

Proceedings of the  
US-LHC Collaboration Meeting  
on  
**ACCELERATOR PHYSICS EXPERIMENTS  
FOR  
FUTURE HADRON COLLIDERS**

**Brookhaven National Laboratory  
Upton, New York  
February 22-23, 2000**

**Editors  
W. FISCHER and F. PILAT**

Brookhaven National Laboratory  
Brookhaven Science Associates  
Upton, New York 11973  
Under Contract No. DE-AC02-98CH10886  
with the United States Department of Energy

## CONTENTS

FOREWORD	iv	V. SHILTSEV Compensation of Beam-beam Effects in Tevatron with Electron Beams: R&D Status and Plans ( <i>Slides</i> )	57
F. PILAT, W. FISCHER, R. TALMAN, M. SYPHERS and O. BRÜNING Summaries	1	V. PTITSIN Beam-beam Studies at RHIC	81
<i>Single Beam Investigations</i>		<i>Experimental Techniques</i>	
T. ROSER, W. FISCHER and F. PILAT RHIC RUN 2000 Plans	4	P. BAGLEY Local, Linear, Transverse Coupling in Storage Rings ( <i>Slides</i> )	84
C. MONTAG and B. HOLZER Persistent Current Effects in HERA-p	7	W.C. TURNER, P.S. DATTE, P.F. MANFREDI, J.E. MILLAUD, N.V. MOKHOV, M. PLACIDI, V. RE, H. SCHMICKLER Status Report on the Development of Instrumentation for Bunch by Bunch Measurement and Optimization of Luminosity in the LHC	112
W. FISCHER, S. PEGGS, F. PILAT, S. TEPIKIAN and D. TRBOJEVIC RHIC Dynamic Aperture and Beam Lifetime Studies in 2000	10	F. SCHMIDT Detuning, Resonances and the Complete Nonlinear Model Determined from Turn-by-turn Pick-up Data	119
F. PILAT Local, Nonlinear Interaction Region Correction	13	G. ARDUNI, H. BURKHARDT, K. CORNELIS, Y. PAPAPHILIPPOU F. ZIMMERMANN and M.P. ZORZANO Measurements of Coherent Tune Shift and Head-Tail Growth Rates at the SPS	128
D. TRBOJEVIC Beam Growth Studies with Primary and Bent Crystal Collimators ( <i>Slides</i> )	17	M. BAI, M. METH, B. PARKER, S. PEGGS, T. ROSER and D. TRBOJEVIC Measurements with AC Dipoles	136
<i>Colliding Beam Investigation</i>		W. FISCHER, B. PARKER and O. BRÜNING, Transverse Echos in RHIC	139
P. BAGLEY Tevatron Run II Plans	23	LIST OF PARTICIPANTS	144
T. SEN Beam-beam Studies for the Tevatron	38		
M.A. FURMAN Beam-beam Simulations for Separated Beams	50		

## FOREWORD

The US-LHC Collaboration Meeting on Accelerator Physics Experiments for Future Hadron Colliders was held at Brookhaven National Laboratory, Upton, New York, on February 22 and 23, 2000. It was attended by 24 participants from 6 institutions.

Future hadron colliders face new challenges. The Meeting focused on plans for accelerator physics experiments at existing machines that are relevant to the operation of the LHC and to the design of future hadron colliders. Synergies between short-term and long-term experimental efforts were identified and experimental groups organized.

The session on Single Particle Investigations, chaired by R. Talman (Cornell), discussed the possibilities of studies and experiments during the upcoming Tevatron and RHIC runs. Emphasis was given to dynamic aperture, beam lifetime and persistent current investigations as well as local nonlinear interaction region corrections and collimator studies.

The session on Colliding Beam Investigations, chaired by M. Syphers (FNAL), discussed possible beam-beam

studies at the Tevatron and RHIC. Experiments were viewed in light of possible LHC problems and theoretical investigations.

The session on Experimental Techniques discussed an array of advanced methods with which beam data can be obtained. Among these were bunch-by-bunch luminosity measurements for the LHC and the processing of turn-by-turn beam position data. These data can be used to implement local coupling corrections, derive nonlinear accelerator models and obtain broad band impedances. New techniques also included AC dipole measurements and transverse echos.

We thank all participants for their contributions to the success of the workshop. We are grateful to Mary Campbell, Rhianna Bianco and Waldo MacKay for their support in organizing the workshop and in preparing the proceedings. We hope that these proceedings are a useful reference for future collaborative work on accelerator physics experiments.

W. Fischer and F. Pilat

## SUMMARIES

### 1 WORKSHOP SUMMARY

*F. PILAT AND W. FISCHER, BNL*

Participants from CERN, Cornell, DESY, FNAL, LBNL, and BNL discussed beam based experiments relevant for the LHC and other future hadron colliders. The following areas of activity were identified as the most appropriate for a collaborative effort in the short and medium term:

- Interaction region corrections
- Beam-beam effects
- Collimation
- Luminosity measurement
- Studies with AC dipoles

Teams of people were formed to take part in machine studies at RHIC during summer 2000 and possibly during the fall at the Tevatron. Initial studies are a natural evolution of already planned commissioning activities. We envision that successful studies will evolve into formal beam experiments in the medium term (beyond 2002). Such experiments have to be proposed to and approved by the scientific reviewing boards at BNL and FNAL.

For every team, a coordinator is responsible for proposing a plan for machine studies. It is important that initial studies have a limited scope and support commissioning and operations efforts. Formal machine study proposals will be based on contributions from all team members and agreements from home institutions. The following teams were formed:

#### *Interaction Region Corrections*

BNL	F. Pilat, M. Bai, W. Fischer, A. Lehrach, T. Satogata, S. Tepikian
CERN	O. Brüning
FNAL	T. Sen, P. Bagley

The following items are needed to commission and study the RHIC interaction region correction system:

1. Analysis of the instrumentation requirements for the BPM system (turn-by-turn capabilities), kickers (injection and tune meter kickers), tune meter, beam current transformer, beam profile monitor, Schottky system and AC dipole.
2. A realistic model of RHIC at 65 GeV/u, with the commissioning lattice and field errors measured at 3000 A (the quadrupole current for 65GeV/u is 3131 A)
3. A plan to attack non-linearities one at the time, starting with octupole errors. The correction method should be tested with large known and controlled non-linearities. Simulated data should be obtained in advance.

4. An automated way to set the interaction region correctors in the control room according to the action-kick minimization correction. Essential is the capability of interfacing the off-line model to the on-line model used in the control room.
5. An operational procedure to optimize the nonlinear corrector settings. Promising observables for tuning are the measured tune spread and line amplitudes in Fourier spectra of turn-by-turn data.

The written proposal will analyze in detail the above listed points. The goal is to have a first draft by March, an agreed upon proposal by June and beam time in July-August 2000.

#### *Beam-beam Effects*

BNL	W. Fischer, A. Drees, F. Pilat, V. Ptitsin
CERN	O. Brüning
FNAL	P. Bagley, T. Sen, M. Syphers
LBNL	M. Furman

During the workshop two beam-beam studies emerged as starting points for further investigations: the measurement of beam-beam footprints in the Tevatron and RHIC, and the search for coherent modes in RHIC.

Measured beam-beam tune-shifts give a base-line for future studies. In addition, 'folded' footprints, obtained in Tevatron simulations with large bunch numbers, are a cause for concern since they appear to be correlated with a smaller dynamic aperture.

Simulations indicate that coherent oscillation modes due to beam-beam interactions may be observable in RHIC. It is planned to further investigate this prediction and test it experimentally.

Beam-beam studies are being planned at FNAL for the 36 on 36 bunch operation. The participation of FNAL group members in these efforts should ensure coordination with this collaborative inter-laboratory effort.

#### *Collimation*

BNL	A. Drees, N. Catalan-Lasheras, D. Trbojevic
IHEP	V. Biryukov

A novel collimation system, which uses a bent crystal to channel the beam onto a Collimators, is being installed in RHIC. The system may allow precise measurements of transverse diffusion processes. Substantial transverse diffusion is expected from intra-beam scattering during gold operation at storage. The crystal is provided by IHEP, and the collaboration can be naturally extended to beam studies. A written proposal is being prepared.

*Luminosity Measurement*

BNL A. Drees  
LBNL W. Turner

The goal of this collaboration is to establish if the luminosity measurement proposed for the LHC could be tested, at least partially, at RHIC, following the already planned beam test at CERN.

*Studies with AC Dipoles*

BNL M. Bai, W. Fischer  
CERN F. Schmidt

The AC dipole will be possibly installed and commissioned at RHIC in summer 2000. A proposal that details how to use the AC dipole for beam experiments at RHIC will be written and submitted. In addition, the AC dipole in the AGS can be used for tests.

**2 SUMMARY OF SINGLE BEAM INVESTIGATIONS SESSION**

*R. TALMAN, CORNELL*

*Miscellaneous Comments on Presentations*

T. Roser reported on the RHIC test run 1999. In this run the beam diagnostic system performed impressively an lattice measurements are in excellent agreement with model predictions. For 2000 single and colliding beam operation is planned and the gained knowledge would be universal. Specific to RHIC will be the operation with heavy ions for which intra-beam scattering is a dominant effect. This is also of interest to the LHC. Also specific to RHIC is the operation with polarized protons. Gold ions present a good test particle for intra-beam scattering studies and Schottky spectra.

C. Montag showed predicted and observed persistent current effects in the proton ring of HERA. The chromaticity can be predicted to a large degree (within five units) but active on-line correction is still necessary.

W. Fischer presented plans for RHIC machine studies during the year 2000 run. Studies concentrate on establishing an experimental record for many of the basic machine properties. Important study areas are nonlinear detuning and dynamic aperture, intra-beam scattering and persistent current effects. The question arose whether one can study synchro-betatron resonance using a spectral analysis.

F. Pilat discussed plans for compensating interaction region quadrupole field errors in RHIC. There are detailed field measurements and simulations using corrector setting from the the well-established action-angle kick minimization show a significant improvement in the dynamic aperture. For unknown field errors, however, there is no operational compensation algorithm.

D. Trbojevic showed how a bent crystal can be used as a large amplitude diagnostic tool. This may particularly

interesting for transverse intra-beam growth rate measurements.

*Pros and Cons of Inter-laboratory Collaborations*

Collaborations between laboratories have to weigh the advantages and disadvantages of such an approach. Clear advantages are:

- Expertise, algorithms, and codes can be shared
- It is profitable to have small group interaction (e.g. this workshop) and collaborations
- Local advantages, e.g. a modern data acquisition system at RHIC, can establish operational procedures that can be used elsewhere

Disadvantages of inter-lab collaborations are

- A possible loss of focus on local developments
- An exceeding demand for personnel and machine time
- Possible adverse sociological effects (group cohesion)

Past experience, especially with the E778 experiment suggests a number of requirements for a successful collaboration. Among these are

- A strong Institutional support
- A mutual lab interest
- Simple goals
- A minimum of new hardware
- First rate data acquisition systems

Experimental work in a successful collaboration needs to be prepared well in advance. Single particle effects should start with know magnet measurements or expected distributions of magnetic field errors. The study, experiment or correction algorithm should be simulated from these data. The necessary data acquisition systems need to be commissioned as an operational tool. With first experimental results a study or correction algorithm can be refined.

**3 SUMMARY OF COLLIDING BEAM INVESTIGATIONS SESSION**

*M. SYPHERS, FNAL*

From now on the Tevatron Collider will collide 36 on 36 bunches and will have two "pacman" bunches per train. In the future, about 100 bunches will be filled in each ring leading to a bunch spacing of 132ns. In this mode a crossing angle is required which is likely to cause the excitation of synchro-betatron resonances. In addition, simulations resulted in "folded" tune footprints which are a reason for concern since they seem to be correlated with a smaller dynamic aperture. RHIC will primarily run in gold operation. It can be used for strong-strong beam-beam investigations.

Issues that need to be studied for the LHC and other future hadron colliders include control over the beam separation with common interaction region triplets, interaction region correction, the "pacman" effect, the dynamic aperture and lifetime as a function of the crossing angle, and

coherent modes. These issues should be addressed in organized studies and experiments.

Detailed plans should include a precise description of the experimental tools needed (strength ranges, resolution, response functions, ...), the measurement procedures (number of data points, required measurement time, transverse or longitudinal kicks, ...), the observables and the analysis procedure.

For this we need a clear and thorough proposal. A core group of individuals at the Tevatron and RHIC should form a collaborative effort. Actual experimental proposals should be presented to the group at the next collaborating meeting for discussion and feedback.

## 4 SUMMARY OF EXPERIMENTAL TECHNIQUES SESSION

*O. BRÜNING, CERN*

The LHC and future hadron colliders will be complex machines. Almost 3000 bunches will circulate in the LHC, with different orbits, tunes and other parameters. Furthermore, the LHC can only operate with very small beam losses to avoid quenches of the superconducting magnets. Future hadron colliders therefore require the accurate control of a large number of parameters, and fast and non-destructive measurement techniques.

### *BPM Based Measurement*

Beam position monitors are standard equipment in accelerators. A number of techniques were discussed that use turn-by-turn data from beam position monitors, including local coupling correction, broad-band impedance measurements and the deduction of non-linear accelerator models. For local decoupling procedures, it was pointed out by P. Bagley that

- Global coupling correction is different from local coupling correction
- The minimum tune approach is not a coupling correction at the working point
- The one turn transfer map contains all information on coupling

Y. Papahilippou presented a frequency analysis of turn-by-turn data from which the broad band impedance can be obtained. In this approach, the real part is determined from the head-tail growth rate and imaginary part from the tune change with time.

F. Schmidt's complex Fourier analysis of turn-by-turn data results in the coefficients of the one-turn map. The technique works best with two beam position monitors 90 degrees apart shows promise for the correction of individual resonances.

### *New Techniques*

W. Turner showed plans to use collision by-products for measuring various parameters with instrumentation inside

the LHC TAS and TAN absorbers. Among these are the luminosity  $L$ , the relative offset  $\Delta x$ , the crossing angle  $\alpha$  and the beam sizes  $\sigma_x$  and  $\sigma_y$ . Instrumentation inside the absorbers has to be radiation hard equipment to be reliable.

M. Bai reported on the construction for an AC dipole driven with a frequency close to the betatron frequency. Using an adiabatically turn-on the AC dipole can create large coherent oscillations ( $\approx 3\sigma$ ) without emittance increase. Despite its original purpose as a spin flipper, the device can be used to obtain betatron phases and beta functions and an analysis of the beam frequencies can reveal the nonlinear characteristics of the machine.

W. Fischer reported on the possibility of transverse echo measurement in RHIC. For this a fast quadrupole is required. Transverse echo measurements would be a novel tool to investigate transverse diffusion mechanisms.

## RHIC RUN 2000 PLANS\*

T. Roser, W. Fischer and F. Pilat, BNL, USA

### Abstract

After the 1999 test run, the year 2000 run will complete the RHIC commissioning and will also be the first run for physics. The main goal is to achieve 10% of the design luminosity at 70% of the design energy in gold operation. In addition, polarized protons will be stored and accelerated in one of the two rings.

### 1 INTRODUCTION

In 1999 the two RHIC rings were tested in a two months long run. Gold beam was stored at injection energy in both rings and accelerated by a small amount in one of the rings. Most of the systems and instrumentation were commissioned.

For the 2000 run the plan is to accelerate gold beams to 70% of the design energy and collide the beams, producing up to 10% of the design luminosity. More instrumentation systems, notably tune measurement systems, are to be commissioned. For the first time polarized beam will be transferred into one of the rings and accelerated.

### 2 RHIC STATUS AFTER TEST RUN AND MAINTENANCE PERIOD

During the 1999 test run the injector chain, consisting of the source, Tandem, Booster and the AGS, worked well and reliably. The intensity per bunch of the gold beam reached 50% of the design value. Transverse and longitudinal emittances, as measured in the AGS, were within the design specifications.

Fig. 1 shows the preparation of bunches in the AGS. 20 bunches are injected from the Booster. One out of 6 bunches is lost in the transfer due to insufficient kicker pulse length. At injection energy the beam is then debunched and rebunched into 4 bunches. The debunch-rebunch process takes 100ms and results in bunches with an area of  $0.3\text{eV}\cdot\text{s/u}$ .

During the test run the refrigerator worked well and all RHIC magnets were tested up to 40% of the maximum operating field. Beam was circulated and captured by the rf in both rings despite a severely restricted physical aperture (see below). Fig. 2 shows the beam current at injection in the Blue ring with a lifetime of 19 minutes. Beam could be stored for up to 45 minutes in the Blue ring and for a few thousand turns in the Yellow ring. Beam in the Blue ring was accelerated by a modest amount, about  $1\text{GeV/u}$ .

\* Work performed under the auspices of the US Department of Energy.

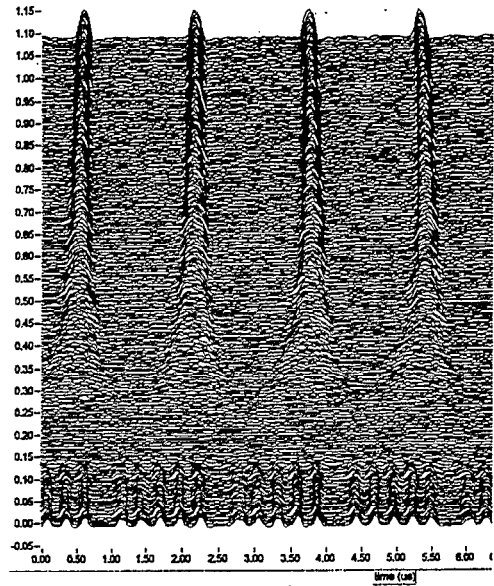


Figure 1: RHIC bunch preparation in the AGS. 24 bunches are injected, debunched and rebunched into 4 bunches with an longitudinal area of  $0.3\text{eV}\cdot\text{s/u}$ . The time from debunching to rebunching is 100ms.

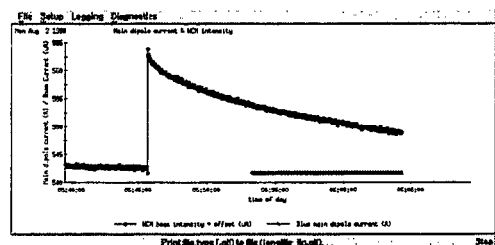


Figure 2: Beam current in the Blue ring showing a lifetime of 19 minutes.

Beam instrumentation systems were commissioned. The beam loss monitors and beam position monitors reached operational performance. It was demonstrated that a novel Ionization Profile Monitor (IPM) can record transverse profiles turn-by-turn.

Measurements of the RHIC lattice properties were performed. In Fig. 3 such a measurement is shown where a predicted difference orbit is compared with a measured one. The difference orbit is taken from closed orbits with and without a vertical orbit corrector. Measured and pre-

dicted difference orbits agree very well except for a few BPMs, which are reversed. For these, agreement is also good after sign reversal. Difference orbits were used to identify reversed BPMs. Fig. 4 shows a measurement of multi-turn orbit rms from which the  $\beta$ -functions can be deduced.

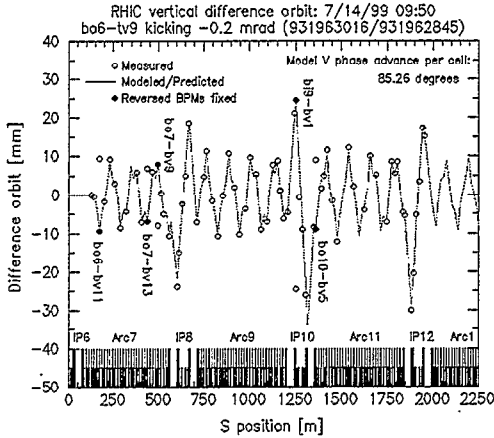


Figure 3: Measured and predicted difference orbits in one half of the ring. The difference orbit is taken from orbits with and without a vertical orbit corrector. The difference orbit was used to identify four reversed BPMs. Except for these predicted and measured difference orbits agree very well.

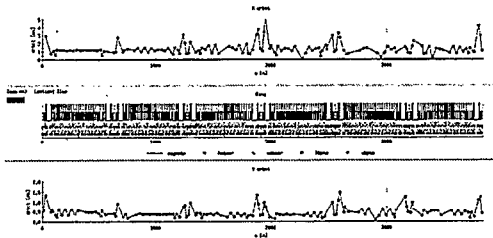


Figure 4: Multi-turn orbit rms in the Blue ring for a  $\beta$ -function measurement.

In 1999, the physical aperture in both rings was severely limited by distorted beam tube bellows (see Fig. 5). During high pressure tests of the Helium process lines, the dummy sections (drift lines without magnets) moved sideways. All 192 dummy inter-connects had to be opened and the bellows repaired.

The power supply systems was not fully completed in 1999. Not all of the interaction region shunt power supplies were delivered in time. This made it necessary to run with a small  $\beta^*$  of 3m in all interaction regions instead of the nominal injection optics that has a  $\beta^*$  of 10m. In addition, the power supply system did not yet provide the nominal ramp rates for acceleration. Measurements of transfer functions and field errors were performed for different ramp rates (see Fig. 6 for a quadrupole measurement). Neither the transfer functions nor the field errors depend on the

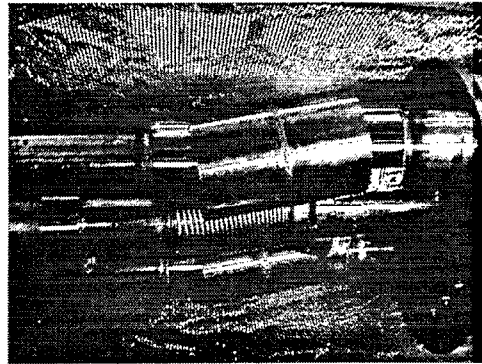


Figure 5: Distorted bellows of Helium process lines in a dummy section.

ramp rate which will make it easier to slowly increase the ramp rate to the nominal value in the next run.

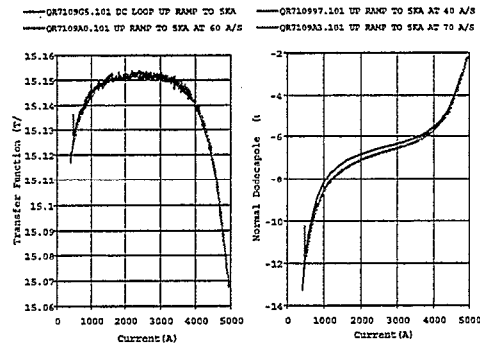


Figure 6: Transfer function and dodecapole measurement of and arc quadrupole at different current ramp rates. There is practically no difference between ramp rates.

### 3 GOALS FOR RUN 2000

There are two main goals for the RHIC Run 2000. First, gold beams are to be accelerated in both rings to 65 GeV/u and brought into collision. The target luminosity is 10% of the design value of  $2 \cdot 10^{26} \text{cm}^{-2} \text{s}^{-1}$ . For this, close to 60 bunches have to be accelerated and stored in each ring. With established collisions, the RHIC physics program will begin. The second goal is to inject polarized protons in one ring, measure the polarization and accelerate the polarized proton beam.

To achieve gold acceleration to the target energy, the transition energy has to be crossed in a superconducting machine for the first time. The RHIC design included a  $\gamma_t$ -jump in order to minimize the beam time close to the transition energy. Nominally, 48 quadrupoles in each ring would be turned off within 60ms to change the  $\gamma_t$  fast with a steadily accelerating beam (see Fig. 7). However, the pulsed power supplies for this scheme are not yet available.

Instead, before reaching transition, the orbit radius will be first reduced. This results in a beam energy that is lower

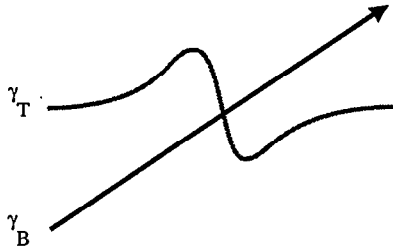


Figure 7: Schematic of a transition crossing with a  $\gamma_t$ -jump. Pulsed quadrupoles are needed for this scheme.

than with a constant radius. To cross transition, the beam will then be accelerated as fast as possible. This will result in an increased orbit radius. The radius can then be lowered slowly to bring the beam again in the middle of the beam pipe. This scheme is shown in Fig. 8.

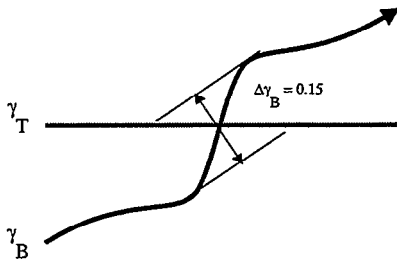


Figure 8: Schematic of a transition crossing with a radius and thereby energy jump. Sufficient radial aperture is needed for this scheme.

In gold operation, intra-beam scattering will be an important effect at injection and storage. Intra-beam scattering will grow all three beam dimensions during stores, and computations predict a significant drop in the instantaneous luminosity due to this effect. Fig. 9 shows the result of such a computation for a storage time of 10 hours.

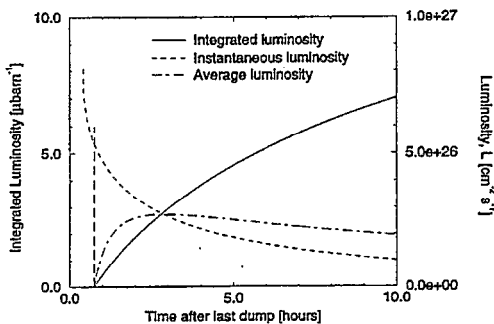


Figure 9: Computed instantaneous, integrated and average luminosity as a function of time. The instantaneous luminosity drops with time since the beams grows in all three dimensions primarily due to intra-beam scattering.

After the end of the gold run, it is planned to operate RHIC with polarized protons. Ultimately, each RHIC ring

will have two Siberian snakes (each consisting of four helical magnets) to overcome depolarizing resonances, and four spin rotators (also consisting of four helical magnets) that allow to collide longitudinally polarized protons at two of the RHIC experiments, STAR and PHENIX. Each ring will also be equipped with a polarimeter.

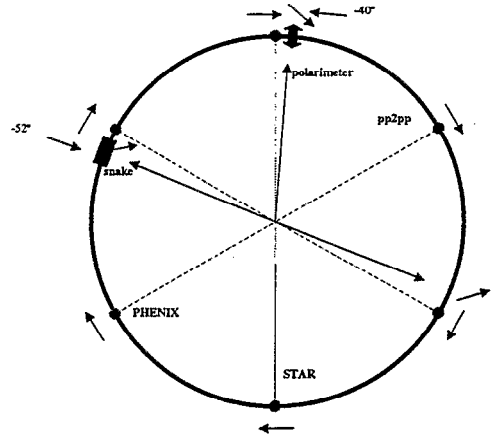


Figure 10: Location of the snake and the polarimeter in the Blue ring that are available for the Run 2000.

For the Run 2000, a new source for polarized protons will be available, one Siberian snake and a polarimeter in the Blue ring (see Fig. 10). Polarized proton operation will therefore be restricted to one ring. The goal for the test run with polarized protons is to inject polarized protons into the RHIC Blue ring, measure polarization with the polarimeter, operate the Siberian snake and finally accelerate beam while preserving polarization.

After the operating period with beam, the quench protection system for the DX magnets will be fully commissioned. This will allow to ramp the rings up to the full design energy in the next run.

Fig. 11 depicts the schedule for the year 2000. Operation with beam will start in March. It is planned to inject and store beams at injection in both rings, accelerate them and establish collisions. Polarized proton operation is at the end of the run.

	Jan-00	Feb-00	Mar-00	Apr-00	May-00	Jun-00	Jul-00	Aug-00
RHIC Status		Ring cold	Hi					
RHIC PS testing/kevt. integr.								
High Intensity proton op.								
Au operations								
Injector set-up								
Inject and circulate in RHIC								
Set-up acceleration in RHIC								
Set-up collisions in RHIC								
RHIC Hi Physics								
Injector set-up for pol. Prot.								
RHIC pol. proton studies								

Figure 11: Schedule for the RHIC 2000 run.

#### 4 ACKNOWLEDGMENTS

This review of the 1999 RHIC performance and the plans for the RHIC Run 2000 reflects the work of the whole Collider-Accelerator Department at BNL.

## Persistent Current Effects in HERA-p

C. Montag\*, B. Holzer, DESY, Hamburg, Germany

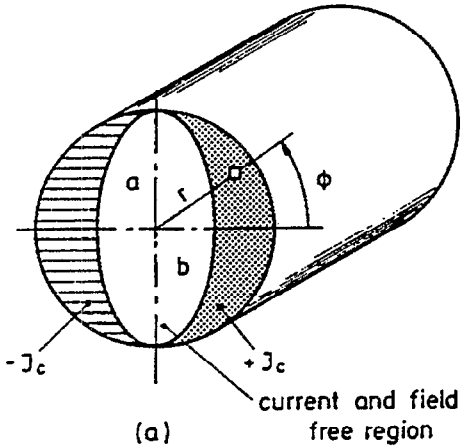


Figure 1: Schematic view of persistent currents inside a filament, running back and forth at a critical current  $J_c$  [1]

### Abstract

Eddy currents in the filaments of superconducting magnets, so called persistent currents, are of great concern for any accelerator using superconducting magnets, like HERA, RHIC, TEVATRON, or LHC. Persistent current effects on the chromaticities in the HERA proton machine during injection are presented, with an emphasis on their predictability and reproducibility.

## 1 INTRODUCTION

In recent years superconducting magnets have become the state-of-the-art technology for high energy hadron machines, like HERA, TEVATRON, RHIC, or LHC. As for all accelerators, the reproducibility and predictability of magnetic fields and thus optics parameters is of great importance for the successful operation of the machine.

Persistent currents are eddy currents induced within the filaments of superconducting magnet windings by changes of the magnetic fields. These persistent currents circulate inside the filaments at a constant current density, as schematically shown in figure 1. Since they contribute to the multipole components of the magnetic field, persistent currents severely affect the quality of a superconducting magnet, especially at low magnetic fields. The azimuthal field component  $B_\theta$  as a function of the radius  $r$  and the azimuth

angle  $\theta$  can be expanded in a series of normal and skew components as

$$B_\theta(r, \theta) = B_{\text{main}} \cdot \sum_n \left(\frac{r}{r_0}\right)^{n-1} \cdot [b_n \cdot \cos(n\theta) + a_n \cdot \sin(n\theta)], \quad (1)$$

with

$r_0$	reference radius
$b_n$	normal multipole coefficient
$a_n$	skew multipole coefficient
$B_{\text{main}}$	main field (dipole field, or quadrupole gradient $\cdot r_0$ ).

In the case of HERA, the chosen reference radius  $r_0 = 25$  mm equals approximately the free-bore radius of the beam pipe.

The effect of persistent currents on the multipole components of the superconducting magnets can be completely neglected at high magnetic fields of about 5 Tesla, which in the case of HERA corresponds to a proton energy of 920 GeV. As measurements have shown, all higher-order multipole coefficients are of the order of  $10^{-4}$  in that case. This changes drastically at the injection energy of 40 GeV, corresponding to 0.2667 Tesla. Here, multipoles of all orders allowed by the coil geometry are induced, i.e.  $n = 1, 3, 5, \dots$  within dipole magnets and  $n = 2, 6, 10$  in the case of quadrupole magnets.

As a consequence, the chromaticities of the HERA proton ring at injection energy are completely dominated by persistent current sextupoles. While the natural chromaticities amount to  $\xi_x = -44$  in the horizontal and  $\xi_y = -47$  in the vertical direction, the contribution of the induced persistent current sextupoles due to the  $b_3$  component in the dipole magnet of  $b_3 \approx 3.2 \cdot 10^{-3}$  is about a factor of 5 higher [3]:

	natural	$b_3$ (dipoles)
$\xi_x$	-44	-275
$\xi_y$	-47	+245

To make things even worse, the influence of persistent currents on machine performance depends strongly on the history of the magnets – duration of the previous run, quenches, etc. Additionally, persistent current effects vary with time due to their decay [4]. For successful operation of the accelerator some means of compensation is therefore necessary.

\* Email: christoph.montag@desy.de

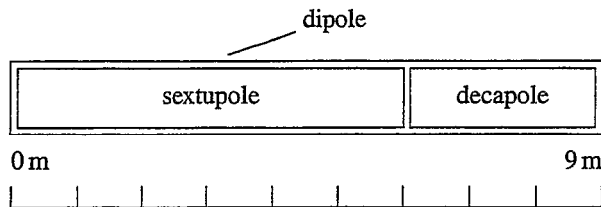


Figure 2: Schematic view of a superconducting HERA dipole with its sextupole and decapole correction windings.

## 2 THE HERA PERSISTENT CURRENT SEXTUPOLE CORRECTION SCHEME

The superconducting HERA dipoles are equipped with quadrupole and sextupole windings in order to correct field distortions. While the total length of the dipole is 9.0 m, the length of the sextupole winding is only 5.9 m. Furthermore, the sextupole coil is not longitudinally centered with respect to the dipole winding, but is shifted to one end, while the remaining space is equipped with a decapole coil. This is schematically shown in figure 2. To compensate the effects of decaying persistent currents at injection and of induced persistent currents during the ramp, two reference magnets are connected in series with the main HERA-p dipoles [5]. These reference magnets are equipped with various measurement devices, like NMR, hall probes, and rotating coils, in order to determine the actual multipole components of the magnetic field [6]. During injection, these measurements are used to compensate time-dependent contributions of decaying persistent currents to the dipole and sextupole fields, while during the first stage of the ramp, from injection energy to 150 GeV, this system counteracts the “snap-back” effect of the newly induced persistent currents.

At the end of a luminosity run, the magnets are cycled in a well-defined procedure in order to achieve reproducible injection conditions of the magnetic fields on their hysteresis curve. During this procedure, persistent currents are induced which would lead to extremely unstable injection parameters.

When the injection energy is finally reached, these persistent currents decay exponentially. Since the absolute field variation is large immediately after cycling the magnets, the compensation of the effect of this decay on the chromaticity starts with a delay of 300 sec in order to keep the necessary sextupole correction fields small. The effect of the obtained persistent current sextupole contribution on the chromaticities is automatically kept constant using the two sextupole families installed in the HERA proton ring. Figure 3 shows the chromaticities at injection during 30 minutes with and without this sextupole correction. When the sextupole correction is switched off, the decaying persistent currents lead to a rapid change of the chromaticities. With the sextupole correction switched on, the chromatici-

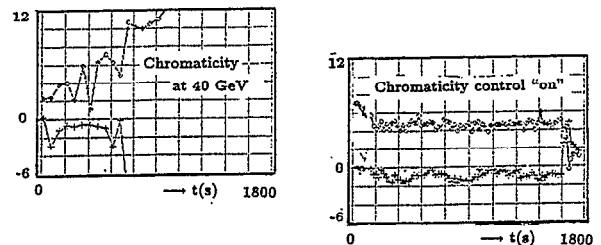


Figure 3: Chromaticities of the HERA proton ring during 30 minutes at injection energy. The left plot shows the rapidly changing chromaticities due to decaying persistent currents when the sextupole correction is switched off. With the sextupole correction switched on, the chromaticities remain constant (right plot) [2].

ties stay constant within the measurement accuracy.

## 3 REPRODUCIBILITY AND PREDICTIBILITY OF PERSISTENT CURRENT SEXTUPOLES

While the HERA persistent current sextupole correction scheme presented in the previous section compensates the effect of the persistent current decay, the absolute values of the chromaticity are adjusted using measurements on beam. For this purpose, a test beam of 10 proton bunches is injected which is used to measure and correct several parameters, such as energy (dipole field), tune, coupling, and chromaticities. When these parameters are adjusted, the test beam is dumped, and the luminosity fill of  $3 \cdot 60 = 180$  bunches is injected.

Since the persistent current sextupole contribution is known from the reference magnet measurement, one might think of using it for the adjustment of the absolute chromaticities instead of the beam-based measurement. To test the feasibility of such a scheme the chromaticities are calculated using the measured  $b_3$  component and the actual sextupole fields necessary to obtain chromaticities of about  $\xi_{x,y} = +2 \pm 1$ , as required for stable operation of the machine. If these calculated chromaticities are constant within one or two units, the reference magnet field measurements should be sufficient to adjust the chromaticities.

Figure 4 shows the optics of one of the 104 FODO cells in the arcs of the HERA proton ring. The persistent current sextupoles, which have the same length and location as the dipole coils, are represented by a thin sextupole of 10 mm length, located in the longitudinal center of the decapole winding (see figure 2). The correction sextupoles are assumed to be located in the longitudinal center of their actual winding, with a length of 10 mm.

Within the four dipole magnets, both the square-root of the  $\beta$ -functions,  $\sqrt{\beta_{x,y}}$ , and the horizontal dispersion,  $D_x$ , vary approximately linearly with the longitudinal coordinate  $s$  along the orbit. Since the contribution of sextupoles

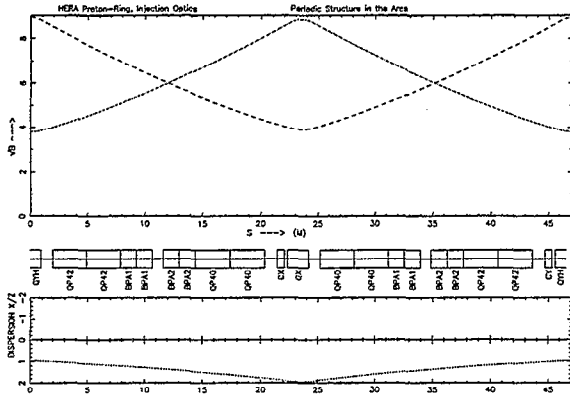


Figure 4: FODO cell optics used for the calculation of the chromaticities due to persistent current sextupoles and correction sextupole settings.

with strength  $m(s)$  to the chromaticities depends linearly on the  $\beta$ -function and the horizontal dispersion,

$$\xi_{x,y,sext} = \frac{1}{4\pi} \oint D_x(s) \beta_{x,y}(s) m(s) ds, \quad (2)$$

the appropriate representation by thin lenses between dipole slices is a crucial issue.

Figure 5 shows the chromaticities as obtained from the  $b_3$  measurement and the actual sextupole settings. In both planes the calculated chromaticities are found within a band of about  $\pm 5$ . As usual, the chromaticities are aimed to be  $\xi_x = \xi_y = +2 \pm 1$ , and must not be negative in order to avoid the head-tail instability. Since the measured bandwidth of  $\pm 5$  would frequently lead to negative chromaticities, this shows that the  $b_3$  measurement in the reference magnets is not sufficient to predict and correct the chromaticities of HERA-p. A possible explanation is the simplified optics model used in this calculation, which does not reflect the longitudinal positions of the persistent current sextupoles and the "real" machine sextupoles well enough. Additionally, the reference magnets might not reflect the average persistent current sextupoles in the entire machine to a sufficient accuracy.

#### 4 SUMMARY AND OPEN QUESTIONS

As has been shown, the predictability of persistent current effects on the chromaticities in the superconducting HERA proton ring at injection energy does not seem to be sufficiently accurate to ensure a successful operation of the machine without chromaticity measurements using a test beam. At present it is still unknown whether this irreproducibility is probably just due to the simplified optics model used in these investigations. In order to improve this situation, a refined optics model will be developed for further studies, with a more realistic representation of both persistent current and correction sextupoles by an increased number of slices.

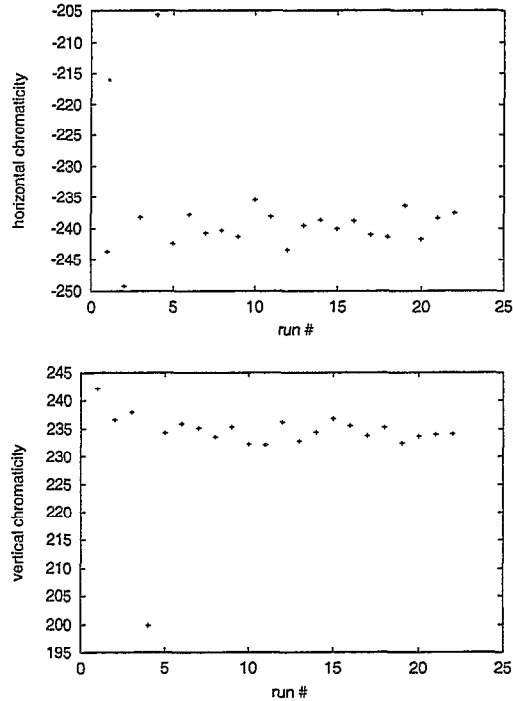


Figure 5: Calculated chromaticities versus run number. The large deviation from the mean value during run 4 is likely to be due to errors in data taking.

Furthermore it is planned to study the reproducibility and predictability of persistent currents on the machine energy, i. e. the dipole field, the tunes, and the betatron coupling.

#### 5 REFERENCES

- [1] C.P. Bean, Phys. Rev. Lett. 8 (1962) 250
- [2] B. Holzer, Part. Acc. 55 (1996)
- [3] O. Meincke, Measurement and Control of Q-Values and Chromaticity in the HERA Proton Ring (in German), DESY-HERA 92-08, 1992
- [4] H. Brueck et al., Time Dependence of Persistent Current Field distortions in the Superconducting HERA Magnets, Proc. EPAC90, Nice, 1990
- [5] C. Daum, J. Geerinck, P. Schmueser, R. Heller, H. Moeller, H. Muto, S. Schollmeier, P. Bracke, DESY-HERA 89-09, 1989
- [6] P. Schmueser, R. Meincke, Y. Zhao, Methods of Harmonic Measurements in the Superconducting HERA Magnets and Analysis of Systematic Errors, DESY-HERA 91-13, 1991

# RHIC DYNAMIC APERTURE AND BEAM LIFETIME STUDIES IN 2000\*

W. Fischer, S. Peggs, F. Pilat, S. Tepikian and D. Trbojevic, BNL, USA

## Abstract

Commissioned during the summer of 1999, RHIC is still a new machine, and its basic properties must be explored in detail. Among such investigations dynamic aperture and beam lifetime measurements are central. During the first year of operation an experimental record for the dynamic aperture and beam lifetime should be established under operational conditions. Further investigations should concentrate on intra-beam scattering, the effectiveness of local nonlinear interaction region correction, and persistent current effects.

## 1 INTRODUCTION

The two RHIC rings were commissioned during the summer of 1999. In the Blue ring a lifetime of about 45 min was achieved, while the lifetime in the Yellow ring was only a few thousand turns (less time was spent commissioning the Yellow ring). The next run calls for a systematic investigation of the effects that limit the dynamic aperture and the beam lifetime and thereby the achievable luminosity. Studies should concentrate on four objectives:

1. Measurement of the dynamic aperture and beam lifetime under operational conditions with varying parameters
2. Measurements of beam growth times due to intra-beam scattering
3. Test of the local nonlinear interaction region correction algorithm
4. Measurement of persistent current effects

Measurements of the dynamic aperture and the beam lifetime can be compared with calculations and simulations (see for example Ref. [1]). This will show how well certain aspects of the RHIC performance can be modeled. The collected data will provide a starting point for improvements.

Of special interest in these efforts is intra-beam scattering, expected to be the most important lifetime limiting effect in RHIC when operated with gold ions [2, 3]. Longitudinal growth times at injection are in the order of minutes.

RHIC uses a novel scheme for the local correction of the nonlinear magnetic errors in the interaction region triplets. A similar scheme will be used in the LHC. No operational experience for such a correction scheme exists and it is of great importance for RHIC and the LHC to establish a

Table 1: RHIC dipole kickers at injection energy.  $\sigma_{x/y}$  denotes the transverse rms beam size.

Kicker	Strength range		Kick length
	[ $\mu$ rad]	$\sigma_{x/y}$	
Injection (ver)	300–1500	4.7–23.5	60 ns
Tune (hor)	0–11	0–0.2	90 ns
Tune (ver)	0–11	0–0.1	90 ns
Abort (hor)	250–2500	4.2–390	> 12 $\mu$ s

working procedure. This topic is dealt with in detail in a separate paper [4].

Bench measurements indicate that time-dependent persistent current effects should only play a minor role in RHIC. A measurement with beam should confirm this.

## 2 EXPERIMENTAL TOOLS

In dynamic aperture measurements the available aperture will be filled with beam and the largest amplitudes at which particles can survive will be measured. A smooth closed orbit and retracted collimators are necessary to ensure that the dynamic aperture is not obstructed by the physical aperture.

In RHIC the vertical aperture will be filled with a single kick using the injection kickers. The horizontal aperture could be filled by the abort kicker, but safety concerns make an implementation of this scenario difficult (after the abort kicker is fired, it would not be available for some time thus making the magnets and other equipment vulnerable). Alternatively the horizontal and vertical aperture can be filled in many turns using the tune kickers. Tab. 1 summarizes the kick strengths of the available kickers at injection energy. At storage the strengths drop to one tenth of the stated values.

The dynamic aperture will be observed with an ionization profile monitor (IPM), which has been successfully tested last summer. The IPM is capable of recording profiles turn-by-turn, although such a high time resolution is not needed for dynamic aperture measurements. For reliable measurements the IPM has to be commissioned as an operational tool and its sensitivity must be determined experimentally. Fig. 1 shows a vertical turn-by-turn profile from the IPM with injection oscillations and the effect of coupling.

The beam lifetime will be measured with a beam current transformer. In Fig. 2 such a signal is shown. An application will fit the data and deliver the lifetime [6].

\* Work performed under the auspices of the US Department of Energy.

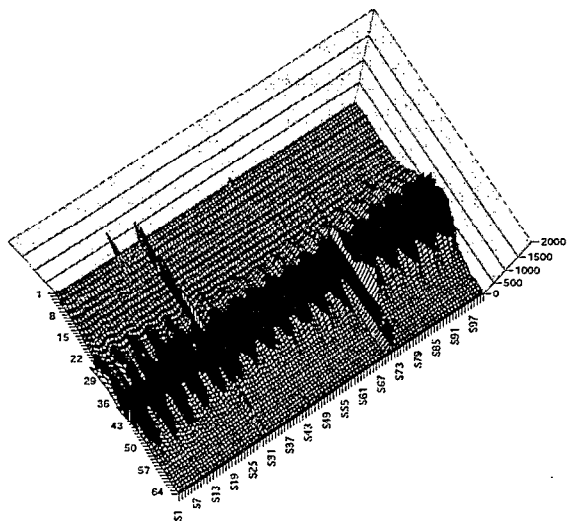


Figure 1: Vertical turn-by-turn profiles from an Ionization Profile Monitor, showing injection oscillations and the effect of coupling (7/27/99 15:00h) [5].

### 3 PARAMETER SCANS

The dynamic aperture and beam lifetime depend on numerous machine parameters. To find the best working point a systematic scan of the most important parameters can be done. These are

- Closed orbit
- Tunes
- Chromaticity
- Nonlinear detuning
- Local nonlinear interaction region correction
- Intensity

Measurements of nonlinear dynamic effects due to magnetic field errors are best done with protons or a gold beam with a small local phase space density (after a kick).

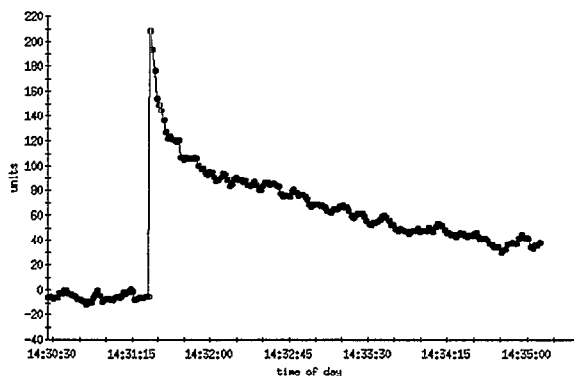


Figure 2: Total beam current versus time, without rf, showing a beam lifetime of about 3 minutes (7/27/99 14:36h).

### 4 INTRABEAM SCATTERING

Intra-beam scattering effects in gold beams are important at injection and storage. At injection, below transition, the longitudinal growth time for a gold beam is in the order of minutes [2, 3] and can be observed with a wall current monitor. The signal from this detector is shown in Fig. 3.

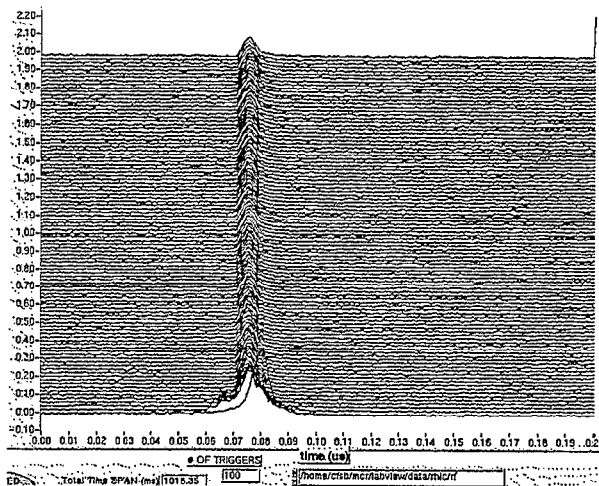


Figure 3: RF wall current monitor, showing captured beam surviving cleanly for the first second (7/19/99 07:20h).

At storage, above transition, the gold beam will grow in the longitudinal and both transverse dimensions. The longitudinal growth will be measured with the wall current monitor, while the IPM allows the observation of the transverse growth rate.

### 5 PERSISTENT CURRENT INVESTIGATIONS

Persistent current effects in RHIC are not as strong as in the HERA proton ring or in the LHC. RHIC's rigidity ratio between storage and injection energy is only 10, while it is 20 for HERA and the LHC.

During the commissioning run in 1999 some time dependent effects were observed. Although it was not possible to determine the cause of these effects, time-dependent persistent current effects might have played a role.

Once the main magnets of RHIC are ramped to the injection level, the persistent currents decay with time and change the sextupole component of the magnetic field. This leads to a slow change of the chromaticity. When the acceleration ramp starts the sextupoles will change back to their original value in a short time interval thereby changing the chromaticity rapidly. This effect is known as snap-back.

Bench measurements of the time dependent sextupole field in the dipoles have been made at 660A, somewhat above the injection level of 460A. Fig. 4 shows the measurements of 20 RHIC arc dipoles. Typically, the sextuple field changes by 1 unit in 5 minutes. We assume that the

persistent currents are approximately independent of the main current [7], and scale the measurements at 660A accordingly to lower values of the dipole current.

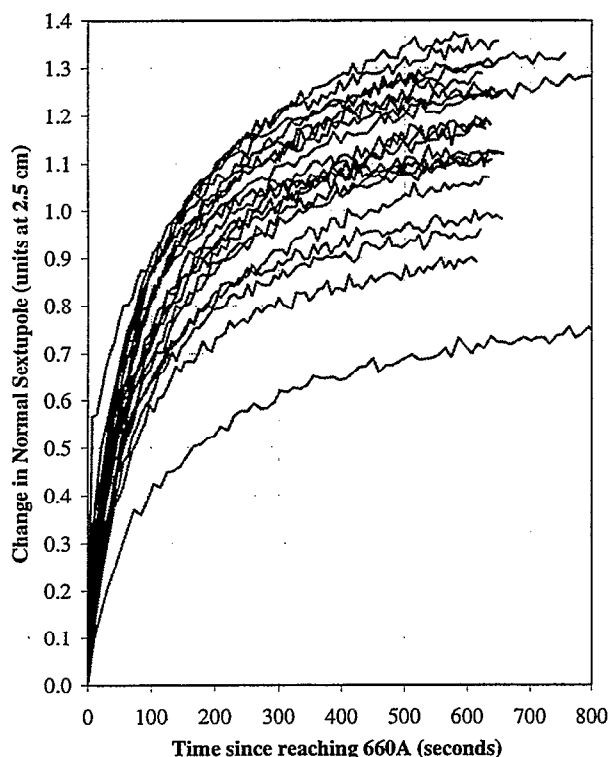


Figure 4: Time-dependent change of the sextupole coefficient in 20 RHIC dipoles, in units of  $10^{-4}$  at a reference radius of 2.5cm [7].

Tab. 2 shows the change in horizontal chromaticity  $\xi_x = \Delta Q_x / \Delta p/p$  for different injection energies after 5 minutes. With a momentum spread  $\Delta p/p$  of about 0.001 off-momentum particles experience a change in the horizontal tune of up to 0.008 within 5 minutes when the relativistic  $\gamma$  is as low as 10.2.

Table 2: Change in the horizontal chromaticity due to persistent currents for different injection momenta after 5 minutes.

Relativistic $\gamma$	[1]	12.0	11.4	10.8	10.2
$I_{dipole}$	[A]	543	524	489	462
$\Delta \xi_x$ after 5min	[1]	-6.4	-6.7	-7.1	-7.5

The chromaticity can be measured at the injection level in 4 second intervals and monitored over several minutes. Chromaticity measurements should be in agreement with the results above that were derived from test bench measurements.

## 6 SUMMARY

Many phenomena and operational scenarios need to be explored for a good understanding of the RHIC machine per-

formance. Dynamic aperture and beam lifetime studies are central to these efforts.

The study of nonlinear effects that stem from magnetic field errors is best done with protons, since growth effects may be masked by intra-beam scattering effects when performed with gold. Gold, of course, should be used to study intra-beam scattering.

## 7 REFERENCES

- [1] W. Fischer and T. Satogata, "A Simulation Study on Tune Modulation Effects in RHIC", BNL RHIC/AP/109 (1996).
- [2] J. Wei, "Intra Beam Scattering in RHIC", RHIC/AP/63 (1995).
- [3] W. Fischer, W. MacKay, S. Peggs and J. Wei, "Emittance Growth in RHIC During Injection", proceedings of the LHC96 Workshop on High Brightness Beams for Large Hadron Colliders, Part. Acc. Vol. 58, pp. 181-191 (1997) and BNL RHIC/AP/112 (1996).
- [4] F. Pilat et al, "Local Nonlinear IR Correction Studies", these proceedings.
- [5] R. Connolly, private communication.
- [6] A. Lehrach, private communication.
- [7] A. Jain, private communication (1999).
- [8] M. Conte, W.W. MacKay, "An Introduction to the Physics of Particle Accelerators", World Scientific (1991).
- [9] E. Keil, "Lattices for Collider Storage Rings", in "Handbook of Accelerator Physics and Engineering" edited by A.W. Chao and M. Tigner, World Scientific (1999).

## Local, non-linear Interaction Region Correction Studies

F. Pilat, Brookhaven National Laboratory, Upton, NY 11973, USA

### 1 INTRODUCTION

The main goal of the interaction Region (IR) Correction system is to improve the performance of a collider by:

(i) correcting locally the effect of the **nonlinear field errors** in the Interaction Region (IR) triplets, and beam separation dipoles (DX and D0 in RHIC).

(ii) correcting locally **coupling effects** arising from field errors and misalignment in the IR magnets.

IR Correction significantly improves the dynamic aperture in simulation (RHIC and LHC). However, given the inherent complexity of nonlinear effects and the lack of straightforward observables, possible improvement of machine performance requires careful planning and machine studies to achieve the goal.

I will overview here the method (*action-kick minimization*) used for IR corrections, the implementation of the correction system for RHIC and its comparison with the system proposed for the LHC. I will then describe the modeling studies that guided the design of the system as well as modeling studies planned for the commissioning. A plan for IR machine studies is then discussed. The plan is conceptually divided in a "*commissioning phase*", that is, the steps necessary to make the system operational, and a "*study phase*" proper, in which parameter spaces as well as their effect on the quality of correction are explored. Finally, I discuss how IR machine studies may form the basis for collaborative studies.

### 2 THE CORRECTION METHOD

The field quality of magnets in the IR's and beam-beam effects are fundamental factors limiting the performance of hadron colliders. The IR Correction system addresses the first factor and corrects the effect locally, taking advantage of the fact that the error sources are local and that there are well defined phase relations between the IR triplets. The action-kick method (first proposed by J.Weil [1]) minimizes the action-angle kick produced by the IR magnets at every order. The action-kick is defined as:

$$\Delta J_x = - \sum_{k, m = -\infty}^{\infty} ik \Delta J_{km}$$

$$\Delta J_y = - \sum_{k, m = -\infty}^{\infty} im \Delta J_{km}$$

$$\Delta J_{lm} \approx - \int ds A_{km} e^{ik \int_0^s \frac{1}{\beta_x} ds' - im \int_0^s \frac{1}{\beta_y} ds'}$$

The above expression for the actions greatly simplify by observing that actions are almost constants of motion and that there are simple phase relations within the IR magnets: there is almost no phase advance in within one triplet and a phase advance of about  $\pi$  between triplets in one IR. It can be demonstrated that, with these approximations, a minimum of 2 correctors per multipole is needed in every IR to correct for the contribution of all IR magnets. By placing the correctors in symmetric locations around the Interaction Point (IP), and exploiting the IR optics anti-symmetry, the one next to a maximum of  $\beta_x$  will be effective horizontally and the one next to a maximum of  $\beta_y$  vertically. The *strengths of correctors* are obtained by minimizing the following quantities:

$$\int_L C_z c_n ds + (-1)^n \int_R C_z c_n ds \quad z = x, y$$

$$C_x = \begin{cases} \frac{n}{\beta_x^2} & \text{for } b_n \\ \frac{n-1}{\beta_x^2} \frac{n}{\beta_y^2} & \text{for } a_n \end{cases}$$

$$C_y = \begin{cases} \frac{n}{\beta_y^2} & \text{for even } b_n \\ & \text{or odd } a_n \\ \frac{1}{\beta_x^2} \frac{n-1}{2} & \text{for odd } b_n \\ & \text{or even } a_n \end{cases}$$

It is worth noticing that the action-kick minimization method does not account for *feed-down* effects. The effect of feed-down has to be evaluated by simulation, at design time, and machine studies, at operations time.

### 3 THE RHIC IR CORRECTION SYSTEM

The RHIC IR correction system consists of nonlinear correction layers located in the C1, C2 and C3 corrector packages located next to the IR triplets, and related power supplies.

All IR's in the Blue and Yellow rings are equipped with correction layers, but in run 2000 only layers at 6 and 8 o'clock (where the large experiments are located) are connected to 50A corrector supplies. A detailed layout of the IR regions can be seen in Figure 1.

In addition, 2 skew quadrupoles per IR (both in the Blue and Yellow Ring) are installed in every C2 package. All IR skew quadrupoles have a 50A independent supply, for a total of 24. These skew quadrupoles to compensate the local coupling

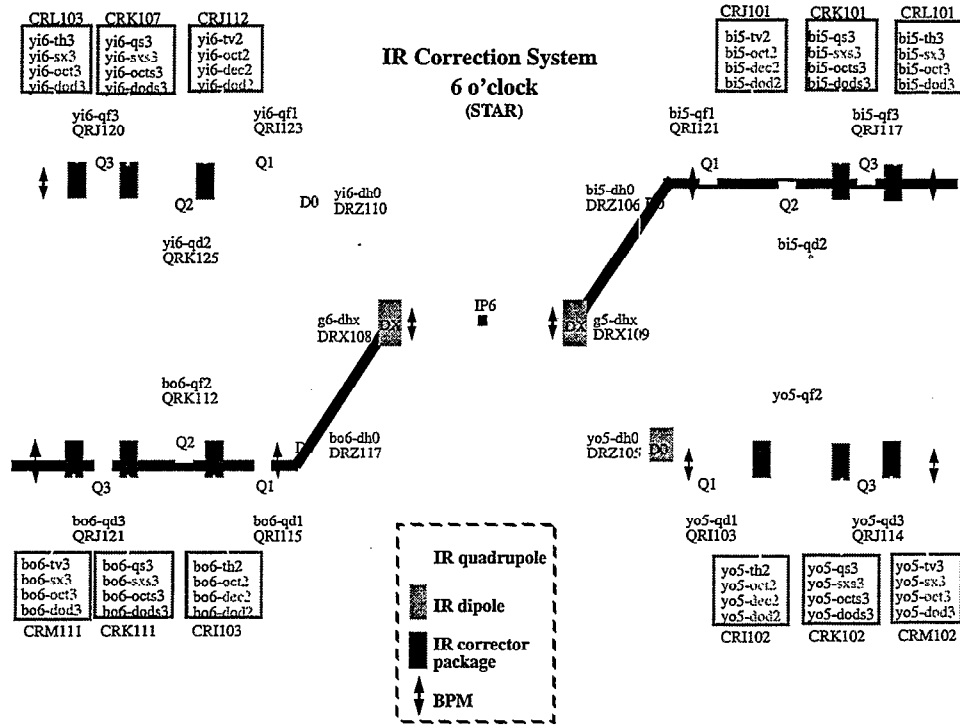


Figure 1. Schematics of the corrector system (nonlinear and skew quadrupoles) around the 6 o'clock IP

from the IR's are in additions to the skew quadrupole families that are used for globally decoupling the machine by minimization of the tune separation at the coupling difference resonance.

#### 4 THE LHC IR CORRECTION SYSTEM

The IR correction system planned for the LHC is based on the same principle of the RHIC IR system.

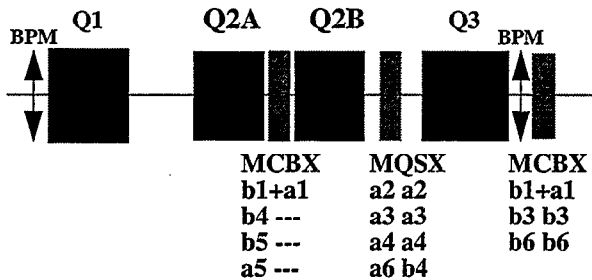


Figure 2. IR Correction system for the LHC. (European notation for the multipoles)

Figure 2 shows a schematic view of the LHC IR Correction system: 3 corrector packages are placed respectively in the middle of the Q2 cryostat (MCBX-Q2), between Q2 and Q3 (MQSX) and after Q3 (MCBX-Q3). The original IR correction scheme was studied and finalized at the US-LHC BNL Workshop in 1999 [2]. Every MCBX contains a horizontal and

vertical dipole corrector, and MQSX a skew quadrupole. The other layers contain high order multipole windings. Recently, a simplified version of the system has been considered, where MCBX-Q2 only retains the 2 dipole correctors, MQSX the skew layers (a2, a3 and a4) and the b4, and MCBX at Q3 contains sextupole and dodecapole windings in addition to the dipole correctors. Overall, the b5, a5, a6 layers were dropped from the original scheme since the corrector strengths required, on the basis of recent LHC IR magnet measurements, are rather weak.

#### 5 THE MODEL

A complete set of simulation results exists for the *nominal RHIC collision lattice*, ( $\beta^*=1\text{m}$  at IP6 and IP8, and  $10\text{m}$  in all other IP's). The RHIC *off-line model* includes the measured field errors for all relevant magnets in the machine, measured at 5000A (current corresponding to  $\sim 100\text{ GeV}$ ). The model includes also the "IR filter" that calculates the IR correction settings by the "action-kick" minimization procedure, and the *local decoupling algorithm* to set the IR skew quadrupole correctors operationally.

A new modeling effort is necessary to simulate the effect of controlled nonlinearity in the machine (see below) for the *run 2000 lattice* (feb2000a,  $\beta^*=1\text{m}$  at IP6,  $\beta^*=8\text{m}$  at IP10 and  $\beta^*=3\text{m}$  in all other IP's) and possibly field errors measured at 3000 A (current for which we have data closest to 70 GeV).

We also need to bridge the *off-line* to the *online model* by implementing in the latter the capability of reading and writing

SXF files [3].

## 6 SYSTEM COMMISSIONING

The commissioning of the IR correction system consists of several steps. The prerequisite is to have 1 RHIC Ring (presumably Blue first, then Yellow) *operational* and *stable*. That specifically means: stable circulating beam (lifetime > 1h), orbit corrected in the IR's to <1mm,  $\Delta Q_{\min} < 0.005$ , and possibly 1 IP (IP6) squeezed to 1m. Commissioning with  $\beta^* = 3\text{m}$  is possible but all IP's at 3m would contribute equally, a less desirable situation).

### 6.1 Systems required for IR Correction Commissioning

Other systems, other than the triplet correctors, are necessary for IR Corrections:

*Tune Meter.* Tune measurements. Possible measurement of tune spread.

*Schottky detector.* Possible measurement of tune spread.

*BPM's (turn-by-turn).* FFT analysis (or frequency analysis) of turn-by-turn data to identify spectral lines due to nonlinear fields. For the 2000 run the capability exists of recording 128 turns at every BPM, and ten-thousand's of turns on selected channels.

*Orbit Display.* Display and correction of orbit. Setting up of IR bumps, off axis in the triplets to measure coupling locally by observing the off plane response and to measure effect of nonlinear fields.

*DCCT.* Measurement of beam lifetime and beam current. Real time (every 10 sec) monitoring and optimization of machine performance.

*Ionization Profile Monitor (IPM).* Beam profile measurements.

*Kickers.* To generate oscillations for turn-by-turn BPM acquisition, dynamic aperture measurements, etc. The *tune meter kickers* can be used resonantly. Should that not give a sufficient kick at collision, *injection kickers* can be used for vertical kicking. *Abort kickers* may be used to generate a horizontal kick at collision (in a low intensity machine run, and possibly only with a reduced number of kicker modules active)

*AC Dipole.* This is the ideal tool to generate a coherent oscillation for IR studies, and will be used for this purpose as soon as on line, likely in the 2001 RHIC run.

### 6.2 IR Non-linear Correctors

The challenge for the system commissioning is to identify beam observables by which to guide and judge corrector performance. The plan is to test *1 corrector layer (order) at the time* in the following order (american notation for multipoles here):

- normal octupole* (b3)
- normal dodecapole* (b5)
- normal sextupole* (b2)
- normal decapole* (b4)
- skew sextupole* (a2)
- skew octupole* (a3)
- skew dodecapole* (a5)

Octupole is first because it generates tune spread, a good potential observable. Dodecapole follows since it is an allowed harmonic of the triplet quadrupoles, and also produces tune spread. Skew octupole and dodecapole are at the bottom of the list since they are not powered for this run, given their predicted minimal impact on machine performance.

For every correction layer the following should be done:

1. A "Controlled experiment": apply a known corrector strength, measure the effect on the machine (tune spread, lifetime, spectral lines in turn-by-turn data), and compare with model data. Repeat that at positions of large  $\beta_x$  and  $\beta_y$  if we have 2 correctors in the same triplet (b3, b5 layers).
2. Compensate the effect with a nearby corrector (for the b3 and b5 layers) or with correctors across the IP. Verify the effect on the machine.
3. Set the corrector at the value calculated by the "IR filter" to dead-reckon the measured field error.
4. Operational setting of the corrector based on machine observables (tune spread, real time DDCT, spectral lines).
5. Measurement of machine performance (lifetime, dynamic aperture) with and without correction.

### 6.3 IR Skew Quadrupole Correctors.

During the early phase of the Year 2000 run a clear coupling effect has been observed in the IR's. By kicking the beam with a horizontal dipole corrector just before an IR, the measured vertical difference orbit shows a clear effect due to the horizontal kick. The horizontal response is in very good agreement with the design machine model. Experimental setting of a triplet skew quadrupole cancels the effect of the orbit. Likely causes of IR coupling are a roll in the IR triplets and skew quadrupole errors in the DX and D0 dipoles at low current.

The plan for IR coupling correction include:

1. Setting up the IR skew quadrupole correctors on the basis of difference orbits analysis. Multiple kicks with different phases will be used to confirm the correction.
2. Measure of local coupling via analysis of turn-by-turn BPM data and local correction (local decoupling algorithm) is planned for the machine run in 2001.

## 7 IR STUDIES

Once the IR correction system is commissioned there are several IR studies that can increase the knowledge and hopefully the performance of the machine, for instance:

1. Measure the effect of going *off-axis* in the triplets. That will allow to study the effect of feed-down as a function of bump amplitude.
2. Parametric dependence on  $\beta^*$  at IP6. In the 2000 run IP6 is the only IR with beta squeeze capability (not all IR power supplies were delivered on time). In 2001 it will be possible to squeeze IP8 as well.
3. Effect of *crossing angle*. The design crossing angle at RHIC is zero, however it is possible to achieve crossing angles up to a few mrad by trimming the DX and D0 magnets. A tunable crossing angle opens the possibility of studying the interplay of IR field quality and beam-beam effects, which is very impor-

tant for the LHC. That is particularly interesting with a proton beam where beam-beam effects are expected to be more significant.

## 8 CONCLUSIONS AND PLANS

The main goal of the IR correction system is improvement of RHIC performance. The IR correction system planned for the LHC is very similar to the RHIC system, so both IR Correction commissioning and IR studies at RHIC are of relevance for the LHC, and in particular for the US-LHC Collaboration. This workshop on "Beam experiments for future hadron colliders" was successful in identifying potential collaborators from which we will benefit during the commissioning and study phases. Collaborative studies, if successful, have the potential to lead in the future to more formally organized beam experiments.

## 9 REFERENCES

- [1] J.Weil, "*Error compensation in insertion region magnets*", Particle Accelerators, 55 439-448(1996).
- [2] Proceeding of the "*Workshop on LHC Interaction region correction systems*", Ed. W.Fischer and J.Weil, BNL-52575 and LHC Project Note 199.(1999)
- [3] H. Grote, J. Holt, N. Malitsky, F. Pilat, R. Talman, C.G. Trahern, "*SXF (Standard eXchange Format): definition, syntax, examples*", RHIC/AP/155, August 1998.

## **Accelerator Physics Experiments for Future Hadron Colliders**

*EXPERIMENTS IN RHIC (summer 2000 ??):*

### **Beam Growth Studies with Primary and Bent Crystal Collimators**

- **Introduction**
- **Previous Experience**
- **Predictions for the Intrabeam Scattering**
- **Bent Crystal Channeling**
- **Experimental Set-Up**

Submitted by Dejan Trbojevic, BNL

## ***Introduction:***

- **Motivation for the experiment:**
  - Show that ***intrabeam scattering*** is a dominant effect on the beam life time and on the emittance growth in RHIC  $_{197}\text{Au}^{79+}$  (important also in the future LARGE Hadron colliders).
  - Experimentally find out the exact scale of the problem. Why?
    - Find the optimum mode for operation!
    - Plan a correct way for the luminosity upgrade
      - RD projects - what kind?
  - Connect the experiment with luminosity optimization and Background reduction.
  - Use the impact parameter measurements to show the way of beam growth:
    - First by using the Primary Collimator jaws
    - Second with the CRYSTAL collimation.

## *Previous Experience:*

- **Major “rules”:**
  - Measure a signal downstream of the collimation point without reducing the luminosity
  - Fit a response curve to the predicted beam growth (Intrabeam scattering?, Diffusion?)
- **SPS measurements (LHC note 117):**
  - Measurements of the transverse diffusion speed and the impact parameter-b
- **Diffusion and 778 experiments in the Tevatron**
- **HERA measurements (Bruning et al.)**

## Intra Beam Scattering Predictions:

- **INTRA-BEAM multiple Coulomb scattering has cross section:**
  - $\sigma \cong Z^4/A^2$
- **Particles in the bunch exchange longitudinal and transverse momenta by Coulomb scattering**
- **D.C background, beam halo, or trapped particles in the empty buckets, could be created by the escaped particles from the RF bucket ( initial bucket area of ~0.3 eVs/u -> ~1.3 eVs/u ).**
- **COMPARISONS BETWEEN EXPERIMENTAL STUDIES with THEORY show a factor of two over-estimate by theory.**
- **Beam Growth at  $\gamma \gg \gamma_t$ :**
  - $1/\sigma_x d\sigma_x/dt = Z^4 N C_0 / (A^2 \epsilon_x \epsilon_y S \gamma_t) d/n_c$
  - $\tau^{-1} \sim Z^4 N / (A^2 \epsilon_x \epsilon_y S)$

## Measurement of the impact parameter $b$ :

- **Measurements of the impact parameter  $b$  by using the edge of the primary collimator or:**
- **Using a bent Si crystal ( $L=5$  mm) (Valery Biryukov Phys. Rev. E 52 (1995) 2045). One looks at the efficiency  $F$  dependence on  $t$  (thickness of the septum  $x'L$ ):**
  - Accuracy  $\delta b = \delta x' * L = 1 \mu\text{rad} 5 \text{ mm} = 5 \text{ nm!}$   
If we plot  $F(x') - F(-x')$  as a function of  $t$  beam distribution over the impact parameter  $b$  at crystal (BPM resolution 0.1 mm).
  - $\theta = 0, t = x'L (x' > 0), t = x'L (x' < 0)$

## *Why Bent Crystal Collimation?*

- **The Lindhard Critical angle significantly larger ( 8.9 times -  $79^{1/2}$  ) :**
  - $\psi_c = 2[ Z_1 Z_2 e^2 / d p v ]^{1/2}$ , where  $d$  - is the crystal lattice parameter,  $p$  - momentum,  $v$  is the speed.
- **Shorter Crystal ( 5 mm instead of 4 cm) improves efficiency and reduces the nuclear scattering beam loss**
- **Smaller bending angle (0.5 mrad) reduces angle problems (4-5 mrad previously)**

## TEVATRON RUN II PLANS

P. Bagley\* for the Tevatron Group  
Fermi National Accelerator Laboratory#, P.O. Box 500, Batavia, IL, 60510

### Abstract

This is a brief overview of the Tevatron plans for the upcoming Collider Run II [1] with special attention to beam beam problems. Presently we have finished the Fixed Target Run and are in the process of switching over to Collider Mode. The Fixed Target run went well and was a successful first pass at incorporating the new Main Injector into the Fermilab complex of accelerators. Although there will be several shutdowns, we will remain in Collider mode indefinitely (at least until the LHC is running).

### 1 THE SCHEDULE [2]

**Early May 2000** – The Tevatron is scheduled to turn back on.

**May 2000** – Most of May will be spent re-commissioning Power Supplies and doing high energy testing. As the culmination of several years of work, the top beam energy of the Tevatron will be raised from 900 GeV to at least 980 GeV and hopefully to 1 TeV.

**May to end of July 2000 – The Engineering Run.** We will mainly be working only with protons (no pbars) re-commissioning the machine.

**First 2 weeks of Aug. 2000** – After at least one 36 X 36 store, we will shutdown and an incomplete CDF detector will be rolled into the beam line. It will be missing its Silicon Vertex Detector and possibly parts of a few other sub-systems.

**Mid Aug. 2000 to the end of Oct. 2000 – The Commissioning Run.** We will be establishing Colliding Beam conditions and CDF will begin to shake out their upgraded detector.

**Nov. 2000 to the end of Feb. 2001** – Shutdown for the D0 experiment to roll into the beam line. Also, CDF will roll out, install their Silicon Vertex Detector and any other needed components, and roll back in.

**March 2001** – Run II begins!

### 2 CHANGES FROM RUN IB

The biggest change from Run I is the increase from 6 to 36 bunches per beam. 36 bunches per beam corresponds to a minimum bunch spacing of 396 nsec.

#### 2.1 Motivation for 36 bunches

The peak luminosity achieved during Run IB was  $2.8e31/(cm^2 sec)$ . For 6 X 6 bunch operation, this corresponds to about 4.9 inelastic interactions per bunch crossing. Multiple interactions per crossing makes the event reconstruction and physics analysis more difficult. The number of interactions per crossing (IC) the experiments can tolerate is an involved question and depends on the type of physics analysis being attempted. Generally, CDF would prefer no more than about 3-4 IC, and D0 would prefer no more than about 1-2 IC.

The limit on the number of interactions per crossing combined with the experiments' obvious desire for more luminosity, pushes us to more bunches.

#### 2.2 Changes to the Other Machines

This will be the first Collider run with the Main Injector (MI). The Main Injector has performed well in the Fixed Target Run, but for Collider operations, it will have many more roles to perform.

There have been major upgrades to the Pbar Source (the Debuncher and the Accumulator). Almost every stochastic cooling system has been replaced, the lattice of the Accumulator has been changed, and they will have to deal with much more beam on target. One of the big questions for Run II is just how many pbars will we have available? What will be the pbar stacking rate?

The Recycler is a new machine that is still being commissioned. It is located in the Main Injector tunnel, above the Main Injector and is a permanent magnet pbar storage ring at 8.9 GeV/c. It will use a combination of Stochastic Cooling and eventually Electron Cooling of the stored pbars. It has 2 major roles. First, pbars from the Pbar Source will be transferred to it at intervals of about 30-90 min. This will allow the Accumulator to always run with small stack sizes (less than about 20 to 40e10), where it is most efficient. Second, at the end of a store in the Tevatron, rather than throw away the remaining pbars, we will attempt to decelerate and recover them in the Recycler. If the Recycler works as designed, it will provide a large increase in the supply of pbars. However, another of the big questions for Run II is how well will the Recycler work and how efficiently will we be able to recover and re-use the pbars remaining at the end of a store?

Recycling the pbars requires a lot of effort for the other machines as well. Previously at the end of a store in the Tevatron, we could just fire the abort kickers, dumping

\* Email: ppb@fnal.gov

# Operated by Universities Research Association, Inc., under contract with the U.S. Department of Energy.

both the protons and the pbars. Now we will have to take the beams out of collision and quickly remove the  $36 \times (240 \cdot e9) = 8.6e12$  protons without quenching. (We will use a set of collimators in the E0 straight section to scrape away the protons. To direct the spray away from the cold magnets, we have installed 4 warm conventional magnets here to make a dogleg. The movement of the collimators will be computer controlled and will use fast feedback on local loss monitors.) Once the protons are gone, we will turn off all the separators, return from the low beta optics to the injection optics and decelerate the pbars to 150 GeV. They will then be transferred to the MI and decelerated through transition and down to 8 GeV. In order to get the large longitudinal emittance pbars through transition, they will change from the 53 MHz RF used above transition to the 2.5 MHz RF system previously used only for coalescing. Finally the pbars will be transferred to the Recycler and cooled for use in a later store.

### 2.3 Changes for the Tevatron

There are many upgrades and changes for the Tevatron :

- 36 X 36 bunches (396 nsec bunch spacing)
- pbar recycling
- 1 Tev upgrade. This is important to the experiments as a 10% increase in beam energy corresponds to an increase of about 30% in top quark production. We will be using the cold compressors to selectively (on a house by house basis) reduce the operating temperature of the ring. We are also shuffling magnet locations to put weaker magnets in colder locations. Also we are putting in prototypes for high  $T_c$  superconductor power leads and recoilers in spool pieces to improve the heat transfer between the 1 phase and the 2 phase helium.
  - use of the Main Injector
  - no ramps between stores to reset hysteresis and persistent currents. This used to take about 30 min. We want to skip this in order to reduce the time it takes to put in a store. Although conceptually simple, this requires accurate predictions of the size of any hysteresis effects and of the time dependent persistent currents on both the front and the back porch. The persistent currents depend upon the time spent at flattop and on the front and back porches and may "remember" several previous stores.
  - different "Approach to Collisions". In Run IB, we brought the beams into collision longitudinally. We used an RF manipulation (cogging) to longitudinally move the pbars relative to the protons. This moved their crossing point from a region where they were separated to the IP where they collided head on. This method doesn't work with 36 bunches as there is no "cogging" where some proton and pbar bunches do not collide. For Run II, we will bring the beams into collision transversely, by collapsing separation bumps at the IPs. We believe this will be a slower process than before.

- new proton injection kickers. These new kickers will have a rise time of less than 396 nsec, the minimum bunch separation.

- new collimation scheme. In Run I, scraping the halo off the beams at the start of the store was a manual process that took about 30 min. For Run II, we have new targets and collimators which form a 2 stage collimation system. We aim to do this in about 5 min. with an automated process using feedback from beam loss monitors just downstream of the collimators. A separate set of collimators will use a similar system to quickly remove all the protons at the end of a store. (Firing the abort kickers would also kill the pbars, which we hope to recycle.)

- new "feed down sextupole" circuits. At locations where the protons and pbars are separated, we use sextupoles and skew sextupoles to act as quads and skew quads with opposite effects on the two beams. In Run I, we had circuits to adjust the horizontal and vertical tunes and one component of the transverse coupling. For Run II, we are adding another circuit that will adjust the other component of the transverse coupling that affects the minimum tune split.

- New Transverse and Longitudinal Damper systems. With the increase in the number of bunches, we are concerned about multi-bunch instabilities. These damper systems will probably use a combination of several narrow band channels (to damp individual modes) and a weak wide band system.

- new tune measurement system. The standard system in use during Run I looked at all the beam. There were some mechanisms in place to try to null out the proton signal so that we could see the pbar tunes. However, delicate tuning of the system was required for this and so typically we could not distinguish the pbar tunes during normal operation. The new system will allow us to easily see the tunes of individual proton or pbar bunches. It will also allow us to do "transfer function" style measurements, lightly exciting any bunch and observing its response.

- slightly different separator configuration. We have moved one horizontal separator and since the injection point into the Tevatron has moved from E0 to F0, the injection helix has also changed slightly.

- slight differences in the lattice. The D0 experiment is adding Forward Proton Detectors for Run II. These require additional warm space outside of the final focus triplet magnets. To provide this room, we were able to find lattice solutions that did not use one pair of the low beta quads. These quads have been removed. Also there is a minor perturbation to the lattice in E and F sectors. This uses the tune quads to adjust the separation between the beams at one of the collimator stations.

- Luminosity Leveling. If we are doing very well with luminosity, but are not yet ready to go to the 132 nsec bunch spacing, an intermediate way to limit the number of interactions per crossing (IC) is to artificially reduce

the luminosity at the start of a store. We propose to do this by starting the store at a larger value for the  $\beta^*$ . As the store progresses and the luminosity falls (due to emittance growth and loss of beam), we can reduce the  $\beta^*$ , increasing the luminosity to its earlier levels. Although this keeps the IC at a more reasonable level, it also reduces the integrated luminosity delivered to the experiments.

- new method for controlling the low beta squeeze. This is required for Luminosity Leveling. Basically rather than doing the low beta squeeze as a time table triggered by an event, we will broadcast a parameter (on an MDAT frame) that tells the many control cards and power supplies where we are in the squeeze.

- faster shot setups. In Run I, it typically took about 3 hours to put in a store. For Run II, we want to reduce this to 30-60 minutes.

- new Collider Data Acquisition software.

Before they work well, each of these will require significant effort and machine time. Most of the Engineering Run and much of the Commissioning Run will be devoted to these projects.

### 3 EARLY RUN II (36 X 36)

The filling pattern has a 3 fold symmetry. For each beam, the 36 bunches are in 3 trains of 12 bunches. The trains are separated by abort gaps of 2.617  $\mu$ secs and within a train the bunches are separated by 396 nsec. This corresponds to a bunch spacing of 21 RF buckets.

Because the bunches are **not** evenly spaced around the ring, different bunches within a train encounter the bunches in the opposing beam at different places in the ring. This can cause differences between the bunches in a train. The 3 fold symmetry means that if all the bunches in the opposing beam are identical, then we only have to look for differences between the 12 bunches within a train. The 3 bunches at a given location (for example the second from the last bunch in the train) in the 3 trains should all behave identically. We will often refer to the bunches by their position in a train from 1 to 12.

#### 3.1 Beam Beam Concerns

The main beam beam concerns for 36 bunch operations are :

- In all conditions from injection to the final collision condition, we have many more near misses through the arcs (about 70 instead of about 10). Also at this bunch spacing, there is an unfortunate coincidence that the distance between crossing points is almost exactly the cell length. There will be the same phase advances between many of a bunch's near misses. Also, between separators, the horizontal and vertical separations advance like the phase advances, and so the separations at many near misses will also follow a pattern. This will certainly drive certain families of resonances while suppressing others.

- 150 GeV lifetime - In Run IB, with frequent tuning, we could typically keep about a 13 hour lifetime for the pbars in the presence of protons. For Run II, the new damper systems and better control and understanding of the persistent current effects should allow us to greatly reduce the large (20-30 units) chromaticities at 150 GeV. These were known to cause lifetime problems but were used to prevent/control instabilities either while we were at 150 GeV or at the start of the ramp. Also for Run II, we expect to spend less time at 150 GeV (faster shot setups) which will reduce the effects of a poor 150 GeV lifetime.

- the transition from the injection to the collision helix. For certain reasons, we cannot use the same separation scheme in the injection and in the low beta optics. We change from the "injection helix" to the "collision helix (with separation bumps at the IPs)" part way through the low beta squeeze. Given the placement of the separators and the phase advances between them, we believe that it is inevitable that at some point during this transition, through some section of the ring, there is a region of poor separation. We can make this region short, but there are still several points where the beams will briefly (several seconds) collide at very small separations.

The Run I experience gives us some hope that this may be tolerable. At that time we were unaware of this problem. In Run I, there were many fewer bunches, but this poor separation extended over a much larger region, again resulting in several crossing points with poor separation. Despite this we rarely had problems with emittance blow up or beam loss during the transition from the injection to the collision helix.

If this becomes a major problem in Run II, we have a plan to inject into optics with a smaller  $\beta^*$  so that we can use the collision helix in our injection conditions.

- bringing the beams into collision. This was already briefly discussed as the Approach to Collisions.

- At the first "near misses" on either side of the interaction points, we do not have as much separation as we would like. This is shown in figures 1 and 2 below.

#### 3.2 Separations Between the Beams

Figure 1 shows 4 views of the separation around the entire ring. The horizontal axis on each of these figures has units of half RF buckets. The harmonic number of the Tevatron is 1113, so the points shown are from 1 to 2226. These figures start just after, and end at the B0 Interaction Point. The D0 Interaction Point is at 742, 1/3 or 2/3 of the ring from B0. Protons travel in the direction of increasing half bucket number on this graph. Pbars travel in the opposite direction. Crossing points for the first pbar bunches in the 3 trains are marked by squares, for the 6th pbar bunch by asterisks, and for the last (12th) pbar bunch by diamonds. The bottom and 2nd from the bottom figures show the center to center horizontal and vertical separation between the pbars and the protons. The

signs of these separations are for the displacements of the pbars relative to the center of the proton bunches. The second figure from the top shows the diagonal separation, the quadrature sum of the horizontal and the vertical separation, that is  $\sqrt{x^2 + y^2}$ , where  $x$  and  $y$  stand for the horizontal and vertical separations, respectively. The top figure shows the diagonal sigma separation (dss), that is the  $\sqrt{(x^2/\sigma_x^2) + (y^2/\sigma_y^2)}$ . The  $\sigma$ 's used in the top figure assume a beam energy of 1 TeV, transverse normalized 95% emittances of  $20\pi$  mm-mrad and fractional momentum spreads of  $0.087e-3$ .

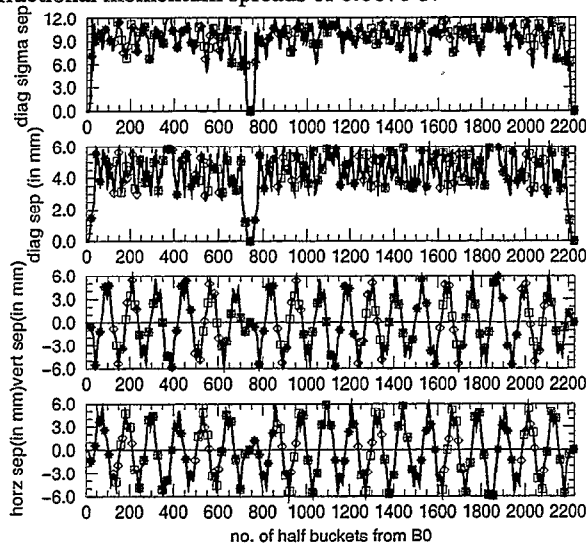


Figure 1 : Four views of the separation around the ring for 36X36. The CDF Experiment is at B0 which is at 0 and 2226 in the figure. The D0 Experiment is at D0 which is at 742 in the figure. From bottom (a) to top (d) : (a) Horizontal separation (in mm), (b) Vertical separation (in mm), (c) Diagonal separation (in mm), (d) Diagonal Sigma separation. Version: v3h15av2.cf045b.nppn2.

Of particular concern in figure 1 are the first crossing points on either side of the interaction points. At these points, the pbars have already passed the separators, but are still close enough to the separators so that there is little separation between the beams. Although the diagonal sigma separation (dss) does not appear much worse than many of the other points, the diagonal separation for these is well below all the others. We will see that the tune shifts (for pbars with zero betatron amplitudes) and the tune spreads (for pbars with a range of betatron amplitudes) from these points are much larger than those from all the other points. With the exception of the first and last bunches in the 3 trains, all the bunches meet bunches from the opposing beam at these points.

### 3.3 Tune Footprints

Figure 2 shows the tune spreads for pbars with a range of betatron amplitudes. This was calculated for bunch 6, in the middle of a train. These assume proton intensities of  $270.e9$ /bunch and as for figure 1, these assume a beam energy of 1 TeV, transverse normalized 95% emittances of  $20\pi$  mm-mrad and fractional momentum spreads of  $0.087e-3$ . Points are shown for pbars with betatron amplitudes of from 0 to  $4\sigma_{\beta z}$  in steps of  $0.5\sigma_{\beta z}$ , where  $z$  may stand for either  $x$  or  $y$ . These figures assume that the pbars have no synchrotron motion. The fractional momentum spread is only used for the opposing proton beam. When we refer to a particle with a horizontal

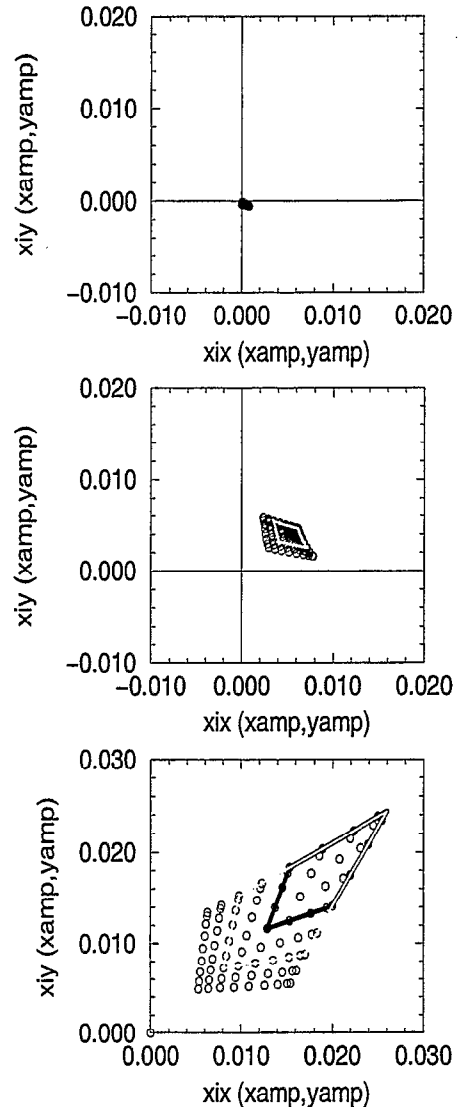


Figure 2: Tune footprints for 36X36, pbar bunch 6. From top (a) to bottom (c) : (a) Contribution from 66 crossing points. All crossings except for the IPs and crossing points next to the IPs. (b) Contribution from 70 crossing points. All crossings except for the IPs. (c) Tune Footprints including the effects of all 72 crossing points. Version: v3h15av2.cf045b.nppn2.

betatron amplitude of  $\sigma_{\beta_x}$ , we mean a particle whose maximum horizontal displacement is  $\sigma_{\beta_x}$ . As a guide to the eye, figures 2b and 2c also show contours at " $2\sigma_{\beta}$ " and " $3\sigma_{\beta}$ ". For example the contour at " $2\sigma_{\beta}$ " connects the points with horizontal and vertical betatron amplitudes of  $(0, 0) \rightarrow (2\sigma_{\beta_x}, 0) \rightarrow (2\sigma_{\beta_x}, 2\sigma_{\beta_y}) \rightarrow (0, 2\sigma_{\beta_y}) \rightarrow (0, 0)$ .

Figure 2a shows the contributions to the tune spreads from 66 of the 72 crossing points. The only crossing points not included are the main IPs and the first crossing points on either side of the IPs. Both the tune shifts and the tune spread in figure 2a are very small. Figure 2b shows the contributions to the tune spreads from 70 of the 72 crossing points. In addition to all the points for figure 2a, this also includes the effects of the first crossing points on either side of the IPs. The effects from these 4 points are much larger than the combined effects of the other 66 points. This tune footprint has the same "sense" as a head on footprint, the zero amplitude particles are at the upper right, the pbars with large horizontal amplitudes and zero vertical amplitudes are at the upper left, etc. The horizontal tune shift and spread come almost entirely from the crossing point downstream (in the pbar sense) of the IP and similarly the vertical comes from the upstream crossing point. (The strengths of the quads are anti-symmetric about the IPs, so near the IP, the horizontal optics on one side become the vertical optics on the other side.)

The large tune spread suggests that these crossing points will also drive resonances strongly. Since the beams are separated at the first crossing points next to the IPs, these points can drive both even and odd order resonances.

We would like to improve the separation at these points, but there is little we can do. The separators are already running about as hard as they can. (If we increase the voltage on them, we believe they will spark much more frequently and a separator spark can ruin a store.) The separation could also be improved by modifying the optics in this region, for example by increasing the phase advance between the separators and these points. However we only have a few quads that are not on the main Tevatron bus and the optics through this region are already highly constrained. There is little we can do.

Finally figure 2c shows the tune spreads for all 72 crossing points, including the IPs. The tune shift parameter from each IP is .00989 and a comparison of figures 2b and 2c show that the total tune spread is still dominated by the effects of the IPs.

Figure 3 shows the tune spreads for all the pbar bunches in a train. Since the filling pattern is 3 fold symmetric, the 3 bunches at a given location (for example the second from the last bunch in the train) in the 3 trains should all behave identically, and we only have to look at 12 bunches.

The tune shifts for pbars with zero betatron amplitudes are shown as open circles. We have assumed gaussian

distributions for the horizontal and vertical displacements and angles of the pbars, from these calculated their horizontal and vertical betatron amplitudes, and then interpolated between our previously calculated tune shifts with amplitudes to get the tunes for each pbar. The darker the spot in figure 3, the more pbars have those tunes.

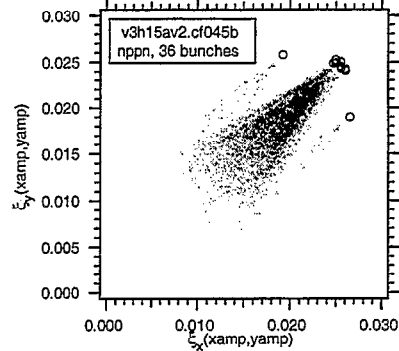


Figure 3: Gray scale plot showing the tune footprints for all 12 pbar bunches in a train for 36X36. The darker the point, the more pbars have those tunes. No synchrotron motion for the pbars. The open circles show the tunes for pbars in each bunch with zero betatron amplitudes.

Version: ts2.v3h15a.cf045b.nppn2

This figure shows that the tune footprints for most of the bunches are almost identical. However, pbar bunches 1 and 12 are shifted from the others because they do not see protons at the first crossing point upstream or downstream (in the pbar sense) of the IPs, respectively. As we saw earlier, these particular crossing points have much smaller separation and much stronger effects than any of the other crossing points (except for the IPs). As a result the pbars take up more space in the tune plane. This may make it more difficult to find operating conditions that are acceptable for all the pbar bunches. If this becomes an intractable problem, we are considering the possibility of not using (not filling) pbar bunches 1 and 12. This would give us stores of 36 proton bunches X 30 pbar bunches. There are other problems with this approach, but it is a possibility.

Figure 4 shows the tune plane near our normal operating point. This shows both even and odd resonances of up to 10th order. In Run IB, our nominal horizontal and vertical tunes in colliding beam conditions were about 0.581 and 0.576. These are the peaks for the proton tune lines on the spectrum analyzers. We believe that the pbar tunes were close to these, but the pbar tunes were never easily read. This operating point is between the  $3/5=0.6000$  and the  $4/7=0.5714$  resonances in figure 4. These resonances could have strong effects on the beams and we had to take care to stay clear of them. Not shown on this plot is the  $7/12=0.5833$ . On some days, we felt we could see effects from this resonance, but on other days, it didn't seem to matter.

The lines shown in figure 4 are only part of the story. These show the locations of the resonances, but not their

strengths or widths and not how these strengths and widths depend on a particle's betatron amplitudes. During Run I, the 3/5 seemed to generally be much stronger and much wider than the 4/7. If either of these resonances are much more strongly driven by the operating conditions for Run II, they may engulf the clear space between resonances. On the other hand, if part of the tune footprints overlap a resonance line, it may not be a problem depending on how strong that resonance is for the particular amplitudes of the particles with the tunes on the resonance.

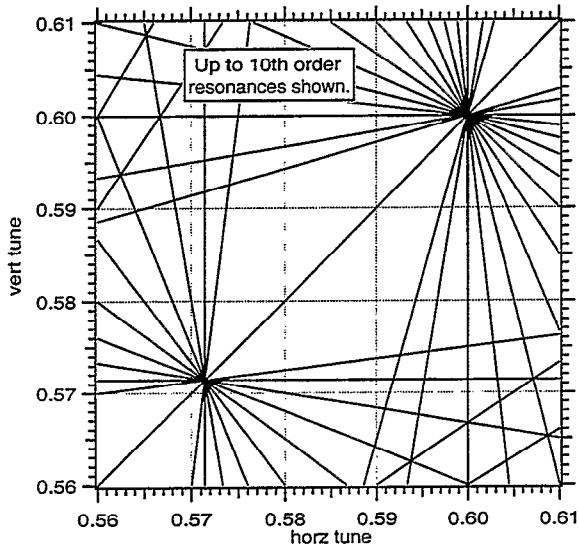


Figure 4: Resonance lines in the tune plane near our working point.

The two main resonances we are near, the 3/5 and the 4/7, are both odd and so, to lowest order, should **not** be driven by the beam beam interaction at the IPs. If the beams collide head on at the IPs, then the IPs should only drive these as 10th and 14th order resonances. But because the beams are separated at the first crossing points, those points can drive these as 5th and 7th order resonances. This is true for all the crossing points in the arcs, but we are more concerned about the first crossing points on either side of the IPs since the separation is small there and we have seen that they produce much larger tune shifts and spreads than the other crossing points. (To further complicate matters, the 3/5 and 4/7 will generally also be driven by the sextupole distribution.)

These are very simple calculations and very simple considerations, but they begin to hint at the problems involved. We would certainly like to have more detailed beam beam simulations and calculations to help us understand what we will see as we re-commission the Tevatron. (There are some efforts underway.) Although we will have many challenges, the 36 X 36 bunch conditions are similar enough to what we had in Run I that we are fairly confident we can make this work.

## 4 LATE RUN II (140 X 103 ?)

As Run II progresses, we expect the pbar stacking rates to increase and that we will start recycling pbars. With an increased supply of pbars and only 36 bunches, the number of interactions per crossing will also increase and again becomes an issue. As discussed earlier, luminosity leveling is a temporary fix, but has a significant cost in integrated luminosity. We are planning to eventually reduce the minimum bunch spacing to 132 nsec. This will allow us to put in about 140 proton bunches on about 103 pbar bunches.

### 4.1 Filling Pattern for 140 X 103

Assume for the moment that we keep the same basic filling pattern as for 36 X 36, except with 1/3 the bunch spacing. We do not plan to improve the abort kickers, so we need to keep the abort gap the same length. In each of the 3 trains, we would then have  $(3 \cdot 11) + 1 = 34$  bunches, for a total of 102 bunches per beam.

The filling pattern for 36 X 36 is 3 fold symmetric with 3 abort gaps in each beam. But for the beam abort we only need 1 abort gap per beam. If we fill 2 of the abort gaps, we can fit in  $2 \cdot 19 = 38$  more bunches per beam, for a total of 140 bunches per beam. The abort gaps in the 2 beams must meet at A0, the location of the abort. The D0 experiment is diametrically opposite A0, so the abort gaps would also meet there, giving D0 140 bunch collisions per revolution time. However at B0, the location of the CDF experiment, the abort gaps do not meet, and CDF would only see 121 bunch collisions per revolution time. We must treat the 2 experiments equally, so we choose to fill 2 abort gaps in the proton beam and only 1 abort gap in the pbar beam. This has 140 X 121 bunches and provides 121 bunch collisions per revolution time to both experiments. This means that most proton bunches will collide with a pbar bunch at both B0 and D0, but that 19 proton bunches will only collide with a pbar bunch at B0 **or** at D0. All the pbar bunches will collide with proton bunches at both B0 and D0.

Finally, we plan to upgrade the proton injection kicker to have a rise time of slightly less than 132 nsec, but the pbar injection kicker rise time will stay at just under 396 nsec. The flattop of the pbar kicker can accommodate 10 bunches at 132 nsec spacing, so after sets of 10 bunches, we have to leave 3 "empty 132 nsec slots" for the rise time of the pbar injection kicker. This reduces the number of pbars we can use and leaves us with 140 proton bunches X 103 pbar bunches.

The proton beam has only one abort gap, so all 140 proton bunches make up one long train. The pbar beam has 2 abort gaps, so there are 2 pbar trains, a short train containing 30 pbar bunches and 2 "injection gaps" and a long train containing 73 pbar bunches and 7 "injection gaps".

## 4.2 Crossing Angles

At a bunch spacing of 132 nsec, the first crossing points on either side of the main Interaction Points are **before** the electro-static separators. The second crossing points are just beyond the separators, but without a crossing angle, the separation at these points is only about  $0.7 \sigma$ . Without a crossing angle, for each Interaction Point, we would have 3 head on collisions and 2 crossings with a separation of about  $0.7 \sigma$ . This is unacceptable and so for this bunch spacing, we require a crossing angle. Unfortunately this requires large crossing angles.

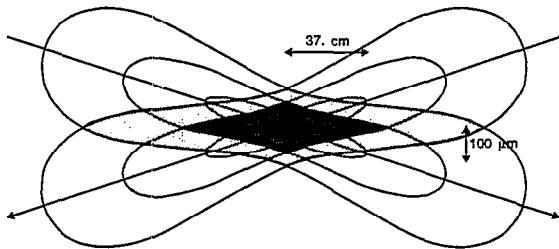


Figure 5: A sketch of two bunches crossing at an IP with  $\beta^*$  of 35 cm, bunch length of 37 cm, and half crossing angle per plane of  $136 \mu\text{rad}$ , corresponding to about  $4\sigma$  separation at the first parasitic crossing points. The direction of motion for the two bunches is indicated by the arrows and they are viewed from the angle where the separation appears largest. This drawing is to scale, however the horizontal and vertical scales are very different, causing the crossing angle to appear to be much larger than it is.  $1\sigma$ ,  $2\sigma$ , and  $3\sigma$  contours are shown with the shaded areas indicating the overlap of these contours.

For separations of about 3-5  $\sigma$  at the first few crossing points, the crossing angle significantly reduces the bunch overlap at the Interaction Point, and hence the peak luminosity. The reduction in overlap is shown graphically in Figure 5, a sketch of 2 bunches colliding with our expected parameters, and in figure 6, a plot of the reduction in the peak luminosity with the crossing angle. The calculation used for the points in figure 6 includes both the hourglass effect (the reduction in luminosity due to the variation in the  $\beta$  over the bunch length) and the crossing angle. The dotted line in figure 6 ignores the hourglass effect. For our parameters, the crossing angle reduces the longitudinal extent of the bunch overlap, the "luminous region". It confines the overlap of the bunches to the region where  $\beta$  is very near its minimum and so the hourglass effect has little effect on the luminosity. Here the length of the luminous region is mainly determined by the transverse size of the beams at the IP and by the size of the crossing angle, **not** by the bunch lengths.

Since we have round beams, the loss in peak luminosity does not depend on the orientation of the crossing angle, only on its size. For reasons related to our

specific lattice and to the separation at the first few crossing points near the IP, we choose to use equal horizontal and vertical crossing angles.

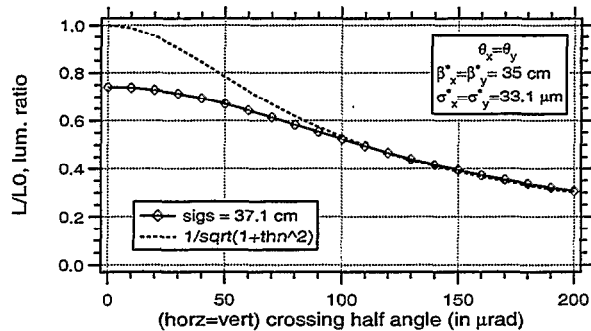


Figure 6: The dependence of the luminosity ( $L/L_0$ ) on the crossing half angle in each plane. The points and the solid line include the hourglass effect. The dotted line shows the approximation that ignores the hourglass effect.  $L_0 = (fBN_{\text{pilot}}N_{\text{pbar}}/4\pi\sigma_{x0}\sigma_{y0})$ , the luminosity if ( $\beta^* \gg$  bunch length) and no crossing angles. This uses a bunch length of 37.1 cm.

The dramatic loss in peak luminosity is a strong incentive to keep the crossing angles as small as possible. But the crossing angle also essentially determines the separation at the first 2 crossing points on either side of the IPs. (This is a total of 8 crossing points.) With both these considerations in mind, we presently plan for half crossing angles of  $\pm 170 \mu\text{rad}$  in both the horizontal and the vertical plane. This gives a total angle between the beams of  $2\sqrt{2} (170 \mu\text{rad}) = 480 \mu\text{rad}$  and corresponds to separations of about  $5\sigma$  at the first crossing points.

There are several implications of these large crossing angles:

- Loss of peak luminosity
- Integrated luminosity concerns
- Change in size and shape of the tune shift footprints from the main IP
  - Synchro-betatron resonances driven by the beam beam interaction at the main IPs. Consider a particle with zero betatron amplitudes, but a non-zero synchrotron amplitude. When it arrives early at an IP, it will have a horizontal and a vertical displacement as it passes the longitudinal center of the opposing bunch. When it arrives late at an IP, it again has horizontal and vertical displacements, but now of the opposite sign. This correlation between its arrival time and its displacement will drive synchro-betatron resonances. The synchrotron tune for the Tevatron at 1 TeV is about 0.00073 (35 Hz), so the synchro- betatron lines are tightly clustered around the pure betatron resonances. The 2 resonances closest to our working point are both odd, the 3/5 and the 4/7 (see figure 4). The head on beam beam interaction can only drive these as 10th and 14th order resonances. With a crossing angle, the beam beam interaction at the IPs will drive the synchro-betatron lines off these resonances.

These synchro-betatron lines will be higher than 5th or 7th order, but lower than 10th or 14th.

- Strong effects from the first few crossing points. We will see that the tune spreads from these points are not small. Since the beams are separated, the beam beam interaction at these points can drive both even and odd resonances.

- Large displacements (2-3.5 mm) in the low beta quads. We have some evidence that the multipole content in these quads may cause problems with displacements of about this size. (This is the reason we are adding a new "feed down sextupole" circuit for Run II. But if the multipole content is a problem, this feed down circuit will only let us compensate one aspect of one multipole term.)

### 4.3 Integrated Luminosity Estimates

Figure 6 shows that we expect to lose about a factor of 2 in peak luminosity with a crossing angle. But this does not directly translate into a loss of integrated luminosity.

Estimates of the sustainable integrated luminosity depend on many factors related to how well the entire accelerator complex is working. A great many details of the performance of the accelerator complex are summarized as 2 parameters, the pbar stacking rate and the pbar recycling efficiency. Unfortunately, we don't yet have a clear idea of the values of these 2 parameters in Run II.

We will guess at these parameters (and several others) to make some estimates of the sustainable integrated luminosity for 2 conditions. The main tool for these estimates is a program that, given the initial beam and machine parameters, simulates the evolution of the beam intensities, beam emittances, and the luminosity during a store. This code was originally written by D. Finley [3] and includes 3 effects :

- Intra-Beam Scattering (IBS). This blows up the longitudinal and horizontal emittances. Coupling is assumed to split the horizontal emittance growth equally into the horizontal and vertical planes, keeping the horizontal and the vertical emittances equal.

- Beam loss from "Luminosity" Events. It uses the total cross section (elastic + inelastic) for particles lost from the beam and uses only the inelastic cross section for the number of interactions per crossing.

- Vacuum effects. These are weak compared to the other two.

J. Marriner later modified this code to include the effect of crossing angles on the luminosity and a recycling efficiency that depends on the pbar emittances at the end of the store.

This code does **not** make any attempt to include effects from the beam beam dynamics. It **assumes** that we can find "good" operating conditions where the beam beam effects are weak compared to the other effects it does include. While this was true for Run I, where we had only 6 X 6 and no crossing angles, we are not confident that

this will be the case for late Run II. As a result, the estimates of the integrated luminosity below, particularly for the case with a crossing angle, may be very optimistic.

We will make estimates for 2 different conditions.

Condition 2 has 396 nsec bunch spacing, 36 X 36 bunches, and if necessary, the luminosity is leveled to be less than  $1.7e32/(cm^2 \text{ sec})$ . This corresponds to less than 5 interactions per crossing on average.

Condition 9 has 132 nsec bunch spacing, 100 bunch collisions per turn at each detector (this is very close to the 103 we would get with the 140 X 103 filling pattern),  $\pm 170 \mu\text{rad}$  half crossing angles in the horizontal and vertical planes, and if necessary, the luminosity is leveled to be less than  $3.8e32/(cm^2 \text{ sec})$ . This corresponds to less than 4 interactions per crossing on average.

For both of these conditions, we assume a 1 hour shot setup time during which we are not stacking and a 20% loss in getting pbars from the Accumulator to colliding beam conditions in the Tevatron.

Table 1 : Integrated Luminosity Estimates

Stack Rate (e10/hr)	Recyc. Effic.	Cond.2 ave.lum. 1/(pb hr)	Cond.9 ave.lum. 1/(pb hr)	diff.
20	0	0.389	0.221 (1.2)	-43%
20	60%	0.487	0.385 (2.5)	-21%
20	80%	0.525	0.434 (2.5)	-17%
40	0	0.518	0.516 (3.6)	0%
40	60%	0.548*	0.685 (4)	+25%
40	80%	0.548*	0.761 (4)	+39%

\* means that there is a surplus of pbars  
 diff. = (Cond.9-Cond.2)/(Cond.2)

The ave. lum. in Table 1 is the luminosity (averaged over a store) that we can maintain with the stated stacking rate and recycling efficiency. The "pbar economics" are included in these. For Condition 9, the average number of Interactions per Crossing at the start of a store is shown in parenthesis next to the average luminosity. All of the cases for Condition 2 stores start at their luminosity limit of  $1.7e32/(cm^2 \text{ sec})$  with an average of 5 Interactions per Crossing.

When the Recycler works and the pbar stack rate is above about 20 or 25e10/hr, we do not lose too much integrated luminosity with 132 nsec. In these conditions, the change to 132 nsec will either cut the number of IC by about a factor of 2 or increase the integrated luminosity. Again this assumes that we can find "good operating conditions" for 132 nsec bunch spacing.

### 4.4 Separations Between the Beams

Figure 7 shows 4 views of the separation around the entire ring with  $\pm 170 \mu\text{rad}$  horizontal and vertical crossing half angles at each IP. This shows the same

quantities and the same setup as figure 1 except that here the squares mark the crossing points for a pbar bunch near the middle of the short train and the diamonds for a pbar bunch near the middle of the long train.

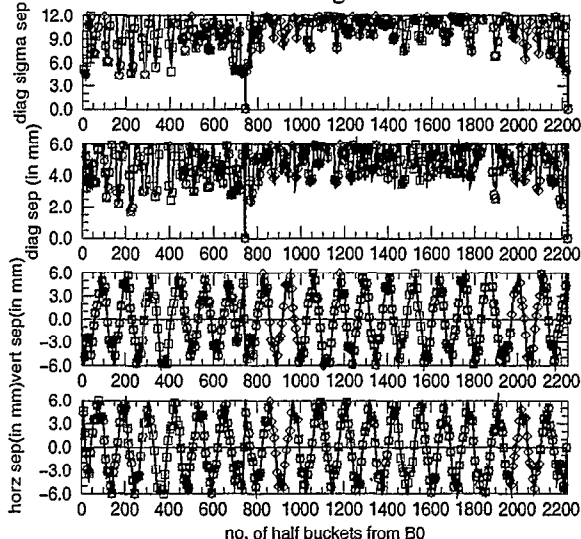


Figure 7 : Four views of the separation around the ring for 140X103. The CDF Experiment is at B0 which is at 0 and 2226 in the figure. The D0 Experiment is at D0 which is at 742 in the figure. From bottom (a) to top (d) : (a) Horizontal separation (in mm), (b) Vertical separation (in mm), (c) Diagonal separation (in mm), (d) Diagonal Sigma separation.

Version:v3h15av2.cf045b,sb4(a0h),a103a,nppn.170pnpn2

The crossing angles completely determine the separation at the first crossing points on either side of the IPs. At the second crossing point, the kick from the separators does have some influence and, depending on the relative sign of this kick and the crossing angle, this can either increase or decrease the separation. At the third crossing point, the separations from the crossing angles and the separators are similar in size and so the relative signs are important. There are many combinations of the signs for the crossing angles and the signs of the separators, but there are also some constraints on these. Figure 7 shows one of our favorite configurations.

In figures 7c and 7d, in the region from about 100 to 420 half buckets from B0, there are several crossing points with relatively "poor" separation. These dips in the diagonal separation are caused by the horizontal and vertical separations being too close in phase. Ideally, they should be  $\pi/2$  out of phase, so that the horizontal separations are near a maximum when the vertical separation is near zero and vice versa. Other crossing angle configurations with different signs for the crossing angles have better separation in this region, but slightly worse separation at some of the points near the IPs. We believe that the configuration in figure 7 may be a good trade off, because the tune spreads due to these points in

the arcs remain small. (See figure 8a. The  $\beta$ s in the arcs are smaller than the  $\beta$ s at the first few crossing points.)

#### 4.5 Beam Beam Dipole Kicks

Each time a bunch encounters a bunch from the opposing beam, they both receive kicks. If the beams are separated, then the average kick received by the bunch will be non-zero. The average kicks received by both beams will change their orbits and hence their separation. The change in separation in turn changes the average kicks the bunches give each other. This is an involved problem to handle correctly, as each bunch encounters the other beam in different places. We make 2 approximations to this problem. First we assume that the proton bunches do not move and use the sum of the proton and the pbar intensities for the kick given to the pbar bunch. (The pbar intensities are expected to be about a factor of 4 less than the protons.) Second we use the kick given to a zero amplitude pbar as an approximation to the average kick given to all the pbars in that bunch.

After calculating the changes to the separations, we adjust the separator settings to fix the average effect at the IPs on all the pbar bunches. Of course, this change in the separators changes the separations which in turn changes the beam beam dipole kicks. It typically takes 2 iterations to get this right. Even after we have corrected the average effects, there are still bunch to bunch variations.

For 36 X 36, both the changes to the separator settings and the remaining bunch to bunch variations were fairly small. After adjusting the separators, the separations at the IPs were less than  $1.5 \mu\text{m}$  (for our nominal parameters, the beam size at the IPs is  $33.1 \mu\text{m}$ ) and the total crossing angles were less than  $11 \mu\text{rad}$ .

For 140 X 103, these beam beam dipole kicks have much larger effects. The maximum separation at the IPs is  $7 \mu\text{m}$  and the rms separation is  $1.6 \mu\text{m}$ . Considering only the pbar bunches in one train or the other, the rms variation in the crossing angles at the IPs is about  $3 \mu\text{rad}$ . But there are also systematic differences between the crossing angles for pbar bunches in the long and the short trains. At B0, this systematic difference is almost purely horizontal, at D0, it is almost purely vertical. At B0, the average horizontal crossing angle for pbar bunches in the long train is about  $333. \mu\text{rad}$  and for pbar bunches in the short train is about  $356. \mu\text{rad}$ , a difference of  $23. \mu\text{rad}$ . At D0, the average vertical crossing angle for pbar bunches in the long train is about  $-332. \mu\text{rad}$  and for pbar bunches in the short train is about  $-358. \mu\text{rad}$ , a difference of  $26. \mu\text{rad}$ . (For both of these, the desired magnitude of the crossing angles is  $2*170 \mu\text{rad}=340. \mu\text{rad}$ .)

These are large enough to concern us and merits further investigation, but we aren't sure what we can do about it.

#### 4.6 Tune Footprints

Figure 8 shows the tune spreads for pbars with a range of betatron amplitudes. This was calculated for pbar bunch

152, in the middle of the long train. This uses the same parameters as figure 2.

Figure 8a shows the contributions to the pbar tune spreads from 262 of the 280 crossing points. The only crossing points not included are the main IPs and the first 4 crossing points on either side of the IPs. Both the tune shifts and the tune spread in figure 8a are very small. In figure 7, we saw several crossing points with relatively "poor" separation in the region from about 100 to 420 half buckets from B0. The contributions of these points are included in figure 8a and are small.

Figure 8b shows the contributions to the tune spreads from 278 of the 280 crossing points. In addition to all the points for figure 8a, this also includes the effects of the first 4 crossing points on either side of the IPs. The effects from these 16 points are much larger than the combined effects of the other 262 points. This tune footprint has the opposite "sense" as a head on footprint, the zero amplitude particles are at the lower left, the pbars with large horizontal amplitudes and zero vertical amplitudes are at the lower right, etc.

The area enclosed by the " $3\sigma$ " contour is fairly small, but the tune spread increases substantially if pbars out to " $4\sigma$ " are included. This is not surprising since there is about  $5\sigma$  separation at the first crossing points. Pbars with amplitudes of  $4\sigma$  are starting to explore the beam beam kicks at  $1\sigma$  from the center of the opposing beam. This is where the kicks are strong and very non-linear.

The large tune spread suggests that these crossing points will also drive resonances strongly. Since the beams are separated at the first crossing points next to the IPs, these points can drive both even and odd order resonances.

Figure 8c shows the tune spreads and shifts from one of the two interaction points. We have shown it at twice the scale to ease comparison with the other contributions. This calculation uses a bunch length (longitudinal sigma) of 37.1 cm and a transverse beam size (sigma) of  $33.1 \mu\text{m}$ . Both the size and the shape are modified from the head on footprint. If there were no crossing angle, the tune shift for zero amplitude particles is .00989. The decrease in the overlap reduces this by more than a factor of 2. The shape of the footprint is also much narrower. The changes in the tune spreads suggest changes to how the beam beam interaction at the main IPs drives resonances.

Figure 8d shows the total tune shifts and spreads for all 280 crossing points. These are significantly smaller than the footprints shown in figure 2c for the 36 X 36 case. There are 2 main reasons for this. First, the tune spreads from the main IPs are greatly reduced by the crossing angle. Second, the footprints shown in figure 8b, which are almost entirely due to the first few crossing points on either side of the IPs, have the opposite sense as the footprints from the main IPs, leading to some cancellation and compression of the total tune spreads. Although not immediately evident, the footprint in figure

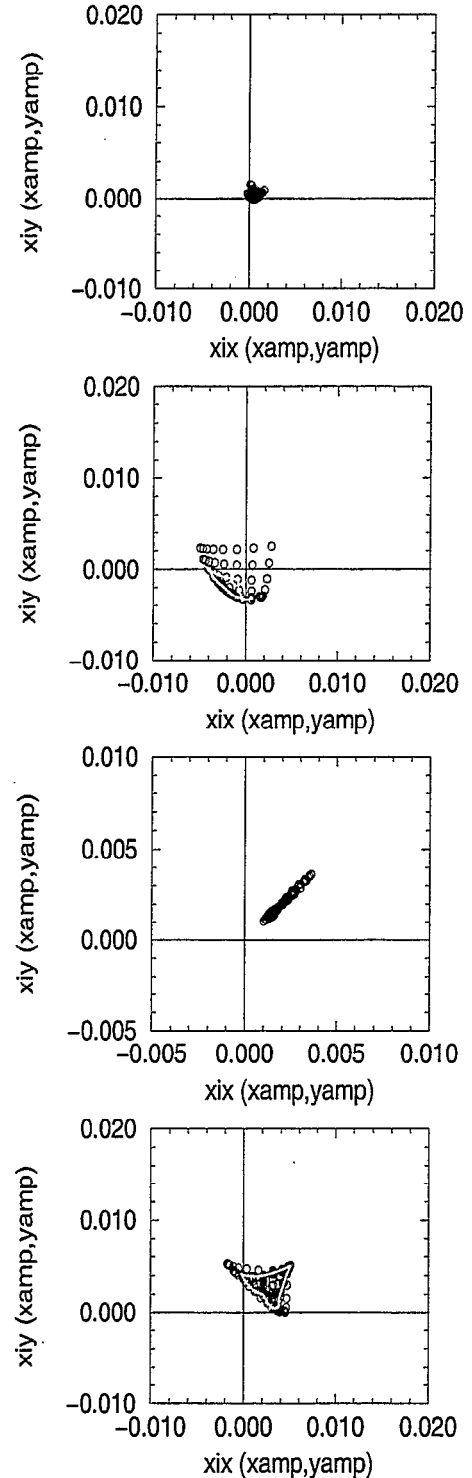


Figure 8: Tune footprints for 140X103, pbar bunch 152. From top (a) to bottom (d) : (a) Contribution from 262 crossing points. All crossings except for the IPs and the first 4 crossing points on either side of the IPs. (b) Contribution from 278 crossing points. All crossings except for the IPs. (c) Tune footprint from one of the two IPs only. Note the different scale. (d) Tune Footprints including the effects of all 280 crossing points. Version: v3h15acsb4a103a.nppn.170nppn2.

8d is "folded". Pbars with horizontal and vertical betatron amplitudes of about  $(4\sigma_{\beta x}, 4\sigma_{\beta y})$  have about the same tunes as those with betatron amplitudes of  $(0, 0)$ . For small amplitude particles, the tunes decrease with increasing amplitude due to the main IPs and the tune changes due to the first few near misses are small. For larger amplitude particles, the tunes increase with increasing amplitude due to the first few near misses and the tune changes due to the main IPs are small. Taken together, the competition between these effects leads to the fold in the footprint.

On the good side, these folds mean that the beam occupies less area in the tune plane and if the resonances have not become stronger and wider, we may have more room in the tune plane between resonances. On the bad side, the folds mean that a particle can have a larger amplitude range for a given range of its tunes. Certain amplitude particles will not detune off of resonances as quickly and so a resonance that aligns properly with the fold could cause a greater amplitude change than it could without the fold. We tend to view these folds as a bad sign and as an indicator of strong non-linearities, but we don't know if these views are justified.

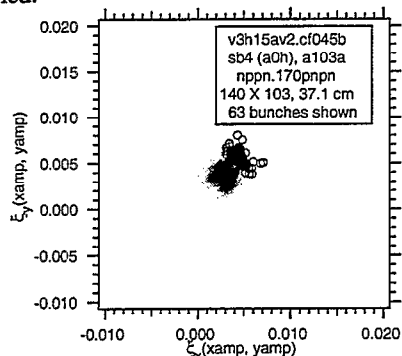


Figure 9: Gray scale plot showing the tune footprints for 63 representative pbar bunches for 140X103. All the bunches in the short train are shown. About 10 bunches from the beginning, middle, and end of the long train are shown. The darker the point, the more pbars have those tunes. No synchrotron motion for the pbars. The open circles show the tunes for pbars in each bunch with zero betatron amplitudes.

Version: v3h15av2.cf045b.sb4a103a.nppn.170pnpn2

Figure 9 shows the tune spreads for 63 representative pbar bunches. Each of the 30 pbar bunches in the short pbar train are shown as well as about 10 bunches from the start, middle, and end of the long pbar train. Because we don't have any symmetry in the 132 nsec filling pattern, no two pbar bunches encounter the protons at exactly the same set of crossing points and generally every pbar bunch has a slightly different footprint.

The spread between bunches is smaller here (in figure 9) than for 36 X 36 (in figure 3). This is mainly

because the crossing angles have improved the separation at the first few crossing points on either side of the IPs.

#### 4.7 Hardware Requirements

Surprisingly little new accelerator hardware is needed for 132 nsec operation.

- More pulsers/power supplies for the proton injection kicker. The proton kicker that is presently being installed can be used for either 396 nsec operation or 132 nsec operation. The magnet is composed of 5 modules. For 396 nsec, we will have 2 sets of positive and negative pulsers/power supplies. One set will power 2 modules, the other set will power 3 modules, giving a rise time of slightly under 396 nsec. For 132 nsec operation, each module will have its own set of pulsers/power supplies, giving a rise time of a little under 132 nsec.

- More separators. Although we can make crossing angles with our present complement of separators, a few additional separators will greatly expand our options for the signs on the crossing angles. This is important because at some of the first few crossing points near the IPs, the separations due to the crossing angles and due to the separator kicks are similar and the relative signs determine whether these add or subtract from each other. We are ordering 1 new horizontal separator module and 3 new vertical separator modules. These will be run off of existing power supplies.

- Coalescing upgrade for the Main Injector. The present coalescing system uses 2.5 MHz RF. If we attempt to coalesce multiple proton bunches at the same time, they will have 396 nsec bunch spacing. For 132 nsec operation, we have to change the fundamental frequency for coalescing to 7.5 Mhz, and add a second (15 MHz) and a third (22.5 MHz) harmonic. The higher harmonics are needed to make the RF waveform more linear over the 5 53 MHz buckets that contain beam.

- Damper work. With many more bunches at a closer bunch spacing, we may see new multi-bunch modes causing problems and need additional narrow band feedback channels to control them. We may also require an upgrade of the weak wide band feedback systems.

- Instrumentation Upgrades. Much of the present instrumentation will have to be upgraded to deal with the many more bunches and the more closely spaced bunches. We will also have to learn how to deal with the tremendous amounts of returned data.

We do not believe that any of these technological issues will present serious problems.

#### 4.8 Conclusions

The 132 nsec bunch spacing with large crossing angles at the IPs is not guaranteed to work. We are very concerned about the synchro-betatron resonances driven by the beam beam interaction at the IPs and by the possible strong effects from the first few near misses on either side of the IPs. We are also concerned about the further

increase in the number of crossing points in the arcs and the resulting increase in the size of effects from the beam beam dipole kicks.

We suspect it will be a challenge to find good operating conditions and, if we can find them, they may be quite different from what we used for either Run I or 36 X 36 bunch operation.

## 5 CROSSING ANGLE STUDIES

### 5.1 Specifics

With the above uncertainties about 132 nsec bunch spacing, an important study is to simply try putting in a large crossing angle with either a 36 X 36 store or a 2 X 1 store. This would be a very direct test of the concerns about the synchro-betatron resonances. (However, even if we find good conditions in these studies, that is not a guarantee that 132 nsec will work. There are still concerns about the small separation at the first near misses and the very large number of near misses around the ring. Also, the problem may not be any of these individually but may be how these effects **combine/interact.**)

We will be installing additional separator modules for 132 nsec operation. However, even with the present complement of separators, for one particular set of signs of the crossing angles, we can make large crossing angles at the IPs. The resulting separations around the ring are shown in figure 10.

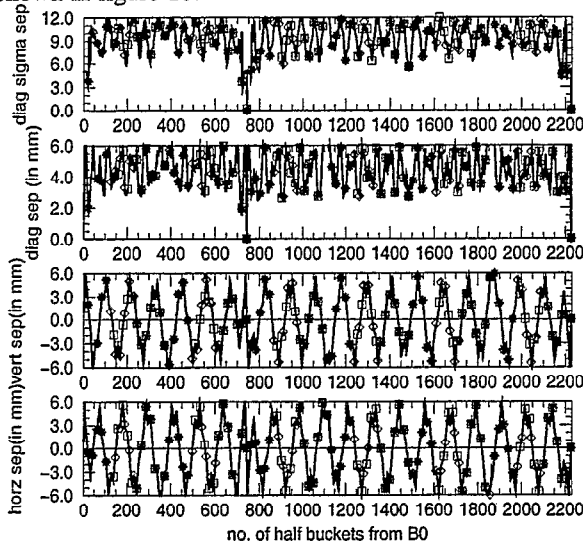


Figure 10 : Four views of the separation around the ring for crossing angle study with 36X36. The CDF Experiment is at B0 which is at 0 and 2226 in the figure. The D0 Experiment is at D0 which is at 742 in the figure. From bottom (a) to top (d) : (a) Horizontal separation (in mm), (b) Vertical separation (in mm), (c) Diagonal separation (in mm), (d) Diagonal Sigma separation.

Version: v3h15av2 sa1 (d48h) nppn.170ppnn2.

Since we are proposing this as a study during 36 X 36 operations, the markers on figure 10 show the crossing points for 36 bunches, as was done in figure 1.

Comparing figure 10 to figure 7, in figure 10 the separation through the arcs is good, but there is a crossing point near each of the IPs (at 21 and 721 half buckets from B0) where the separation is not as large as we would like. (We may be able to improve these points slightly.) This shows the difference in separation that can result from a different choice of signs on the crossing angles.

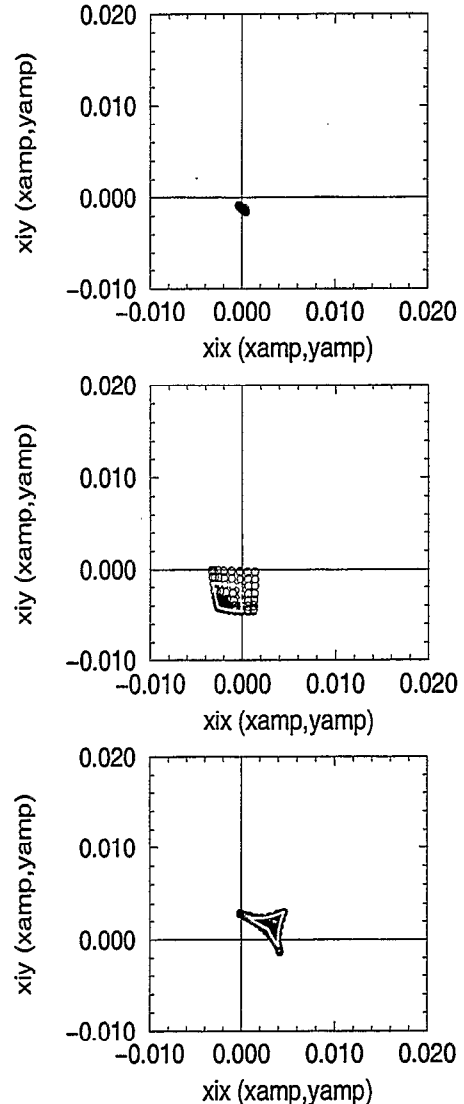


Figure 11: Tune footprints for crossing angle study with 36X36, pbar bunch 6. From top (a) to bottom (c) : (a) Contribution from 66 crossing points. All crossings except for the IPs and crossing points next to the IPs. (b) Contribution from 70 crossing points. All crossings except for the IPs. (c) Tune Footprints including the effects of all 72 crossing points.

Version: v3h15asa1.nppn.170ppnn2.

Figure 11 shows the tune footprints for pbars with a range of betatron amplitudes. This was calculated for pbar bunch 6, in the middle of a train, and uses the same parameters as figure 2. Figure 11a shows the contributions from 66 of the 72 crossing points. The only crossing points not included are the IPs and the first crossing points on either side of the IPs. As usual, the tune shifts and the tune spreads are very small. Figure 11b shows the contributions from 70 of the 72 points. The only crossing points not included are the 2 IPs. As in figure 8b, this tune footprint has the opposite "sense" as a head on footprint. Even with only 36 bunches, the effect of the first crossing points are more similar to the 140 X 103 case.

The contributions to the tune footprints from the IPs is the same as was shown in figure 8c. Finally, figure 11c shows the total tune shifts and spreads from all 72 crossing points. The size and shape are similar to what we saw in figure 8d for 140 X 103 bunches.

Although there are still important differences between this 36 bunch study and the 132 nsec operation, this encourages us that the study may be a good test of some of the 132 nsec problems.

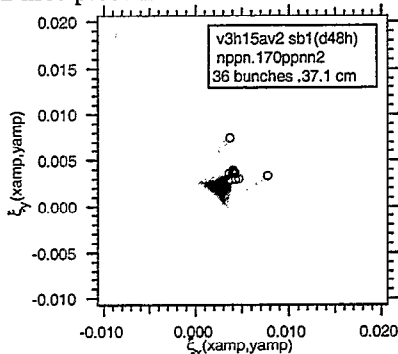


Figure 12: Gray scale plot showing the tune footprints for all 12 pbar bunches in a train for crossing angle studies for 36X36. The darker the point, the more pbars have those tunes. No synchrotron motion for the pbars. The open circles show the tunes for pbars in each bunch with zero betatron amplitudes.

Version: v3h15asa1.nppn.170ppnn2

Finally figure 12 shows the tune shifts and spreads for all 12 pbar bunches in a train. As in figure 3, the footprints for 10 of the 12 bunches are nearly identical, but the first and last bunches in the train are different because they do not see protons at the first crossing point upstream or downstream of the IPs.

This looks like a worthwhile study to get an early view of how difficult 132 nsec bunch spacing will be. Because no special equipment is needed, we could try this as soon as the Commissioning Run in Fall 2000.

Although this is presented as a study, depending on what we find, it may be more of a long development process. We may use these conditions to try to diagnose

our problem and to test possible solutions or tuning algorithms.

## 5.2 Generalities

How would we go into this study ? For now assume that we do this as end of store studies. (Later we will have some comments on the relative advantages of doing end of store vs. dedicated studies.)

- Start from head-on colliding beam conditions (1 Tev,  $\beta^* = 35$  cm, 36 X 36 bunches).

- Turn up the horizontal and the vertical crossing angles together until the losses or lifetimes get bad.

- Re-tune to try to bring down losses and/or improve the lifetime. There are many things to try : Separation bumps at the IPs (Our "crossing angle" bumps may have slight errors that change the separation at the IPs.), tunes, chromaticity, coupling, orbit bumps, cogging, possibly the sextupole distributions and/or octupoles, etc. We may also have to re-scrape the beams to remove any halo that we generated while at small crossing angles or while we were changing the crossing angles.

- If successful, continue increasing the crossing angles. We want to try to get out to angles of about  $\pm 136 \mu\text{rad}/\text{plane}$  or  $\pm 170 \mu\text{rad}/\text{plane}$ .

- Depending on how often we have to re-tune, we may just try "jumping" to these angles.

- If things are really bad, maybe try again with smaller proton intensities or larger  $\beta^*$ .

There are some games we can play to try to separate the contributions from different mechanisms, but the combinations may be important.

- The strengths of the synchro-betatron resonances from the main IPs can be varied by varying the size of the crossing angle.

- The effects of being off-center in the low  $\beta$  quads are also linked to the size of the crossing angle. **IF** there is enough aperture in these quads, we could try to center the pbars and push the protons twice as far off the centerline.

- How do the resonance driving terms from the 2 Interaction Points (B0 and D0) combine ? We may be able to get a very rough, general feel for this by comparing 2 X 1 stores with 1 X 1 stores. For the 1 X 1 stores, we can adjust the cogging so that the bunches collide at B0 or at D0. For a 2 X 1 store, we would be set up so that the single pbar bunch collides with one of the proton bunches at B0 and with the other at D0.

- First few near misses. These are not an issue in a dedicated 2 X 1 store. With 36 X 36 bunches, there are 2 crossing points with diagonal  $\sigma$  separation of only about 3.7. In some ways (tune spread from the first few near misses, size and shape of the tune footprint for all collisions), this is similar to what we would have for 132 nsec bunch spacing. However in many other ways, the situations are quite different (2 "bad" points vs. several). This may give us some idea of the problems, but

it is a significant difference between the studies and the real 132 nsec situation.

- Beam beam dipole kicks. These are very small with 2 X 1 stores and are still small with 36 X 36 stores. With 140 X 103 bunches, these become more of a problem. Again, this is a significant difference between the studies and the real 132 nsec situation.

- Larger  $\beta^*$ . This reduces the divergence at the IP by  $1/\sqrt{\beta^*}$ , so less crossing angle is needed for a given separation at the first near misses. Also it makes the  $\sigma^*$  larger by  $\sqrt{\beta^*}$ . For the same separation at the first crossing points, the parameter  $(\delta\sigma_s/\sigma^*)$  is smaller by  $1/\beta^*$ .

### 5.3 Some General Comments on Beam Beam Studies

There are some basic steps involved in these studies.

0) Get to the point where we can try it. We should be wary of beam beam experiments or studies before we've established "reasonable" colliding beam conditions. For beam beam experiments, almost everything has to be working. Also, for a valid test, we need realistic conditions. The pbars may be fine against proton intensities of 100.e9/bunch, but falling out against 300.e9/bunch. We don't expect to get many pbars during the Engineering Run (May to July 2000). Most of what we get will probably go to establishing 36 X 36 colliding beam conditions. So at the earliest, we would try this study during the Commissioning Run in Fall 2000.

1) Give it a try. Put in the crossing angle and see what happens. There are many beam beam experiments that are basically intended to "try out an idea". In my experience, for many of these : If it "works" or looks promising with more tuning, then great, its adopted. But if it doesn't work, its dropped, often without much effort at understanding **why** it didn't work. If we have problems with crossing angles, we may not have the luxury of dropping it.

1.5) If there are problems, are the conditions pretty much what we expect them to be ? Is something really wrong ? This is a big part of why we need to establish "reasonable" 36 X 36 (head on) colliding beam conditions before starting crossing angle studies. Are the linear optics OK ? Check for  $\beta$  waves, adjust the  $\alpha^*$  bumps, check  $\eta^*$ . Check the separation between the beams at the IPs. Check the cogging. Is the separation in the arcs OK ? Do the separator bumps (both for separation at the IPs and for crossing angles at the IPs) do what's expected ? Are there problems with single beam resonances ?

Also as part of this, look at some "basic" measurements related to the crossing angles : the luminosity, tunes, and tune spectra as a function of crossing angle. Are these what we expect ?

2) If things are still bad even with the expected conditions, then we've got to try to **understand** what's happening. From simulations, what are the

**mechanisms** by which particles get to large amplitudes? What are the important resonances and for what particle amplitudes are those resonances important ? What drives these resonances, the main IP, the first few near misses, the many crossings in the arcs ?

The conditions in the simulations will never be quite the same as what we have in the machine. We need to have a feel for why the simulations behave as they do if they are to give us some insight into what we need to change in the machine to improve performance.

### 5.4 End of Store Studies VS. Dedicated Stores

For End of Store Studies :

- Bigger emittances, smaller intensities
- Saves an hour or two of shot setup
- Has been easier to get machine time
- Slightly less prone to downtime. We get handed a working machine with beams in a "reasonable", stable condition.
- How much emphasis will there be on trying to recycle pbars ?
- We may at least start with the end of stores.

For Dedicated Stores :

- We have to do a full shot setup. If something breaks during shot setup, it still counts as time spent in our machine studies.
- We need dedicated stores to do 2 X 1 stores, 1 X 1 stores, or other "unusual" conditions. If we are doing unusual conditions, we may have trouble getting the beam to colliding beam conditions.
- Will have smaller emittances and higher intensities since we are getting the beams at the start of the store, rather than after they've been colliding for many hours. (Of course, we can always reduce the intensity or blow up the emittance if we desire.) The pbar intensity could be much higher if we only take a single bunch.

In either case :

How do we get to the crossing angle configuration ? Knob Separators ? Do we need to take out the lattice modifications for the collimation scheme ? Is the present collimation scheme OK for our proposed crossing angle configuration ? We should try the modifications to put in the crossing angle with a single beam first and make sure the mechanics work before we try it with colliding beams.

Also we want to make sure that any special instrumentation, diagnostics, or techniques for our studies are already checked out and working. If we're trying something special, we should try to establish the technique as much as possible with single beams in "easy conditions". As a simple example, we don't want to establish pbar tune measurements on crossing angle studies time.

The HEP experiments, CDF and D0, seem interested in 132 nsec bunch spacing. It looks like they will be encouraging us to make it work and put it into operation as soon as possible, provided of course there isn't too much loss of integrated luminosity. This will be a big help in getting machine time to do these studies.

The next year will be a very busy, exciting, interesting time at Fermilab. There is already a great deal of work to do and many unexpected problems are sure to crop up. Although it may not be easy, we feel that 36 bunch (396 nsec bunch spacing) operation can be made to work. This is sufficient for peak luminosities up to  $1-2 \times 10^{32}/(\text{cm}^2 \text{ sec})$ .

Hopefully even before Run II officially starts in March 2001, we will begin some crossing angle studies to prepare for 132 nsec bunch spacing. These will be important to let us see what the problems are and to give us time to start to address them. At best, we expect 132 nsec operation with crossing angles to be difficult, and we may not be able to make it work at all.

## REFERENCES

- [1] Although it needs to be revised, the Run II Handbook is still a valuable reference. It is on the Web at [http://www-bd.fnal.gov/lug/runII\\_handbook/RunII\\_index.html](http://www-bd.fnal.gov/lug/runII_handbook/RunII_index.html)
- [2] An up to date version of the Long Range Schedule for Fermilab should be available on the Web at [http://www.fnal.gov/directorate/program\\_planning/PPO.html](http://www.fnal.gov/directorate/program_planning/PPO.html)
- [3] "Calculation of Integrated Luminosity for Beams Stored in the Tevatron Collider", D.A.Finley, FERMILAB-TM-1607, Mar 1989, 4pp. Also published in IEEE Part. Accel. 1989 :1834-6.

## Beam-beam studies for the Tevatron

Tanaji Sen, FNAL, Batavia, IL 60510

### 1 MOTIVATION FOR RUN II BEAM-BEAM STUDIES.

In the first stage of Run II, the Tevatron will be operated with 36 bunches in each beam with bunch separations of 396 nanoseconds. The expected peak luminosity is  $\mathcal{L} = 8.6 \times 10^{31} \text{ cm}^{-2} \text{ sec}^{-1}$  with an average number of 2.3 interactions per bunch crossing. In the second stage of Run II, the goal is to increase the luminosity to about  $1.5 \times 10^{32} \text{ cm}^{-2} \text{ sec}^{-1}$ . If the bunch spacing were kept constant, the average number of interactions per bunch crossing would increase to about 4. This is thought to be unacceptably large and might saturate the efficiency of the detectors. This is the main reason for decreasing the bunch spacing at higher luminosities.

One possibility is to reduce the bunch spacing to 132 nanoseconds which lowers the average number of interactions to an acceptable value of 1.4. This shorter bunch spacing however has several consequences on beam dynamics. Collisions between bunches will now occur every 19.78m. This is shorter than the distance of the nearest separators from the main IPs at B0 and D0. Consequently the beams will not be separated at the parasitic collisions nearest to the IPs if the geometry of the orbit is left unchanged. A sketch of this orbit is seen in the top part of Figure 1. This will lead to unacceptably large beam losses and background. Moving the separators closer to the detectors does not separate the beams sufficiently at the locations PC1L and PC1R. The phase advance from the first available position for the separators to these points is too small for the separator strengths that are available [1].

One way to increase the transverse separation between the beams is to make the beams cross at an angle at the IPs. The optimum crossing angle depends upon a number of issues and requires a detailed investigation. The issues include a reduction in the luminosity, change in the beam-beam tune spreads, excitation of synchro-betatron resonances, orbit offset in IR quadrupoles which increases the nonlinear fields seen by the beams, required separation between the beams at the nearest parasitic collisions, the dispersion wave generated by the orbit offset, increase in the strength of the coupling etc. A crossing angle of  $\sim \pm 200 \mu\text{rad}$  in the 45 degree plane separates the beams by  $\sim 4\sigma$  at the first parasitic collision. A sketch of the orbits with a crossing angle is shown in the bottom part of Figure 1.

The crossing angles that are thought to be necessary have a major impact on the luminosity. If  $\mathcal{L}_0$  is the nominal luminosity without a crossing angle, then the luminosity with

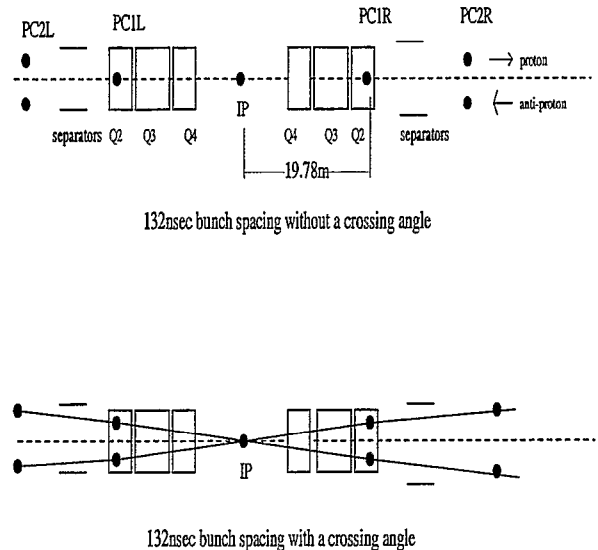


Figure 1: Sketch of the locations of the main beam-beam collisions and the next two parasitic collisions, e.g. PC1R, PR2R on the right, with respect to the triplet quadrupoles and the separators. The top figure shows the geometry without a crossing angle, the bottom figure shows the geometry with a crossing angle.

a total crossing angle of  $2\phi$  is

$$\mathcal{L} = \frac{1}{\sqrt{1 + (\sigma_s \phi / \sigma_\perp)^2}} \mathcal{L}_0 \equiv \mathcal{R} \mathcal{L}_0 \quad (1)$$

where  $\sigma_\perp$  is the transverse beam size at the IP. Figure 2 shows the relative loss in luminosity as the crossing angle is increased. For example at a half crossing angle of  $200 \mu\text{rad}$ , the luminosity is only 38% of its value without a crossing angle. The smaller overlap between the beams which lowers the luminosity also decreases the beam-beam tune shift. If one assumes that we can replace the beam size  $\sigma_\perp$  at the IP by  $\sigma_\perp \sqrt{1 + (\sigma_s \phi / \sigma_\perp)^2}$  then the head-on tune shift parameter is reduced from its value  $\xi_0$  at zero crossing angle to  $\xi = \mathcal{R}^2 \xi_0$ . Figure 2 shows that with this assumption, the relative tune shift at a half crossing angle of  $200 \mu\text{rad}$  is about 28% of its value at zero crossing angle. This hand-waving estimate of the beam-beam tune shift with a crossing angle is useful only as a rough guide. The beam-beam tune shift with a crossing angle depends on the synchrotron oscillation amplitude so it is not enough to specify only the transverse amplitudes when computing the tune shift. However it is true that at any betatron amplitude, the tune shift at all synchrotron amplitudes except zero is smaller than the tune shift without a crossing angle.

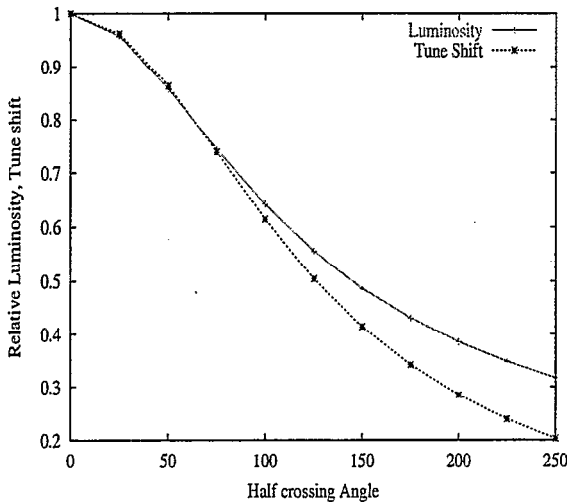


Figure 2: The relative decrease in luminosity and the head-on tune shift parameter as a function of the half crossing angle in the  $45^\circ$  plane.

Once the crossing angles are introduced with more than one hundred bunches in each beam, several beam dynamics issues become important. Some of them are listed here:

- Single beam issues

Dynamic and physical aperture resulting after off-axis excursion in IR quads. At the first parasitic interaction which occurs within the quadrupole Q2, the beam size is about 2mm. Assuming that a minimum of  $4\sigma$  separation is necessary, they will be apart by about 8mm. Coupled with the large beam size, this orbit relatively far from the quadrupole axis will make both beams more sensitive to the nonlinear fields of the triplet quadrupoles. In addition, orbit perturbations could lead to larger beam loss due to the tighter physical aperture in these quadrupoles.

- Beam-beam issues

- Long range interactions at collision. The long-range interactions distort the tune footprint significantly. For example, the zero amplitude tune shift can lie within the interior of the footprint and there can be folds within the footprint. In such cases the tuneshifts at large amplitudes may be greater than at smaller amplitudes. The impact of these folds on the stability needs to be investigated. From studies on the SSC and the LHC [2], it is known that the amplitude in phase space where diffusive motion begins is smaller than the separation between the beams if all the long-range kicks occur at the same phase. This diffusive amplitude  $r_{diff}$  can be expressed as

$$r_{diff} = r_{sep} - \Delta \quad (2)$$

where  $r_{sep}$  is the average separation between the beams and  $\Delta \propto \sqrt{N_{PC}N_p}$  where  $N_{PC}$  is the number of parasitic collisions and  $N_p$  is the intensity of the strong bunch. In the Tevatron the long-range kicks occur at different phases so this expression may not be directly applicable. Nevertheless if there are enough such interactions where the tails of the beams overlap, diffusive motion and eventually particle loss may start at amplitudes less than the average separation.

- Crossing angle induced synchro-betatron resonances. The strength of these resonances is often characterized by the Piwinski parameter  $\chi = \sigma_s \phi / \sigma_\perp$ . The typical requirement is that this parameter should be much less than one for these resonances to have negligible effect. This would favour shortening the bunch length. However resonance strengths cannot increase monotonically with  $\chi$  because at large crossing angles the overlap between the beams decreases and the strength of the beam-beam force and the resonances decrease. Nevertheless, a detailed study of these resonances and how they combine with the long-range interactions to affect growth of particle amplitudes needs to be done.
- Bunch to bunch variations in orbit. A separator scheme to ensure that collisions of most bunches are well centered will be essential. However dipole kicks due to the long-range beam-beam collisions will also produce significant variations in orbits from bunch to bunch.
- PACMAN bunches. Bunches which are the furthest away from the center of a train might be in a different tune region and therefore more susceptible to losses.
- Long-range interactions at injection and during the ramp. As the beams are ramped to top energy, the separation helix changes and the separation is very small at some locations. This could be a problem when there are nearly two hundred interactions. However, the beams are larger during the ramp so beam-beam kicks are smaller.

Figure 3 shows the sequence of collisions for different bunches in a train. The head of the train will meet the head of the opposing train at the IP and all subsequent long-range encounters with the other train will be downstream of the IP. A bunch in the center of the train will experience half of its long-range encounters upstream of the IP and the remaining encounters downstream of the IP. The last bunch in the train will have all long-range encounters upstream of the IP. Figure 4 shows the anti-symmetric optics around the IP. As a consequence of the anti-symmetry, there is no reflection symmetry about the center of the train and the strength of the beam-beam kicks is different for each bunch. In Run IIa where there will be three trains of 12 bunches each, there

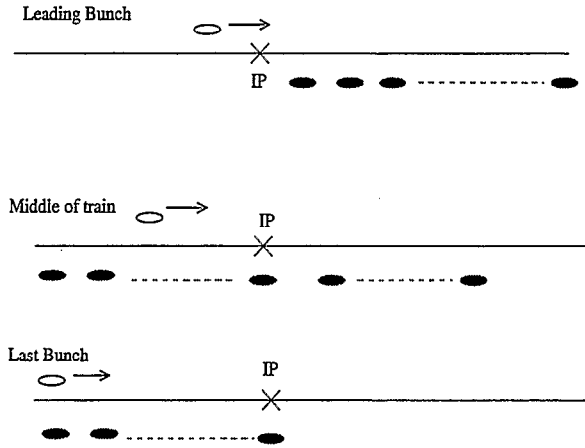


Figure 3: Schematic of the collision scheme for different bunches in a train.

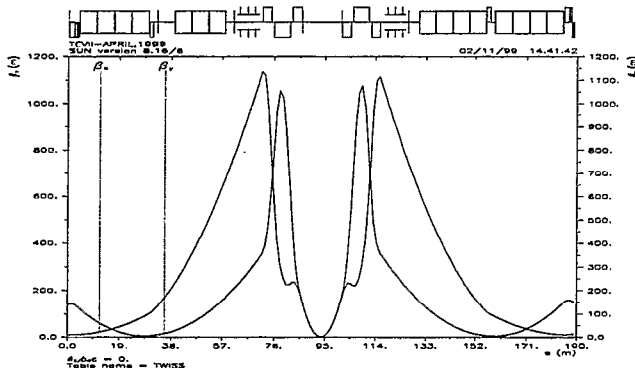


Figure 4: Plot of the beta functions around the IP showing that the optics is anti-symmetric around the IP.

is a three-fold symmetry so there are twelve equivalence classes of beam-beam kicks. In Run IIb with  $140 \times 105$ , there will possibly be one train of proton bunches meeting two trains of anti-proton bunches. This is required so that every anti-proton bunch meets a proton bunch at B0 and D0. There is no symmetry in this scenario so there will be 105 different equivalence classes of beam-beam kicks for the anti-proton beam. Table 1 shows a set of basic parameters for Run IIb. These values are subject to change.

Some of the questions which a study of the beam-beam interactions must answer include:

- Do the beam-beam interactions with crossing angles excite significant synchro-betatron resonances?
- Which of the long-range interactions have an important influence on the beam?
- What is the optimum crossing angle?
- Which of the following effects have an important influence on the beam?

**Static:** Transverse coupling, bunch to bunch intensity variations, unequal emittances, phase advance errors from IP to

	Run IIb
Luminosity	$14.0 \times 10^{31}$
Number of bunches ( $p \times \bar{p}$ )	$\sim 140 \times 105$
Interactions/crossing	1.3
$N_p$ per bunch	$2.7 \times 10^{11}$
$N_{\bar{p}}$ per bunch	$3 \times 10^{10}$
Total $\bar{p}$ 's	$3.15 \times 10^{12}$
Bunch separation [nsec]	132
Emittances ( $p/\bar{p}$ )	20/15
$\sigma^*$ ( $p/\bar{p}$ ) [ $\mu\text{m}$ ]	33/29
$\sigma_s$ ( $p/\bar{p}$ ) [cm]	37/37
Half crossing angle $\phi$ [ $\mu\text{rad}$ ]	$\sim 200$
Beam-beam tune shift - 2IPs ( $p/\bar{p}$ )	$(0.77/6.0) \times 10^{-3}$
Transverse tunes	20.581/20.575
Synchrotron tune	$7.2 \times 10^{-4}$
Piwinski parameter $(\sigma_s/\sigma^*)\phi$ [ $\mu\text{rad}$ ]	2.1/2.5
No. of long-range interactions	208

Table 1: Basic parameters for Run IIb with a 132 nanosecond bunch spacing. Some of these parameters such as the number of bunches and crossing angle represent best estimates at present.

IP, chromatic variation in  $\beta^*$ , ...

**Time dependent:** Tune modulations and/or fluctuations, beam offset modulations and/or fluctuations.

- What measures are useful in improving the lifetime? e.g. resonance compensation, reduction of tune shift with amplitude, beam-beam compensation, ...

## 2 BEAM-BEAM INTERACTIONS WITH A CROSSING ANGLE

The impact of all the beam-beam interactions with Run IIb parameters requires a detailed study before we will know if the beams are sufficiently stable. As a start we have begun investigations of the effect of the synchro-betatron resonances excited by the crossing angle at the main IPs. In this section I will report on our simulation studies with a crossing angle.

Figure 5 shows the simulation model for treating the beam-beam interactions at a crossing angle. This model has the following features:

- 6D interactions at B0 and D0. This includes the change in energy from the beam-beam interaction.
- Strong beam bunch (protons) is sliced into 9 disks to account for the crossing angle. The transverse distance of the anti-proton from the center of each disk is used to calculate the beam-beam kick from that disk and then the kicks are summed over all disks. All of these kicks are delivered at the same instant so the anti-proton is not propagated from disk to disk.
- Transverse size of the disks increases away from the IP. This takes into account the hourglass effect.
- Equal crossing angles in both planes - the crossing plane

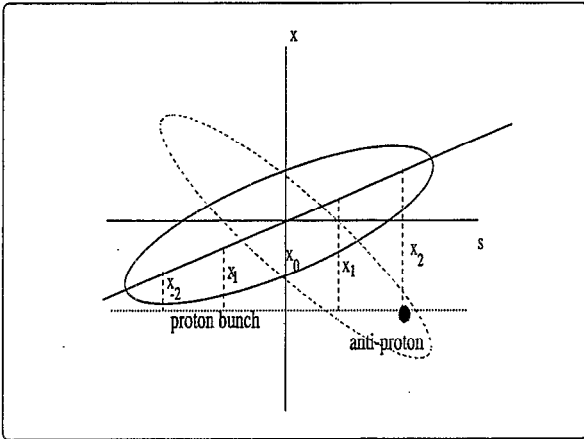


Figure 5: Simulation model for beam-beam interactions

is at  $45^\circ$  to the horizontal plane.

- 6D Linear transport through interaction region and arcs.
- Phase advance between B0 and D0 is taken from a recent lattice model of the Tevatron [3].
- Particles are tracked for 1 million turns ( $\sim 21$  seconds).

Tune footprints at various crossing angles have been calculated with this model. Figure 6 shows the footprints at zero crossing angle and a total crossing angle of  $400\mu$  radians or  $283\mu$  radians each in the horizontal and vertical planes. Also shown are the sum and difference resonances up to twelfth order. At the desired tunes, the beam straddles the sum twelfth order resonances with fifth and seventh order sum resonances outside the beam distribution. As mentioned earlier, the tune footprint at the crossing angle of  $400\mu$  radians is considerably smaller than without a crossing angle because of the smaller overlap between the beams. Without a crossing angle, only resonances of the form  $2m_x\nu_x + 2m_y\nu_y = n$  can be excited ( $m_x, m_y = 0, \pm 1, \pm 2, \dots$ ) while a crossing angle will excite resonances of the form  $m_x\nu_x + m_y\nu_s + m_s\nu_s = n$ . We observe that at zero crossing angle, all the twelfth order resonances with even coefficients cross the beam distribution starting at amplitudes around  $2.5\sigma$ . However all the nearby difference resonances have at least one odd coefficient so they are not excited by the beam-beam interactions. The tune footprint with the crossing angle shrinks sufficiently so that the sum resonances  $2\nu_x + 10\nu_y, \nu_x + 11\nu_y, 12\nu_y$  do not cross the distribution but all other sum twelfth order resonances are excited and are "seen" by the beam at amplitudes greater than about  $3\sigma$ . None of the difference resonances are seen by the beam when the crossing angle is  $400\mu$  radians.

While the footprints are useful in determining the resonances that may cause amplitude growth, long term tracking is essential in order to determine their impact on the beam. Figure 7 shows the results obtained after tracking a beam distribution with and without a crossing angle. At each angle, the initial distribution was composed of two sets

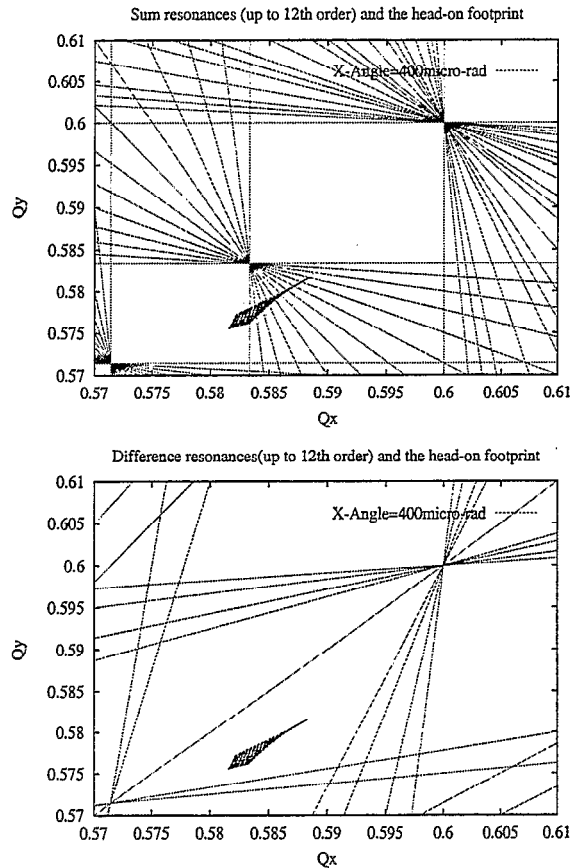


Figure 6: Beam-beam tune footprints with only the interactions at the main IPs. In the top figure, the footprints without a crossing angle and with a total crossing angle of  $400\mu$  radians in the  $45$  degree plane are shown superposed on all the nearby sum resonances up to twelfth order. The bottom figure shows these footprints superposed on the difference resonances up to 12th order.

of particles: a uniform distribution of 1000 particles between 0 and  $4\sigma$  and another uniform distribution of 1000 particles between  $4$  and  $10\sigma$ . Particles within the core are well represented and this choice of distribution also enables us to determine amplitude growth in the tails with a significant number of particles which would not be the case with a Gaussian distribution. During the tracking the maximum and minimum amplitude reached by each particle is recorded and the ratio of these limits is taken as the maximum swing of the particle. Figure 7 shows the maximum swing for each particle in the distribution first at zero crossing angle and then at  $400\mu$  radians. At zero crossing angle, the swings are in an absolute sense quite small but are relatively large between  $5$  and  $6\sigma$  - the region crossed by the  $12\nu_x$  and  $10\nu_x + 2\nu_y$  resonances. These resonances are also the twelfth order resonances with the largest widths. Tracking shows that the amplitude swings are large where the resonance widths are large, as they should be. Overall

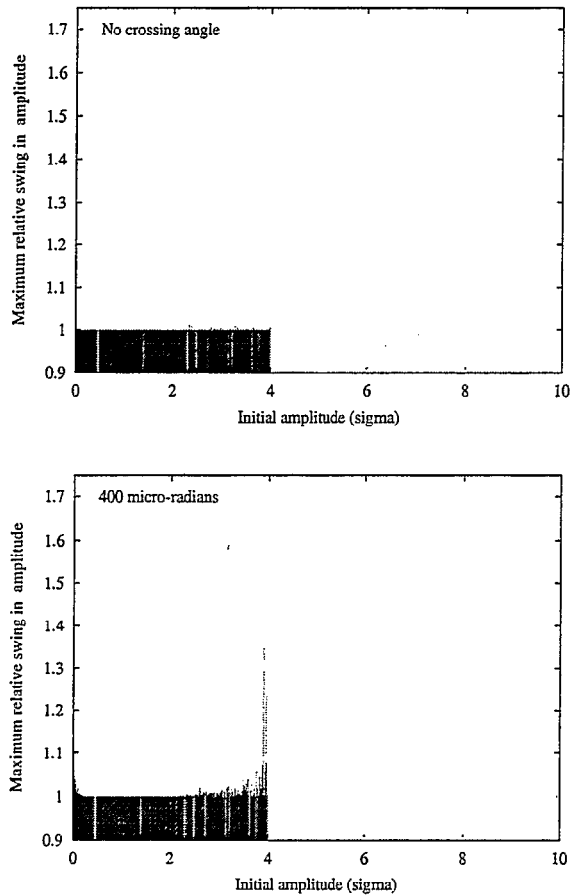


Figure 7: The maximum relative amplitude reached over a million turns as a function of the initial amplitude. Each line represents a particle. The top figure shows the amplitudes without a crossing angle and the bottom figure shows results with a crossing angle of  $400\mu\text{radians}$ . The amplitude swings are relatively large in the region crossed by the twelfth order resonances and their synchrotron sidebands.

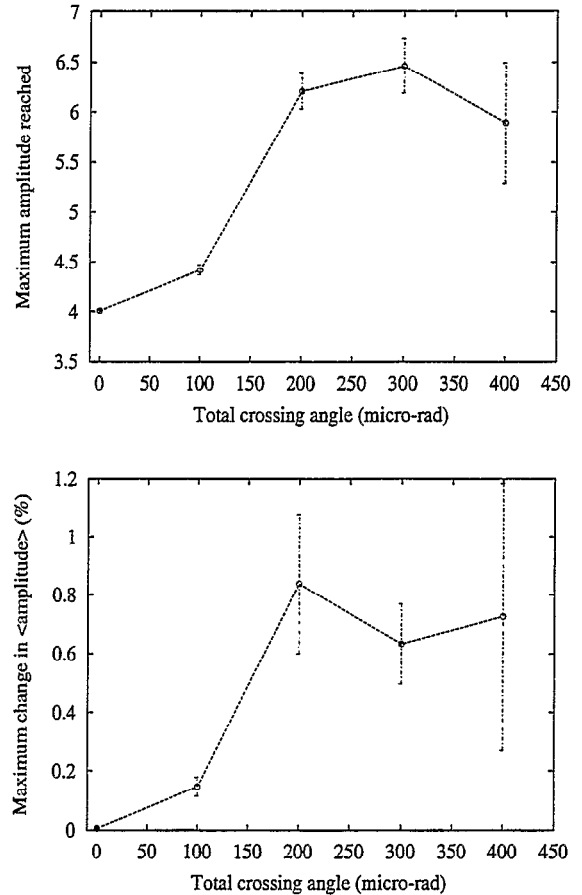


Figure 8: Top: Maximum amplitude reached by any particle within  $0$  to  $4\sigma$  averaged over three initial distributions as a function of the crossing angle. The error bars represent rms deviations over the three distributions, each of which had a uniform distribution of 1000 particles between  $0$  and  $4\sigma$ . Bottom: The maximum change in the average amplitude of the distribution, also averaged over the three initial distributions.

at zero crossing angle, the amplitude swings of all particles in the distribution are small enough that there is no increase in the size of the distribution. All particles stay well within the physical aperture ( $\sim 18\sigma$ ). The crossing angle generates new betatron resonances and synchrotron sidebands of these resonances leading to a more intricate web of resonances. The bottom part of Figure 7 shows that now there is a greater amplitude swing from  $\sim 3.5\sigma$  all the way out to  $10\sigma$ . This region has many more resonances than before. The core however (amplitudes less than  $3\sigma$ ) is relatively unaffected because no resonances cross this region, as seen in Figure 6. Overall even though the amplitude swings are larger in the tails, they are still not large enough for any of the particles in the distribution to reach the physical aperture.

The amplitude growth observed in the simulations is likely to depend on the initial distribution, especially when

there are many more resonances in phase space. Figure 8 shows the results of the amplitude growth observed with three initial distributions, each with a uniform distribution of 1000 particles between 0 and  $4\sigma$ . The top figure shows the maximum amplitude reached by any particle in the distribution as a function of the crossing angle. At zero crossing angle, there is no growth in the distribution and the rms deviation over the distributions is also negligible. As the crossing angle increases, the average of the maximum amplitude reached increases until a crossing angle of  $300\mu\text{radians}$  before decreasing at  $400\mu\text{ radians}$ . However the rms deviations also increase and at  $400\mu\text{ radians}$ , the fluctuations are the largest. This is to be expected since the network of resonances in phase space has a more complicated structure as the crossing angle is increased in this range so some particle distributions may experience the effects of these resonances more than others. Taking into account the error bars, the difference in amplitude growth between 200, 300 and  $400\mu\text{ radians}$  is not statistically significant. The bottom figure shows the maximum change in the sum amplitude averaged over the beam distribution as a function of the crossing angle. The changes are less than 1% in most cases with larger fluctuations between distributions as the crossing angle is increased. The growth of this averaged amplitude with time is not monotonic for any distribution but has more of a "diffusive" nature. The differences in the averaged amplitude between 200, 300 and  $400\mu\text{ radians}$  are also not statistically significant.

Synchro-betatron resonances excited by the crossing angle create synchrotron sidebands around the betatron resonances. Modulation of the betatron tune also creates sidebands around the betatron resonances at the modulation frequency. A natural source of tune modulation occurs when the chromaticity is non-zero (expected to be set to +5 units in Run II to combat head-tail instabilities). Off momentum particles undergoing synchrotron oscillations experience a betatron tune modulation at the synchrotron tune. Particles with the rms energy deviation  $\sigma_E/E \simeq 1 \times 10^{-4}$  for example will experience tune modulation at 35Hz with an amplitude  $5 \times 10^{-4}$ . Power supply ripple in quadrupoles causes tune modulation over a whole spectrum of frequencies and with different amplitudes. Since tune modulation will be present, it is useful to compare the relative effects of synchro-betatron resonances excited by the crossing angle and those excited by tune modulation.

Figure 9 shows the maximum amplitude beating with an initial distribution between 0 and  $4\sigma$ , without a crossing angle and with a crossing angle of  $400\mu\text{ radians}$ . The tune modulation increases the amplitude beating range significantly, especially for particles at amplitudes beyond  $3.5\sigma$ . In this region particles can reach amplitudes nearly three times their initial amplitude. Tune modulation completely dominates the effects due to the crossing angle - the amplitude beating at  $400\mu\text{ rad}$  is only slightly different from the case without a crossing angle.

Figure 10 shows the maximum amplitude reached and the maximum change in the averaged amplitude for two

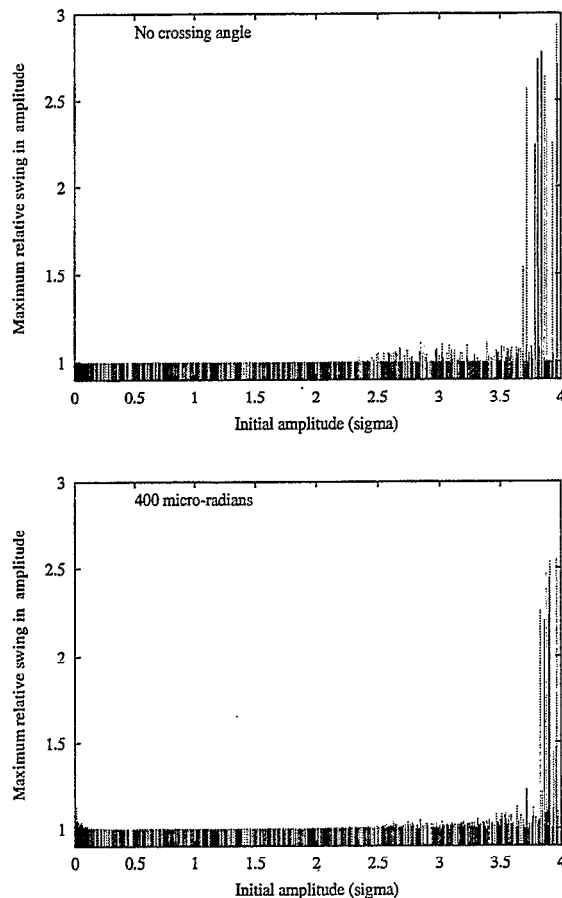


Figure 9: Same as Figure 7 except for two differences. The initial distribution has particles uniformly distributed between 0 and  $4\sigma$  and there is tune modulation at an amplitude of 0.001 and frequency 35Hz. Even without a crossing angle, there is much larger amplitude beating for particles at amplitudes beyond  $3.5\sigma$  compared to the case without tune modulation. The amplitude beating is slightly smaller at  $400\mu\text{ radians}$ .

tune modulation amplitudes -  $5 \times 10^{-4}$  and  $10^{-3}$  - and averaged over three initial distributions. The maximum amplitude reached is the largest at zero crossing angle and then decreases as the crossing angle is increased. This is easily understood - increasing the crossing angle decreases the overlap of the beams, and hence the beam-beam force, so the nonlinear effects of the beam-beam force and tune modulation are reduced. There is a competition between the resonances excited by the crossing angle and those excited by the tune modulation but at the typical modulation amplitudes considered here, the latter appear to be dominant. The maximum change in the averaged amplitude has a somewhat different behaviour with crossing angle. With the lower modulation amplitude, the change is relatively flat from 100 to  $300\mu\text{ radians}$  while at the larger modulation, the change peaks at  $200\mu\text{ radians}$  and falls off steeply on either side. Overall, the growth in the averaged amplitude with

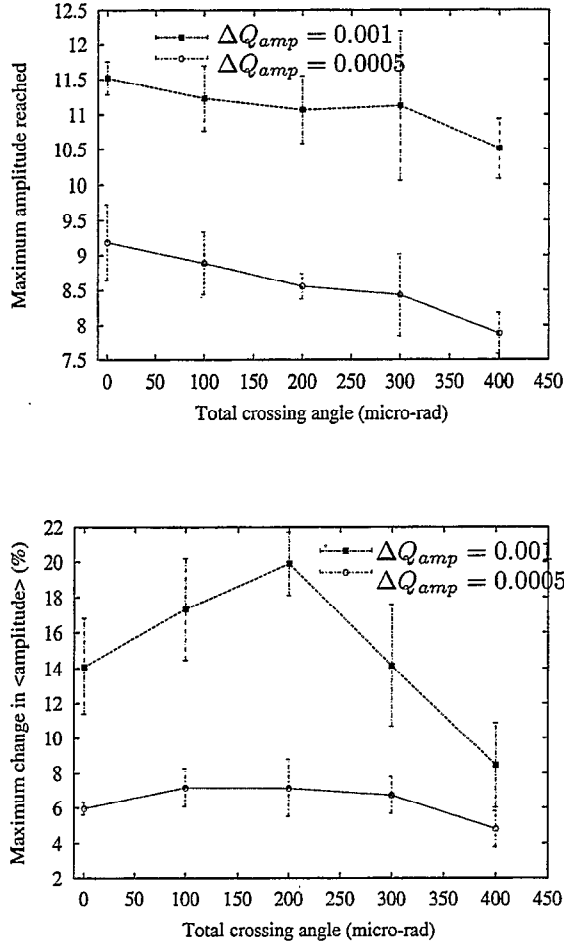


Figure 10: Same as Figure 8 but with added tune modulation at 35Hz and two different amplitudes  $5 \times 10^{-4}$  and  $10^{-3}$ . The amplitude growth with tune modulation is significantly larger than without modulation.

tune modulation is significantly greater than without.

In the simulations done to date, only the main beam-beam interactions have been considered. The long-range interactions, specially the ones nearest to the IPs, will have a significant effect on the particles as will the nonlinearities in the IR quadrupoles. The nearest neighbour long-range interactions will favour larger crossing angles while the magnetic nonlinearities of the IR quadrupoles will favour smaller angles. These effects must be considered before the range of the optimum crossing angle is known.

There is another feature of the main beam-beam interactions which has not been considered until now. The bunches at the Tevatron are long and are comparable in size to the beta function at the IP. This introduces new effects considered in the next section.

### 3 ANALYTICAL STUDIES OF BUNCH LENGTH EFFECTS

It was pointed out nearly ten years ago by Krishnagopal and Siemann [4] that the phase advance experienced by a particle as it propagates through the opposing bunch can have a strong effect on the strength of the beam-beam interactions. They considered a simplified version of the problem assuming (i) that the beta function stays constant over the interaction length and (ii) one transverse degree of freedom and the longitudinal. Under these assumptions they found that the beam-beam harmonics are of the form

$$V_{m_x m_s} = T_{m_x}(J_x) J_{m_s} \left( \frac{m_x a_s \sigma_s}{2 \beta^*} \right) \exp \left[ -\frac{1}{2} \left( \frac{m_x \sigma_s}{2 \beta^*} \right)^2 \right] \quad (3)$$

where the tunes are close to the resonance  $m_x \nu_x + m_s \nu_s = n$ . The main point to emphasize here is the exponential decay of the resonance strengths with the square of the bunch length. This rapid fall-off in strength is primarily due to the assumption that the beta function stays constant and therefore the phase advances linearly over the interaction length.

This problem has recently been studied [5] without the major assumptions made in the earlier study. The results show that instead of a monotonic decay with bunch length, the resonance strengths oscillate as a function of the bunch length. Here I present a summary of these results. I will assume that the beams are round over the interaction length, an assumption that is true at the Tevatron and in most hadron colliders.

For infinitely short bunches the Hamiltonian is

$$H(J_x, \phi_x, J_y, \phi_y) = \frac{\nu_x}{R} J_x + \frac{\nu_y}{R} J_y + H_s + \frac{1}{R} U(J_x, \phi_x, J_y, \phi_y) \delta_P(\theta) \quad (4)$$

$(J_x, \nu_x), (J_y, \nu_y)$  are the linear actions and tunes in the horizontal and vertical planes respectively,  $R$  is the radius of the ring. Here we have assumed that the lattice is completely linear.  $H_s$  is the Hamiltonian describing the non-linear longitudinal motion.  $U$  is the beam-beam potential,  $\delta_P(\theta)$  is the periodic delta function with period  $2\pi/N_{IP}$

when there are  $N_{IP}$  equally distant interaction points in the ring.

The beam-beam potential has the Fourier expansion

$$U = \frac{N_p r_p}{\gamma p} \sum_{m_x=0}^{\infty} \sum_{m_y=0}^{\infty} U_{2m_x, 2m_y}(J_x, J_y) \times \cos 2m_x \phi_x \cos 2m_y \phi_y \quad (5)$$

The Fourier coefficients  $U_{2m_x, 2m_y}$  for a potential due to a Gaussian distribution can be found in a straightforward fashion. This coefficient will be the dominant harmonic in the Fourier expansion if the tunes nearly satisfy the resonance condition

$$2m_x \nu_x + 2m_y \nu_y = n \quad (6)$$

If the bare tunes  $(\nu_{x0}, \nu_{y0})$  are close enough to this resonance condition, then due to the tune shift with amplitude the resonance condition may be exactly satisfied at an amplitude called the resonant amplitude. The equation for the resonant amplitude can be written as

$$\begin{aligned} \mathcal{R}(a_x, a_y) &\equiv \delta + \Delta\nu_x(a_x, a_y) + \frac{m_y}{m_x} \Delta\nu_y(a_x, a_y) = 0 \\ \delta &= \nu_{x0} + \frac{m_y}{m_x} \nu_{y0} - \frac{n}{2m_x} \end{aligned} \quad (7)$$

Here  $\Delta\nu_x, \Delta\nu_y$  are the tune shifts with amplitude. For a Gaussian distribution of charge, the resonant amplitudes lie on a one-parameter ( $r$ ) family of curves determined by the equation

$$\begin{aligned} \mathcal{R}(a_x, r a_x) &= \delta + N_{IP} \xi \int_0^1 \frac{du}{u} \exp\left[-\frac{(1+r^2)a_x^2 u}{4}\right] \\ &\left\{ \left[ I_0\left(\frac{a_x^2 u}{4}\right) - I_1\left(\frac{a_x^2 u}{4}\right) \right] I_0\left(r^2 \frac{a_x^2 u}{4}\right) \right. \\ &\left. + \frac{m_y}{m_x} \left[ I_0\left(r^2 \frac{a_x^2 u}{4}\right) - I_1\left(r^2 \frac{a_x^2 u}{4}\right) \right] I_0\left(\frac{a_x^2 u}{4}\right) \right\} = 0 \end{aligned} \quad (8)$$

where  $a_y = r a_x$ . These resonant amplitudes  $(a_x, a_y)$  can be found by numerical integration and are very close to the locus of stable fixed points corresponding to these resonances. The resonance islands are centered on the stable fixed points.

When the bunches are of finite length, the beam-beam potential seen by a particle is

$$V(x, y, s) = \rho_l(s+ct)U(x, y) \equiv \sum_{\vec{m}, n} V_{\vec{m}, n} \exp[i(\vec{m} \cdot \vec{\psi} - n\theta)] \quad (9)$$

$\rho_l$  is the longitudinal density of the bunch whose center is a distance of  $s+ct$  from the particle. Remarkably enough, the Fourier harmonics of the potential for round beams factorize into a product of two terms

$$V_{2m_x, 2m_y, m_s, n} = \frac{N_b r_p}{\gamma p} U_{2m_x, 2m_y}(J_x, J_y) L_{2m_x, 2m_y, m_s, n}(a_s) \quad (10)$$

where  $U_{2m_x, 2m_y}$  depends only on the transverse actions and is independent of the longitudinal variables. The dependence on the bunch length  $\sigma_s$  and the synchrotron oscillation amplitude of the particle  $a_s$  is all contained in  $L_{\vec{m}}$ . Assuming that the longitudinal density distribution of the opposing bunch is Gaussian and that the tunes are sufficiently close to a resonance so that

$$\Delta = 2m_x \nu_x + 2m_y \nu_y + m_s \nu_s - n \ll 1 \quad (11)$$

the longitudinal harmonic is of the form

$$L_{\vec{m}} = \frac{1}{(2\pi)^{3/2}} \exp\left[-\frac{a_s^2}{4}\right] \sum_{j=-\infty}^{\infty} (-1)^j I_j\left(\frac{a_s^2}{4}\right) F_j \quad (12)$$

$$F_j = \int_0^{\infty} du e^{-2u^2} \cos[2m_+ \tan^{-1}\left(\frac{\sigma_s u}{\beta^*}\right)] I_{2j}(2a_s u). \quad (13)$$

where  $m_+ = m_x + m_y$ . The complicated argument of the cosine in Equation (13) is a consequence of the growth of the beta function as  $\beta(s) = \beta^* + s^2/\beta^*$  where  $s$  is the distance from the IP. The transverse harmonics  $U$  decrease with increasing  $m_x, m_y$  as is well known but for finite bunch lengths there is another multiplicative factor  $L_{\vec{m}}$  which also decreases as  $m_+$  increases. These expressions can be analytically evaluated to extract the dependence on the bunch length  $\sigma_s$ , synchrotron oscillation amplitude  $a_s$  of the particle and the resonance harmonic numbers  $m_x, m_y$ . The most useful result is obtained in the limit of high resonance numbers - this is usually the case at most accelerators where tunes are chosen to avoid resonances of order lower than or equal to ten. An asymptotic expansion in the limit that  $m_+ \rightarrow \infty$  shows that

$$\begin{aligned} \lim_{m_+ \rightarrow \infty} L_{\vec{m}} &= \frac{1}{2(2\pi)^{3/2}} \frac{1}{\sqrt{m_+ \lambda}} \cos[2m_+ \arctan(\lambda)] \\ &+ O\left(\frac{1}{m_+}\right), \quad \lambda = \frac{a_s \sigma_s}{2\beta^*} \end{aligned} \quad (14)$$

This predicts a damped oscillatory dependence on the bunch length. We may define a quasi-wavelength of these oscillations as  $(\pi/m_+)(\lambda/\arctan(\lambda))$  which in the limit  $\lambda \ll 1$  is  $\pi/m_+$  while in the opposite limit  $\lambda \gg 1$  is  $2\lambda/m_+$ . Figure 11 shows the behaviour of  $L_{\vec{m}}$  in the asymptotic limit for  $m_+ = 8, 9, 10$  as a function of  $\lambda$ . At small  $\lambda$  the quasi-periods of the oscillations are short while at large  $\lambda$ ,  $L_{\vec{m}}$  approaches zero asymptotically. Thus at short bunchlengths, observables such as beam lifetime (due to the beam-beam interactions) are likely to change quickly with bunchlength while at long bunchlengths the lifetime may be somewhat insensitive to the choice of bunch length. This oscillatory behaviour is in contrast to the exponential decay predicted by the earlier analysis [4].

One measure of the influence of the bunch length can be seen in the resonance widths. Assuming, as is usual, that the resonances are isolated the half widths in action are given by the expressions

$$(\Delta J_{x,w}, \Delta J_{y,w}) = (m_x, m_y) \times \left(\frac{|N|}{|D|}\right)^{1/2}$$

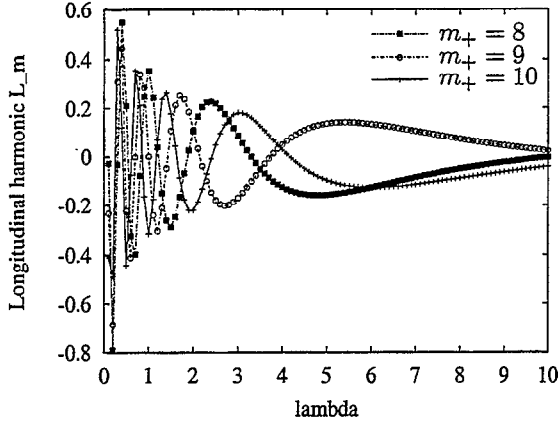


Figure 11: Asymptotic behaviour of the longitudinal part of the beam-beam harmonics,  $L_{\bar{m}}$  for large  $m_+$  at  $m_+ = 8, 9, 10$  as a function of  $\lambda = a_s \sigma_s / (2\beta^*)$ .

$$N = 2U_{m_x, m_y}(I_{1,s}, I_2)L_{\bar{m}} \quad (15)$$

$$D = L_0 \left[ m_x^2 \frac{\partial^2}{\partial J_x^2} + 2m_x m_y \frac{\partial^2}{\partial J_x \partial J_y} + m_y^2 \frac{\partial^2}{\partial J_y^2} \right] U_{0,0}$$

Figure 12 shows the resonant amplitudes and the widths of the twelfth order sum resonances. It is necessary for the neighbouring islands to touch or intersect in action space in order for the islands to overlap but it does not prove that they do in fact overlap in phase space. Overlapping in action space is therefore a necessary but not sufficient condition for resonance overlap. We observe that for zero length bunches it is possible for the  $10\nu_x + 2\nu_y$  and  $8\nu_x + 4\nu_y$  resonances to overlap but not for the other sum resonances. The bottom figure shows the resonance widths now calculated for Tevatron bunch lengths and  $a_s = 1$ . These widths are smaller by an order of magnitude - hence none of these resonances can overlap as is clear from this figure. This is consistent with observations at the Tevatron - in past operations when the working point was chosen to straddle these twelfth order resonances, there was no significant effect on the lifetime. This calculation makes it clear that bunch length effects have a major impact on the beam-beam resonance strengths.

The analytical predictions can be tested by particle tracking. The model to incorporate bunch length effects described here is similar to that in Section 2 but with two additional features. The longitudinal density of each disk falls off as a Gaussian from the center of the bunch and the particle is propagated from the center of each disk to the next by the appropriate transfer matrix. Tracking was done for different bunch lengths, first with all 1000 particles in the distribution at the same initial synchrotron amplitude  $a_s = 1$  and then with a Gaussian distribution in  $a_s$  with a cutoff at  $a_s = 3$ . These simulations were done at three different tunes: the Tevatron tunes  $\nu_x = 0.581, \nu_y = 0.575$ , close to a fourth integer resonance  $\nu_x = 0.257, \nu_y = 0.251$ ,

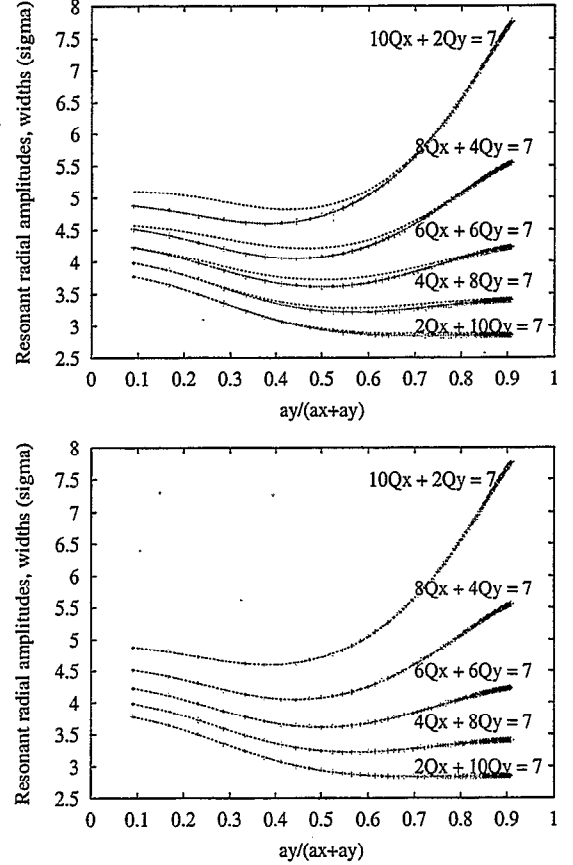


Figure 12: The top figure shows the locations of resonant amplitudes and the widths of sum twelfth order resonances calculated for infinitesimally short bunches,  $\beta^* = 0.35\text{m}$  as a function of  $r = a_y / (a_x + a_y)$ .  $Q_x, Q_y$  denote the horizontal and vertical tunes respectively. The curves in red show the locations of the resonant amplitude while the curves in blue and green on either side show the width of the resonance. We see that there is the possibility of overlap between the  $10Q_x + 2Q_y$  and  $8Q_x + 4Q_y$  resonances for  $\sim 0.15 < r < 0.3$ . At the bottom we show the same resonances and widths calculated with a bunch length of 36cm and  $a_s = 1.0$ . The resonance widths are all reduced by an order of magnitude. Now there is no possibility of overlap between any of these resonances.

and close to a sixth order resonance  $\nu_x = 0.175, \nu_y = 0.169$ . The maximum relative swing of the distribution was recorded for each simulation.

Figures 13 to 15 show the dependence of the swing on the bunch length. At the Tevatron tunes, the maximum swing is close to the value it would be without the beam-beam interaction indicating that the resonances do not have a significant effect. As a function of bunch length however, the maximum swing oscillates with decreasing amplitudes. Close to the lower order resonances the swings are much larger as expected and they also oscillate with the bunch length. The results of these simulations at three different tunes are in qualitative agreement with the analytical predictions.

The best test of these predictions would be an experimental measurement. This would require that the bunch length be varied over a range and an observable such as the lifetime be measured at each bunchlength of the strong beam. It would be sufficient to have only a single bunch in each beam. At the Tevatron, it is not possible to shorten the bunch length much below its value of around 36cm. However the bunch can be lengthened either by an injection mismatch or with the addition of RF noise. In order to have a clear signature that the observed effects are due to the change in bunchlength, it will be desirable to have other parameters such as bunch intensity, emittance, tunes etc. constant. With careful preparation, it should be possible to carry out such a test.

#### 4 PROPOSED EXPERIMENTS

In RunII the performance limitations may well arise due to the several long-range interactions. This is also true for the LHC where there will be about 60 long-range interactions and almost all at the same phase. In addition, the LHC will be the first hadron collider where both beams will be of the same intensity so strong-strong effects (about which not much is known) might also be important. There are a number of experiments that would address questions relevant to the weak-strong regime (appropriate to the Tevatron) and the strong-strong regime. I will focus here on weak-strong experiments.

- Impact of synchro-betatron resonances.

It would be useful to measure their impact without the complications of the long-range interactions. The only published observations with crossing angles at hadron colliders were at the SPS [6]. There experiments with two colliding bunches found no significant differences in background losses up to crossing angles of  $600\mu\text{rad}$ . Compared to the Tevatron however, the Piwinski parameter  $\chi$  was substantially smaller ( $\chi_{max} = 0.7$ ) due to the shorter bunch lengths. At the Tevatron the experiments can be done with one anti-proton bunch and two proton bunches so the anti-protons collide with a bunch at B0 and D0. At the least one would measure the lifetime, and background losses at different

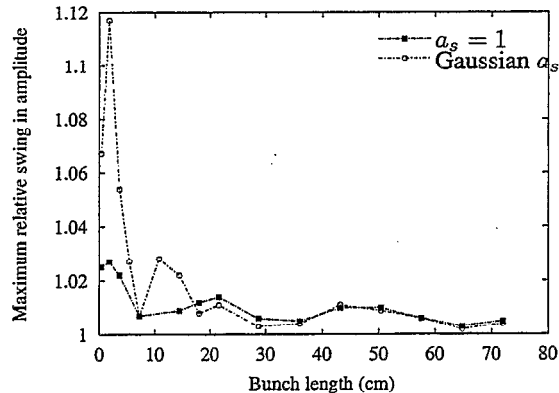


Figure 13: Maximum relative swing amongst 1000 particles tracked for 100,000 turns at each bunchlength with the Tevatron tunes  $\nu_x = 0.581, \nu_y = 0.575$ . Bunch length effects such as phase advance over the bunch and the longitudinal Gaussian density distribution of the disks are included in these simulations.

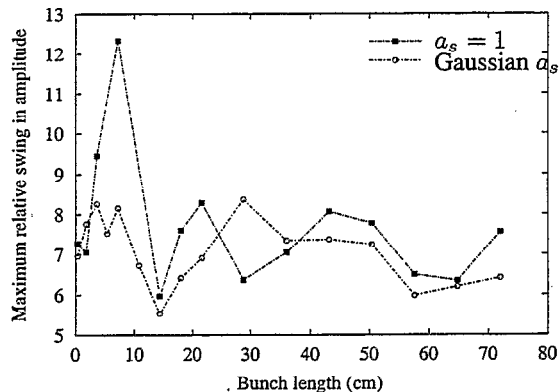


Figure 14: Same as above but close to fourth integer resonances,  $\nu_x = 0.257, \nu_y = 0.251$ .

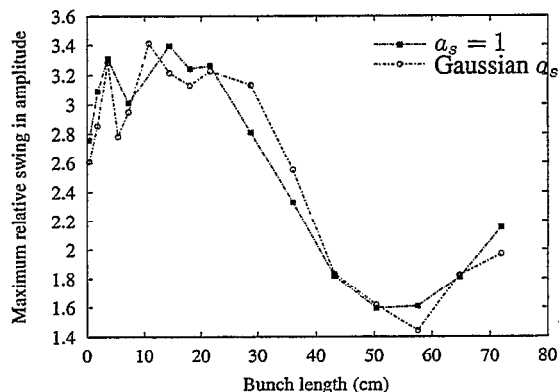


Figure 15: Same as above but close to sixth integer resonances,  $\nu_x = 0.175, \nu_y = 0.169$ .

crossing angles. Orbit effects due to the crossing angles will need to be eliminated, thus it would be useful to first measure the single beam lifetime without and with crossing angles. Limitations due to physical aperture can be determined this way. The lifetime with colliding beams may depend on the relative signs of the crossing angles at the two IPs. Of all the possible combinations of signs, some may be ruled out because they would not separate the beams by the required distances when there are 100 or more bunches in each beam. It would be useful to determine the lifetime for each of the useful sign combinations. These measurements may reveal that there is a crossing angle beyond which the effects due to the nonlinear fields of the IR quadrupoles and the synchro-betatron resonances lead to unacceptably large losses. This can be compared with the results of simulations and would determine if the important physics is contained in the models.

- Impact of long-range interactions.

Tune footprints are severely distorted when the long-range interactions are included and the footprint changes from bunch to bunch. Preliminary tracking results with  $36 \times 36$  bunches indicate that these interactions reduce the dynamic aperture by a significant amount. The interactions closest to the IP on either side are at the smallest separations and have the largest effect. As a first experimental test it would be desirable to have a few bunches (say four) in the proton beam and spaced so that each anti-proton bunch experiences only the nearest neighbour interactions in each IR but not the head-on interactions. The lifetime could be measured as a function of the proton intensity and also as a function of the beam separation at these nearest neighbour points. The dependence on separation will be a useful input towards determining the minimum crossing angle while the dependence on intensity may be useful in determining the maximum useful luminosity. This set of experiments will be very useful in testing the predictive power of the simulations with long-range interactions. If the observations are close to the simulation results, then simulations may be used with more confidence in predicting the outcome with 100 or more bunches in each beam. With the bunch spacing at 396 nanoseconds, perhaps the most useful experiment to determine the feasibility of shortening the spacing to 132 nanoseconds would be to collide an anti-proton bunch with 36 proton bunches with crossing angles at B0 and D0. This can be accomplished with the present set of separators. In this experiment the impact of both the synchro-betatron resonances and the long-range interactions will be felt. Observations over a range of crossing angles will go a long way towards our understanding of these phenomena.

- Tune footprint due to the beam-beam interactions.

Measurement of the footprint is the most basic test of the nonlinearity of the beam-beam force and the machine lattice. A comparison with the theoretical footprint will reveal if all important effects have been included in the theoretical model. The tune as a function of amplitude could be measured with a pencil anti-proton bunch which can be kicked to different amplitudes in both transverse planes. If this pencil bunch is sufficiently narrow, it will probe the force within a small region of phase space where the tune is nearly constant. Following the kick this probe bunch will decohere due to the nonlinear beam-beam force and its emittance will grow as it fills out phase space by shearing. Figure 16 shows an example of the decoherence of the beam centroid following an initial kick which placed it at a distance of about  $5\sigma$  from the center of the opposing bunch. Some of the issues which must be addressed in such an experiment include:

- The time to measure the tune should be less than the decoherence time.

- The decoherence time will depend on the kick amplitude and the machine chromaticity.

- The minimum size of the pencil bunch may depend on the minimum intensity required to trigger the beam position monitors if turn by turn data is used to measure the tunes.

- If scraping is used to reduce the beam size, then it might be useful to scrape in regions of high dispersion to remove some of the momentum spread. It may also take some time to learn how to scrape efficiently without losing the beam.

If the bunch decoheres significantly following a tune measurement at a particular amplitude, it may be unusable for a subsequent measurement. In that case we may want a train of pencil bunches, each of which will be kicked to a different amplitude, to obtain the tune footprint. An alternative possibility could be to use an AC dipole, as suggested for other measurements at RHIC, to kick the beam adiabatically and thereby avoid the emittance growth. If this works in practice, then each pencil bunch could be used to measure the tune at more than one amplitude.

## 5 CONCLUSIONS

The beam-beam interactions will have a major impact on beam stability in Run II. Crossing angles at the main interaction points and the nearly two hundred long-range interactions will be new sources of lifetime limitations. This will be further complicated by the fact that the effects will vary from bunch to bunch. Detailed theoretical and experimental studies are required to know whether this mode of operation will be feasible.

The working point of the Tevatron has been chosen so that the tune footprint does not cross resonances of order less than twelve. When crossing angles are introduced, the footprint shrinks in size. Some twelfth order betatron reso-

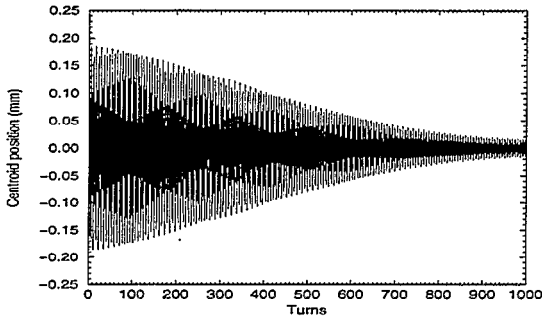


Figure 16: Decoherence of the beam centroid due to the nonlinear beam-beam force between two beams that are initially offset from each other by about  $5\sigma$ .

nances now do not cross the beam distribution and new resonances are excited. In addition synchrotron sideband resonances develop around the betatron resonances and these are a source of concern.

The simulations reported here have studied the effects of the crossing angles but not those of the long-range interactions. These show that the synchro-betatron resonances induced by the crossing angles do not appear to affect the core of the beam up to crossing angles of  $400\mu$  radians. The amplitude growth found at crossing angles between  $200\mu\text{rad}$  to  $400\mu\text{rad}$  are statistically about the same. These simulations also show that tune modulation at typical modulation depths causes large amplitude growth and dominates the effects due to the crossing angles. Analytical and simulation studies have shown that the long length of the bunches in the Tevatron have a major impact on the strength of the beam-beam resonances. The analytical studies predict that the resonance strengths oscillate as a function of the bunch length. This has been confirmed with simulations. Resonance widths calculated for the Tevatron bunches are about an order of magnitude smaller than those calculated for zero length bunches. These results suggest that it would be very worthwhile to conduct a beam-beam experiment where the bunch length is varied to the extent possible. At longer bunch lengths there is a loss of luminosity due to the hour-glass effect but it may turn out that the gain in lifetime is sufficiently high that the integrated luminosity is larger. In any event, the phase averaging effect due to the long bunch is significant and needs to be taken into account in all theoretical models.

The amplitude growth within the beam distribution may change qualitatively when the long-range interactions are included. The footprint changes and the changes are different from bunch to bunch. The transverse core of some bunches may be excited by resonances. This is now under study.

In the near term, experimental observations with crossing angles appear feasible during the machine studies period at the Tevatron in the fall of 2000. The first stage of Run II

will operate with 36 bunches in each beam. This will give us an opportunity to observe the effects of the several long-range interactions. When the faster kickers are available, operation with the shorter bunch spacing of 132 nanoseconds will be tested. It will also be desirable to conduct basic tests of beam-beam models by measuring the tune footprint and perhaps further out, measure the dynamic aperture with beam-beam interactions. These experiments can just as well be conducted at other colliders, especially RHIC when the AC dipoles are available.

## 6 REFERENCES

- [1] J. Johnstone, FNAL Internal note (1994)
- [2] J. Irwin, SSC preprint SSC-233 (1989)
- [3] MAD lattice from P. Bagley, ca. April 1999.
- [4] S. Krishnagopal and R. Siemann, *Phys. Rev. D*, **41**, 2312 (1990)
- [5] T. Sen, *The beam-beam interaction of finite length bunches in hadron colliders*, FNAL preprint Pub-00/093-T (2000)
- [6] K. Cornelis, W. Herr, M. Meddahi, CERN preprint CERN SL/91-20 (1991)

## BEAM-BEAM SIMULATIONS FOR SEPARATED BEAMS\*

Miguel A. Furman,<sup>†</sup> Center for Beam Physics, LBNL, Berkeley, CA 94720

### Abstract

We present beam-beam simulation results from a strong-strong gaussian code for separated beams for the LHC and RHIC. The frequency spectrum produced by the beam-beam collisions is readily obtained and offers a good opportunity for experimental comparisons. Although our results for the emittance blowup are preliminary, we conclude that, for nominal parameter values, there is no significant difference between separated beams and center-on-center collisions.

### 1 INTRODUCTION AND SUMMARY.

In this note we present first results for beam-beam simulations for the LHC and RHIC with separated beams. There are two main motivations for these kind of simulations: (a) to assess undesirable effects from LBNL's sweeping luminosity monitoring scheme for the LHC [1], and (b) to assess undesirable effects from the process of bringing initially-separated beams into collision. In addition, we want to simulate conditions that might be testable at RHIC in order to test our understanding of strong-strong beam-beam dynamics in hadron colliders.

For the cases presented here, we have not found any indications of adverse effects for nominal parameter values. However, these simulations have been run for a maximum of  $T = 10^5$  turns, which amount to only a brief interval of real accelerator time, so our conclusions are subject to change upon more detailed scrutiny.

The results presented here were obtained with a three-dimensional strong-strong gaussian code whose features are described below. This investigation represents a direct extension of the work by Krishnagopal [2], and Zorzano and Zimmermann [3].

### 2 SIMULATIONS.

#### 2.1 Code features.

Our code is both an extension and a simplification of the code TRS [4]. It is a strong-strong simulation code in which the two colliding bunches are represented by a given number  $M$  of macroparticles that are initially distributed gaussianly in 6-dimensional phase space. The beam and

ring parameters for the two rings are fully independent. The heart of the code is the beam-beam module: at every turn, just before the beam-beam collision, the centers  $\bar{x}$  and  $\bar{y}$ , and rms sizes  $\sigma_x$  and  $\sigma_y$  of the two distributions are computed from the macroparticle distributions, and these four dynamical quantities are fed into the Bassetti-Erskine [5] formula for the field of a relativistic gaussian distribution. The electromagnetic kick is computed from this expression and applied to each particle of the opposing beam. Then the role of the two beams is reversed before proceeding. Finite bunch-length effects are taken into account by slicing the bunch longitudinally into a certain number  $K$  of slices, each of which acts as a kick on the particle as it goes through the kicking bunch. A weak-strong mode is available as an option controlled by an input switch.

After the beam-beam kick, the beams are transported along the rings by the action of a linear Courant-Snyder one-turn map that depends on the machine tunes and beta functions at the interaction point. A synchrotron rotation is performed on the longitudinal coordinates. Radiation damping and quantum excitation are applied once per turn by the action of a localized kick.

Our code can also describe beam-beam collision with separated beams by means of an input-specified closed-orbit displacement. This displacement can be static or time-dependent, and can be independently specified for either (or both) of the two beams. In addition, the code can optionally simulate a beam feedback element whose action is to shift the transverse position of the macroparticles so that their centroid is brought back to the specified closed orbit at every turn. Finally, the code can describe beams of various particle species, namely  $e^+$ ,  $e^-$ ,  $\mu^+$ ,  $\mu^-$ ,  $p$ ,  $\bar{p}$  and  $\text{Au}^{79+}$  ions in any desired combination. An extension to any other kind of ion is straightforward.

The code has, at present, several simplifications in the modeling of the collider. In particular, the beam-beam collisions have zero crossing angle; there is only one bunch per beam, so that there are no parasitic collisions; there is only one interaction point in the ring. These simplifications will be removed in future versions.

An intrinsic deficiency of the soft-gaussian approach is the introduction of an inconsistency in the calculation: although the actual macroparticle distribution deviates from the gaussian shape as time evolves, the beam-beam kick is always computed under the assumption of a gaussian shape. This inconsistency is, in principle, more serious for hadron simulations than for  $e^+e^-$  simulations, since

\*Work supported by the US Department of Energy under contract no. DE-AC03-76SF00098. Presented at the US-LHC Collaboration mtg., BNL, Feb. 22-23, 2000; to be published in the proceedings.

<sup>†</sup> mafurman@lbl.gov

the damping times are typically much larger than typical simulation runs in the former case than in the latter. However, for short runs and weak beam-beam parameters, as in the examples presented here, we have checked that the distribution does not deviate significantly from the gaussian shape, and hence this inconsistency is not serious. The question remains, however, whether the gaussian shape is a good approximation to the actual particle distribution expected (or realized) in hadron colliders, particularly after long times following injection. We do not attempt to answer this question here. However, we intend to shed some light on this issue in the future by allowing the code to use distributions other than gaussian.

## 2.2 Simulation conditions.

As mentioned above, in all results in this note the crossing angle is zero, there is only one bunch per beam (no parasitic collisions), and there is only one interaction point in the ring. The damping time for the LHC at 7 TeV is  $T \simeq 10^9$  turns, and is larger for RHIC with Au<sup>79+</sup> ions at 100 GeV/nucleon. Since our runs are for at most  $10^5$  turns, we have turned off radiation damping and quantum excitation in the code, which amounts to setting the damping time to  $\infty$ . The feedback is turned off. In all cases we use  $M = 10000$  macroparticles per bunch. Other parameters are listed in Tables 1 and 2.

## 3 RESULTS.

### 3.1 Results for the LHC.

**Nominal collision conditions.** For reference we present first the results for nominal conditions, with parameters as specified in Table 1 and the beams colliding center-on-center. As seen in Fig. 1, the beam blowup is insignificant over  $10^5$  turns, and the rms sizes show the expected statistical fluctuations of order  $1/\sqrt{M} = 1\%$ .

Table 1: Selected LHC parameters [6].

Beam energy parameter, $\gamma$	7460.52
Protons per bunch, $N$	$1.05 \times 10^{11}$
Beta-function at the IP, $\beta^*$ [m]	0.5
RMS spot size at the IP, $\sigma_0$ [ $\mu\text{m}$ ]	15.9
Nominal beam-beam parameter, $\xi$	-0.0034
Tunes, $(\nu_x, \nu_y)$	(0.31, 0.32)
RMS bunch length, $\sigma_z$ [m]	0.077
Synchrotron tune, $\nu_s$	0.0021

Fig. 2 shows the absolute value of the spectra of the sum and difference of the beam centroids. The coherent modes are clearly seen, with the  $\sigma$  modes at the lattice tunes. The  $\pi$  modes are downshifted from the  $\sigma$  modes by  $\sim 1.1\xi$ . The incoherent spectrum lies in between the two coherent modes.

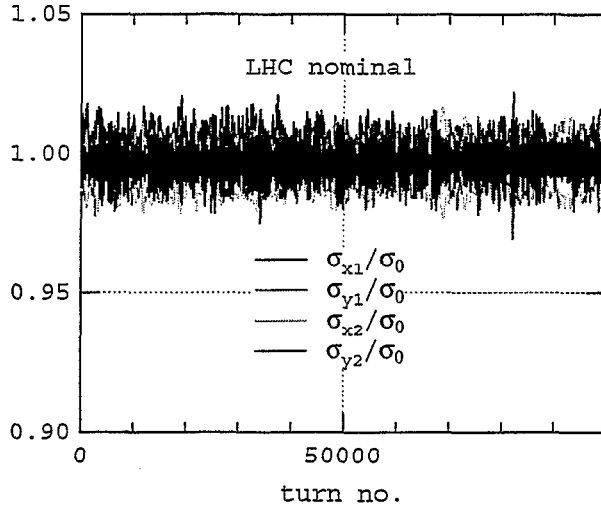


Figure 1: The rms beam sizes for nominal collisions.

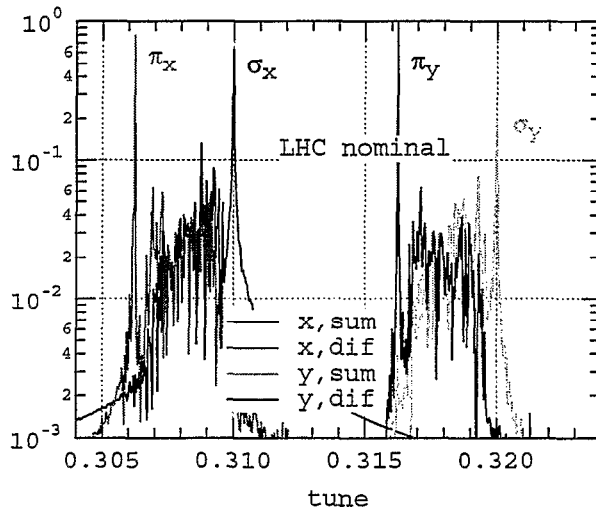


Figure 2: The beam-beam tune spectra during nominal collisions. The four traces are the absolute value of the spectra of the sum and difference of the beam centroids. The normalization is such that the highest peak among the four traces is arbitrarily set to unity; the relative heights of the traces are meaningful. Only the first 25000 turns of the run were used in the computation of the spectra.

**Sweeping one beam about the other.** In the luminosity monitoring scheme being developed at LBNL for the LHC one beam is deliberately swept in a circle about the other, which remains fixed. This sweeping is achieved by an appropriate time-dependent closed orbit bump spanning the interaction point (IP). As a first test we have chosen a sweeping period of 1000 turns and a sweeping radius of  $0.6\sigma_0$  for the closed orbit of beam #2, while the closed orbit of beam #1 remains static and is offset by  $0.2\sigma_0$  from the nominal IP at  $45^\circ$  relative to the horizontal axis. The luminosity per collision is shown in Fig. 3, showing the characteristic fluctuations due to the off-center collisions

with a period of 1000 turns. In practice, this is the signal that will be used to optimize the luminosity, although the period will be significantly larger than 1000 turns. The rms beam sizes (Fig. 4) do not show significant differences with the nominal conditions (Fig. 1). Fig. 5 shows the beam centroid spectra; comparing with the nominal case (Fig. 2) one sees that the  $\sigma - \pi$  tune split is smaller during the sweeping operation owing to the lower effective beam-beam parameter. The difference spectra also show sidebands of the  $\pi$  modes separated by 0.001, corresponding to the sweeping tune.

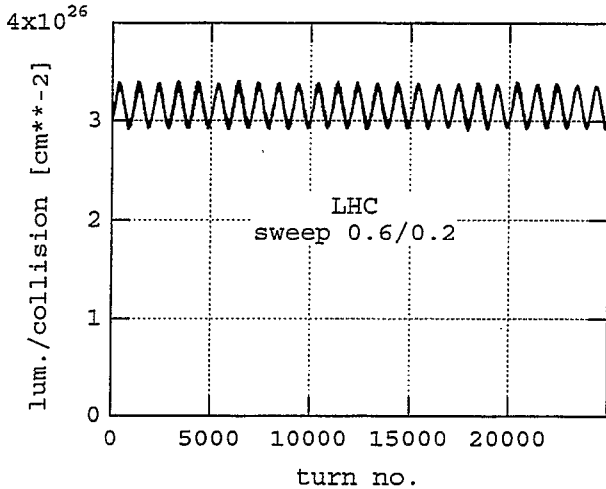


Figure 3: The luminosity per collision during the sweeping process.

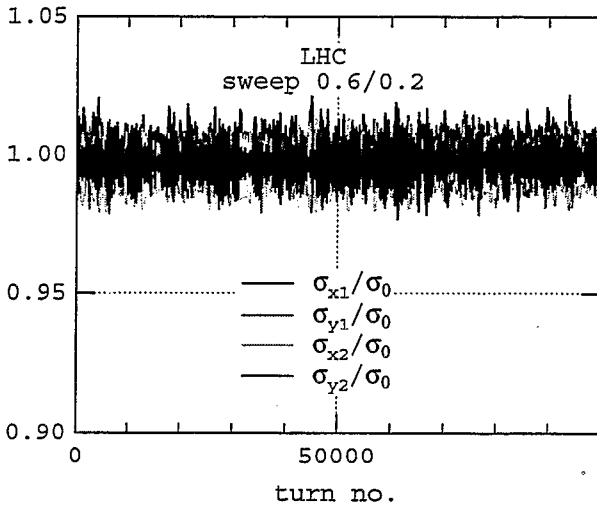


Figure 4: The rms beam sizes during the sweeping process.

**Statically-offset collisions.** We have also tested to see if constantly-separated beams are more sensitive to beam blowup than beams colliding head-on. Fig. 6 shows the rms beam sizes for the case in which the closed orbit of beam

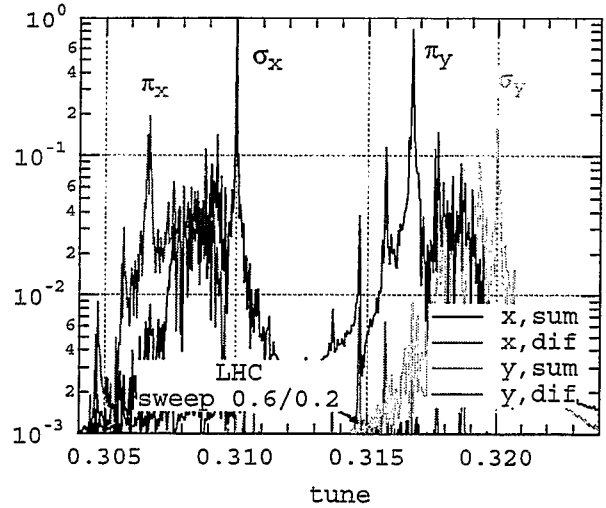


Figure 5: The beam-beam tune spectra during the sweeping process.

#2 is displaced vertically from that of beam #1 by  $3\sigma_0$  and is held fixed in this position. Comparing with the nominal case (Fig. 1), there is no significant difference. Fig. 7 shows the beam centroid spectra. Comparing with the nominal case, Fig. 2, there is an important qualitative difference: the  $\pi_y$  coherent mode is *upshifted* from the  $\sigma_y$  mode rather than downshifted. This change is due to the fact that the slope of the beam-beam force at a separation of  $3\sigma$  has the opposite sign from the slope near the origin. In addition, of course, the  $\sigma_x - \pi_x$  tune split is smaller than in the nominal case owing to the smaller effective beam-beam parameter.

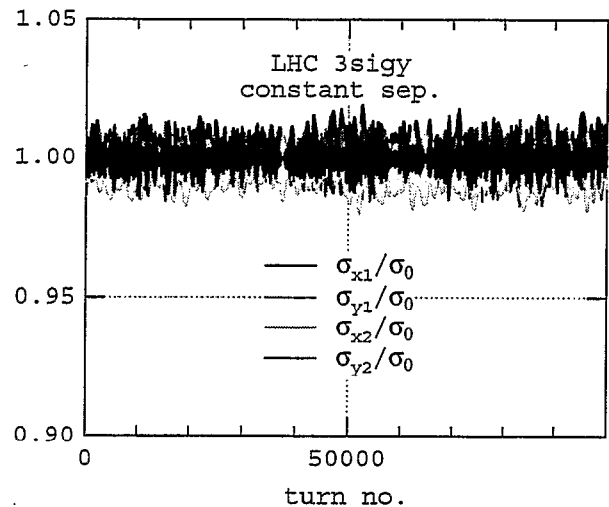


Figure 6: The rms beam sizes when beam #2 is displaced vertically from beam #1 by  $3\sigma_0$ .

**Closed-orbit squeeze.** We have also tested to see if any undesirable effects appear when the beams are brought transversely into collision following the end of the accel-

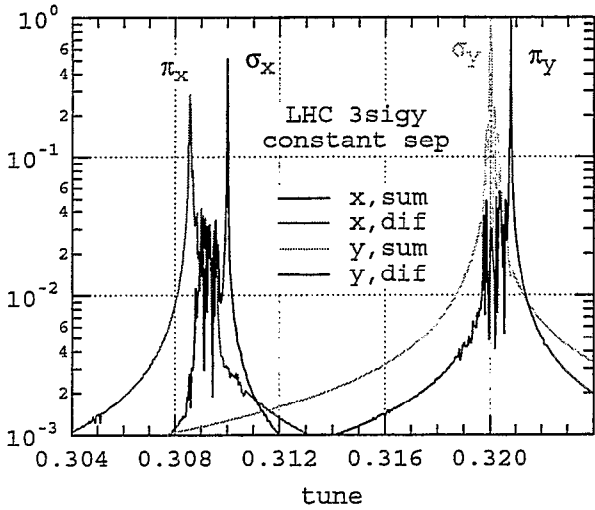


Figure 7: The beam centroid spectra when beam #2 is displaced vertically from beam #1 by  $3\sigma_0$ . Notice that the  $\pi_y$  coherent mode is upshifted from the  $\sigma_y$  mode.

eration ramp. For this purpose we assume that the closed orbit of beam #2 starts out vertically displaced from the nominal IP by  $3\sigma_0$  and is linearly brought down to the nominal IP over a time interval of 25000 turns, while the closed orbit of beam #1 is held fixed at the nominal IP. We ran the simulation for an additional 5000 turns for a total of 30000 turns. Fig. 8 shows the normalized beam centers,  $\bar{x}_i/\sigma_0$  and  $\bar{y}_i/\sigma_0$  as a function of time, for  $i = 1, 2$ . Fig. 9 shows the rms beam sizes, and Fig. 10 shows the luminosity per collision during this process, exhibiting the characteristic gaussian shape as the beam overlap increases.

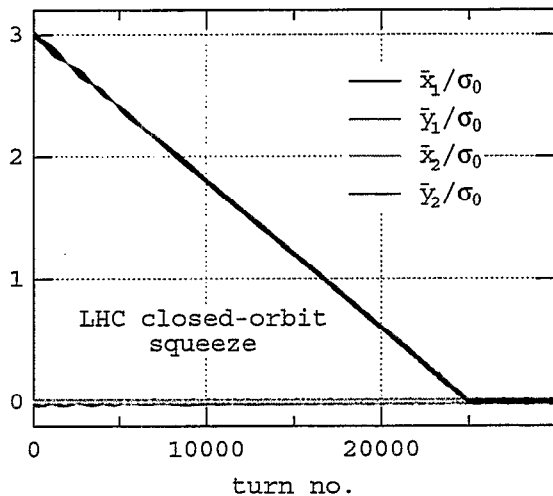


Figure 8: The normalized beam centers as a function of time during a vertical closed-orbit squeeze.

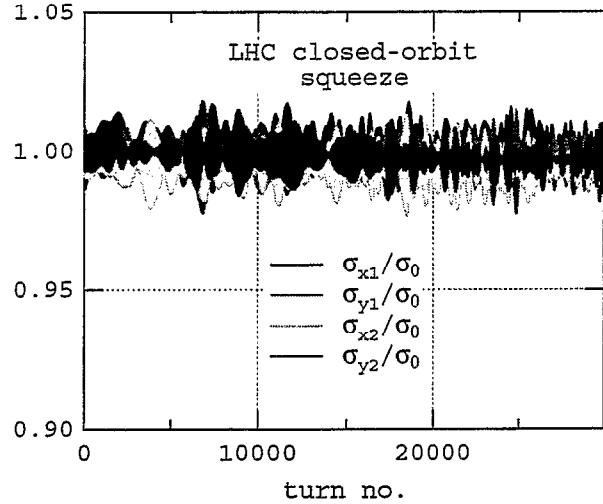


Figure 9: The rms beam sizes as a function of time during a vertical closed-orbit squeeze.

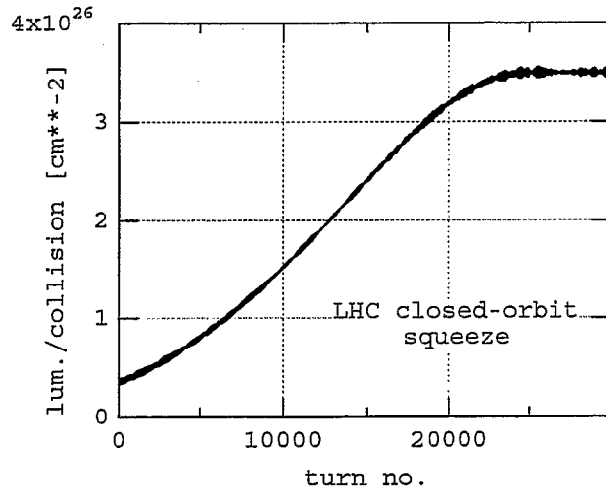


Figure 10: The luminosity per collision as a function of time during a vertical closed-orbit squeeze.

### 3.2 Results for RHIC.

**Nominal collision conditions.** Nominal conditions for RHIC are shown in Table 2. For these conditions, Fig. 11 shows the beam centroid spectra. As in the case of the LHC, the  $\sigma$  coherent modes are located at the ring tunes, and the  $\pi$  modes are downshifted from the  $\sigma$  modes by  $1.1\xi$ .

**Split tunes.** We have run one case in which the tunes of the two rings are split by 0.005, so that all four tunes are different,  $(\nu_{x1}, \nu_{y1}) = (0.190, 0.195)$  and  $(\nu_{x2}, \nu_{y2}) = (0.180, 0.185)$ . In this case, as shown in Fig. 12, all coherent modes have disappeared, as expected from the theory [8].

Table 2: Selected RHIC parameters [7].

Beam energy parameter, $\gamma$	106.5
Au <sup>79+</sup> ions per bunch, $N$	$1 \times 10^9$
Beta-function at the IP, $\beta^*$ [m]	10
RMS spot size at the IP, $\sigma^*$ [ $\mu\text{m}$ ]	396
Nominal beam-beam parameter, $\xi$	-0.0023
Tunes, $(\nu_x, \nu_y)$	(0.19, 0.18)
RMS bunch length, $\sigma_z$ [m]	1
Synchrotron tune, $\nu_s$	0.000745

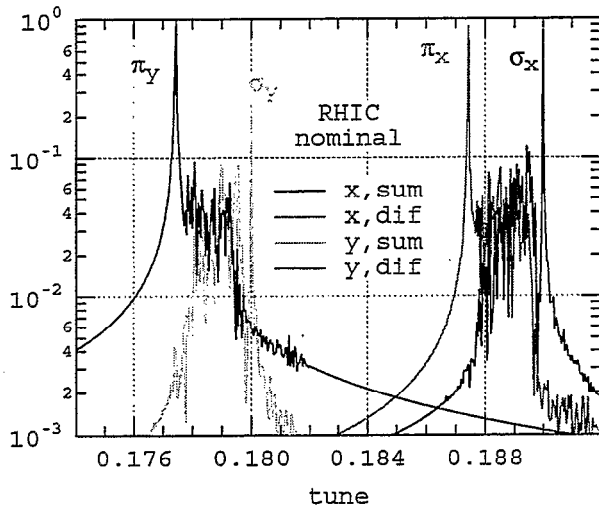


Figure 11: Beam centroid spectra for nominal collision conditions (Table 2).

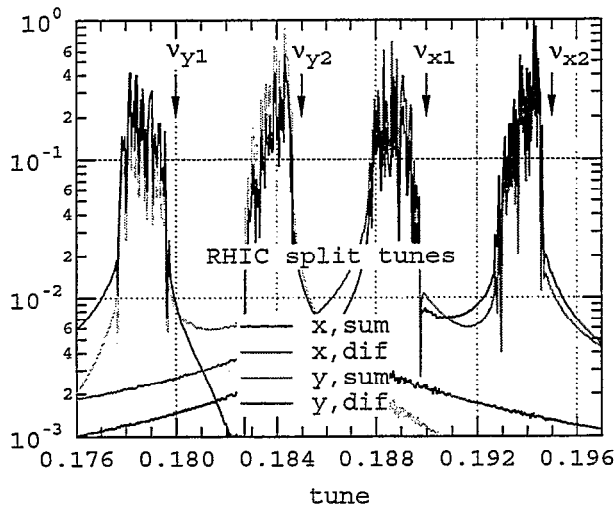
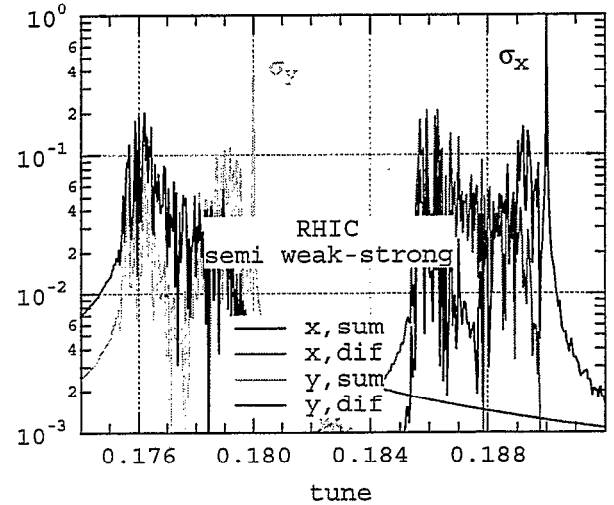


Figure 12: Beam centroid spectra for split tunes, indicated by the arrows. Other parameters are as specified in Table 2. Notice that all coherent modes have disappeared.

**Semi-weak-strong case.** By “semi-weak-strong” we simply mean that the number of particles per bunch is different in the two beams. Specifically, we choose  $N_1 = 2 \times 10^9$ , with other parameters as specified in Table 2. As seen in Fig. 13, the  $\pi$  modes have disappeared because they have shifted into the continuum of the spectrum and hence have Landau-damped, in agreement with theoretical expectations [8].


 Figure 13: Beam centroid spectra for unequal bunch intensities:  $N_1 = 2 \times 10^9$ ,  $N_2 = 1 \times 10^9$ . Other parameters are as specified in Table 2. Notice that the  $\pi$  modes have disappeared.

**Weak-strong case.** Finally, we present a simulation in the “weak-strong” mode that is only of mathematical interest. In this case beam #2 is represented by a mathematical gaussian lens rather than by a collection of macroparticles. Other than this, all parameters are as stated in Table 2; in particular, the number of particles per bunch and the tunes are the same for the two beams. In this case both coherent modes have disappeared, and the spectrum only shows the incoherent part. The sum and difference spectra coincide exactly, since beam #2 is static.

## 4 DISCUSSION.

The appearance of coherent dipole beam-beam modes is perhaps the cleanest manifestation of the beam-beam interaction in strong-strong mode and offers the possibility of simple and meaningful comparisons with experiment. Three examples of such measurements are: (1) the tune shift of the  $\pi$  mode as a function of beam-beam separation; (2) the disappearance of the coherent modes as the tunes of the two rings move away from each other; and (3) the disappearance of the  $\pi$  modes as the bunch intensities of the two beams become sufficiently different. The thresholds and magnitudes of these effects can be readily computed by simulations, as our samples show. Of course, one has

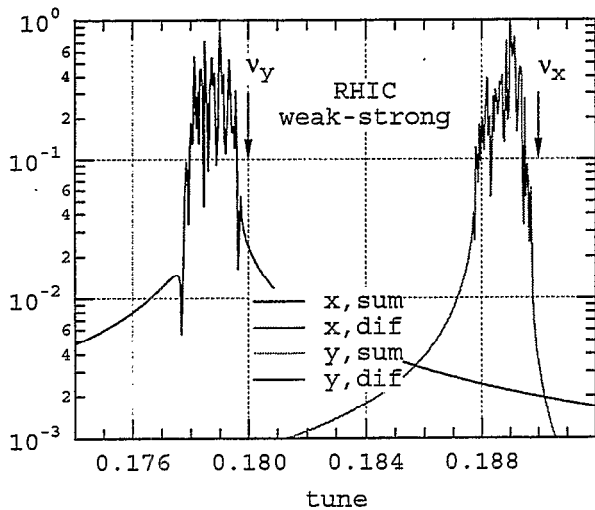


Figure 14: Spectrum for a weak-strong simulation in which beam #2 is represented by a static gaussian lens. All parameters are as shown in Table 2. The sum and difference spectra coincide exactly. Note the absence of coherent modes.

to make sure that the tune spread from lattice nonlinearities is small enough, otherwise the coherent modes might be Landau-damped. Obviously this issue requires further detailed study.

For a few selected cases we have verified that our results are in excellent agreement with those in Ref. 3, lending support to the validity of the two codes.

The coherent beam-beam renormalization factor  $|(\nu_\pi - \nu_\sigma)/\xi|$  has the value 1.1 in our calculations, which appears to be  $\sim 10\%$  smaller than analytic estimates [8,9]. We do not know if this difference is significant.

For the cases with separated beams (static separation, closed-orbit squeeze, and beam sweeping), our results do not show noticeable detrimental effects such as emittance blowup. Of course our conclusions are based on relatively short runs, and may change upon further examination. Nevertheless, it is encouraging that there is no significant difference with the case of nominal, center-on-center, collisions.

Since  $\sigma_z/\beta^*$  is small for both machines, we have used in all cases shown here the impulse approximation ( $K = 1$ ) for the beam-beam collision. We have verified that this is a valid approximation by running sample cases with  $K = 5$ , which show insignificant differences with the  $K = 1$  cases. The advantage of the single-slice calculations is computational speed, since the CPU time is proportional to  $K$ . For  $M = 10000$  in strong-strong mode and a linear lattice map, our runs take  $\sim 5600$  CPU seconds to run for  $T = 25000$  turns on a Cray SV1 computer at NERSC. In this regime the computer speed is limited by the calculation of the beam-beam force, and overall CPU time scales with the product  $T \times K \times M$ . If we turn on the radiation damping and quantum excitation elements, computer speed

is slightly lower.

Although synchrotron motion leads, even in the impulse approximation, to synchrotron coupling, the effects from this coupling are very weak in the cases reported here owing to the smallness of  $\nu_s$  and  $\sigma_z/\beta^*$ . As a result, it is legitimate to ignore the longitudinal motion by setting  $\nu_s = 0$ , although we have not bothered to do so. The implementation of a crossing angle in our calculations might introduce more significant synchrotron coupling effects.

We have initiated sensitivity studies with respect to two parameters that are directly relevant to the cost (in terms of CPU time) and reliability of our simulations, namely: the number of macroparticles per bunch, and the length of the simulation. The beam centroid spectra is quite insensitive to these two parameters: even 100 macroparticles per bunch running for 1000 turns yield very accurately the tunes of the coherent modes. On the other hand, beam blowup is not given reliably when one uses few macroparticles.

As mentioned above, an intrinsic limitation of our code is the gaussian approximation. Although the initial distribution in our simulations is, by construction, gaussian, this shape cannot in principle persist for long times owing to the nonlinearities of the beam-beam force. For the nominal LHC beam-beam parameter value we have verified that the deviations from the gaussian shape of the distributions are insignificant up to  $10^5$  turns, although these deviations become clear (though still a few percent) in sample runs for bunch intensities 10 times the nominal value. Furthermore, in a real hadron collider, the initial particle distribution is sensitive to the injection process, and is unlikely to be exactly gaussian. We plan to augment our simulation code by allowing shapes other than gaussian (but still of a prescribed functional form), and determining the effect of the change on the beam centroid spectra. We also plan to optimize the PIC code CBI [10], which does not make any assumption about the shape of the distribution, by adapting it to a parallel computer.

The gaussian approximation (or, indeed, any approximation of a specific functional form) leads to purely numerical beam blowup that might mask physical blowup effects due to the nonlinearities of the forces. Fig. 15 shows the result for the rms beam sizes for the LHC for bunch intensities 10 times the nominal value. There is an approximately linear increase in beam size whose slope we may call  $\dot{\sigma}$ . By repeating this calculation for  $M = 100$  and  $M = 1000$ , we have found the empirical scaling law  $\dot{\sigma} \propto M^{-p}$  where the scaling exponent is  $p \simeq 0.7 - 0.8$ . Further investigations are planned, particularly the dependence on tune and on beam separation.

## 5 ACKNOWLEDGMENTS.

I am grateful to F. Zimmermann, M. P. Zorzano, W. Turner and S. Krishnagopal for discussions and to NERSC for supercomputer support.

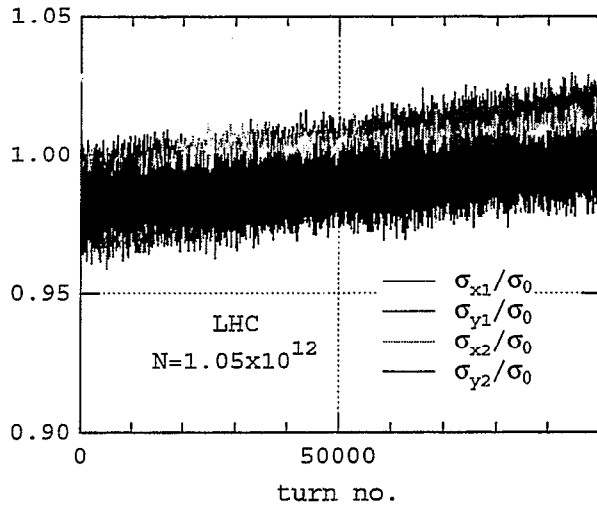


Figure 15: The rms beam sizes for LHC collisions for bunch intensities 10 times the nominal value.

## 6 REFERENCES

- [1] W. Turner, these proceedings.
- [2] S. Krishnagopal, M. A. Furman and W. C. Turner, "Studies of the Beam-Beam Interaction for the LHC," Proc. PAC99, New York City, March 29-April 2, 1999, p. 1674; S. Krishnagopal, "Collective Beam-Beam Effects in the LHC," Proc. Workshop on Beam-Beam Effects in Large Hadron Colliders LHC99, April 12-17, 1999, CERN-SL-99-039 AP, p. 52.
- [3] M. P. Zorzano and F. Zimmermann, "Coherent Beam-Beam Oscillations at the LHC," LHC-PR-314, 2 November 1999.
- [4] J. L. Tennyson, undocumented code "TRS," 1989.
- [5] M. Bassetti and G. A. Erskine, "Closed Expression for the Electric Field of a Two-Dimensional Gaussian Charge," CERN-ISR-TH/80-06.
- [6] "The Large Hadron Collider: Conceptual Design," CERN/AC/95-05(LHC), 20 October 1995.
- [7] "RHIC Design Manual," <http://www.agsrhichome.bnl.gov/NT-share/rhicdm/00.toc1i.htm>.
- [8] Y. Alexahin, "Eigenmodes of Coherent Oscillations in Colliding Beams," Proc. Workshop on Beam-Beam Effects in Large Hadron Colliders LHC99, April 12-17, 1999, CERN-SL-99-039 AP, p. 41, and references contained therein.
- [9] R. E. Meller and R. H. Siemann, "Coherent Normal Modes of Colliding Beams," IEEE Trans. Nucl. Sci. NS-28 No. 3, 2431 (1981); K. Yokoya, Y. Funakoshi, E. Kikutani, H. Koiso and J. Urakawa, "Tune Shift of Coherent Beam-Beam Oscillations," KEK Preprint 89-14; K. Yokoya and H. Koiso, Part. Accel. 27, pp. 181-186 (1990).
- [10] S. Krishnagopal, "Luminosity-Limiting Coherent Phenomena in Electron-Positron Colliders," Phys. Rev. Lett. 76, pp. 235-238 (1996); "Energy Transparency and Symmetries in the Beam-Beam Interaction," PRST-AB 3, 024401 (2000).

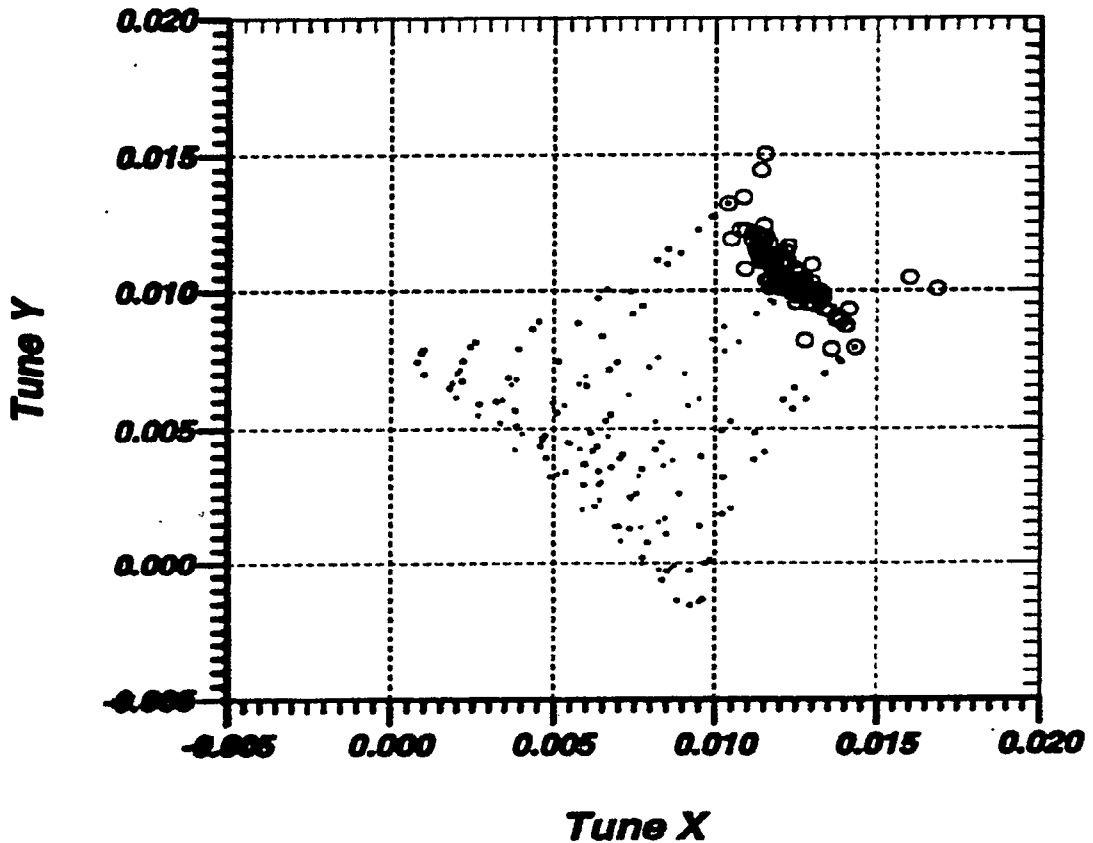
**Vladimir Shiltsev**

**Fermilab / Beams Division**

# ***Compensation of Beam-Beam Effects in Tevatron with Electron Beams: R&D Status and Plans***

1. Introduction: overview of beam-beam compensation with electron beams
  
2. Electron lens experiment:
  - a) goals
  - b) schedule
  - c) design parameters
  
3. Electron beam studies in the Linac lab:
  - a) prototype set-up
  - b) magnetic field
  - c) electron beam

## Tune spread in the $\bar{p}$ beam for TEV33



**Tune spread in the  $\bar{p}$  beam for the TEV33 Tevatron upgrade [P.Badley, *et. al*, 1996]. Large circles are for tunes of core particles in 121 antiproton bunches. Small circles are tunes of non-zero betatron amplitude particles in some bunches.**

$\Delta\nu_{\bar{p}} \approx 0.02$  is about the maximum experimentally achieved value for hadron colliders

→ enhanced diffusion due to high order resonances, increased background, limit on the beam lifetime and luminosity.

**Can these beam-beam effects be corrected?**

**Goal #1: Compensation of bunch-to-bunch tune spread with time variable "electron lens"**

**Goal #2: Compensation of nonlinear beam-beam effects with "electron compressor"**

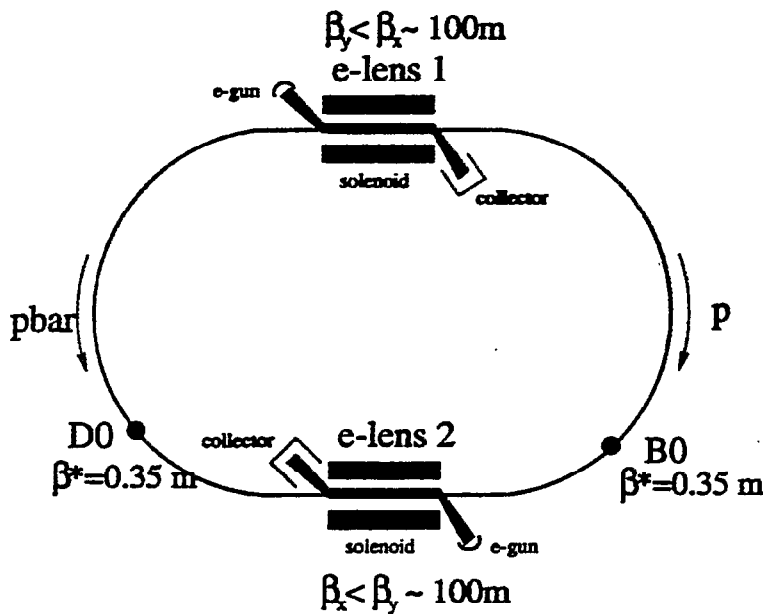
**Goal #3: Beam dynamics studies, TMCI in the Tevatron, TEL as a diagnostics tool, etc.**

# Linear Electron Lens

The linear electron beam lens can compensate the bunch-to-bunch tune spread in the  $\bar{p}$  beam by the electron current variation in time. For a round, constant density electron beam with total current  $J$ , radius  $a$ , and interacting with antiprotons over length  $L$  the tune shifts are

$$\xi_z^e = -\frac{\beta_z (1 + \beta_e)n_e L r_{\bar{p}}}{2 \gamma_{\bar{p}}} = -\frac{\beta_z (1 + \beta_e) J L r_{\bar{p}}}{2\pi e \beta_e c a^2 \gamma_{\bar{p}}}$$

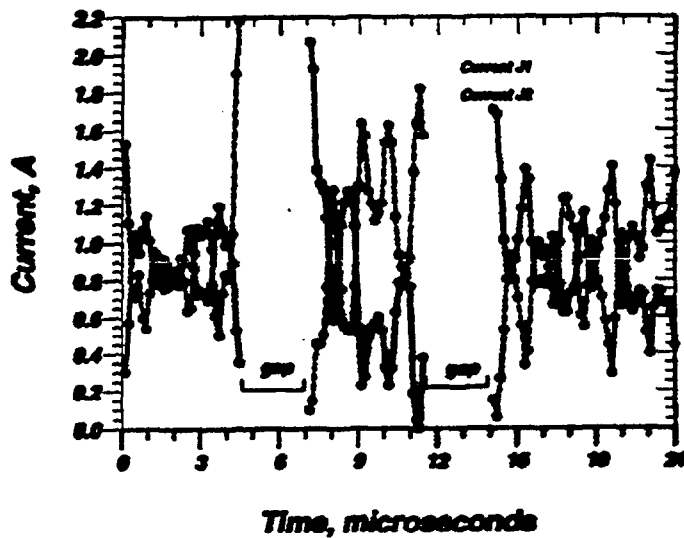
For example the beam with  $J \approx 3.7$  A,  $L = 2$  m,  $a = 1.5$  mm, 10 kV ( $\beta_e = 0.2$ ) gives  $\xi^e \approx -0.01$  in the Tevatron  $\gamma_p \approx 1066$ ,  $\beta_z = 100$  m.



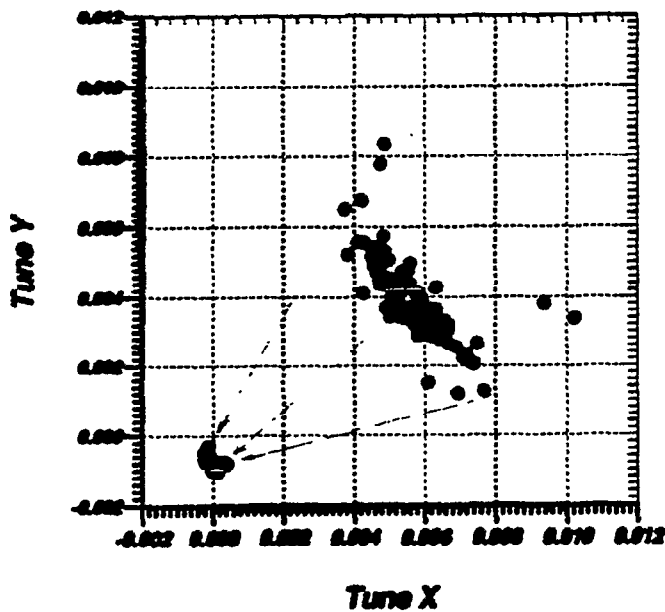
Tevatron layout with two electron lenses. Two electron lenses installed in locations with different  $\beta_x/\beta_y$  allows to compensate both  $x$  and  $y$  bunch-to-bunch tune spread.

The electron lens should be installed so that a) e-beam does not interact with proton beam; b) beta-functions are high enough so the electron current density is reasonable; c) dispersion function is small enough.

## Linear compensation of the bunch to bunch tune spread

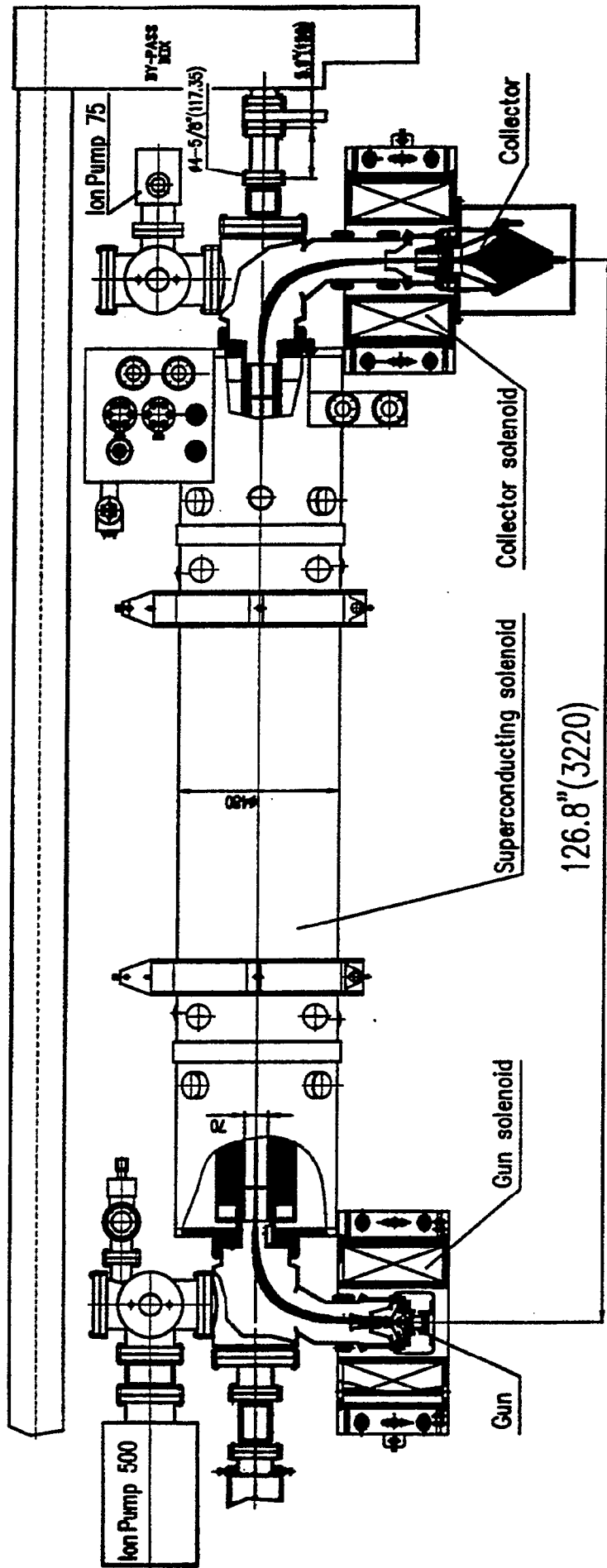


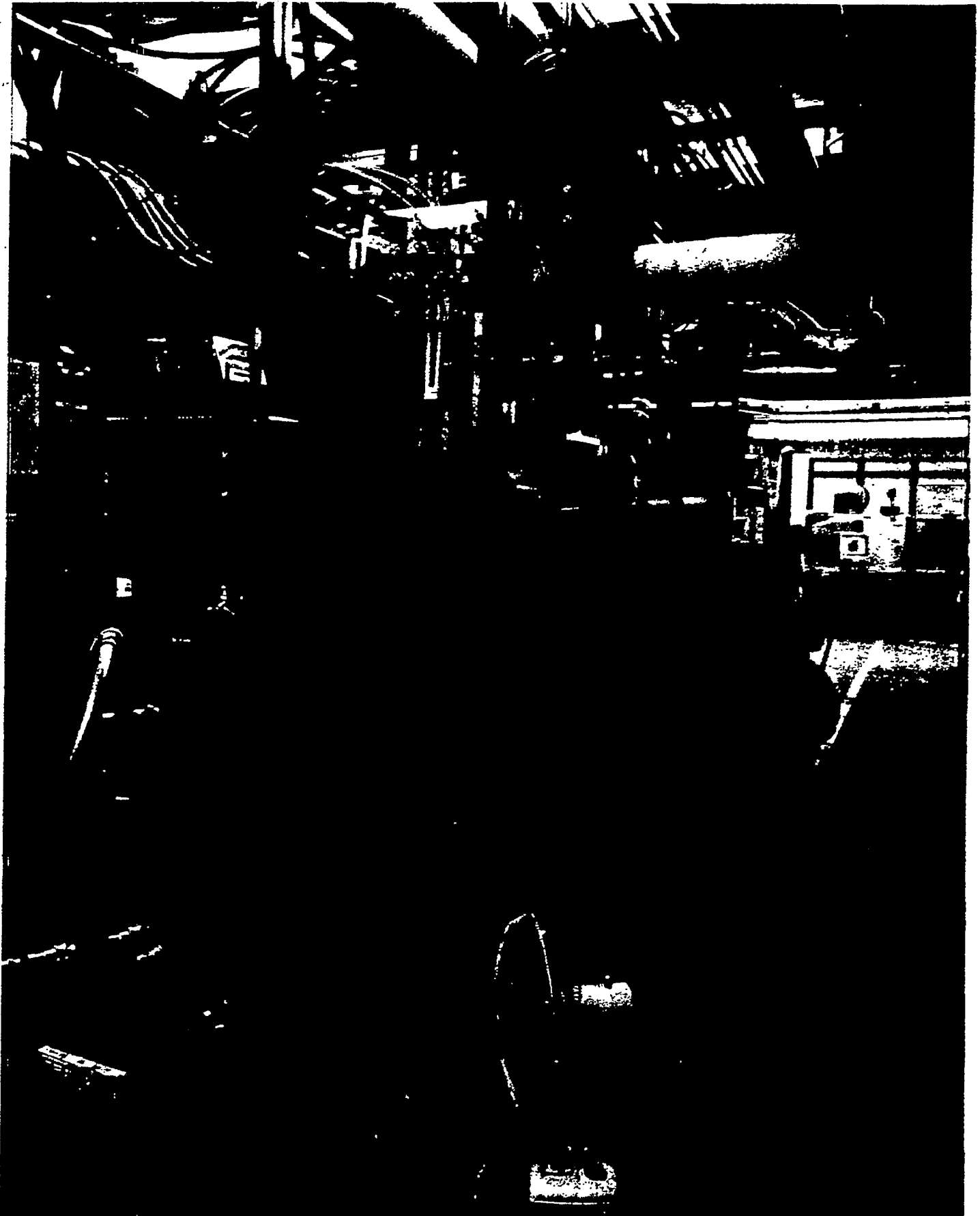
Currents in the two electron lenses to compensate the bunch-to-bunch tune spread in the  $140 \times 121$  bunches scenario.



The initial 121  $\bar{p}$  bunch tunes (core particles only) and the resulting bunch tunes assuming a 10% compensation error.

# Tevatron Electron Lens





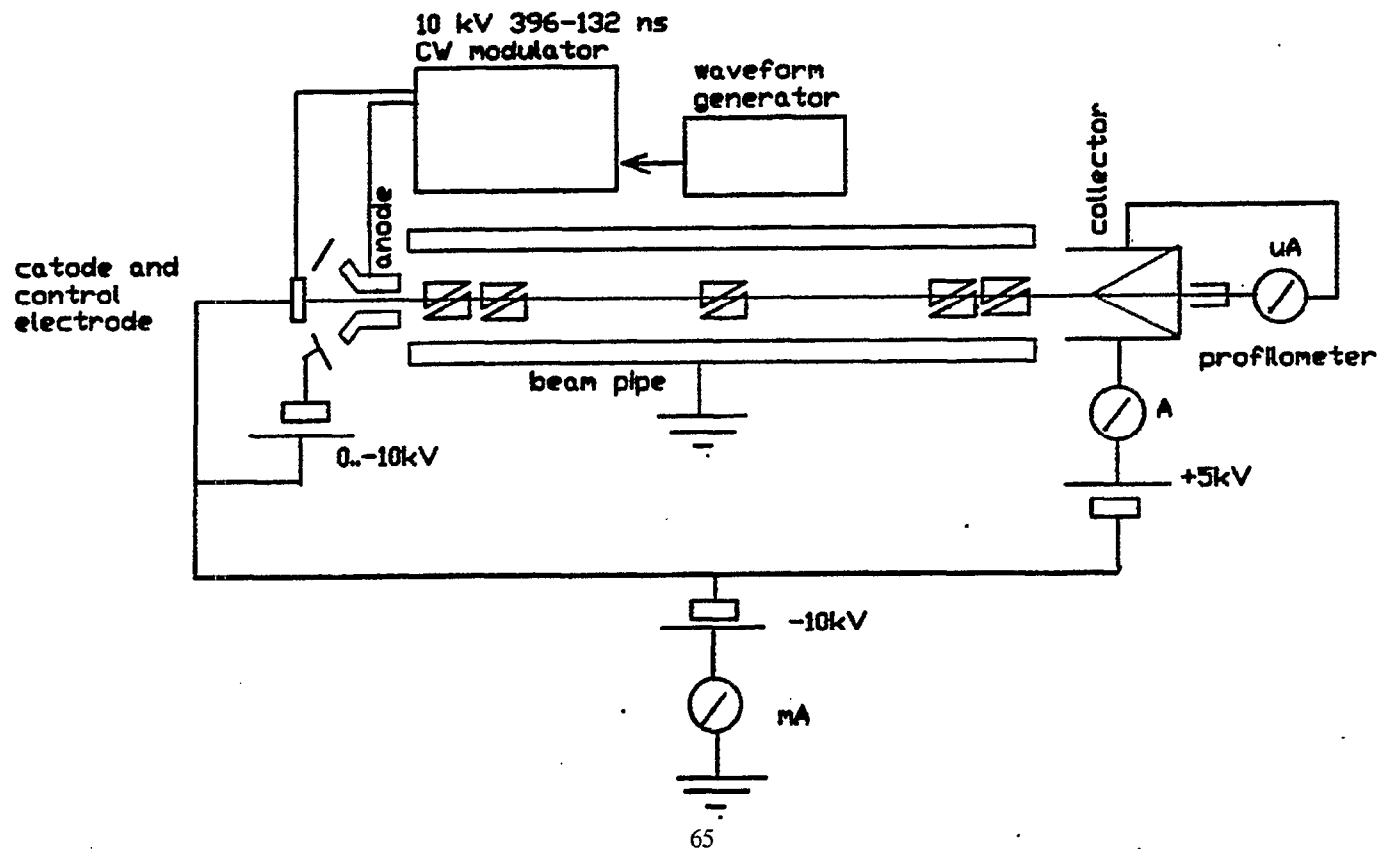
## Electron lens

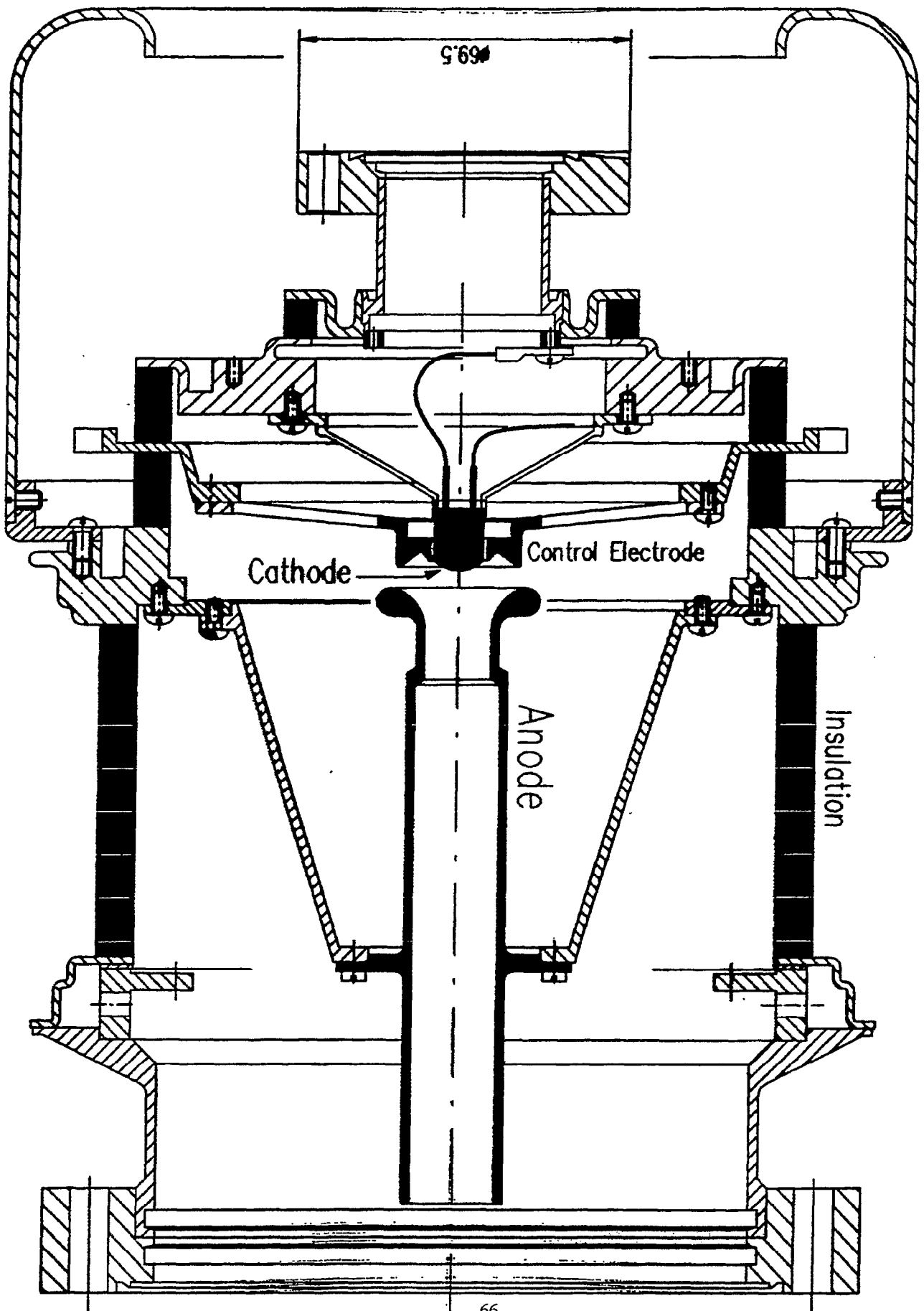
	<b>Linac Lab prototype</b>	<b>Tevatron 1<sup>st</sup> e-lens</b>
<b>main solenoid length</b>	<b>1.96 m</b>	<b>2.50 m</b>
<b>total length</b>	<b>3.26m</b>	<b>3.67 m (v-v)</b>
<b>configuration</b>	<b>straight</b>	<b>2 bends</b>
<b>e-energy</b>	<b>7-20 kV</b>	<b>10-15 kV</b>
<b>max e-current</b>	<b>3A (DC), 12A(pulsed)</b>	<b>2-8 A</b>
<b>current stability</b>	<b>&lt;0.1%</b>	<b>&lt;0.1%</b>
<b>current modulation</b>	<b>160 ns</b>	<b>396 (132) ns</b>
<b>cathode radius</b>	<b>5 mm.</b>	<b>5 mm</b>
<b>e-beam radius</b>	<b>2.5-5 mm</b>	<b>1-2 mm</b>
<b>area compression</b>	<b>upto 4</b>	<b>10-25</b>
<b>B field solenoid/gun</b>	<b>4/1 kG</b>	<b>50/2 kG</b>
<b>B straightness, rms *</b>	<b>0.05 mm**</b>	<b>0.05 mm</b>
<b>beam shape control</b>	<b>yes</b>	<b>yes</b>
<b>vacuum</b>	<b>&lt;10<sup>-7</sup> Torr</b>	<b>&lt;10<sup>-9</sup> Torr</b>

\* over 80 % of length

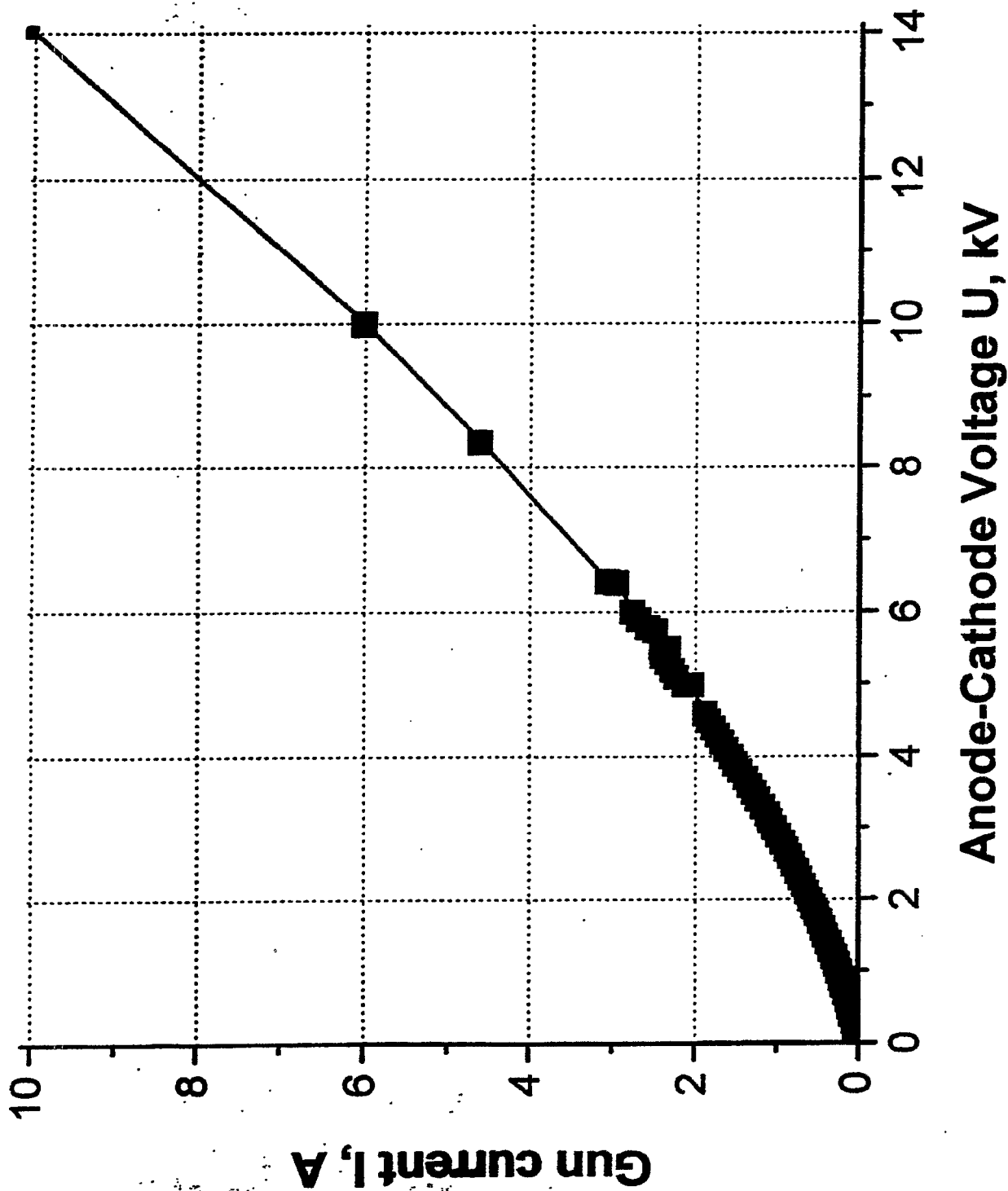
\*\* 0.005 mm with use of corrector coils

# TEL Electric Circuit

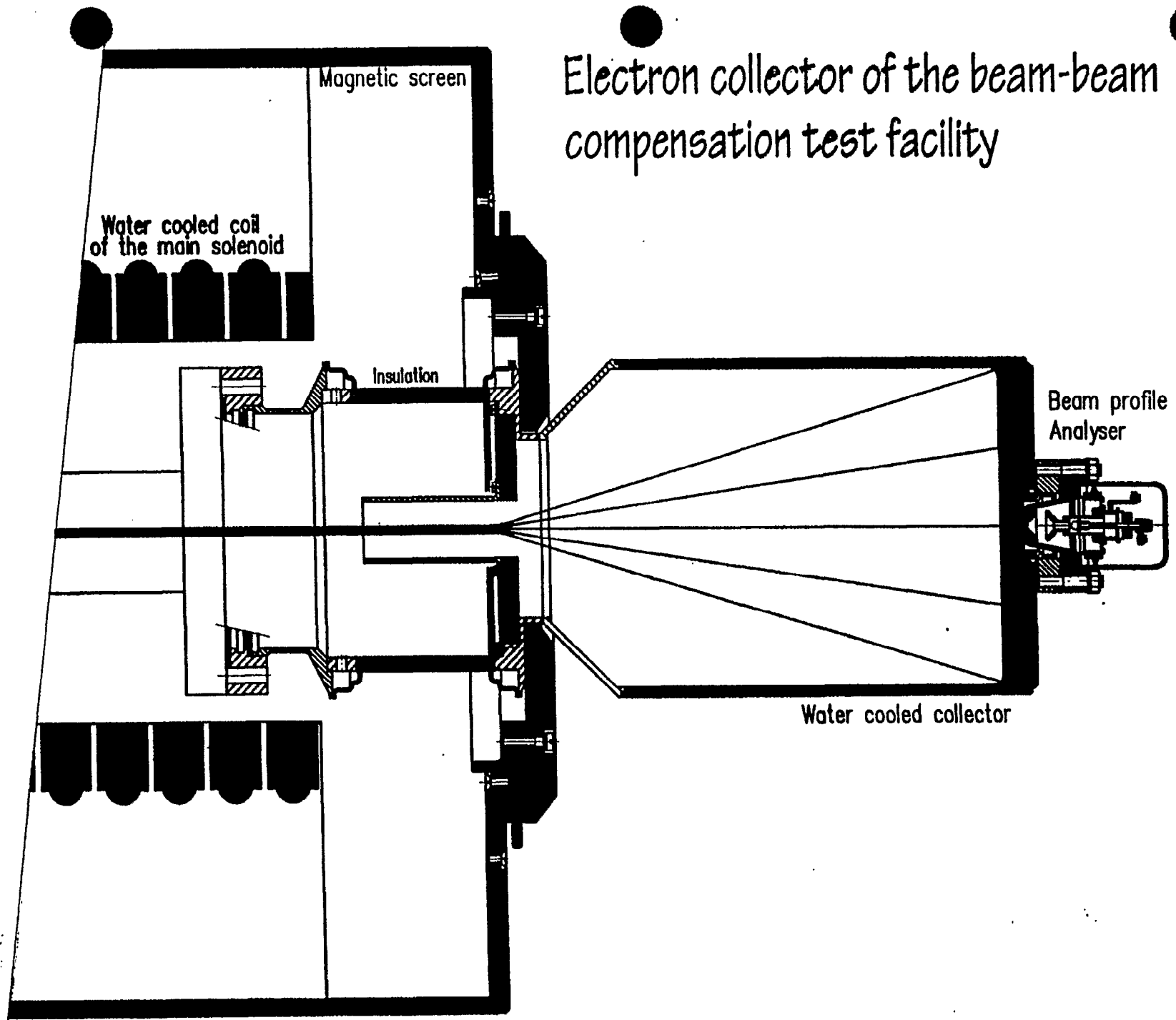




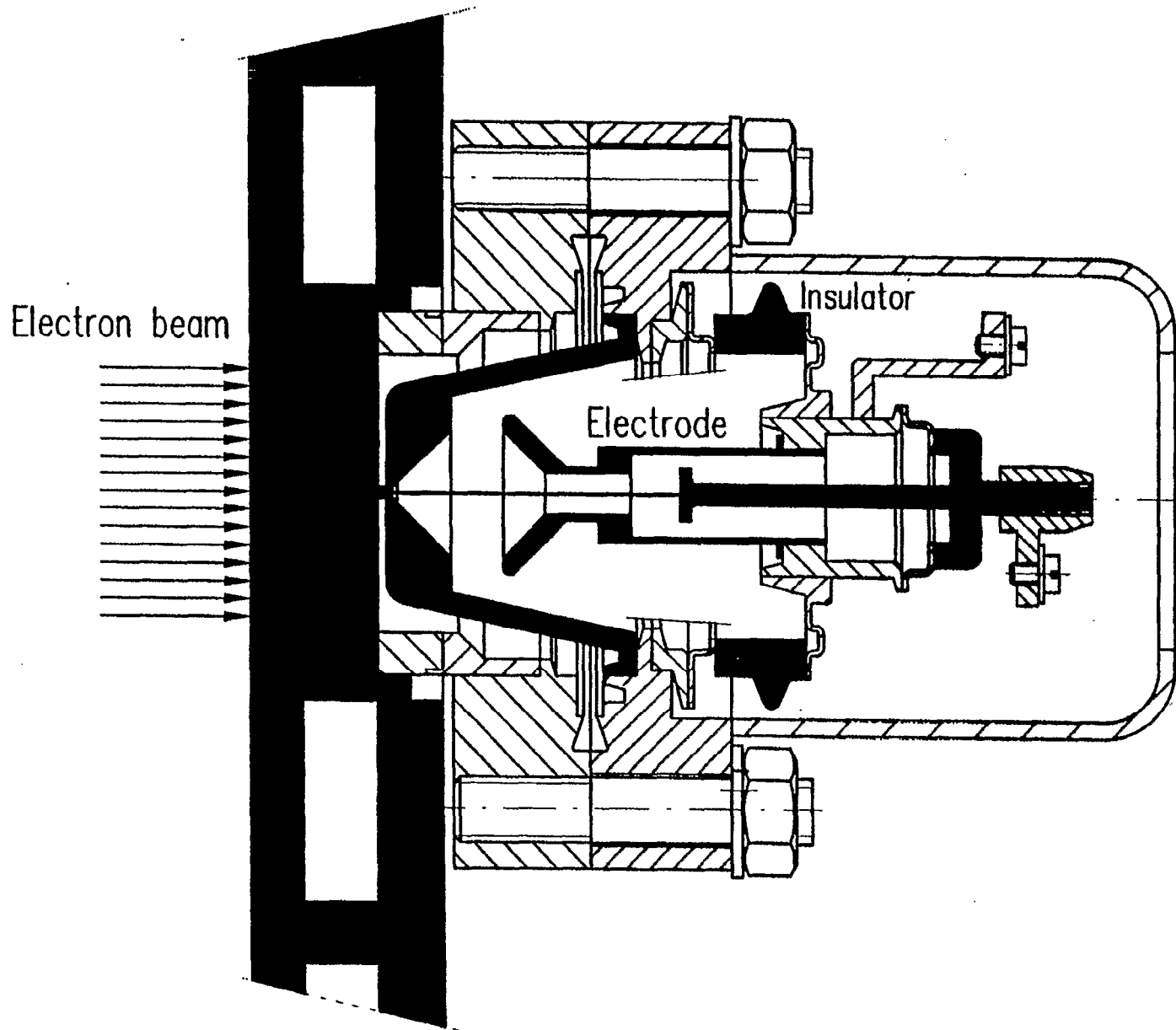
TEL e-Gun Current vs Voltage:  $I = 5.9 \mu A * U^{(3/2)}$



# Electron collector of the beam-beam compensation test facility

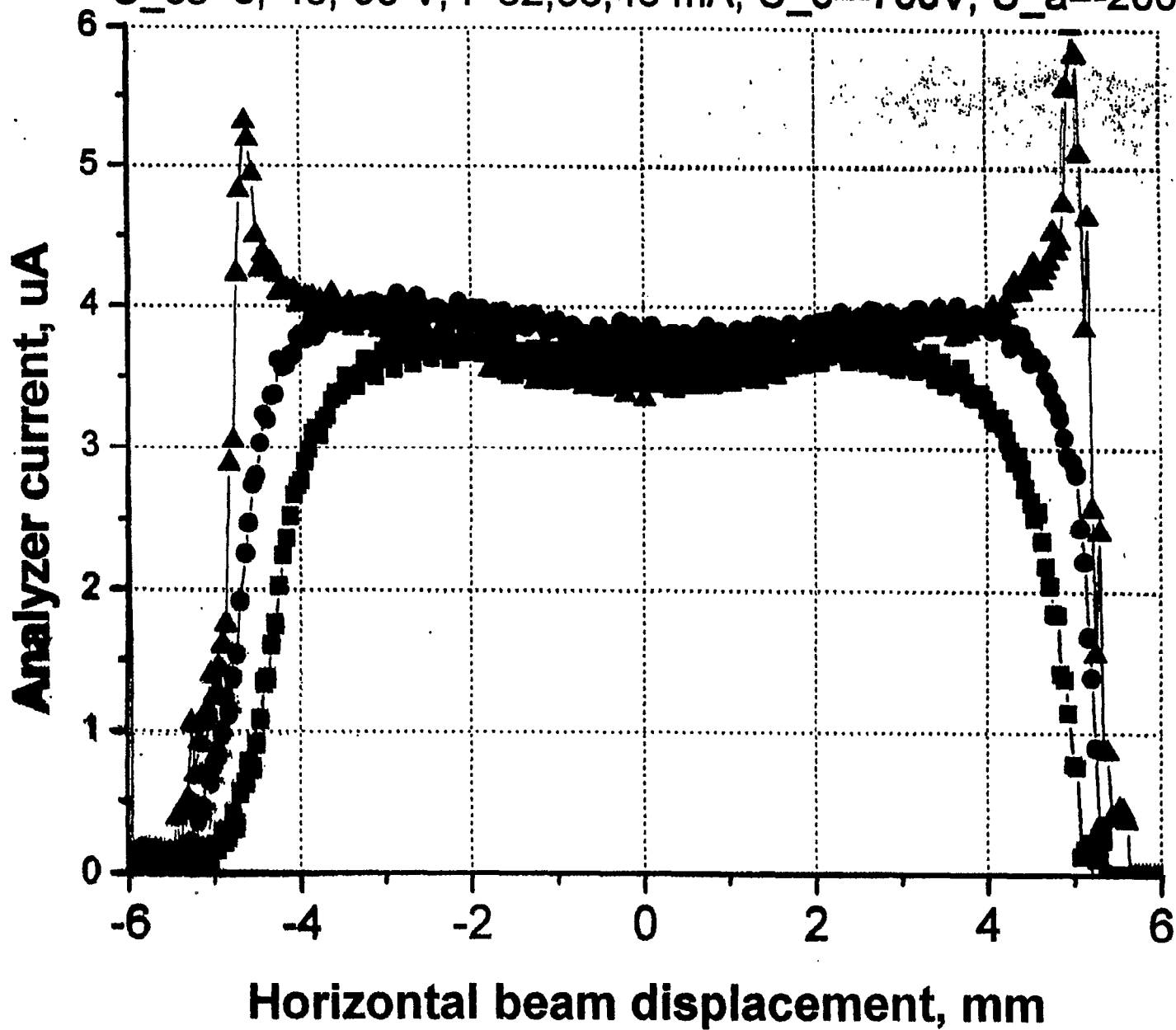


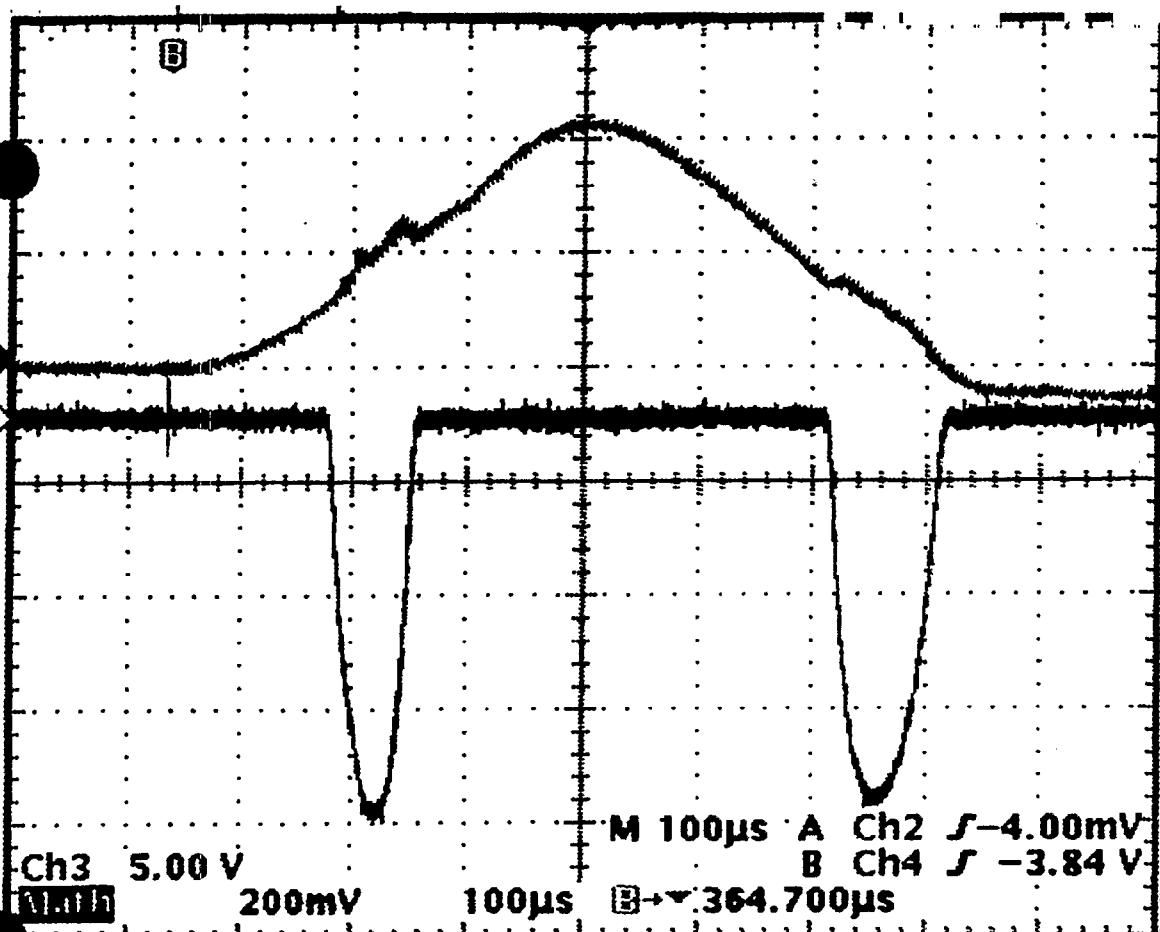
# Beam temperature and profile analyser



# Beam profile vs control voltage

$U_{ce}=0, -45, -90$  V,  $I=62, 56, 46$  mA;  $U_c=-700$ V,  $U_a=-200$ V





**Save Waveform**

 **To File**

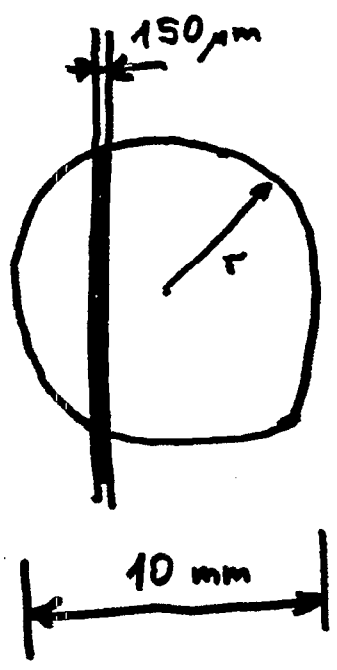
**To Ref1**  
23-Nov-1999  
12:07:24

**To Ref2**  
---

**To Ref3**  
---

**To Ref4**  
---

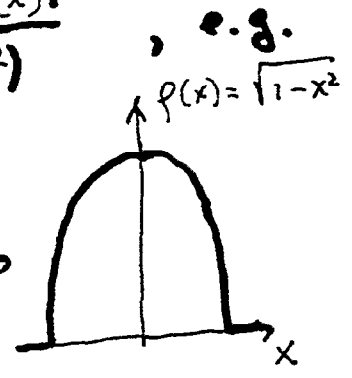
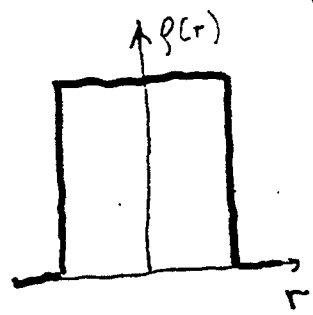
Save Current Setup    Recall Saved Setup    Recall Factory Setup    **Save Waveform**    Recall Waveform    File Utilities



We measure  $p(x)$

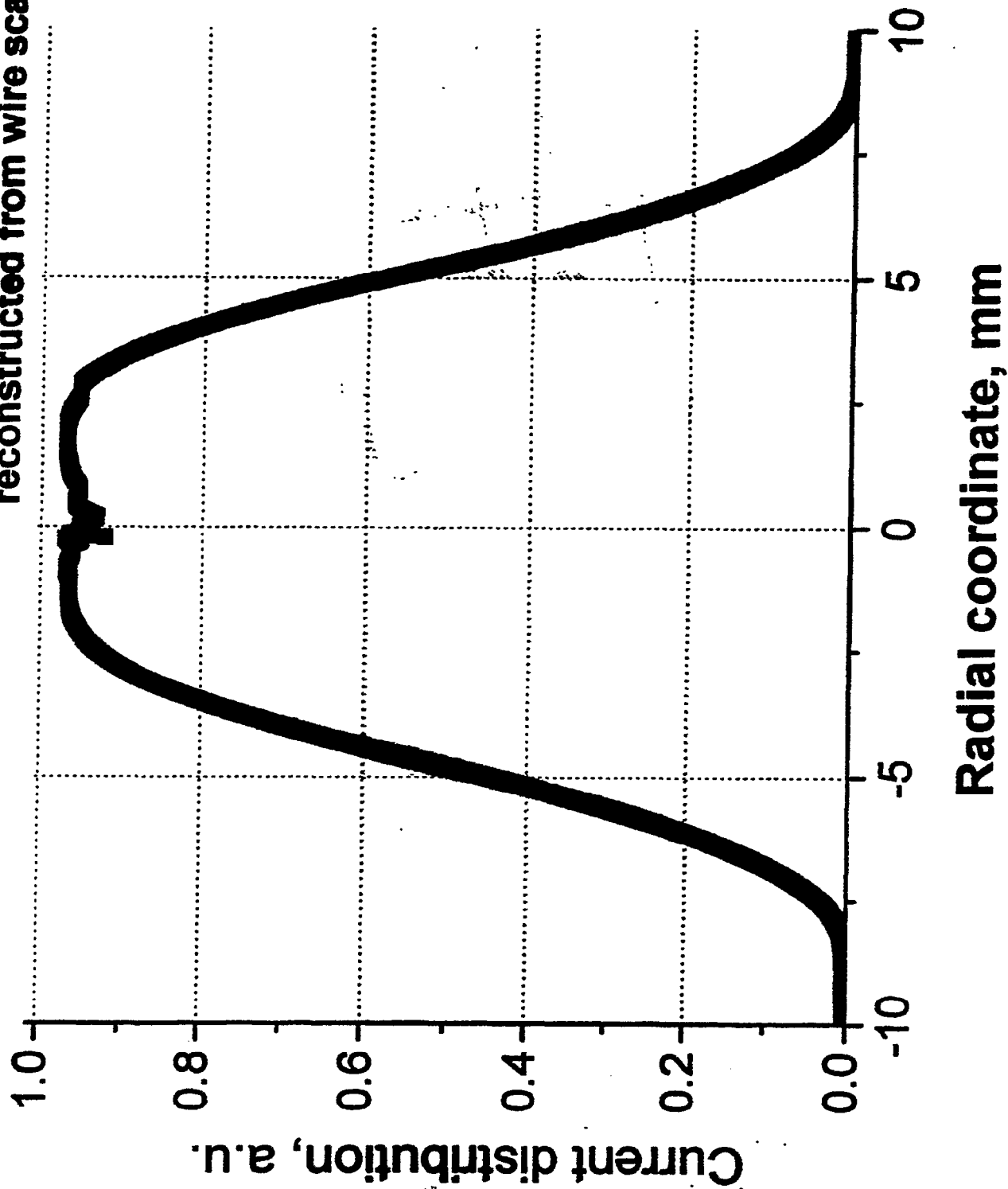
if  $p(x,y) = p(r)$ ,  $r = \sqrt{x^2 + y^2}$

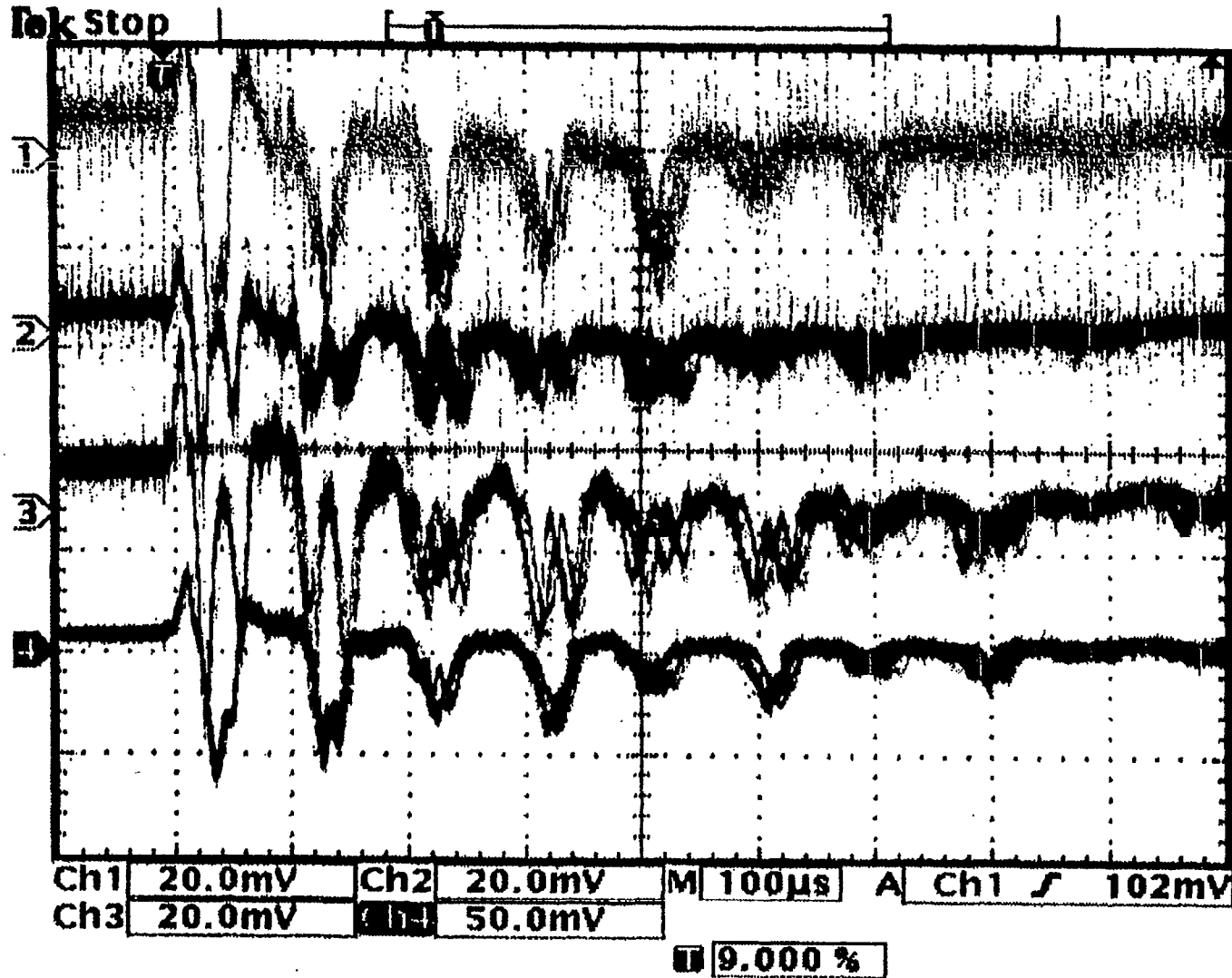
$$p(r) = -\frac{d(p^2(x))}{d(x^2)}$$



# 0.5 A electron beam current density profile

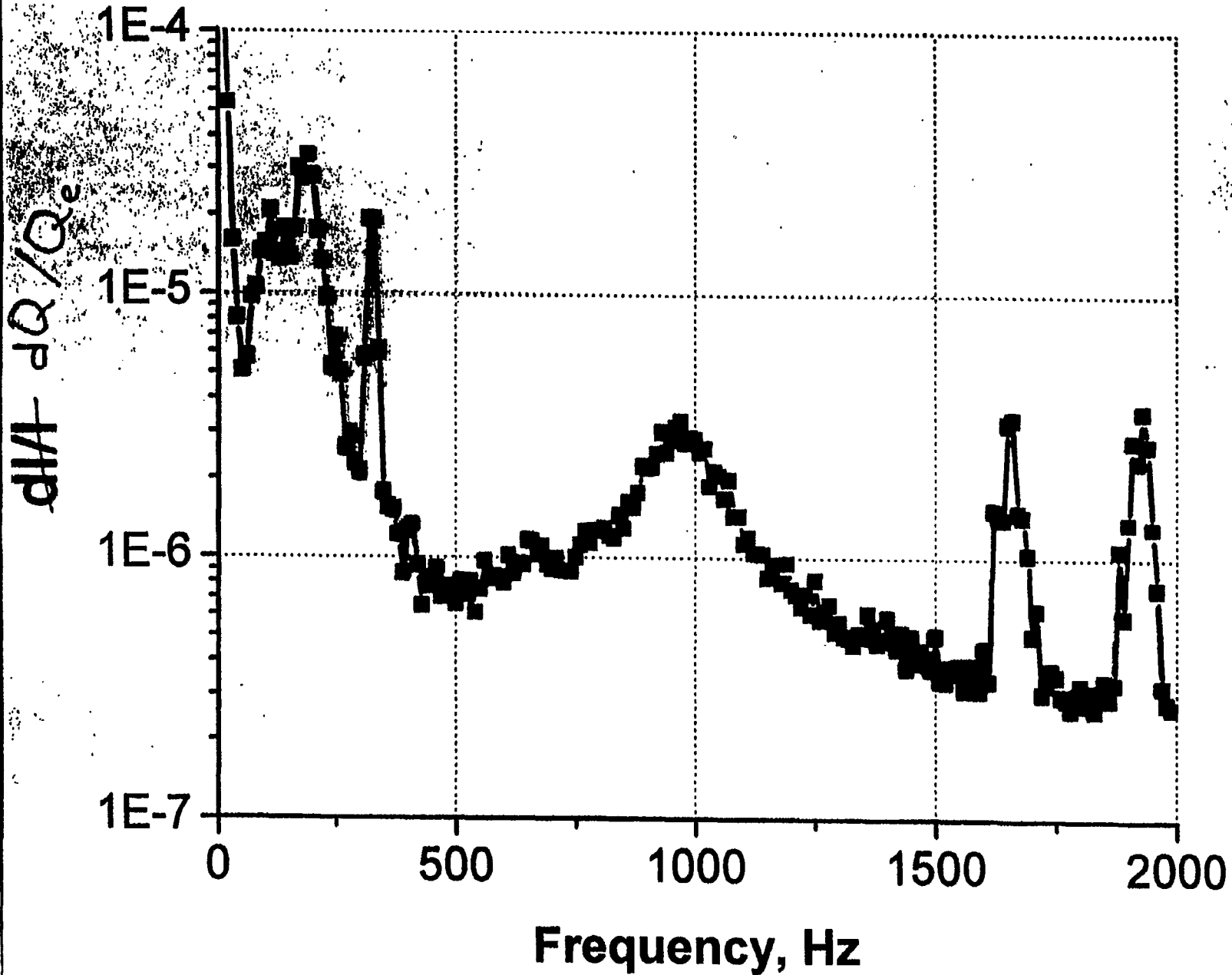
reconstructed from wire scan



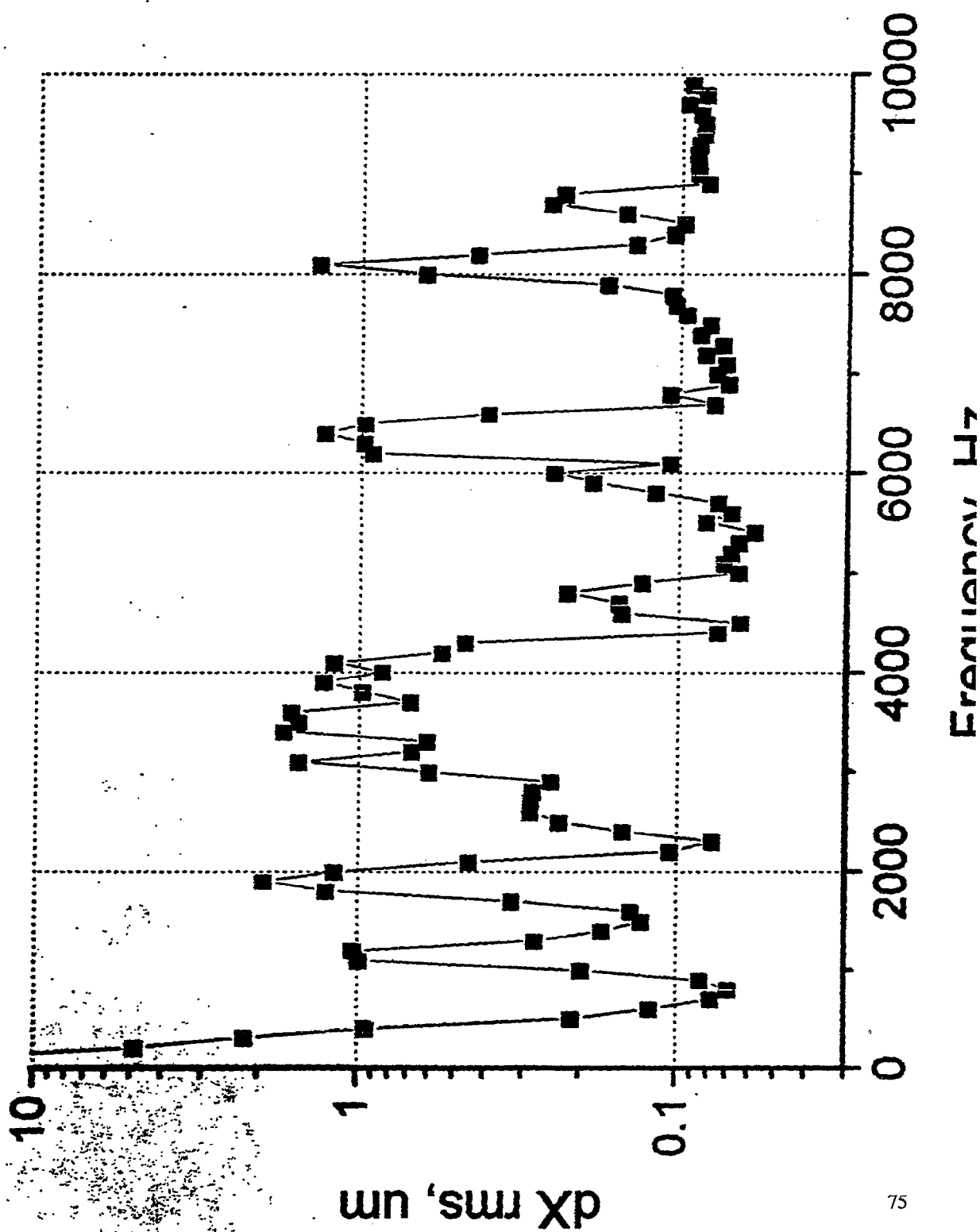


**Large amplitude waves in ion column around 0.1A electron beam:  
 1,2,3,4 – “sum” pick-up electrode signals along 2 m long system,  
 $u = \omega_p a (\ln(b/a)/2)^{1/2} \approx 4 \text{ cm}/\mu\text{s} \rightarrow 1.4 \cdot 10^{10} \text{ ions/m} \rightarrow 17\% \text{ Q-compensation}$**

Spectrum of <sup>charge</sup> ~~current~~ fluctuations in 1 A e-beam

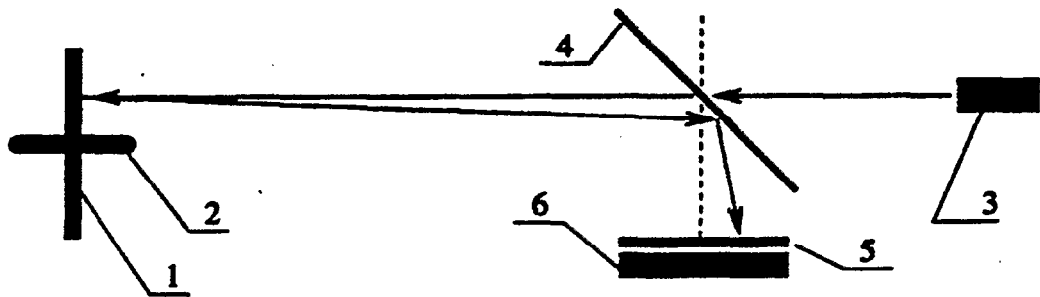


# Spectrum of vertical motion of 0.9 A electron beam

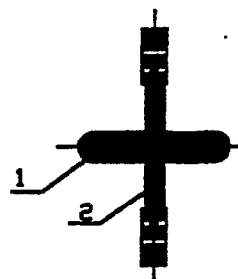
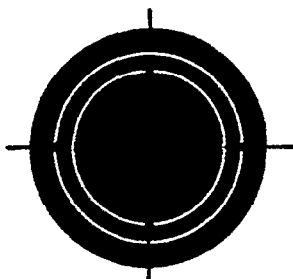


## Magnetic field straightness in the e-lens

Magnetic field in the e-lens should be straight with accuracy  $\sim 1 - 2 \cdot 10^{-4}$  rad.



Scheme of magnetic field straightness measurements. 1 and 2 – mirror with magnetic arrow, 3– diode laser, 4– beam splitter, 5– optical filter, 6– Position Sensitive Device.



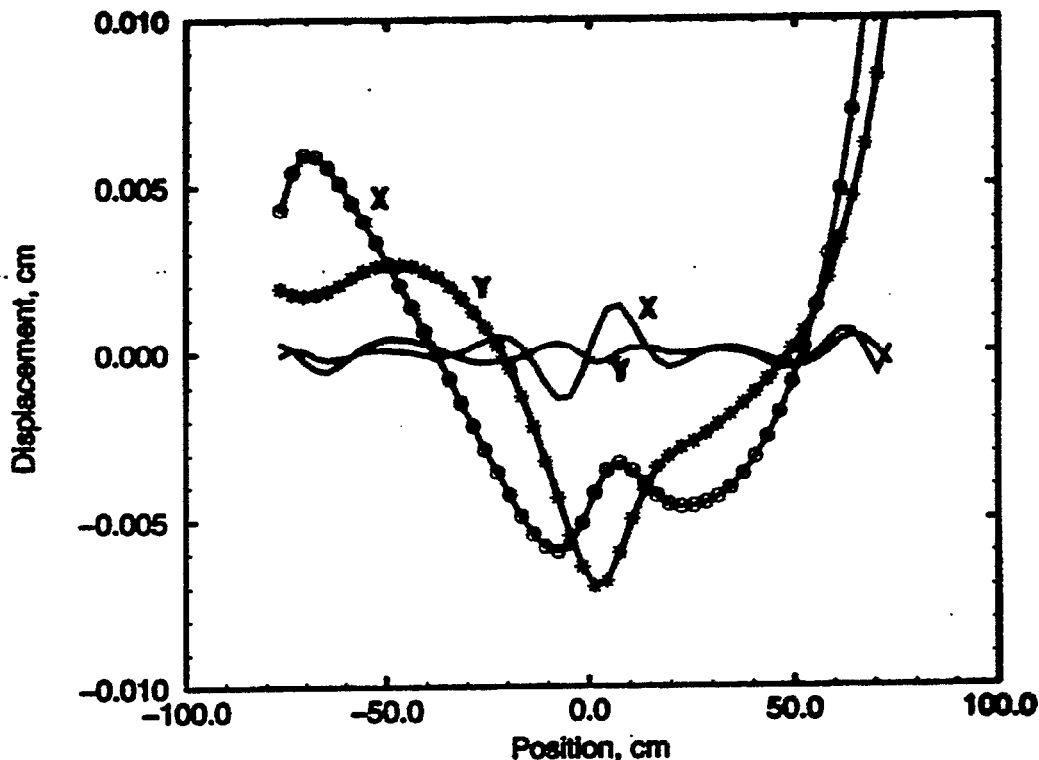
The probe allowed to measure the direction of magnetic field is a flat mirror with an attached magnetic arrow wich has 2 degrees of freedom.

Here 1– arrow, 2– reflective surface.

The precision of the method is  $\alpha_{\text{rms}} \approx 1.5 \times 10^{-4} (1\text{kG}/B)^2$  in low fields with saturation of the arrow at  $B \sim 1.5$  kG. The precision in a higer field of about 4 kG is  $\sim 10-20 \mu\text{rad}$ .

## Magnetic field alignment

Deviation of the electron trajectory (i.e. of the magnetic field line) from the straight line in the "electron lens" should be  $\Delta x_e \lesssim 0.1\alpha$  that is about 0.01 cm.



Deviation of the magnetic field line in the main solenoid of the electron lens prototype without (stars and circles) and with (lines) simulated correction by dipole coils.

The field deviation was measured optically, using a magnetic arrow attached to the mirror which has two rotational degrees of freedom.

# Beam-Beam Compensation Project

## **Summary of accomplishments to date:**

### 1. LINAC LAB:

a) Electron lens prototype in the Linac lab provided some 1000 Ampere-hours of operational experience.

b) We achieved e-beam currents of 3A DC, 5A in pulsed regime 50 kHz rep rate, and 12 A maximum in pulsed regime. That exceeds BBCompensation requirements.

c) Experimentally demonstrated that multi-Ampere electron beams can very stable. High-frequency fluctuations of the electron current can be less than 0.01%. Beam transverse position jitter is some microns. That's better than B.B.Compensation criteria.

d) We have designed, fabricated and tested a number of electron beam diagnostic tools, including ion/electron clearing electrodes, BPMs and low-noise electronics, "staying wire" beam profile monitor.

## 2. TEVATRON ELECTRON LENS:

a) we have designed TEL magnetic system in collaboration with IHEP, Protvino and assured it fits Tevatron infrastructure and safety requirements. Fabrication of the magnetic system is underway in IHEP, Protvino and to be finished in June 2000.

b) 50 kW collector and 8 A electron gun designs are finished. Fabrication started.

c) preparations of the E4R building for the TEL test experiments has been started.

## Near future plans:

- a) finish design and fabrication of the TEL vacuum chamber, beam diagnostics.
- b) finish fabrication of the full scale HV modulator (400 ns, 10 kV CW).
- c) after getting SC solenoid magnet – perform full scale test in E4R building (June-Dec 00)
- d) install the 1<sup>st</sup> TEL at F48

e) Tevatron beam studies:

Plan PB: TEL with  $I=0A$  does not make any harm (vacuum, orbit, QPS)

Plan A: single bunch operation, demonstration of  $dQ=-0.01$

Plan AA: 36 bunch operation @Run II  
 $dt < 400ns$ ,  $dQ = -0.01$

after that decision about the 2<sup>nd</sup> TEL will be made

## BEAM-BEAM STUDIES AT RHIC\*

V. Ptitsin, BNL, USA

### 1 RHIC BEAM-BEAM COLLISIONS

In this talk we discuss possible beam-beam studies that could be done at the RHIC collider. These studies are not only interesting for the understanding of the RHIC operational limits, but also for the operation of future hadron colliders, like the LHC. These studies could verify predictions of analytical calculations and beam-beam simulations, especially in the strong-strong regime.

The RHIC collider is suited for beam-beam experiments, both in the strong-weak and the strong-strong regime. Tab. 1 shows the basic parameters for gold and proton operation at injection and storage energy. The collider consists of two rings which intersect at six interaction points, where equal species collide head-on. Outside the interaction regions the beams are separated in the horizontal plane. Separation is achieved through DX and D0 magnets (see Fig. 1).

During the first years of operation, RHIC will use 60 bunches in each ring. Future upgrade scenarios include up to 360 bunches per ring. With 60 bunches there is enough longitudinal spacing between consecutive bunched so that no parasitic beam-beam collisions occur in the interaction regions. With the increase of the number of bunches to 180 or more a crossing angle up to 1.3 mrad would be required to reduce the effects of parasitic collisions [1].

With the moderate values of the beam-beam parameter  $\xi$  we expect that the beam-beam interaction would not be a dominant effect, especially for gold-gold collisions. On the other hand, beam-beam effects should be observable.

### 2 DIAGNOSTIC AND CONTROL TOOLS

To carry out studies, a set of tools and instruments is necessary for the control and measurement of beam parameters. The basic manipulation required for beam-beam studies is to bring the two beams in and out of collision. This can be done longitudinally and transversely. The transverse orbit control should also provide the ability for a precise change of the beam crossing angle at the interaction point.

In RHIC a crossing angle up to 1.3 mrad can be created through the DX and D0 magnets. Precise interaction point orbit separation and angle control is done by using orbit bumps of 4 interaction region dipole correctors. These horizontal and vertical interaction region bumps will be used to maximize the collider luminosity. The beam-beam separation at the interaction point can be performed with a step

size of 0.02mm. The maximum beam separation that can be obtained through bumps is 9.4mm at the top energy.

The orbit position and angle at the RHIC interaction points can be extracted using the measured beam positions at the DX beam position monitors (see Fig. 1). These dual-direction, dual-plane BPMs are located at both sides of the interaction points. The relative precision of BPM measurements reaches 0.01mm.

The following list presents other beam instrumentation that is useful for beam-beam studies at RHIC:

- A tune meter and Schottky system for the measurement of betatron tunes, tune spread and other beam oscillation modes.
- A tune meter kicker to excite bunches with a single kick or multiple kicks.
- A Ionization Profile Monitors (IPM) for the measurement of the transverse beam profiles. When fully commissioned the IPM can measure individual bunches turn-by-turn.
- A beam current transformer to measure the total beam current and a wall current monitor to measure the current per bunch.
- A Zero Degree Calorimeter for luminosity measurements and optimization.

### 3 POSSIBLE BEAM-BEAM EXPERIMENTS AND STUDIES

The following list of the beam-beam studies is proposed to be carried out at RHIC. Some of them might be important to better understand and improve the RHIC operation while others are of a more theoretical interest.

#### *Weak-strong beam-beam studies:*

- The observation of diffusion caused by the beam-beam interaction. This can be done using the beam size measurements from the ionization profile monitor. In gold operation, this effect will be difficult to detect due to intra-beam scattering.
- The measurement of beam-beam caused tune spread and tune dependence on betatron amplitude  $Q(J)$ . This should follow measurements of amplitude dependent tune shift from nonlinear magnetic effects.

\* Work performed under the auspices of the US Department of Energy.

Table 1: Basic RHIC parameters.

	Au injection	Au top	p injection	p top
Z	79	79	1	1
A	197	197	1	1
$\beta^*$ (m)	10	1	10	1
$Q_{x,y}$	29.18/28.19	29.18/28.19	29.18/28.19	29.18/28.19
$N_b$	$10^9$	$10^9$	$10^{11}$	$10^{11}$
$\gamma$	12.6	108	31.2	268
$\sigma_t$ (m)	0.88	0.17	0.5	0.09
$\Delta p/p$ ( $10^{-3}$ )	0.74	0.64	0.51	0.34
95% $\epsilon_N$ ( $\pi$ mm-mrad)	10	10-40	20	20-30
$\sigma^*$ (mm)	1.15	0.124	1.07	0.112
$\xi$	0.0012	0.0012	0.0037	0.0037

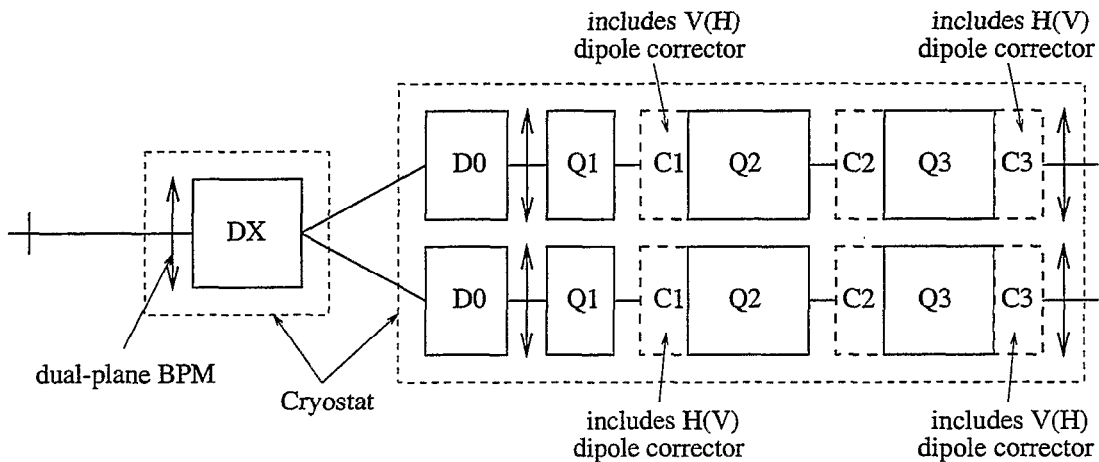


Figure 1: Half side of an RHIC interaction region from the top. DX separates the beams initially and D0 further. Q1,Q2,Q3 are quadrupoles, C1,C2,C3 are multi-layer corrector packages.

- Beam-beam effects as a function of the betatron tunes. Horizontal and vertical betatron tunes can be scanned easily.
- The measurement of the effect of parasitic beam collisions. This can be done with beam separation at 1 or 2 interaction points with the help of the orbit separation bumps [2]. Up to  $10\sigma$  separation is required to approximate the conditions of the LHC.
- The study of synchro-betatron resonances caused by the crossing angle. The effect should be noticeable when the crossing angle  $\alpha$  is of the order of the ratio of the transverse and longitudinal beam sizes. Required crossing angles are:  
 $\alpha/2 = 1.2\text{mrad}$  (storage RF system, top energy)  
 $\alpha/2 = 0.6\text{mrad}$  (acceleration RF system, injection energy)  
 The second option requires the smaller crossing angle that can be created by DX,D0 magnet adjustment.
- The studies of the beam-beam effect with unequal beam emmitances to verify SPS results.
- The observation of whether and how beam-beam collisions affect the beam polarization. This can be done with intense polarized proton beam at injection.

#### Strong-strong beam-beam studies:

- The observation of coherent beam-beam mode tunes. The tune meter kicker can be used to excite coherent beam motion. The Schottky monitor could detect coherent modes. These studies probably require the corresponding betatron tunes in two ring to be equal within 0.002.
- In case the coherent modes are observed, they could be used to optimize beam-beam head-on collisions [3].
- The measurement of beam-beam coherent modes as a function of the betatron tune split between the two

rings. This could test the idea that the coherent motion would be decoupled between two beams with an increase of the tune split [4].

- The study of the coherent modes dependence on the beam separation (long-range interactions) modes.
- The study of the closed orbit distortion by long range beam-beam interactions.

The last two items might have a special interest for the LHC project where the parasitic long-range beam-beam interaction provides the considerable contribution to beam-beam effects.

Some of the studies can be done parasitically at the polarized proton run. With the beam of protons containing many bunches in one ring and few bunches (1-3 bunches) in another ring, only few bunches of polarized beam would be affected by beam-beam interactions.

#### 4 SUMMARY

- We expect that the RHIC nominal operation would not be strongly affected by beam-beam effects, especially in gold-gold collisions. This need to be confirmed by operational experience.
- RHIC is equipped with a variety of diagnostic and control tools that are sufficient for effective beam-beam studies and experiments.
- We are open to and encourage collaboration in this area.

#### 5 REFERENCES

- [1] S. Peggs, RHIC/AP/169
- [2] W. Fischer, F. Zimmerman, RHIC/AP/179
- [3] Suggested and considered for RHIC by W. MacKay and A. Drees
- [4] A. Hoffman, LHC Beam-Beam Workshop, 1999.

Talk dates back to 11/90

US-LHC Collaboration Meeting: Accelerator Physics Experiments for Future Hadron Colliders, BNL, 2000

# Local, Linear, Transverse Coupling in Storage Rings

Peter Bagley, Fermilab

Work was done at CESR, Cornell Univ.

Dave Rubin

Michael Billings

Raphael Littauer

## My main references

Edwards and Teng

Parametrization of Linear Coupled Motion  
in Periodic Systems

IEEE Trans. on Nuc. Sci. Vol NS-20 No 3 June 1973

Peggs

Coupling and Decoupling in Storage Rings

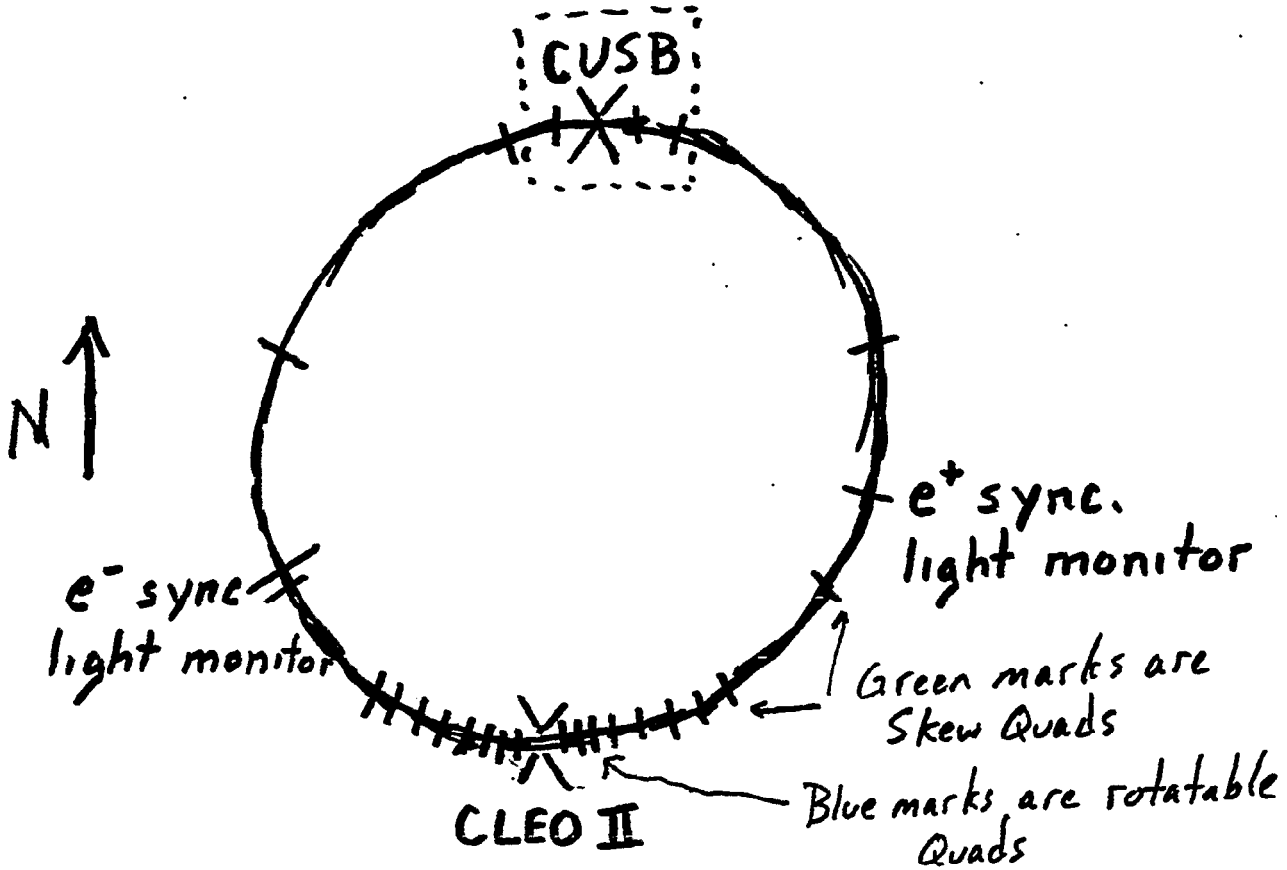
IEEE Trans. on Nuc. Sci. Vol NS-30, No. 4, Aug. 1983

The Projection Approach to Solenoid Compensation  
Particle Accelerators 1982, Vol. 12 pp. 219-229

Billing

The Theory of Weakly Coupled Transverse Motion  
in Storage Rings

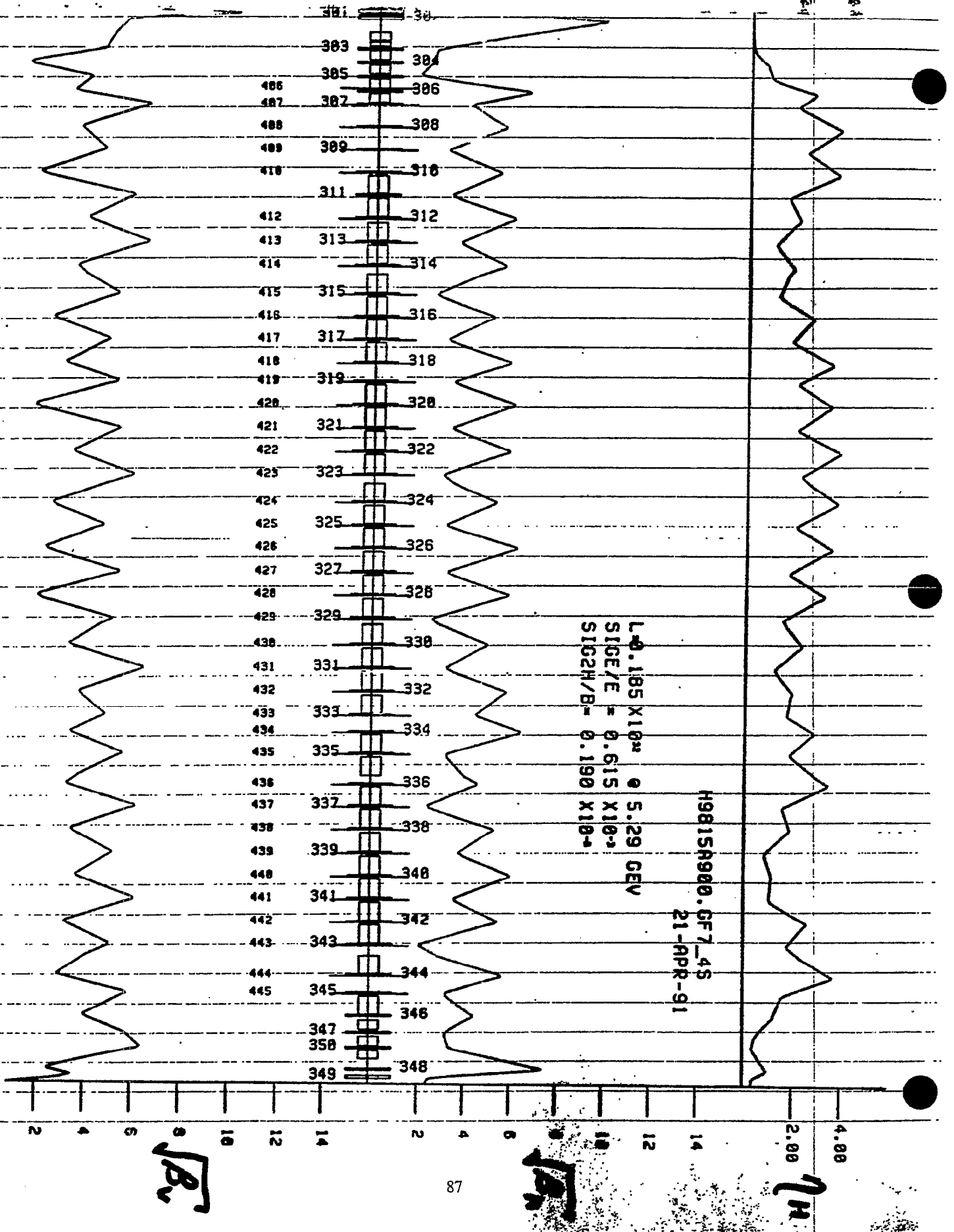
CESR Note CBN85-2



Circumference = 768. m

$e^+e^-$  storage ring

$\Upsilon$  energy region  
( $\sim 5$  GeV/beam)



ETA= VERT HORIZ ETA LUMINOSITY NU CHROMATICITY PAGE # 09:19 21-APR-91  
 0.0158 1.0902 0.004 0.1052E+32 VERT 9.0514 -24.74 SIG2H/B 0.10900E-00 ALP/P 0.015094 H0815A000.GF7\_4S  
 0.4746 5.6019 0.301 0.1464E+31 HORIZ 0.6971 -10.06 SIGE/E 0.01494E-03 CIRC 708.42003M

REA: IR1 LARGE APERTURE IR1 UPTO NORMAL RF STRAIGHT NORMAL LATTICE IR2 LARGE APERTURE GEV= 5.2090  
 PER V 72.642 1ST 351 49.093 1ST 307 30.134 1ST 309 49.545 1ST 350 31.474 1ST 349 MEV/TURN 1.0200  
 ETA V 103.010 1ST 351 41.492 1ST 307 20.845 1ST 309 41.183 1ST 350 12.144 1ST 349 PARTIC /BUNCH 0.1315E+12  
 PER H 90.231 1ST 302 70.001 1ST 308 74.347 1ST 310 78.610 1ST 322 75.522 1ST 348 LIMIT L0  
 ETA H 97.910 1ST 302 42.092 1ST 203 27.823 1ST 310 40.701 1ST 334 54.703 1ST 348 POLIZ 100.3 MIN  
 ETA 0.019 1ST 302 3.701 1ST 300 3.001 1ST 310 3.794 1ST 322 0.950 1ST 348 NBUNCHES= 1  
 3D,EVEN # SEXT STRENGTHS= -0.2193 0.1016

adiation integral values:[wigglers on] I1=0.1235E+02 I2=0.1002E+00 I3=0.2007E-02 I4=0.3039E-02 I5=0.5905E-03 U0= 1.1047  
 H>[at wigglers]= 0.4400E+00 Emittance=0.2448E-00 [Averages at RF] Sv=15.9504E Sh=17.8941E Ets= 3.0303E

104 201 103 0/ 110 351 111 301 112 302 113 203 114 204 115 303 116  
 02 400 101 304 102 202 400 101 305 102 202 400 101 306 102 202 124 307 407 117 110 308 408 109 309 409 109 310 410 1 311  
 1 312 412 120 1 313 413 1 314 414 121 1 315 415 1 316 416 1 317 417 1 318 418 105 319 419 1 320 420 1 321 421 1  
 22 422 1 323 423 122 1 324 424 1 325 425 1 326 426 126 1 327 427 1 328 428 120 1 329 429 123 1 330 430 120 1  
 31 431 1 332 432 120 1 333 433 100 334 434 134 201 103 335 435 139 201 103 135 336 436 130 201 103 337 437 1 338 438 120 1  
 39 439 1 340 440 1 341 441 1 342 442 1 343 443 150 208 151 344 444 127 128 345 445 104 208 151  
 40 400 153 200 145 347 140 207 107 350 147 203 143 141 340 148 349 140/

301	0.6000	-0.428000	334	0.6000	0.211503	201	0.57273	07.89150	101	0.71230	134	0.50030
302	0.9500	0.524700	335	0.6000	-0.102031	202	3.23049	31.65434	102	0.49515	135	2.61376
303	0.6000	-0.270000	336	0.6000	0.220000	203	2.94526	140.62640	103	0.15714	136	0.60354
304	0.6000	0.421200	337	0.6000	-0.213221	204	1.64350	07.89150	104	0.07304	105	0.00000
305	0.6000	-0.379400	338	0.6000	0.209000	200	3.20000	07.89150	105	5.37000	139	1.02550
306	0.6000	0.388270	339	0.6000	-0.102000	207	3.17612	34.81710	106	0.50175	140	2.03000
307	0.6000	-0.295172	340	0.6000	0.102159	208	0.57104	50.00320	107	0.50175	141	1.71999
308	0.6000	0.103343	341	0.6000	-0.203077	109	7.30945		108	0.04000	142	0.50000
309	0.6000	-0.250077	342	0.6000	0.230529	110	0.64000		109	0.30070	143	1.05200
310	0.6000	0.210000	343	0.6000	-0.100000	111	0.30070		110	0.55930	145	0.00300
311	0.6000	-0.241999	344	0.6000	0.202020	112	0.55930		111	4.05370	146	1.10504
312	0.6000	0.100555	345	0.6000	-0.219200	113	0.37721		112	0.60947	147	0.79013
313	0.6000	-0.190217	346	0.6000	0.100000	114	0.60947		113	0.23530	148	2.02000
314	0.6000	0.199337	347	0.6000	-0.055174	115	0.23530		114	5.70945	149	0.00000
315	0.6000	-0.200940	348	0.6000	0.530000	116	5.70945		115	1.60000	150	3.04500
316	0.6000	0.227703	349	0.9500	-0.590407	117	1.60000		116	0.18200	151	0.18200
317	0.6000	-0.202147	350	0.6000	-0.105151	118	0.46000		117	0.18200	152	5.73981
318	0.6000	0.229979	351	1.2200	-0.037000	120	0.22500		118	0.18200	153	1.32000
319	0.6000	-0.209400				121	1.92000		119	0.18200		
320	0.6000	0.207700				122	2.00000		120	0.46000		
321	0.6000	-0.204381				123	1.00000		121	0.22500		
322	0.6000	0.210370				124	0.29001		122	0.20000		
323	0.6000	-0.215007				126	0.22500		123	1.00000		
324	0.6000	0.200019				127	2.39981		124	0.29001		
325	0.6000	-0.270373				128	3.34000					
326	0.6000	0.225074										
327	0.6000	-0.301110										
328	0.6000	0.241073										
329	0.6000	-0.245740										
330	0.6000	0.217103										
331	0.6000	-0.201900										
332	0.6000	0.102235										
333	0.6000	-0.107200										

US-LHC Collaboration Meeting: Accelerator Physics Experiments for Future Hadron Colliders, BNL, 2000

## Global Decoupling Recipe

1) Use normal (upright) quads to bring the tunes together.

Typically there is a minimum tune split

2) Use skew quads to make the tunes equal

3) Use normal (upright) quads to return to the operating point.

Can also measure and correct  $\eta_v$ , but

$\eta_v$  is also generated by vertical bends

No information about skew quads where  $\eta_h$  is small.

# Problems with Global Decoupling

It is not sensitive to  $(\varphi_A + \varphi_B)$  coupling

component.

Not unique. Can typically use any of several SQ's.

Measurement is not made at the operating point.

Minor concerns

When return to the operating pt., change the  $(\varphi_A - \varphi_B)$  component.

Global Decoupling is not defined unless the machine is on the difference resonance.

Depends on how the machine is brought to the difference resonance.

Machine can be globally decoupled and still have a large  $\sigma_v$ . (local coupling)

Another analogy:

global decoupling  $\iff$  correcting the tune

local decoupling  $\iff$  correcting the  $\beta$ 's

$\implies$  Global Decoupling is still a very useful procedure. If the operating point is near the difference resonance can quickly and easily greatly reduce the coupling.

# Decomposition of Full Turn Transfer Matrix into Normal Modes

$$T = \begin{pmatrix} M & n \\ m & N \end{pmatrix} = V U V^{-1}$$

$$= \begin{pmatrix} \gamma I & C \\ -C^+ & \gamma I \end{pmatrix} \begin{pmatrix} A & 0 \\ 0 & B \end{pmatrix} \begin{pmatrix} \gamma I & -C \\ C^+ & \gamma I \end{pmatrix}$$

where  $\gamma^2 + \det C \equiv 1$   $\gamma \approx 1$  usually

$$C = \begin{pmatrix} C_{11} & C_{12} \\ C_{21} & C_{22} \end{pmatrix} \Rightarrow C^+ = \begin{pmatrix} C_{22} & -C_{12} \\ -C_{21} & C_{11} \end{pmatrix}$$

$$A = \begin{pmatrix} \cos 2\pi\nu_A + \alpha_A \sin 2\pi\nu_A & \beta_A \sin 2\pi\nu_A \\ -\gamma_A \sin 2\pi\nu_A & \cos 2\pi\nu_A - \alpha_A \sin 2\pi\nu_A \end{pmatrix}$$

and similarly for B

$$W = \begin{pmatrix} a_A \sqrt{\beta_A} \cos \varphi_A \\ -\frac{a_A}{\sqrt{\beta_A}} (\sin \varphi_A + \alpha_A \cos \varphi_A) \\ a_B \sqrt{\beta_B} \cos \varphi_B \\ -\frac{a_B}{\sqrt{\beta_B}} (\sin \varphi_B + \alpha_B \cos \varphi_B) \end{pmatrix} = V^{-1} \begin{pmatrix} x \\ x' \\ y \\ y' \end{pmatrix} = V^{-1} \begin{pmatrix} x \\ x' \\ y \\ y' \end{pmatrix}$$

The matrix  $V$  translates from the normal mode coordinates to the horizontal and vertical coordinates.

This is true for energy displacements also

$$\begin{pmatrix} \eta_A \\ \eta'_A \\ \eta_B \\ \eta'_B \end{pmatrix} = V^{-1} \begin{pmatrix} \eta_x \\ \eta'_x \\ \eta_y \\ \eta'_y \end{pmatrix} = \begin{pmatrix} \delta I & -C \\ C^+ & \delta I \end{pmatrix} \begin{pmatrix} \eta_x \\ \eta'_x \\ \eta_y \\ \eta'_y \end{pmatrix}$$

Given the normal mode dispersions and twiss parameters, the normal mode emittances may be calculated from the usual recipe (as per Sands).

Actually must be careful with damping partition numbers. (Reference Raubenheimer)

PAC Chicago 1989

Separate the dependence on the twiss parameters.

Peggs  $\bar{W} = GW = \begin{pmatrix} G_A & 0 \\ 0 & G_B \end{pmatrix} W = \begin{pmatrix} a_A \cos \varphi_A \\ -a_A \sin \varphi_A \\ a_B \cos \varphi_B \\ -a_B \sin \varphi_B \end{pmatrix}$

where  $G_A = \begin{pmatrix} \frac{1}{\sqrt{\beta_A}} & 0 \\ \frac{\alpha_A}{\sqrt{\beta_A}} & \sqrt{\beta_A} \end{pmatrix}$

and similarly for  $G_B$

$$\bar{V} = GVG^{-1} = \begin{pmatrix} \delta I & G_A C G_B^{-1} \\ -G_B C^+ G_A^{-1} & \delta I \end{pmatrix} = \begin{pmatrix} \delta I & \bar{C} \\ -\bar{C}^+ & \delta I \end{pmatrix}$$

## Relative Phase and Amplitude

Calculate the horz. and vert. motion that results from a coherent excitation of the "A" mode.

Let the initial state be

$$\bar{W}_0 = (a_A, 0, 0, 0)$$

$n$  turns later

$$\varphi_A = 2\pi n \nu_A$$

$$X_n = V W_n = V U^n W_0 = G^{-1} \bar{V} \bar{U}^n \bar{W}_0$$

$$= \underbrace{\begin{pmatrix} \sqrt{B_A} & 0 & 0 & 0 \\ \frac{-\kappa_A}{\sqrt{B_A}} & \frac{1}{\sqrt{B_A}} & 0 & 0 \\ 0 & 0 & \sqrt{B_B} & 0 \\ 0 & 0 & \frac{-\kappa_B}{\sqrt{B_B}} & \frac{1}{\sqrt{B_B}} \end{pmatrix}}_{G^{-1}} \underbrace{\begin{pmatrix} \gamma & 0 & \bar{C}_{11} & \bar{C}_{12} \\ 0 & \gamma & \bar{C}_{21} & \bar{C}_{22} \\ -\bar{C}_{22} & \bar{C}_{12} & \gamma & 0 \\ \bar{C}_{21} & -\bar{C}_{11} & 0 & \gamma \end{pmatrix}}_{\bar{V}} \underbrace{\begin{pmatrix} a_A \cos \varphi_A \\ -a_A \sin \varphi_A \\ 0 \\ 0 \end{pmatrix}}_{\bar{U}^n \bar{W}_0}$$

$$= \begin{pmatrix} \sqrt{B_A} & 0 & 0 & 0 \\ \frac{-\kappa_A}{\sqrt{B_A}} & \frac{1}{\sqrt{B_A}} & 0 & 0 \\ 0 & 0 & \sqrt{B_B} & 0 \\ 0 & 0 & \frac{-\kappa_B}{\sqrt{B_B}} & \frac{1}{\sqrt{B_B}} \end{pmatrix} \begin{pmatrix} a_A \gamma \cos \varphi_A \\ -a_A \gamma \sin \varphi_A \\ -a_A (\bar{C}_{22} \cos \varphi_A + \bar{C}_{12} \sin \varphi_A) \\ a_A (\bar{C}_{21} \cos \varphi_A + \bar{C}_{11} \sin \varphi_A) \end{pmatrix} = \begin{pmatrix} X \\ X' \\ Y \\ Y' \end{pmatrix}$$

$$= G^{-1} \begin{pmatrix} a_A \gamma \cos \varphi_A \\ -a_A \gamma \sin \varphi_A \\ a_A \sqrt{\bar{C}_{12}^2 + \bar{C}_{22}^2} \cos(\varphi_A + \Delta\varphi_A) \\ -a_A \sqrt{\bar{C}_{11}^2 + \bar{C}_{21}^2} \sin(\varphi_A + \Delta\varphi_A + \Delta\varphi_{AY}) \end{pmatrix}$$

# Relative Phase and Amplitude

16

Calculate the horiz. and vert. motion that results from a coherent excitation of the "A" mode.

Let the initial state be

$$\bar{W}_0 = (a_A, 0, 0, 0)^T$$

n turns later  $\varphi_A = 2\pi n z_A$

$$X_n = V W_n = V U^n W_0 = G^{-1} \bar{V} \bar{U}^n \bar{W}_0$$

Define  $\Delta\varphi_A$  so that

$$\cos \Delta\varphi_A = \frac{-\bar{C}_{22}}{\sqrt{\bar{C}_{12}^2 + \bar{C}_{22}^2}} \quad \sin \Delta\varphi_A = \frac{\bar{C}_{12}}{\sqrt{\bar{C}_{12}^2 + \bar{C}_{22}^2}}$$

Then

$$x = a_A \gamma \sqrt{\beta_A} \cos \varphi_A \equiv X_{\text{amp}} \cos \varphi_x$$

$$y = a_A \sqrt{\beta_B} \sqrt{\bar{C}_{12}^2 + \bar{C}_{22}^2} \cos(\varphi_A + \Delta\varphi_A) \equiv Y_{\text{amp}} \cos \varphi_y$$

$$\left(\frac{Y}{X}\right)_A \equiv \frac{Y_{\text{amp}}}{X_{\text{amp}}} = \frac{1}{\gamma} \sqrt{\frac{\beta_B}{\beta_A}} \sqrt{\bar{C}_{12}^2 + \bar{C}_{22}^2}$$

$$(\varphi_y - \varphi_x)_A = \Delta\varphi_A$$

$$\bar{C}_{12} = \gamma \sqrt{\frac{\beta_A}{\beta_B}} \left(\frac{Y}{X}\right)_A \sin \Delta\varphi_A$$

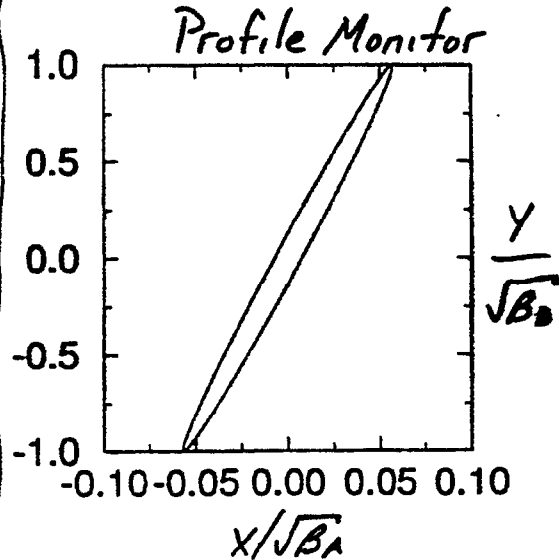
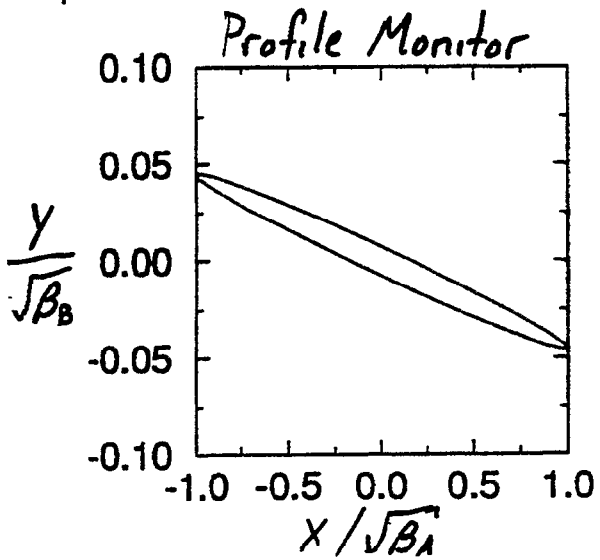
$$\bar{C}_{22} = -\gamma \sqrt{\frac{\beta_A}{\beta_B}} \left(\frac{Y}{X}\right)_A \cos \Delta\varphi_A$$

out of phase  
→ blow up

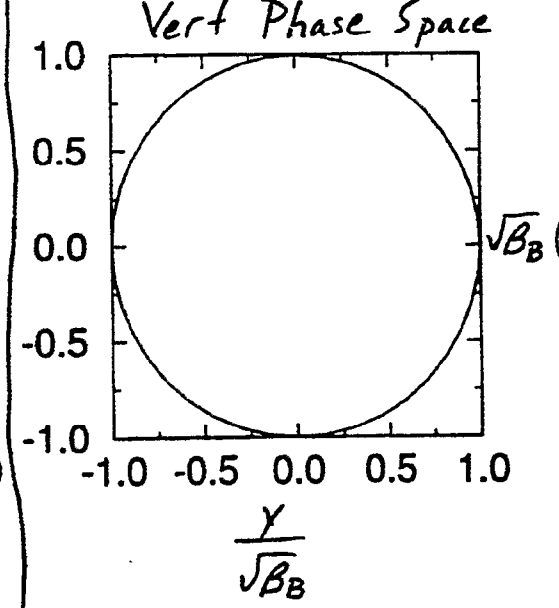
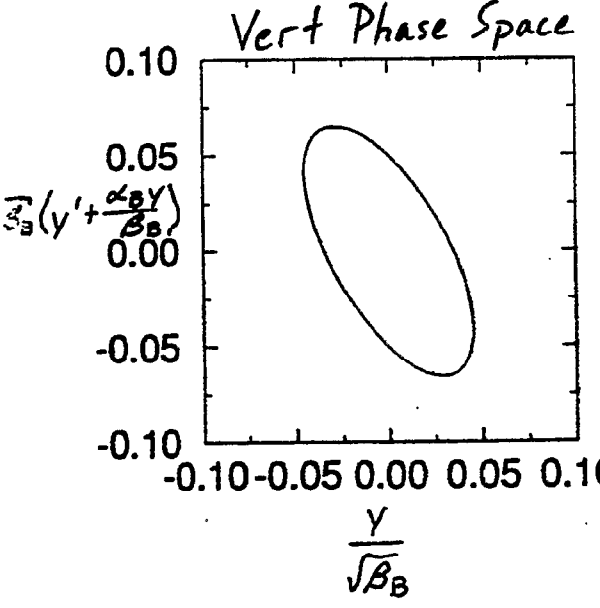
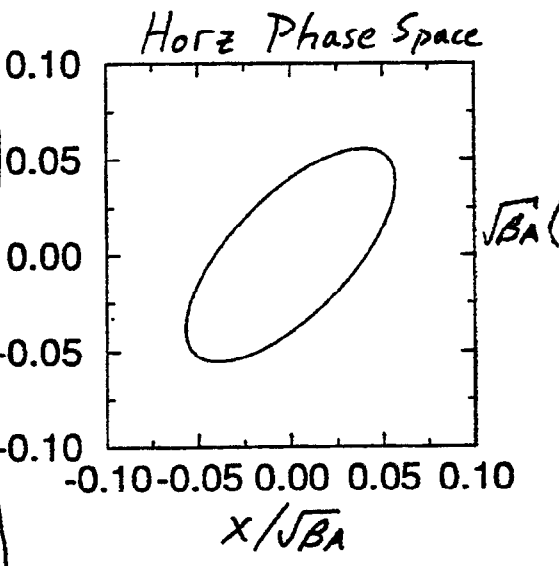
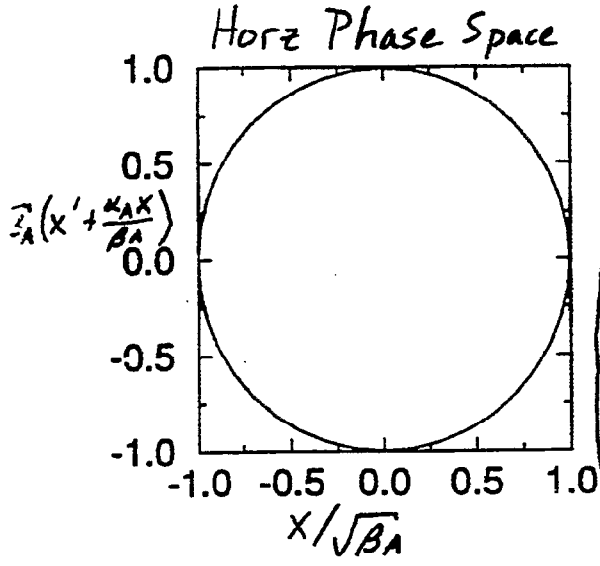
in phase  
→ tilt

# A mode only

# B mode only



$\bar{C}_{11} = .0565$   
 $\bar{C}_{12} = .0075$   
 $\bar{C}_{21} = .0328$   
 $\bar{C}_{22} = .0449$   
 $\gamma = .99885$



Generally must convolute the 2 ellipses.  $\curvearrowright$

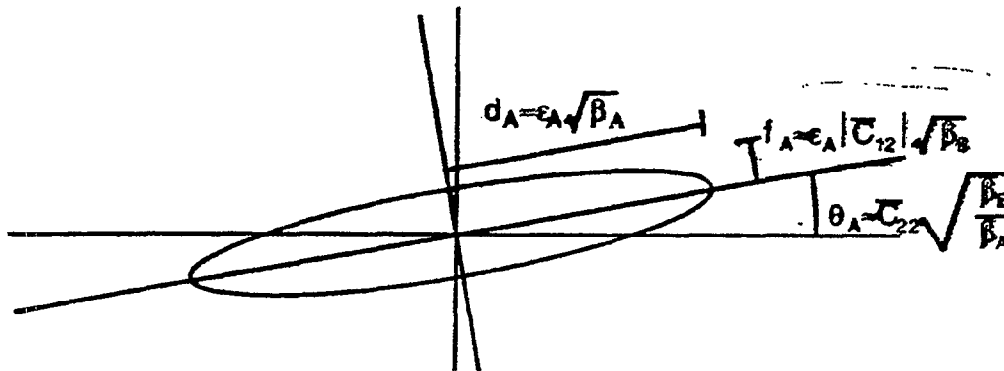


Fig.1A Beam ellipse for weak coupling and the "A" mode excited

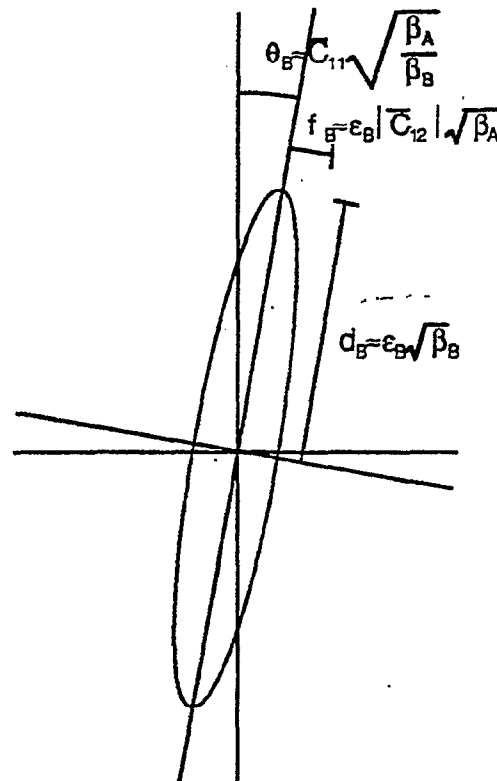


Fig.1B Beam ellipse for weak coupling and the "B" mode excited

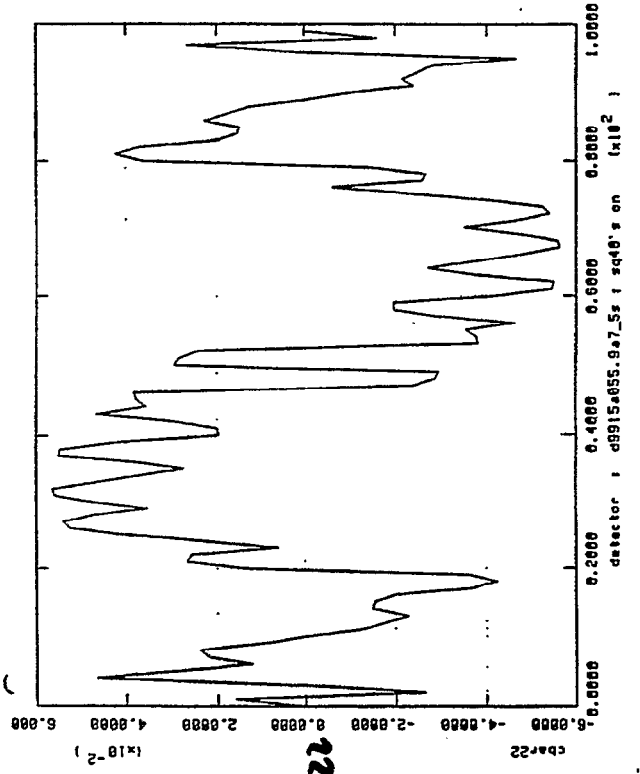
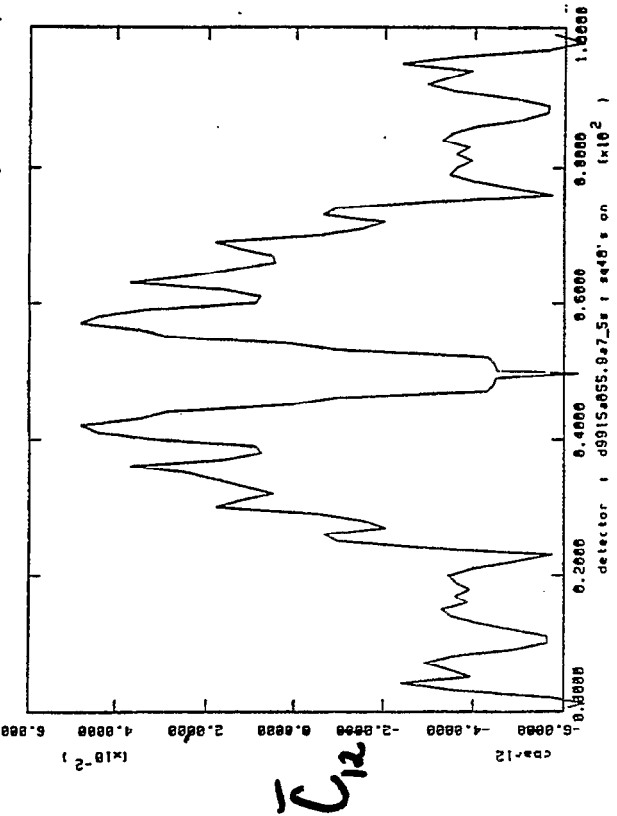
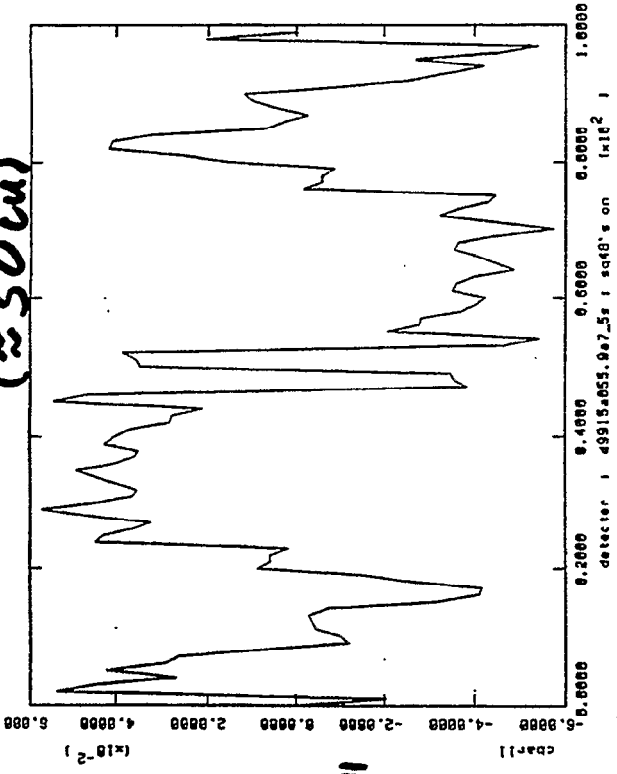
For weak coupling

$$\sigma_v = \sqrt{\epsilon_B \beta_B + \epsilon_A \beta_B \bar{C}_{12}^2 + \left( \gamma \frac{\sigma_E}{E} \right)^2}$$

$$"E_v" = \epsilon_B + \epsilon_A \bar{C}_{12}^2$$

Skew Quads at 48 powered antisymmetrically

86

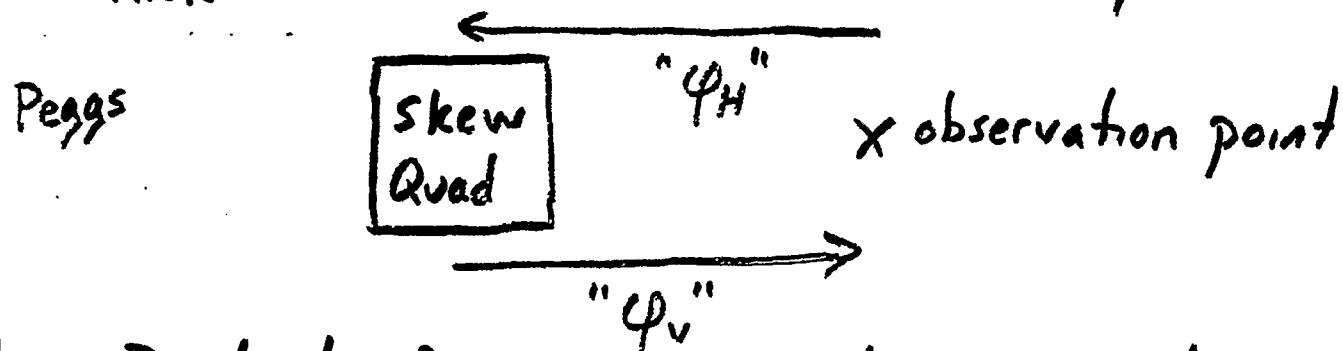


emittances  
 .1756e-6 m  
 .4507e-9 m (.4260e-10m)  
 for sol'n + comp. only  
 tunes 9.4058  
 9.3530

## Propagation of $\bar{C}$

Want to look at the effect of an upstream skew quad.

Project the horz. motion backwards to the skew quad. The horz. displacement at the skew quad produces a vert. kick. Project the vert. kick forwards to the observation point.



Product of these projections give terms that propagate as  $(\phi_A - \phi_B)$  and  $(\phi_A + \phi_B)$

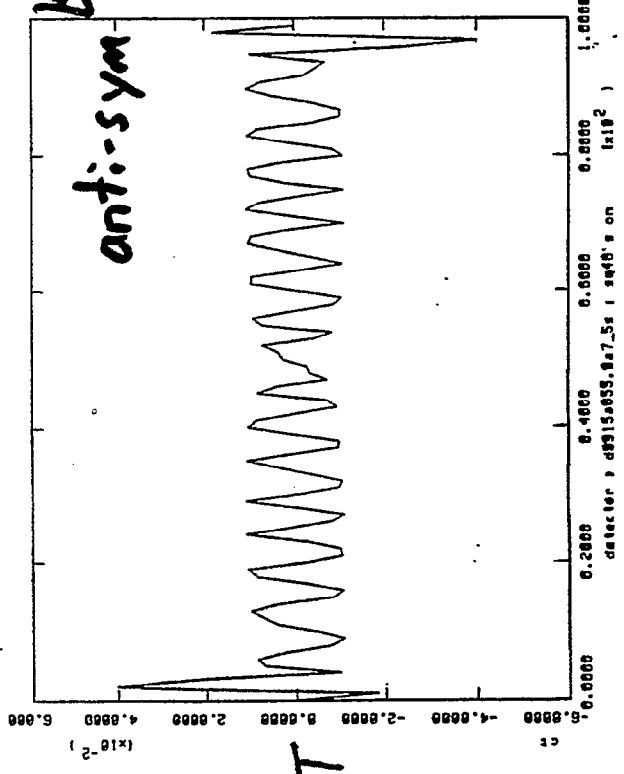
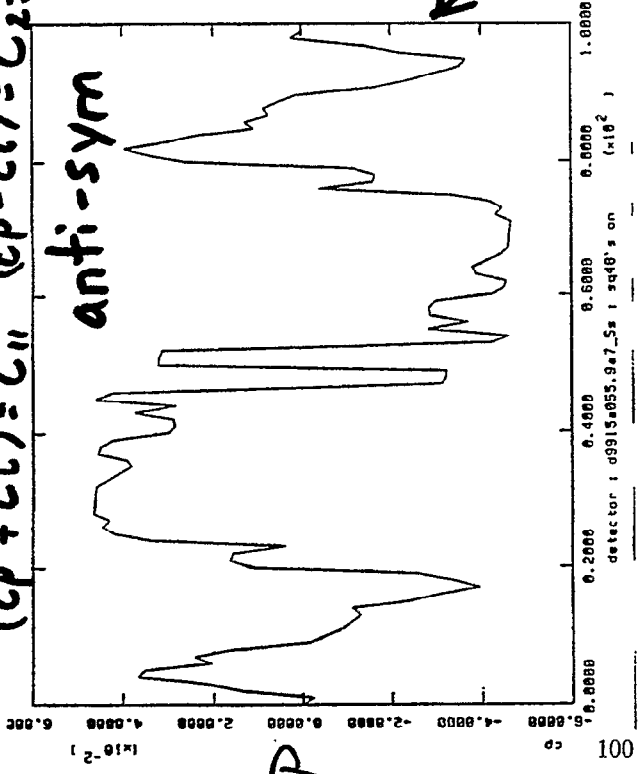
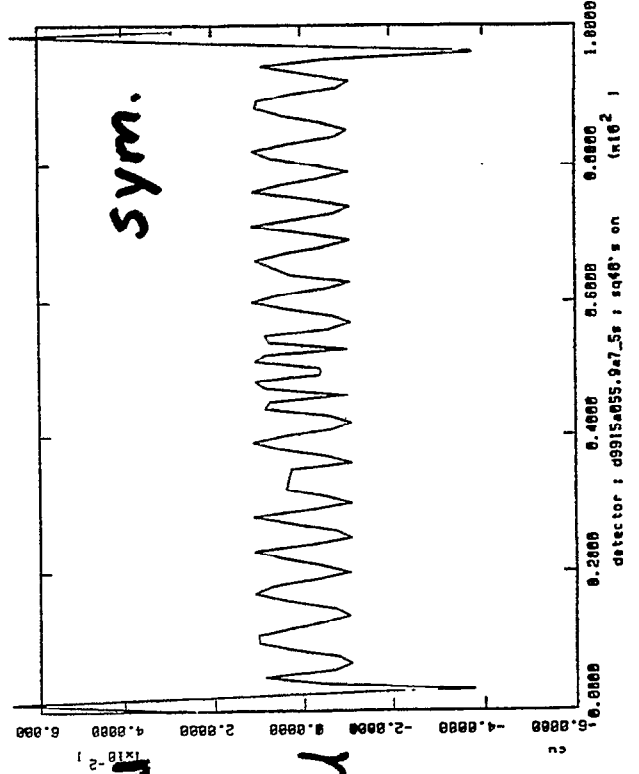
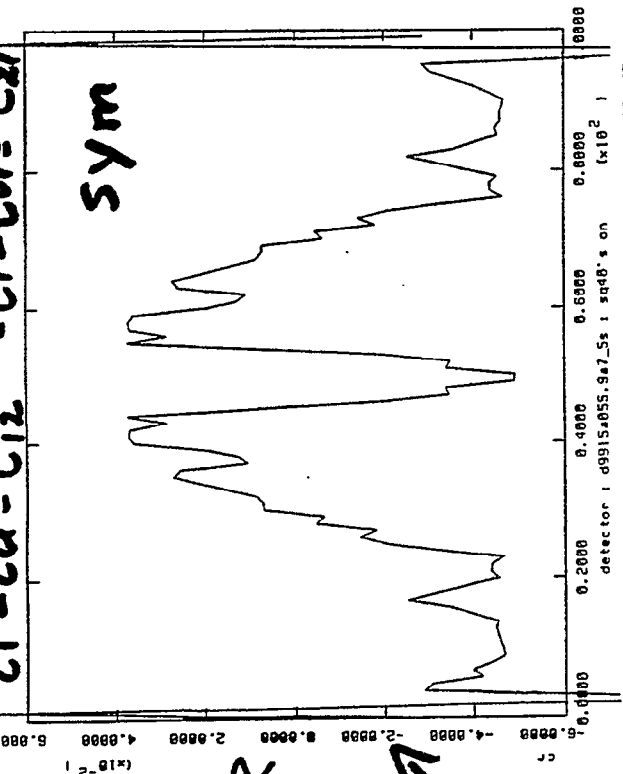
Since coupling propagates as  $(\phi_A + \phi_B)$  and as  $(\phi_A - \phi_B)$ , get resonances at

$$2\nu_A + 2\nu_B = n$$

$$2\nu_A - 2\nu_B = n \Rightarrow \text{Many machines run near here.}$$

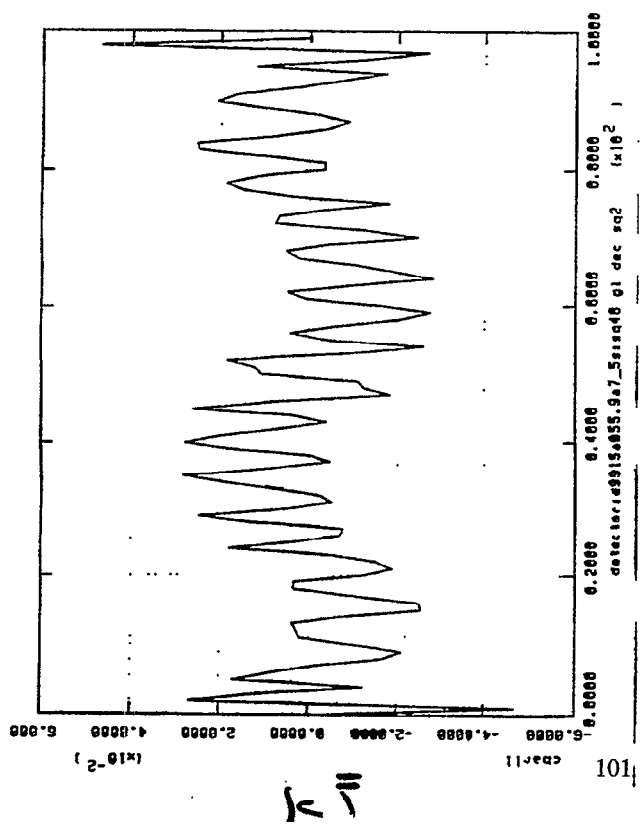
Analogous to how the  $B$  wave from a gradient error propagates.

Skew Quads at 48 powered antisymmetrically  
 $(cp + ct) = \bar{c}_{11}$   $(cp - ct) = \bar{c}_{22}$   
 $cr - cu = \bar{c}_{12}$   $-cr - cu = \bar{c}_{21}$

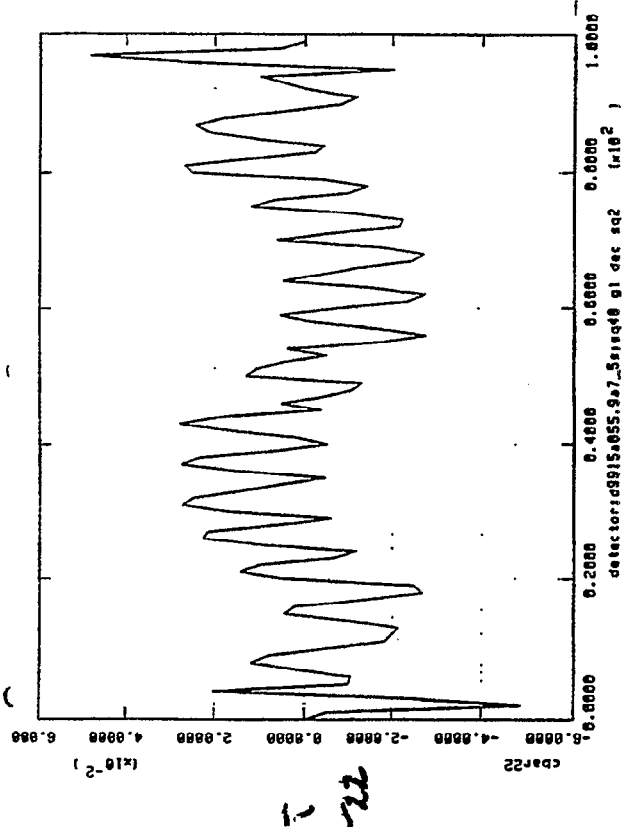


~ factor of 4 due to prox. to cnp. reson.

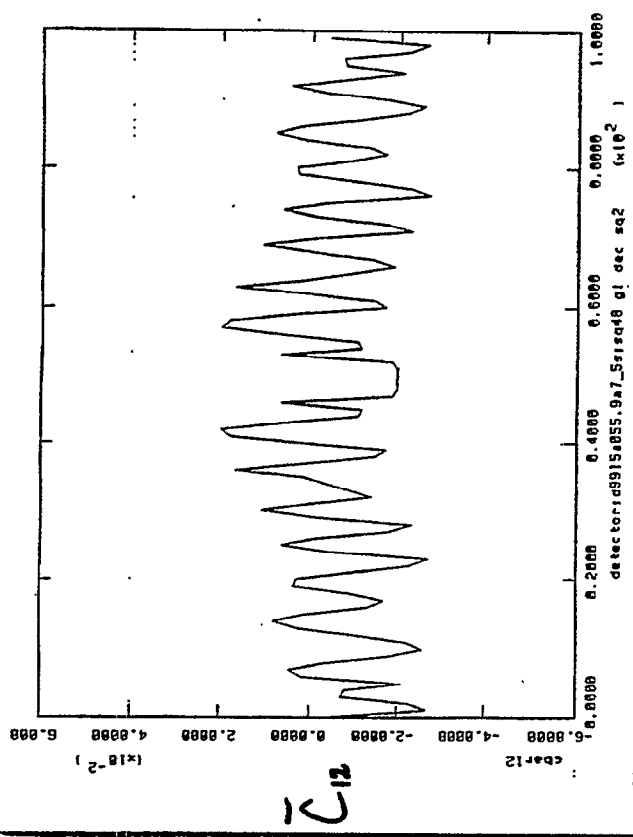
NEW SCANS AT 6000 TO POWERED ON 11-23-78. 210 DAILY CLEANUP



C11



C22

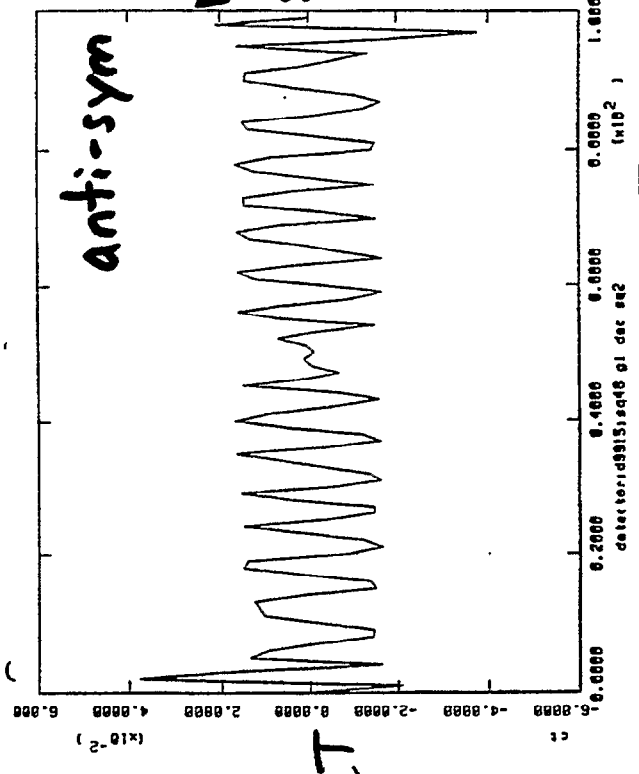
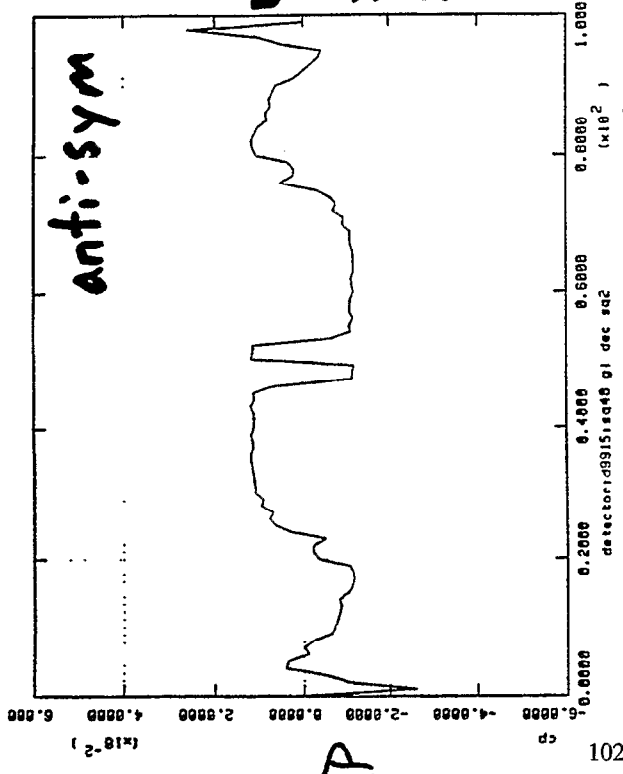
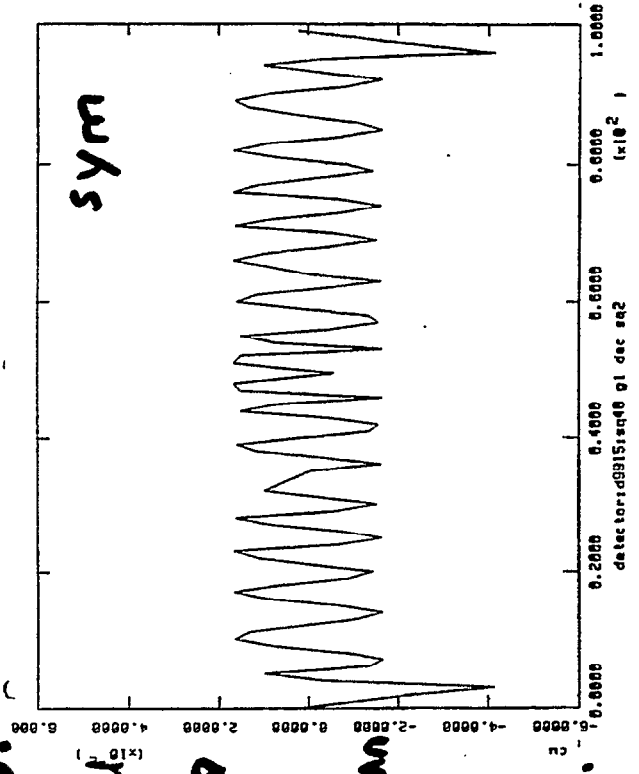
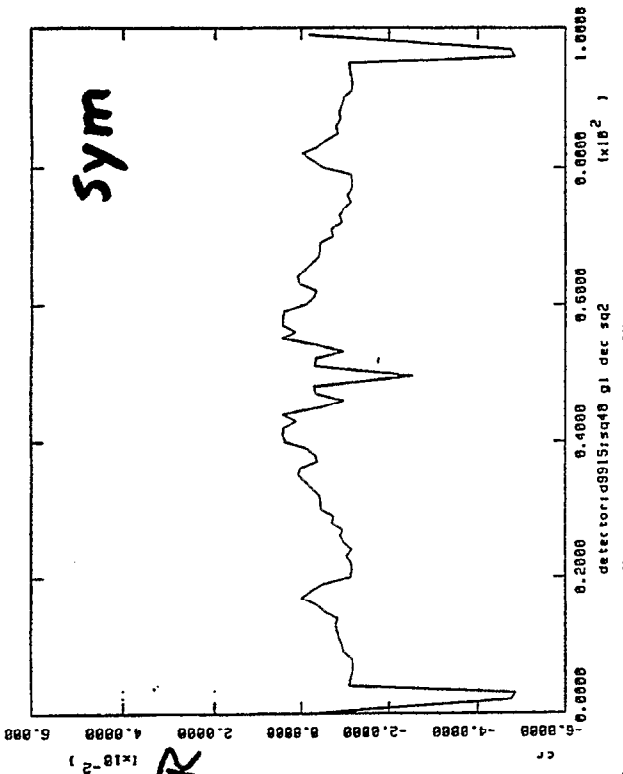


C12

tunes .4058  
.3530

emittances .1761e-6 m  
.1234e-9 m (.4260e-10 m)  
for  
sol'n + comp.  
only

new trends at LHC are to perform anti-sym globally decoupled.



CR

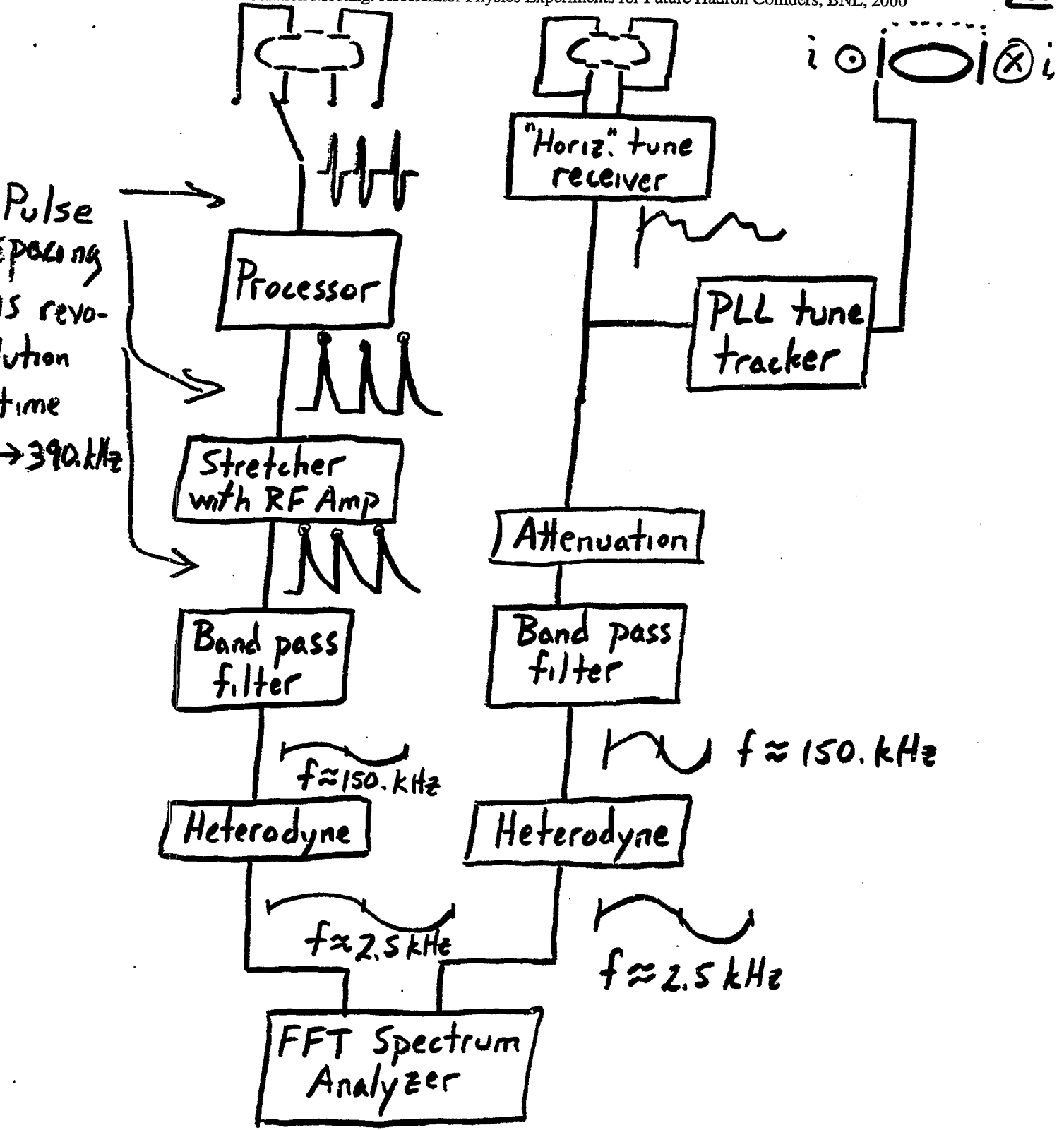
CR

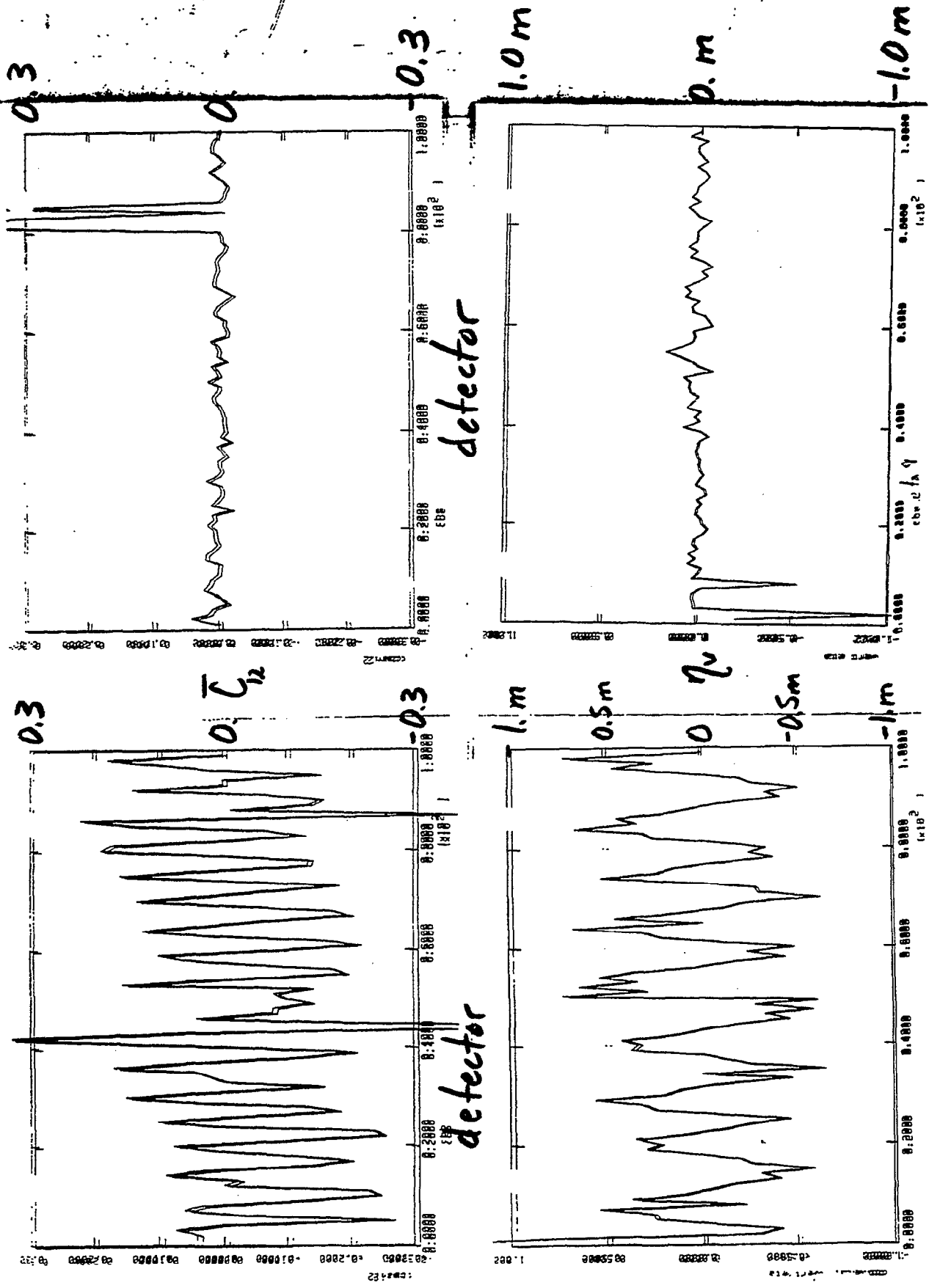
$\neq 0$   
but  $\approx \frac{1}{5}$   
before  
global  
decoupling.

slightly  
larger than  
before  
global  
decoupling.

anti-sym

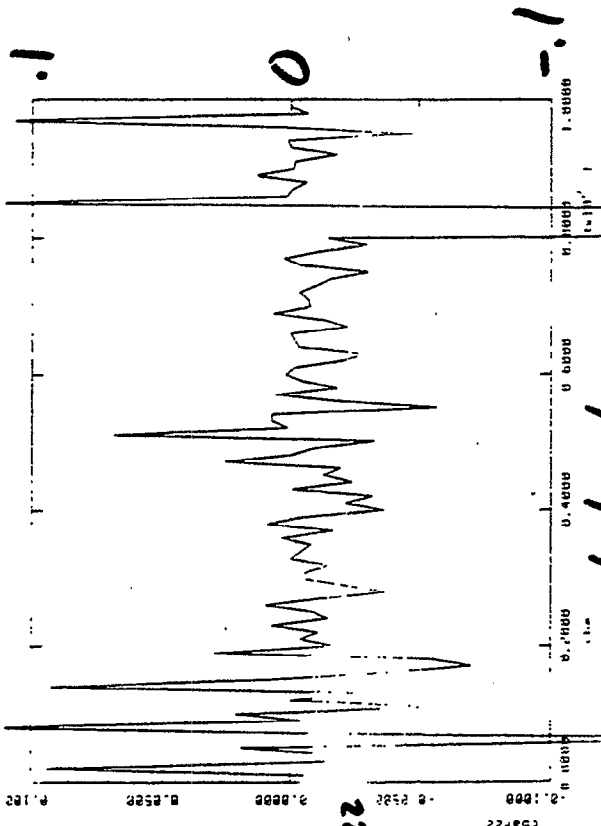
anti-sym





108540 sol'n  
off

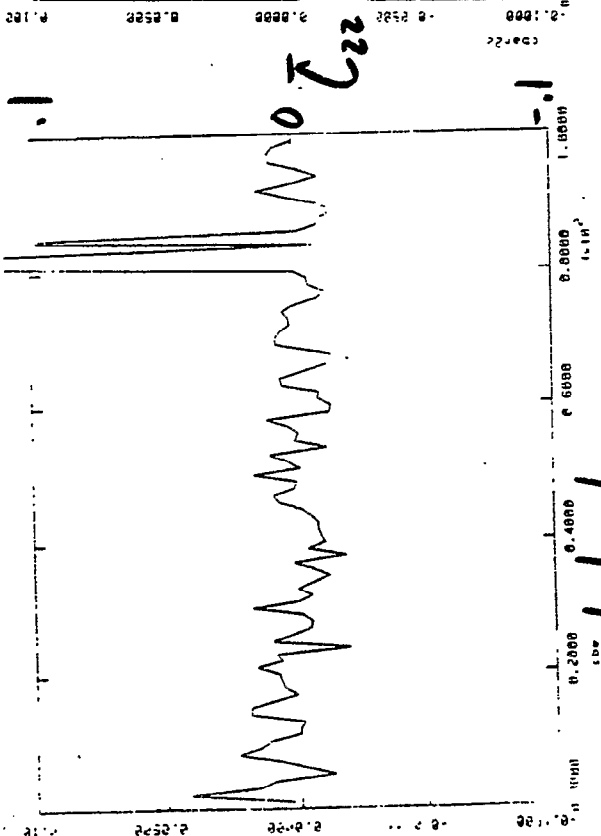
Before



detector

Note that  $Z_{22}$  is much noisier than  $Z_{12}$

CLEO sol'n off

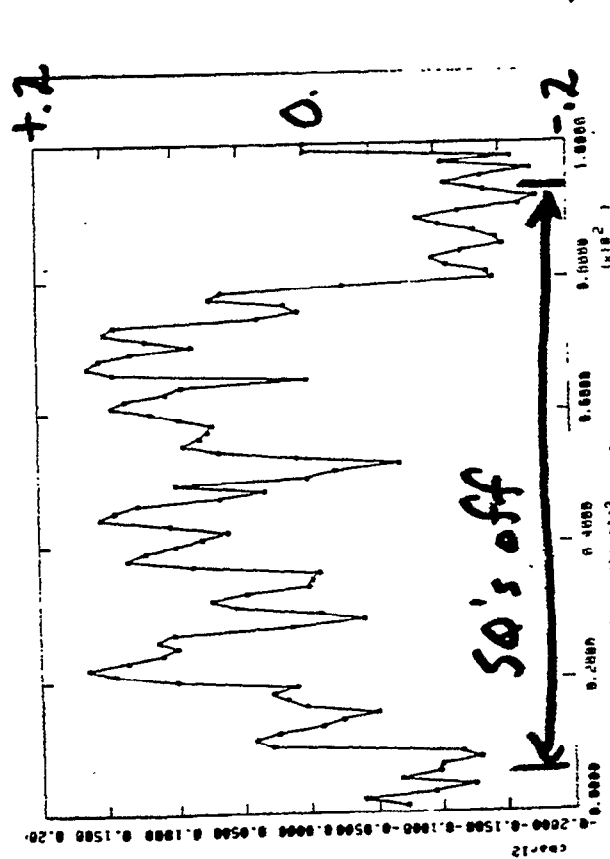
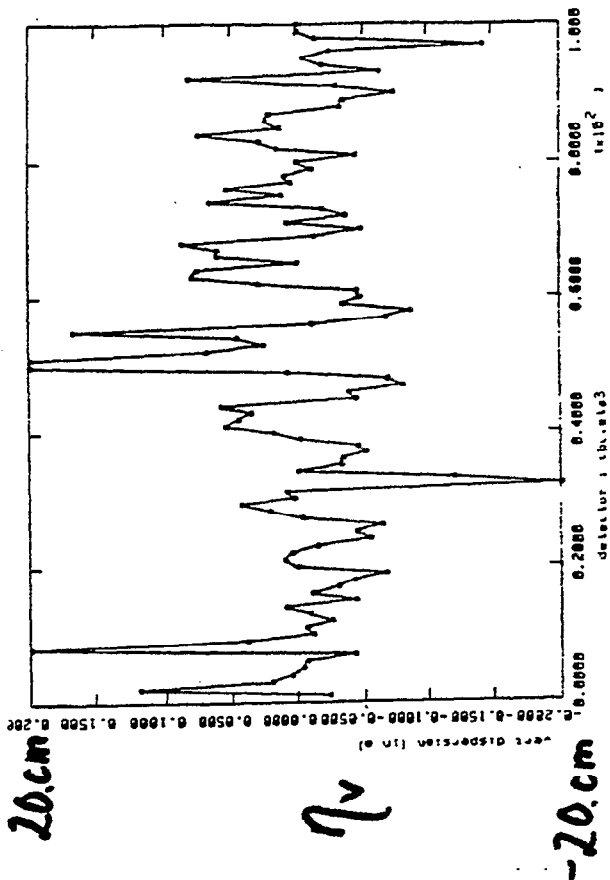


detector

.2m

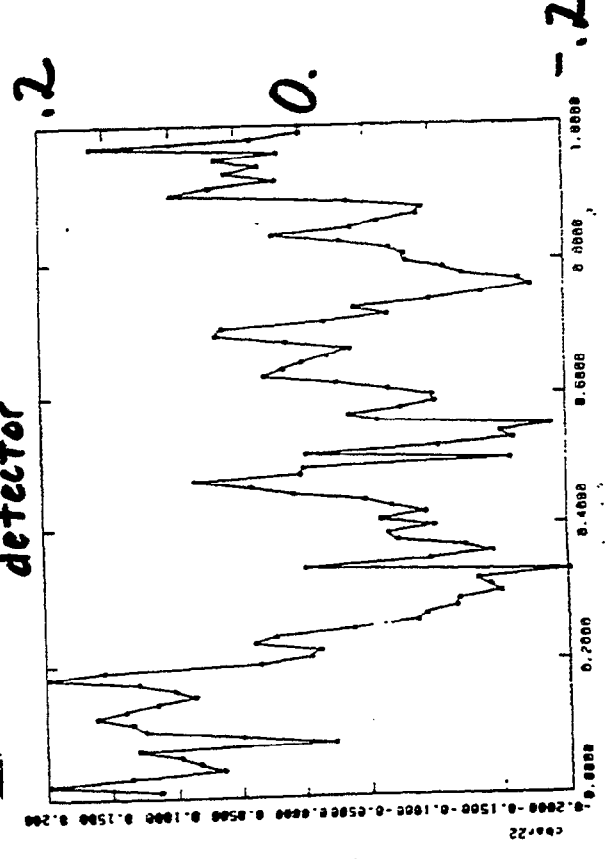
After

Before



detector

detector

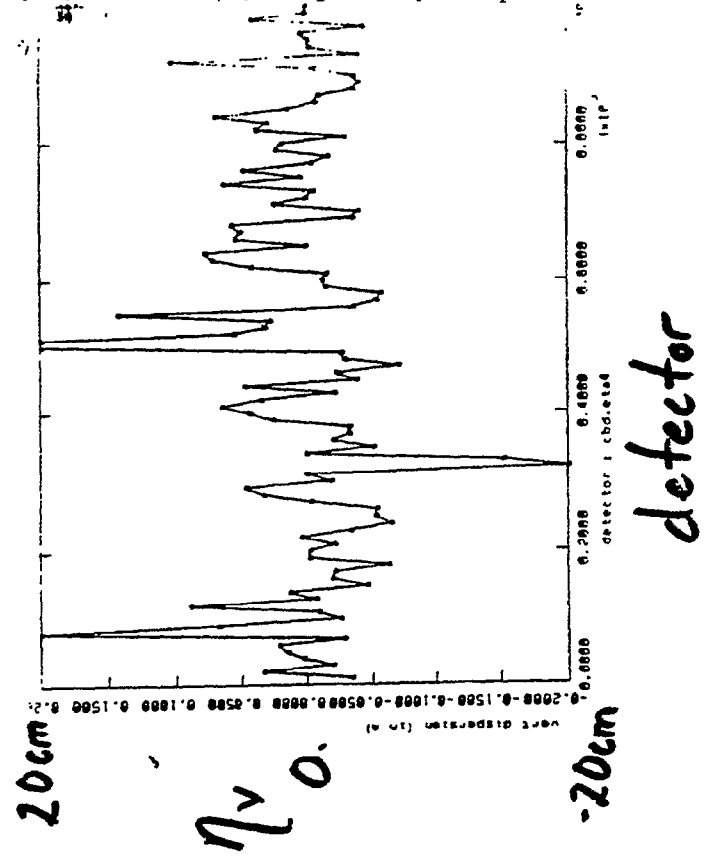
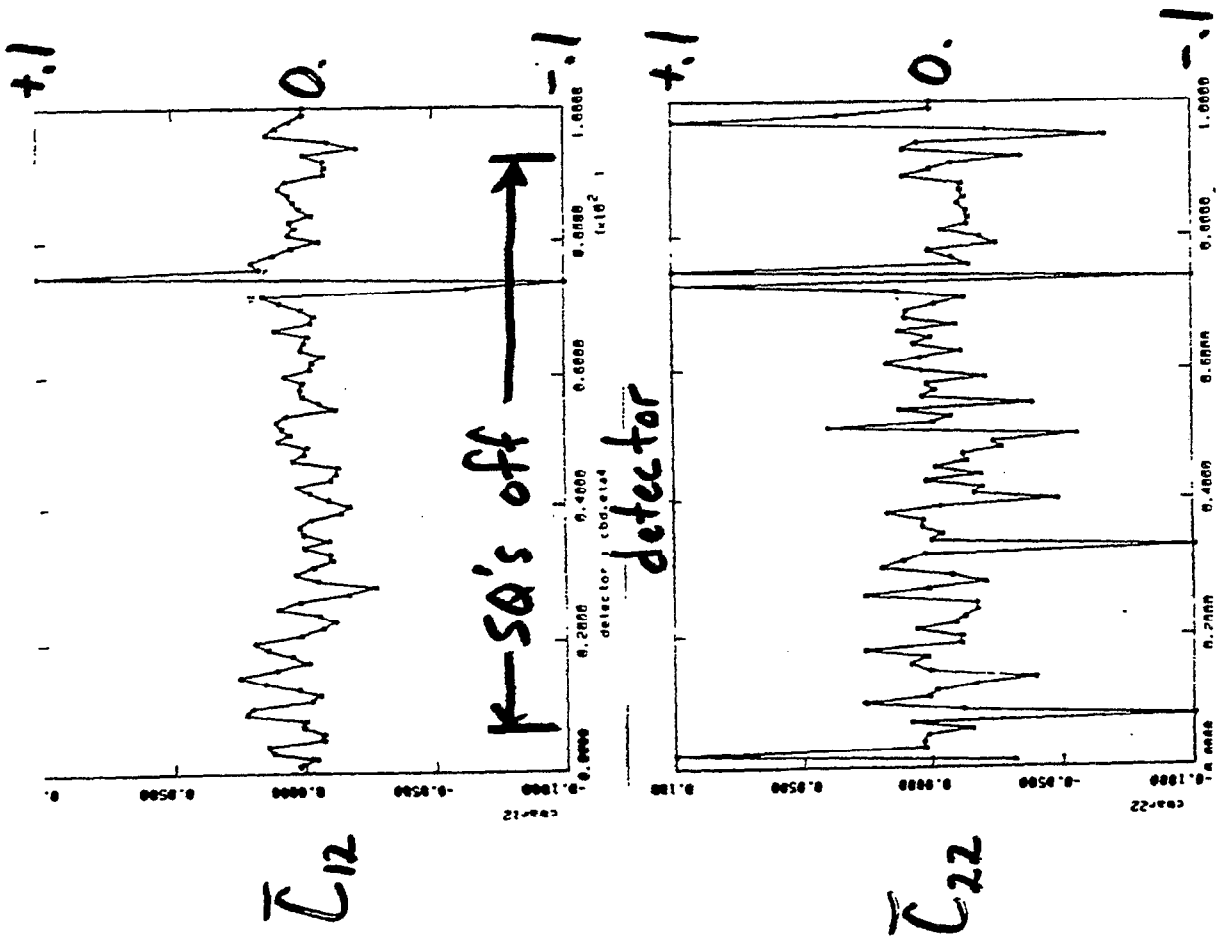


detector

910325

Cleo. soln on  
 $\theta_v = 550 \mu m$  (sync light)

After



detector

910325

Cleo soln on  $\sigma_s = 2.70 \mu m$  (sync/14)

## Conclusions

Less serious for proton machines than for electron machines.

We parametrize the coupling by 4 coupling parameters, the elements of the  $2 \times 2$  matrix  $\bar{C}$ . These relate the normal modes to the horizontal and vertical motion.

The  $\bar{C}_{ij}$  have components that propagate like

$$\varphi_A \pm \varphi_B$$

Global coupling is determined by the components of  $\bar{C}$  that propagate as  $\varphi_A - \varphi_B$ .

It is not sensitive to the component that propagates as  $\varphi_A + \varphi_B$ .

Only defined on the coupling resonance.

We have developed a method for measuring 3 of the 4 coupling matrix elements. We can measure one of these, the  $\bar{C}_{12}$ , very well.

With the measured  $\bar{C}_{12}$  and  $\eta_v$  we can calculate changes in skew quad settings that will locally decouple CESR. This is now a standard procedure at CESR.

# Betatron Phase Measurements in CESR\*

D. Sagan, D. Rubin, and S. Greenwald  
 Laboratory of Nuclear Studies, Cornell University, Ithaca, NY 14853

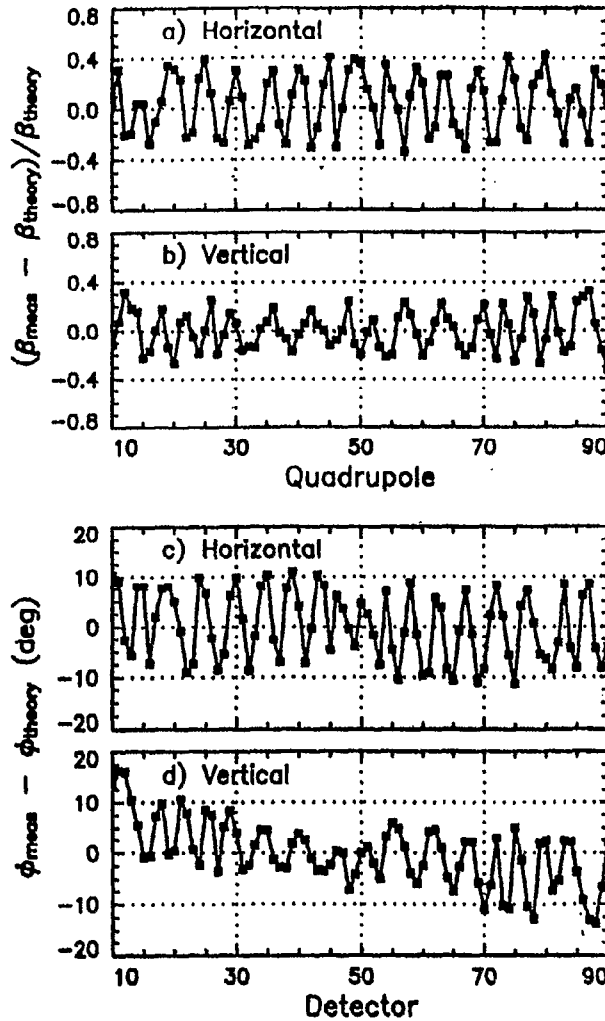


Figure 3: Initial beta and betatron phase relative to the theoretical values. The numbering system in CESR is such that the  $i^{th}$  detector is close to the  $i^{th}$  quadrupole.

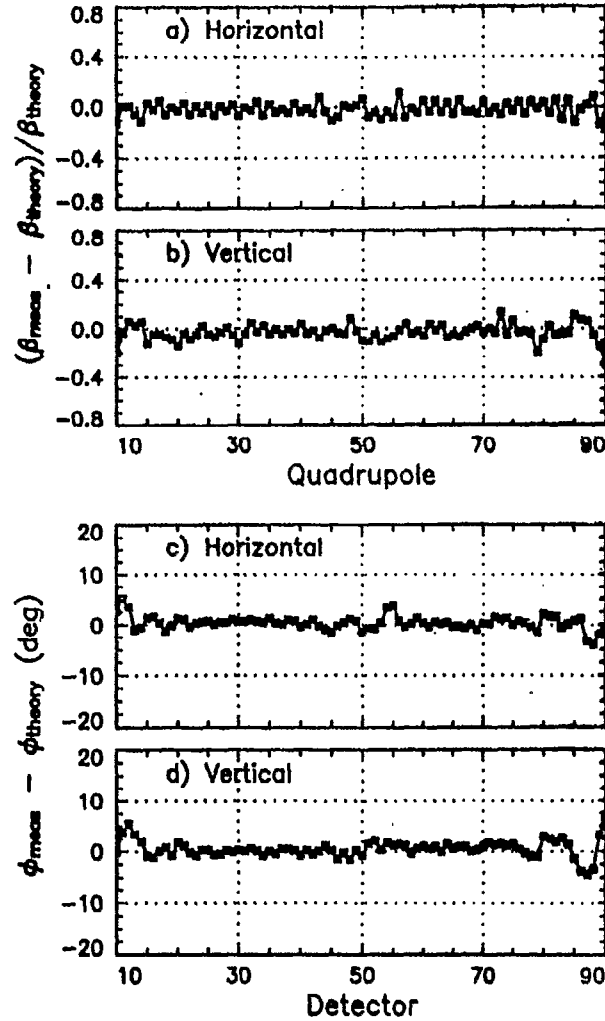


Figure 4: Beta and betatron phase relative to the theoretical values after correcting using only the phase data of the previous figure.

~~With electrons, we could coherently and continuously shake them really hard at the tune.~~

We can't do this with protons.

An obvious method is to kick the beam and look at the turn by turn oscillations.

We would certainly want chromaticities of  $\approx 0$  to get a nice long lasting signal.

Its not clear that this will be a clean enough signal.

Horz and Vert BPM's are NOT at the same locations in the Tevatron.

If we assume no couplers between a detector and its neighbor, this should be easy to handle.

I think we've been in the middle of an upgrade for several years.

In principle, pieces are in place for turn by turn capability (1024 turns) at every BPM.

Still needs work

I believe that it will eventually be able to readout all the BPMs in a house on the same trigger. about 5 BPMs/plane/house

Least Significant Bit is 0.15 mm.

Ming-Jen Yang was doing some good work on this a few years ago, but has since not had time to work on it.

I think it will take a significant effort to get believable, consistent data.

F17 proton injection kicker Horiz  
0.057 mrad at 1 TeV  $\Rightarrow \approx \pm 2.9$  mm peak displacements

Vertical pinger

at 1 TeV  $\Rightarrow \approx \pm 1.3$  mm peak displacements

## Status report on the development of instrumentation for bunch by bunch measurement and optimisation of luminosity in the LHC\*

W.C. Turner<sup>1</sup>, P.S. Datte<sup>1</sup>, P.F. Manfredi<sup>1,5</sup>, J.E. Millaud<sup>1</sup>, N.V. Mokhov<sup>2</sup>,  
M. Placidi<sup>3</sup>, V. Re<sup>4,5</sup>, H. Schmickler<sup>3</sup>

<sup>1</sup>Lawrence Berkeley National Laboratory, Berkeley, CA 94720

<sup>2</sup>Fermi National Accelerator Laboratory, Batavia, IL 60510

<sup>3</sup>CERN, Geneva, Switzerland

<sup>4</sup>University of Bergamo, Bergamo, Italy

<sup>5</sup>INFN, Pavia, Italy

(24 Apr.2000)

### Abstract

The status of development of instrumentation for bunch by bunch measurement and optimization of luminosity in the LHC is described in this paper. Radiation hard, fast, segmented, gas ionization chambers have been designed for installation near the shower maxima in the IR neutral particle absorbers (TAN) and IR front quadrupole absorbers (TAS). Low noise electronics have been developed to allow measurement over the full range of luminosity ( $10^{28} - 10^{34} \text{ cm}^{-2}\text{sec}^{-1}$ ) anticipated for the LHC with reasonable integration times. A prototype system will soon be tested with hadronic showers initiated by 450 GeV protons from the SPS.

### 1 INTRODUCTION

The Large Hadron Collider (LHC) [1] is a 7+7 TeV pp collider being constructed at CERN to operate with very high design luminosity,  $10^{34} \text{ cm}^{-2} \text{ sec}^{-1}$ . The high luminosity has many consequences for machine design. The large number of protons per bunch ( $10^{11}$ ) and the large number of bunches in each ring (2835) are particularly relevant for this paper.

For inelastic cross section 80 mb at 14 TeV cm the forward power of collision products leaving a high luminosity IP in each direction is approximately 1 kW. Absorbers are required to protect IR region superconducting magnets so that less than 1.2 mW/kgm reaches the cold mass. Fig. 1 shows a layout of one half of a high luminosity IR. A front quadrupole absorber (TAS) protects the inner triplet quadrupoles and a neutral particle absorber (TAN) protects the outer beam separation dipole D2.[2] The absorbers are shown filled in black in Fig. 1. Fig. 2 shows contours of power density

in the TAN absorber; one sees that the peak power density of the hadronic/electromagnetic showers inside the TAN is in the range 1-10 W/kgm. Table 1 gives the mean number, mean energy and total energy per pp interaction incident on the absorbers. The power density in the TAN is dominated by the showers initiated by neutrons and photons and in the TAS by charged pions and photons. On average about half of the 14 TeV collision energy is deposited in these absorbers. The peak flux of particles of various types at the shower maximum in the TAN, scaled to 5W/kgm, is given in Table 2 for design luminosity  $10^{34} \text{ cm}^{-2}\text{sec}^{-1}$ . Very high energy neutrons are included in the "hadron flux" in Table 2 but low energy neutrons with energy < 14 MeV are excluded from the "hadron flux" and listed separately.

Bunches in LHC are produced in trains with gaps for kicker magnet rise times. Altogether there are 3564 rf buckets spaced 25 nsec apart with nominally 2835 of them filled. A typical bunch structure is  $3564 = 12 \times 297 = 11 \times [3 \times (81b+8e)+30e] + [2 \times (81b+8e) + 119e]$  where b denotes a filled bucket and e an empty one. A finite crossing angle  $\sim 300 \mu\text{rad}$  is needed to avoid unwanted head on collisions approaching and leaving an IP. Bunches in the middle of a bunch train experience approximately fifteen long range collisions in the common beam tube on each side of an IP. Bunches near the head and tail of a bunch train experience fewer long range collisions (PACMAN bunches). These long range collisions produce orbit distortions and tune shifts in addition to the head on tune shift produced at the IPs.[3] The possibility that bunches experiencing fewer than the nominal number of long range collisions may be unstable has led to the recommendation that the luminosity be measured for each bunch individually.[4]

\* Work supported by the US Dept of Energy under contract no. DE-AC03-76SF00098.

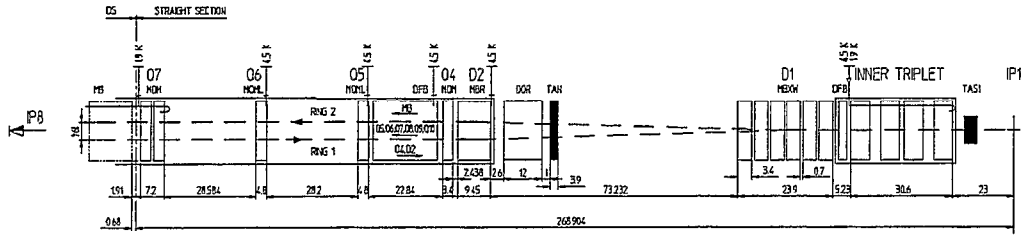


Fig. 1: Layout of one half of a high luminosity insertion IP1(5) of LHC. The front quadrupole absorber (TAS) and the neutral particle absorber (TAN) are shown filled in black.

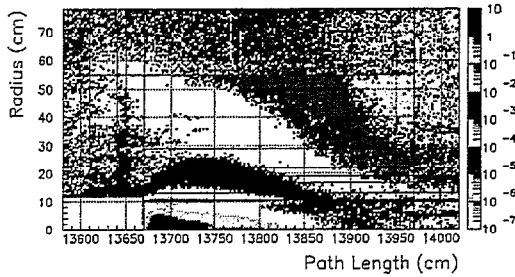


Fig.2: Contours of power density (W/kgm) deposited in the TAN at design luminosity  $10^{34} \text{ cm}^{-2} \text{ sec}^{-1}$ .

Table 1: The mean number, mean energy and total energy per pp interaction incident on the (a) TAN and (b) TAS absorbers at design luminosity  $10^{34} \text{ cm}^{-2} \text{ sec}^{-1}$ .

(a) TAN

Particle type	$\langle n \rangle$	$\langle E \rangle$ (GeV)	$\langle n \rangle \langle E \rangle$ (GeV)
Neutral hadrons	.33	2185.	725
Protons	.06	1215.	73
Charged Pions	.71	125.	88
Photons	151	5.	736
Electron/positron	12.5	1.	8
Muons	.01	25	.25

(b) TAS

Particle type	$\langle n \rangle$	$\langle E \rangle$ (GeV)	$\langle n \rangle \langle E \rangle$ (GeV)
Neutral hadrons	.58	261.	152
Protons	.29	292.	83
Charged Pions	6.8	159.	1081
Photons	8.3	87.	725
Muons	.06	33	.2

Table 2: The flux of particles of various types at the shower maximum in the TAN at design luminosity  $10^{34} \text{ cm}^{-2} \text{ sec}^{-1}$ .

Particle type	Flux( $\text{cm}^{-2} \text{ sec}^{-1}$ )
Hadrons	$3 \times 10^9$
Electron/positron	$1.3 \times 10^{10}$
Photons	$1.5 \times 10^{11}$
Neutrons(<14 MeV)	$\sim 2 \times 10^{11}$

The existence of the TAN and TAS absorbers led to the proposal to instrument them to sample the power deposited by the hadronic/electromagnetic showers and to use this information as a machine tool to keep the LHC operating near optimum luminosity.[5] Scanning the position of one beam at the IP allows measurement of beam-beam separation and transverse beam size. By segmenting the detectors it may also be possible to measure crossing angle and transverse IP position. The particular situation in LHC leads to a different approach than has been used in storage rings in the past for the measurement of luminosity. The very high power density in the absorbers requires strict attention to radiation hardness; there is no possibility of using glass, plastic, fiber optics, PMTs and organic gasses in this environment. Solid state detectors are probably also ruled out. Furthermore the equipment will become highly activated and if necessary to service would require remote handling. A premium is therefore placed on high reliability and maintenance free operation – hopefully for many years. Since there are approximately 20 interactions per bunch crossing at  $10^{34} \text{ cm}^{-2} \text{ sec}^{-1}$  and the multiplicity of particles hitting the absorbers is high there is no possibility of measuring individual events or using coincidence. The detector envisioned therefore measures the locally deposited energy density and relies on cross calibration with a particle detector for absolute luminosity. Single beam backgrounds could cause difficulty with this approach however preliminary

estimates indicate they will be quite small.[5] At very low luminosity with less than one pp interaction per bunch crossing, coincidence of detectors on opposite sides of the IP could be used to suppress single beam background.

## 2 REQUIREMENTS FOR LUMINOSITY MEASUREMENT IN LHC

The requirements of an LHC luminosity monitor for machine operations purposes were established at a mini workshop held at CERN on 15-16 Apr. 1999. They are summarized here.[6]

- Capability of keeping the storage ring tuned within 2% of optimum luminosity
- Correlation of apparent luminosity with position of IP < 1% per mm
- Correlation of apparent luminosity with half crossing angle < 1% per 10  $\mu$ rad
- Dynamic luminosity range  $10^{23}$  to  $10^{34}$   $\text{cm}^{-2} \text{sec}^{-1}$  with "reasonable" integration time
- Bandwidth 40 MHz to resolve luminosity of individual bunches
- Backgrounds less than 10% and correctable
- Cross calibrate with absolute luminosity measurement every few months.

It is important for optimisation of luminosity that the measurement of an apparent change of luminosity not be due to the variation of other beam parameters, such as position of the IP or crossing angle, while the luminosity itself is unchanged. For this reason the correlation of apparent luminosity with IP position and crossing angle are specified to be small; 1% per mm and 1% per 10  $\mu$ rad respectively.

It is planned that the LHC will operate over six orders of magnitude in luminosity. This is needed to accommodate the TOTEM experiment for measurement of forward pp scattering at low luminosity ( $\sim 10^{23} \text{cm}^{-2} \text{sec}^{-1}$ ) and the high  $p_T$  experiments ATLAS and CMS at high luminosity ( $\sim 10^{34} \text{cm}^{-2} \text{sec}^{-1}$ ). A luminosity optimisation tool needs to perform well over the entire range of luminosity.

For the reasons discussed in Sec. 1, it is desirable to measure the luminosity of each colliding bunch pair with 25 nsec bunch spacing which requires 40 MHz bandwidth for electronics.

## 3 CONCEPT FOR OPTIMISATION OF LUMINOSITY

A concept for optimisation of luminosity is shown in Fig. 3. The two beam centers are separated at the IP by a transverse displacement  $D(t)$  which is the sum of an intentional circular sweep of the center of one beam  $d(t)$  and an error  $e(t)$ . If the magnitudes of the intentional

sweep and error displacement are small compared to the rms beam size then to lowest order in the displacements the luminosity is given by

$$L = L_0 \left( 1 - \frac{\varepsilon^2 + d^2}{4\sigma_*^2} \right) - L_0 \frac{\varepsilon d}{2\sigma_*^2} \cos(\omega t - \phi). \quad (1)$$

A detector current proportional to the luminosity then has a quasi-static term proportional to the optimum luminosity  $L_0$  and a linear oscillation term. The magnitude of the oscillation is proportional to the product of the magnitudes of the error offset and the intentional displacement divided by twice the rms beam size in one transverse direction. For the general situation the detector current may be written as

$$I(t) = e\alpha\varepsilon_{\text{det}}m\sigma_{\text{inel}}L \quad (2)$$

where  $\sigma_{\text{inel}}$  is the inelastic cross section,  $m$  is the multiplicity of particles per event which fall within the acceptance of the detector,  $\varepsilon_{\text{det}}$  is the detection efficiency and  $\alpha$  is the number of charge carriers collected per detected particle. The current is integrated over an interval 0 to T, assumed equal to an integer multiple of, or to be large compared to,  $2\pi/\omega$ , to obtain the luminosity and error offset

$$L_0 = \frac{\int_0^T I(t) dt}{e\alpha\varepsilon_{\text{det}}m\sigma_{\text{inel}}T}$$

$$\bar{\varepsilon} = \frac{\hat{e}_x \int_0^T \cos(\omega t) I(t) dt + \hat{e}_y \int_0^T \sin(\omega t) I(t) dt}{\left( \frac{d}{4\sigma_*^2} \right) e\alpha\varepsilon_{\text{det}}m\sigma_{\text{inel}}T} \quad (3)$$

The measurement of  $\bar{\varepsilon}$  can then be fed back to the closed orbit bumpers to reduce it to zero. In practice we imagine that reducing  $\bar{\varepsilon}$  to the level of  $0.1\sigma_* = 1.6\mu\text{m}$  is sufficient. The magnitude of the optimum sweep amplitude  $d$  is equal to the desired residual error, in this case  $0.1\sigma_*$ . Eqns. 3 can be used to derive expressions for the statistical errors of  $L_0$  and  $\bar{\varepsilon}$  as functions of the integration time T.[5]

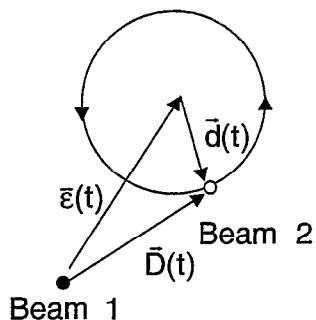


Fig. 3: Concept for optimisation of luminosity;  $e(t)$  = error offset of the two beam centers at the IP,  $d(t)$  = intentional circular sweep of the transverse position of beam 2.

Preliminary investigations have been made of the possibility that beam sweeping indicated in Fig. 3 could increase the beam emittance. So far the simulations have not observed such a deleterious effect for the bunch intensities envisioned for LHC.[7],[8]

#### 4 IONIZATION CHAMBER PROPERTIES

An illustration of luminosity instrumentation in the TAN and TAS absorbers is shown in Fig. 4. The instrumentation is located near the shower maximum

energy density approximately 25 cm behind the front face of the absorbers. The radiation power density in a transverse plane in the TAN is shown in Fig. 5(a). The peak power density is 21 mm from the two beam centerline (symmetry axis of the absorber) owing to the 150  $\mu$ rad half crossing angle. The beam tube on the left in Fig. 5(a) is enlarged compared to the one on the right to allow synchrotron light from the outer beam separation dipole to pass through the TAN to a synchrotron radiation monitor. Since this simulation was made, the location of the synchrotron monitor has been moved to the other side of the separation dipole so the left beam tube is now circular and symmetrically placed relative to the right beam tube. The instrumentation shown in Fig. 4 has been segmented into quadrants to allow measurement of the crossing angle and the transverse position of the IP by measuring the left - right and up - down asymmetry ratios. The sensitivity of the left - right asymmetry ratio as a function of the position of the center of the power profile is shown in Fig. 5(b).

A survey of possible detectors led to the choice of a gas ionization chamber based on considerations of radiation hardness, reliability and low maintenance and simplicity of installation.[9] The key problems to solve with this approach are bandwidth, acceptable signal to noise ratio and impedance matching to the front end electronics. The solution to these problems led to a multi-plate pressurized ionization chamber. The operating gas would be 4 atmospheres of Ar+1%N<sub>2</sub>. Some parameters of the

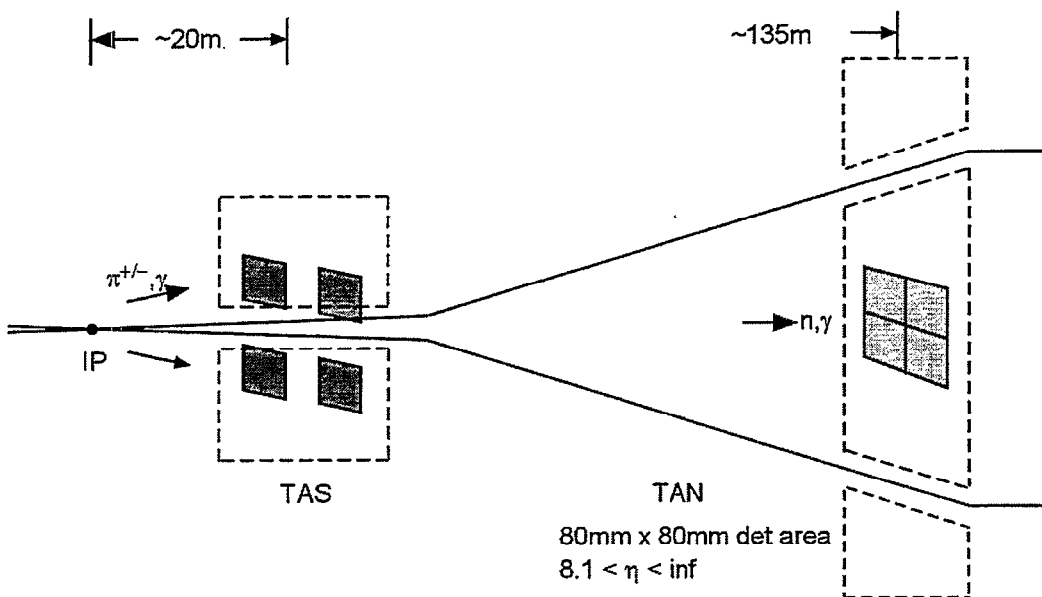


Fig. 4: Illustration of ionization chamber detectors in the TAN and TAS absorbers.

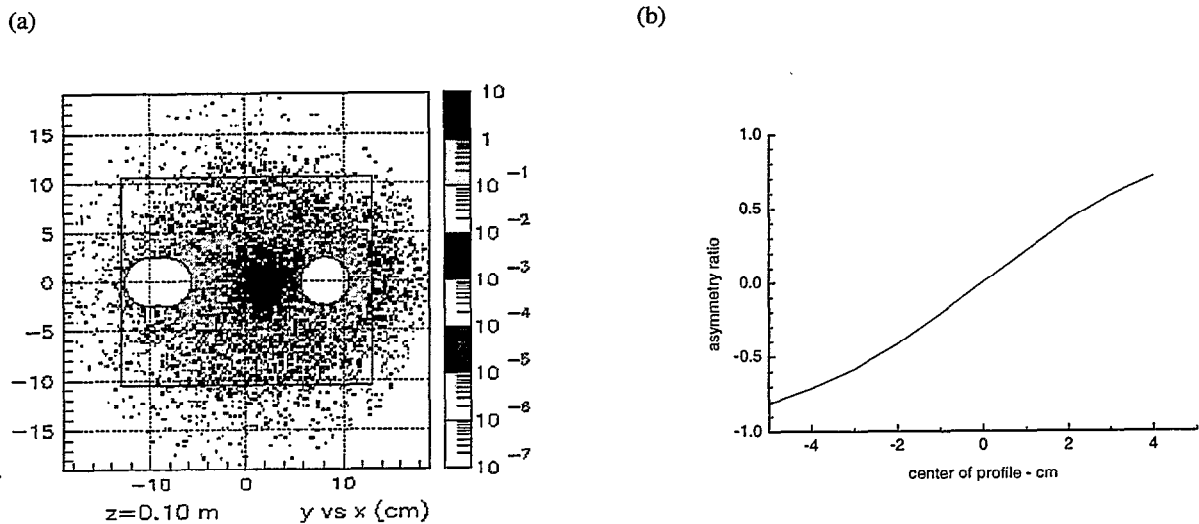


Fig. 5: (a) Contours of radiation power density (W/kgm) in the transverse plane deposited in the TAN at design luminosity  $10^{34} \text{ cm}^{-2} \text{ sec}^{-1}$  and (b) left - right asymmetry ratio as a function of the center of the radiation power density profile.

Table 3: Properties of the ionization chamber.

Property	Value	
Active Area (1 quadrant)	40mm x 40mm	
Plate gap	0.5mm	
No. of gaps	60(electrically 10 parallel x 6 series)	
Capacitance per gap	28.3pF	
Gas	Ar+1%N <sub>2</sub> , 4x760 Torr	
Gap voltage	150V	
Electron gap transit time	21.7nsec	
Bunch freq/Rev freq	40.079MHz/11.2455kHz	
Bunch structure	12x(3x81+2x8+38)=3564	
Inel pp int/bunch xing @ $10^{34} \text{ cm}^{-2} \text{ sec}^{-1}$	20	
mip per pp int	268	
mip per bunch xing @ $10^{34} \text{ cm}^{-2} \text{ sec}^{-1}$	$5.35 \times 10^3$	
Electron-ion pairs/cm-mip	388	
Ioniz e/pp int	$5.2 \times 10^3$ (1 gap)	$5.2 \times 10^4$ (10 gaps)
Ioniz e-/bunch xing @ $10^{34} \text{ cm}^{-2} \text{ sec}^{-1}$	$1.04 \times 10^5$ (1 gap)	$1.04 \times 10^6$ (10 gaps)

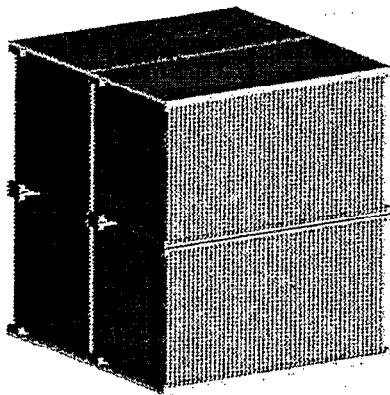


Fig. 6: Illustration of the multi-plate ionization chamber.

ionization chamber are given in Table 3. The gap width 0.5 mm is chosen so the electrons clear the chamber between 25 nsec bunch crossings. The number of gaps and their series-parallel electrical configuration is chosen to match the ionization chamber capacitance plus cable impedance rise time to the front-end amplifier peaking time (2 nsec) and to achieve signal to noise ratio  $\sim 8:1$  for 1 pp interaction ( $5 \times 10^3 e^-$  per gap on average). Our solution to these conditions leads to sixty 0.5 mm gaps arranged in six series groups of ten gaps in parallel. An illustration of the multi-plate, segmented ionization chamber is shown in Fig. 6.

Our solution to the problem of measuring luminosity over six orders of magnitude has been to design a detector and electronics package that can detect a single pp interaction in the LHC. In a single pp interaction on average  $5.2 \times 10^3$  electron-ion pairs are produced per gap. The pre-amplifier and pulse shaper has been designed to produce a 35 mV signal from the induced electron charge collected from ten gaps in parallel ( $1/2 \times 10 \times 5.2 \times 10^3 e^- = 2.6 \times 10^4 e^-$ ). With an equivalent noise charge (ENC) less than  $3 \times 10^3 e^-$ , the signal to noise ratio is  $\sim 8.7$ . Under these circumstances luminosity can be measured to arbitrarily low values, until the single beam background limit is reached, by simply counting ones and zeros as bunches cross. This is the traditional pre LHC era situation. The single beam background limit estimated for beam gas interactions corresponds to luminosity  $\sim 10^{26} \text{ cm}^{-2} \text{ sec}^{-1}$ , two orders of magnitude below the luminosity expected

for TOTEM operation.[5] In the very low luminosity limit, with a small probability of a pp interaction per bunch crossing, the single beam background could be further reduced by operating the ionization chambers on opposite sides of the IP in coincidence. At ultimate luminosity,  $2.5 \times 10^{34} \text{ cm}^{-2} \text{ sec}^{-1}$ , the average number of pp interactions per bunch crossing is fifty. The average induced charge collected from ten parallel gaps is  $50 \times 2.6 \times 10^4 e^- = 1.3 \times 10^6 e^-$  and the pre-amplifier pulse shaper output voltage is 1.25 Volts.

The ion drift velocity is much less than for electrons so that in equilibrium an ion space charge distribution corresponding to  $1.5 \times 10^3$  bunch crossings builds up in the gaps. Even at ultimate luminosity  $2.5 \times 10^{34} \text{ cm}^{-2} \text{ sec}^{-1}$  this ion space charge has been calculated to be well below the level where recombination is significant; the ionization chamber signal remains a linear function of luminosity.[5]

## 5 INTEGRATION TIME

Estimates of the integration times for measurement of luminosity, beam-beam separation, crossing angle and transverse position of the IP are given in Table 4 for luminosities  $10^{34}$  and  $10^{28} \text{ cm}^{-2} \text{ sec}^{-1}$ . The estimates are conservative since they include the statistics of only the hadrons in Table 1. The number of bunches in each proton beam is assumed to be 2835 for  $10^{34} \text{ cm}^{-2} \text{ sec}^{-1}$  and 36 for  $10^{28} \text{ cm}^{-2} \text{ sec}^{-1}$ . The rms precision of each measurement is indicated in the first row; for example  $\sigma_r/L = .01$ . The integration times are given in three units; seconds, turns and bunch crossings. The integration times in Table 3 refer to measurements of the means averaged over all bunches. For measurements of individual bunches to the stated precision the integration times in Table 4 need to be multiplied by the number of bunches. Even for the low luminosity  $10^{28} \text{ cm}^{-2} \text{ sec}^{-1}$  the integration times are sufficiently short to be practical; for example approximately one minute for a 1% measurement of luminosity averaged over the 36 bunches and approximately a half hour for 1% measurement of luminosity of each bunch. At  $10^{34} \text{ cm}^{-2} \text{ sec}^{-1}$  the integration time for 1% measurement of luminosity averaged over all bunches is one turn and the time to measure beam-beam separation to  $0.1\sigma^*$  is 11 turns.

## 6 STATUS OF DEVELOPMENT

As of the writing of this paper a prototype ionization chamber has been designed and is in fabrication. Prototype pre-amplifiers and pulse shaping boards have been bench tested and meet the bandwidth (40 MHz) and noise requirements ( $\text{ENC} < 3 \times 10^3 e^-$ ). In the Summer of 2000 a one week beam test is scheduled in the H4

Table 4: Integration times for measurement of luminosity, beam-beam separation, crossing angle and transverse position of the IP.

Integration time (sec/turns/bunch crossings)				
L (cm <sup>2</sup> sec <sup>-1</sup> )	$\frac{\sigma_L}{L} = 0.01$	$\sigma_\varepsilon = 0.1\sigma^*$	$\sigma_\psi = 1\mu\text{rad}$	$\sigma_{a^*x} = \sigma^*$
10 <sup>34</sup>	6.2x10 <sup>-5</sup>	1.0x10 <sup>-3</sup>	2.55x10 <sup>-4</sup> /	3.8x10 <sup>-3</sup> /
	0.7/	11/	2.9/	42.6/
	2.0x10 <sup>3</sup>	3.1x10 <sup>4</sup>	8.2x10 <sup>3</sup>	1.2x10 <sup>5</sup>
10 <sup>28</sup>	62/	1.0x10 <sup>3</sup> /	2.55x10 <sup>2</sup> /	3.8x10 <sup>3</sup> /
	7.0x10 <sup>5</sup> /	1.1x10 <sup>7</sup> /	2.9x10 <sup>6</sup> /	4.310 <sup>7</sup> /
	2.5x10 <sup>7</sup>	4.0x10 <sup>8</sup>	1.0x10 <sup>8</sup>	1.5x10 <sup>9</sup>

beamline of the SPS at CERN. The prototype four quadrant ionization chamber will be mounted behind a steel absorber. A slow spill of 450 GeV protons will be incident on the steel absorber;  $\sim 10^6$  p per 2.4 sec spill, repeated every 14.4 sec. The ionization chamber will be set up behind the steel absorber to measure the flux of ionizing shower particles. The pulses of electron charge and the ion current reaching the plates will be measured separately by fast and slow electronic circuits. Provisions are made for varying the thickness and A/Z of the absorber plates, the gas pressure and composition and the transverse position of the chamber in the showers. In the future it is planned to continue these measurements with a 25 nsec bunched beam. The experimental set-up is being modelled with the MARS radiation code to allow comparison of the measurements with expectations.[11]

## REFERENCES

- [1] The Large Hadron Collider Conceptual Design, CERN/AC/95-05 (LHC), 20 Oct. 1995.
- [2] W. Turner, E.H. Hoyer and N.V. Mokhov, "Absorbers for the High Luminosity Insertions of the LHC", Proc. Of EPAC 98, Stockholm, 1998, pg. 368.
- [3] W. Herr, "Effect of PACMAN bunches in the LHC", LHC Project Report 39 (1996).
- [4] W. Herr and F. Ruggiero, "Summary of the Workshop on Beam-Beam Effects in Large Hadron Colliders (LHC99)", LHC Project Reprint 277, 9 Aug. 1999. The workshop proceedings may found on the web site: <http://wwwslap.cern.ch/collective/bb-workshop99/>
- [5] W.C. Turner, "Instrumentation for the Absorbers in the Low Beta Insertions of LHC", LBNL-42180, (13 Aug. 1998).
- [6] See H. Schmickler, "Summary Comments" in Proc. Of Tools for Luminosity Optimisation in the LHC,

15-16 Apr. 1999, CERN, Geneva. The proceedings can be found on the web site:

<http://www.cern.ch/CERN/Divisions/SL/groups/bi/conferences/Lworksho/Lworkshop.html>

- [7] S. Krishnagopal, M. Furman and W.C. Turner, "Studies of the beam-beam interaction for the LHC", Proc. PAC99, New York, 29 Mar. – 2 Apr. 1999, pg. 1674.
- [8] M. Furman, "Beam-beam simulations for separated beams", this workshop.
- [9] P. Datte, J. Ludwig, P.F. Manfredi, J.E. Millaud, D.R. Nygren and W.C. Turner, "Preliminary Design Considerations on the LHC Beam Monitor", LBNL internal report dated 13 Dec. 1999.
- [10] W.C. Turner, "The effect of TAN z location on the relative luminosity signal and the correlations of apparent luminosity with crossing angle and IP position", LBNL CBP Tech. Note 203, 27 Mar. 2000.
- [11] N. Mokhov, "MARS Code Developments, Benchmarking and Applications", Proc. ICRS-9 Intl. Conf. on Radiation Shielding", Tsukuba, Japan, Oct. 1999, and references therein. <http://www-ap.fnal.gov/~mokhov/papers/2000/Fermilab-Conf-00-066.ps>

# Detuning, Resonances and the Complete Non-linear Model determined from Turn-by-Turn Pick-up Data

F. Schmidt, CERN, Geneva, Switzerland

## Abstract

Recently, it has been demonstrated that a sufficiently precise FFT spectrum can be used to construct a complete non-linear model of an accelerator like the LHC. Each spectrum line in the FFT from turn-by-turn tracking data has one corresponding term in the distortion function in resonance basis. This distortion function is normally derived from a one-turn map using Normal-Form techniques. Using the same tools one can perform the inverse operation from the distortion function back to the one-turn map which represents the non-linear model of the accelerator. The method requires small amplitude oscillation and is applied in an order by order fashion starting with the sextupole terms.

This method should work equally well for experimental data from turn-by-turn pick-ups given that the noise level of the measurement system is low enough. An additional advantage is the fact, that all linear parameters can be measured as well such that a complete description of the linear and non-linear model should be obtainable.

## 1 INTRODUCTION

Since many years perturbation theory [1] and more recently the Normal Form [2-5] techniques have been used to understand nonlinear motion of single particles in hadron accelerators. This has proven to be very useful in the design phase of an accelerator. When it comes to existing machines these sophisticated tools have been rarely in use up to now. In part this is due to the complexity of the theory but also due to the fact that a nonlinear model of the accelerator cannot be predicted easily. Checking such a model experimentally [6, 7] may prove even more difficult.

One well documented attempt to overcome this problem has been made by Bengtsson [8]. In the framework of the first order perturbation theory he has studied how the real spectra from tracking or experimental turn-by-turn data can be related to resonances. This study has stopped short of a complete solution. An important prerequisite to his analysis was a tune measurement technique superior to the standard FFT [9]. Similar attempts were performed in the field of celestial mechanics [10].

Recently, new techniques were developed [11, 12], allowing an even more precise determination of the tunes. It seems therefore appropriate to review the link between experimental data and theoretical models. The frequency map analysis by Laskar [11] can be used not only to derive the tune, but also to find spectral lines in descending order of magnitude. It has already been shown how these spectra can be applied to remove from a sequence of tracking data unwanted regular complexity. Moreover, this method

has been successfully used to correct resonances excited by sextupoles [13].

## 2 SOME THEORY

The theory has been developed in depth in Ref. [14] a short outline of which can be found in this section.

Complex Fourier spectrum of normalised coordinates can be written as:

$$\hat{x}(N) - i\hat{p}_x(N) = \sum_{j=1}^{\infty} a_j e^{i[2\pi(m_j\nu_x + n_j\nu_y)N + \psi_j]} \quad (1)$$

$m_j, n_j \in \mathbf{Z}$ ,

The connection between one-turn maps and Normal Form can be conveniently described using the Map - Normal Form Diagram (for details see [3, 5]):

$$\begin{array}{ccc} \mathbf{x} & \xrightarrow{\mathbf{M}} & \mathbf{x}' \\ \Phi^{-1} \downarrow & & \downarrow \Phi^{-1} \\ \zeta & \xrightarrow{\mathbf{U}} & \zeta' \end{array} \quad (2)$$

Generating function  $F$  and Hamiltonian  $H$  are given by:

$$\Phi = e^{iF(J, \phi)}, \quad \mathbf{U} = e^{iH(J)} \quad (3)$$

The Normal Form coordinates can then be written as:

$$\zeta = e^{-iF_r} \mathbf{h}, \quad h_z^{\pm} = \hat{z} \pm i\hat{p}_z, \quad (4)$$

with the generating function in resonance basis:

$$F_r = \sum_{jklm} f_{jklm} \zeta_x^{+j} \zeta_x^{-k} \zeta_y^{+l} \zeta_y^{-m} \quad (5)$$

or

$$F_r = \sum_{jklm} f_{jklm} (2I_x)^{\frac{j+k}{2}} (2I_y)^{\frac{l+m}{2}} \times e^{-i[(j-k)(\psi_x + \psi_{x_0}) + (l-m)(\psi_y + \psi_{y_0})]} \quad (6)$$

The generating function in action leads to:

$$\mathbf{h} = e^{iF_r} \zeta = \zeta + [F_r, \zeta] + \frac{1}{2}[F_r, [F_r, \zeta]] + \dots \quad (7)$$

The evolution of linearly normalised coordinates can be written as:

$$h_x^-(N) = \sqrt{2I_x} e^{i(2\pi\nu_x N + \psi_{x_0})} - 2i \sum_{jklm} j f_{jklm} (2I_x)^{\frac{j+k-1}{2}} (2I_y)^{\frac{l+m}{2}} \times \quad (8)$$

$$e^{i[(1-j+k)(2\pi\nu_x N + \psi_{x_0}) + (m-l)(2\pi\nu_y N + \psi_{y_0})]}.$$

As a consequence the terms of the generating function and the spectral lines are related as follows:

Generating Function		Spectral Line
Amplitude	$ f_{jklm} $	$ HSL_{jklm}  = 2 \cdot j \cdot (2I_x)^{\frac{j+k-1}{2}} (2I_y)^{\frac{l+m}{2}}  f_{jklm} $
		$ VSL_{jklm}  = 2 \cdot l \cdot (2I_x)^{\frac{j+k}{2}} (2I_y)^{\frac{l+m-1}{2}}  f_{jklm} $
Phase	$\phi_{jklm}$	$PHSL_{jklm} = \phi_{jklm} + (1 - j + k)\psi_{x_0} - (l - m)\psi_{y_0} - \frac{\pi}{2}$
		$PVSL_{jklm} = \phi_{jklm} - (j - k)\psi_{x_0} + (1 - l + m)\psi_{y_0} - \frac{\pi}{2}$

### 3 APPLICATION IN TRACKING STUDIES

#### 3.1 Fourth Order Resonance

In this section the method is applied to the well studied LHC lattice version 4 [15]. A set of 60 realizations of the random multipolar errors, called seeds in the following, are included in the dipoles and quadrupoles. For each seed a set is generated of  $10^4$  tracking data starting with a small initial amplitude of  $1 \sigma$ . In this region of phase space the amplitude dependence of the lines is to a very good approximation quadratic for the lines generated by third order terms and cubic for the lines generated by fourth order terms. Therefore, it can be concluded that higher order contributions are not relevant at  $1 \sigma$ . Those quadratic sextupoles contributions to the octupole resonances can be neglected, knowing that the sextupole contributions, which are largest in the main dipoles, are quasi-locally corrected. In parallel, the maps and the resonant Hamiltonian in resonance basis are calculated using the DaLie program [16]. As an example, Fig. 1 shows that the Hamiltonian terms of the regular resonance (2, -2) can be predicted with excellent precision from the line spectra of all 60 seeds.

#### 3.2 Reduction of Phase Space Deformations

In a first example (LHC case in Fig. 2a, c) the do-nut shaped horizontal phase space is reduced to a near perfect circle by removing the first 100 dominant lines. It goes without saying that the tune line has to be kept. This procedure does not introduce high order distortions which tend to spoil the usefulness of perturbative techniques like Normal Form.

The strong reduction of phase space distortion can be applied to sharpen the method for detecting the onset of chaos [17]. In Fig. 2b a typical case is shown of the evolution of the angular distance in phase space of initially close-by particles. In the case of regular motion a linear increase of this distance is expected. The large variations of the distance may make it difficult however to decide about the nature of the particle motion.

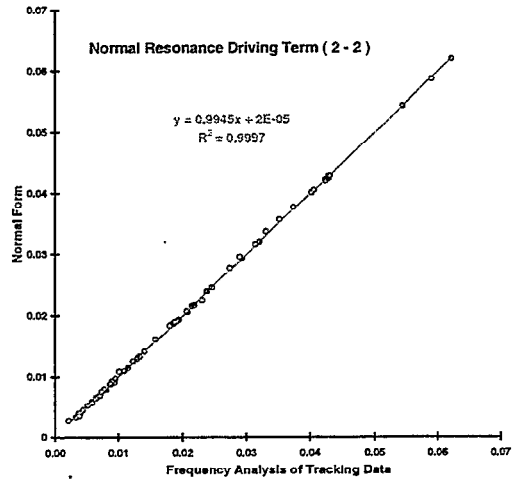


Figure 1: Hamiltonian Term from Normal Form and from Tracking Data for 60 Seeds of the LHC Lattice Version 4

The subtraction of lines (compare part d.) to part b.) offers an easy and reliable method to reduce these variations.

The most difficult test is the study of motion close to resonance structures. The large five islands (SPS case in Fig. 2a) can indeed be reduced to points by the subtraction of lines as seen in part b.). The one essential precondition of this method is however the existence of a well defined tune. The method therefore fails in the case of chaotic motion, here achieved by approaching the vicinity of the separatrix motion. The subtraction of 100 lines that transform part c.) into part d.) does no longer simplify the complexity in phase space.

### 3.3 The Correction of the Resonances in the LHC

A possible exploitation of the techniques discussed so far consist in the correction of the resonance contributions generated by the nonlinear elements in an accelerator lattice. For this purpose tracking data of a realistic LHC model are analysed.

Following well established strategies for the correction of the resonances [18] one has to identify the location and the strength of a set of correctors families to compensate the third order resonances (3, 0) and (1, 2). A family of sextupolar spool pieces, normally used to correct the average  $b_3$  component along the lattice was split into several families to compensate the cosine and sine term of the two resonance. Using tracking data at each location of the correctors the best places for correctors could be identified, i.e. longitudinal locations where the oscillations of the lines have their extreme values (Fig. 3). Two resonances were corrected simultaneously each with two correction family while keeping the  $b_3$  corrected on average. In this way the amplitude of the lines could be reduced by more than 50%. The resulting reduction of the phase space distortions is clearly visible in Fig. (4). In the tracking (Tab. 3.3) it can be seen that the double resonance correction leads to an improvement of the dynamic aperture of almost 10%.

Table 1: Improvement of Dynamic Aperture due to Resonance Correction

Stability Border	Uncorrected LHC lattice	Correction of (3,0) & (1,2) Resonance
Regular Motion	15.5	16.9
Strong Chaos	16.0	17.1
Lost before 1000 Turns	16.9	18.0

## 4 EXPERIMENTS AT ACCELERATORS

### 4.1 List of Observables

This FFT based method should allow to measure all linear and nonlinear observables relevant to single particle dynamics. In particular the aim is to measure the following properties:

- Phase advance between pickups
- $\beta$ -beating
- Linear coupling
- Chromaticity
- Detuning versus amplitude
- Driving terms of resonances

- Full non-linear model of the accelerator

It goes without saying that a pick-up system of high quality is available around the ring. In the future it remains to be shown that the methods is applicable in the presence of pick-up noise and the unavoidable decoherence of the pick-up signal due to filamentation. The following experimental results are first recorded in Ref. [19].

### 4.2 SPS experiment

The SPS is an ideal test bed for this kind of investigation. The machine has practically no multipolar components so that particles exhibit mainly linear oscillations. Moreover, closed orbit, linear coupling and chromaticity have been well corrected. This "ideal" machine is made non-linear with the use of eight strong sextupoles.

In the experiment, the beam is kicked to various amplitudes and the turn-by-turn data is recorded by all pickups in one sixth of the machine (to which the SPS turn-by-turn recording system is presently limited).

As expected from earlier experiments [20] the detuning as a function of the linear invariant (Fig. 6a) is very well predicted by tracking (all solid lines in Fig. 6 are tracking results obtained with SixTrack [21]). Very promising is the agreement between the tracking and the experiment for the (3,0) resonance (Fig. 6b), the experimental data are systematically lower by a few percent only. When studying the first (1,0) resonance (Fig. 6c) a problem of the closed orbit measuring system becomes apparent. This line is the amplitude dependent offset of the FFT signal after the kick. To calculate this line one has to measure and subtract the signal offset before the kick which was not possible with sufficient precision. Moreover, the number of data samples were limited to 170 turns and there had been unavoidable electronic spikes. Lastly, the other (1,0) resonance (Fig. 6d) is presented which should suffer less from the limitations of the measurement system. Indeed, there is less noise signals in that case. However, there is a significant discrepancy with the tracking data which remains to be understood.

### 4.3 LEP experiment

The electron storage ring LEP was used for another experiment. Five different cases were studied with the 90/60 optics used for physics runs in 1997: one tune close to the (3,0) resonance and two tunes at increasing distance to that resonance. In the latter two cases the beam was kicked to 2 different amplitudes (each case is represented by another symbol in Fig. 7). In Fig. 7a the detuning curves are recorded with a sliding window in tune for two different kick strengths. Both curves lie fairly well on top of each other. The effect of radiation can be directly observed and there is no sign of filamentation [22]. Moreover, the detuning is well predicted by tracking (solid line as calculated with MAD [23]). Both terms of the (1,0) resonance (part c.) and d.) of Fig. 7) show good agreement

between the tracking and the experiment after inclusion of radiation (the straight curve in part c.) is obtained without radiation). However, the (3,0) resonance has a significant discrepancy with the tracking data even when radiation is properly treated. There is almost a factor 10 between experiment and tracking. Although there is not yet a full understanding of the cause of this difference it can probably be addressed to random sextupole components which are not included in the tracking.

## 5 CONCLUSIONS

It has been shown that the tune line spectrum can serve as a powerful tool to deal with strong nonlinearities in single particle motion. It is appealing for accelerator designer to have a tool that works without involved mathematical apparatus. It works very well in simulations and is expected to be equally useful in machine experiments. In fact, it has been demonstrated that these lines can be used to suppress unwanted phase space distortions and to correct resonances in a non-perturbative manner.

Preliminary experiments show a promising similarity between experiment and theory. In upcoming experiments it will be studied to which extent this technique allows the evaluation of nonlinearities and their correction.

## 6 REFERENCES

- [1] A. Schoch, "Theory of linear and non-linear perturbations of betatron oscillations in alternating gradient synchrotrons", CERN 57-21, (1958).
- [2] A. Bazzani et al., "Normal forms for Hamiltonian maps and nonlinear effects in a particle accelerator", *Nuovo Cim.*, B **102**, pp. 51-80 (1988).
- [3] M. Berz, É. Forest and J. Irwin, "Normal form methods for complicated periodic systems: a complete solution using differential algebra and lie operators", *Part. Acc.* **24**, pp. 91-107 (1989).
- [4] M. Berz, "Differential-algebraic description of beam dynamics to very high orders", *Part. Acc.* **24**, pp. 109-124 (1989).
- [5] A. Bazzani, E. Todesco, G. Turchetti and G. Servizi, "A normal form approach to the theory of nonlinear betatronic motion", CERN 94-02, (1994).
- [6] W. Fischer, M. Giovannozzi and F. Schmidt, "The dynamic aperture experiment at the CERN SPS", CERN SL/95-96 (AP), *Physical Review E* Vol. **55**, Number 3, p. 3507, March 1997.
- [7] O. Brüning, W. Fischer, F. Schmidt and F. Willeke, "Comparison of measured and computed dynamic aperture for the SPS and the HERA proton ring", presented at the "LHC95 International Workshop on Single-particle Effects in Large Hadron Colliders", Montreux, October 1995.
- [8] J. Bengtsson, "Non-Linear transverse dynamics for storage rings with applications to the low-energy antiproton ring (LEAR) at CERN", CERN 88-05, (1988).
- [9] E. Asseo, J. Bengtsson and M. Chanel, "Absolute and high precision measurements of particle beam parameters at CERN antiproton storage ring LEAR using spectral analysis with correction algorithms", Fourth European Signal Processing Conference, edited by J. L. Lacoume et al., North Holland, Amsterdam, pp. 1317-1320 (1988).
- [10] J. Laskar, "Secular evolution of the solar system over 10 million years", *Astron. Astrophys.* **198**, pp. 341-362 (1988).
- [11] J. Laskar, C. Froeschlé and A. Celletti, "The measure of chaos by the numerical analysis of the fundamental frequencies. Application to the standard mapping", *Physica D* **56**, pp. 253-269 (1992).
- [12] R. Bartolini, A. Bazzani, M. Giovannozzi, W. Scandale, and E. Todesco, "Tune evaluation in simulations and experiments", *Part. Acc.* **56**, pp. 167-199 (1996).
- [13] R. Bartolini and F. Schmidt, "Evaluation of non-linear phase space distortions via frequency analysis", LHC Project Report 98 and in the proceedings of the workshop on: "Nonlinear and Collective Phenomena in Beam Physics", Arcidosso, September 1996.
- [14] R. Bartolini and F. Schmidt, "Normal Form via Tracking or Beam Data", LHC Project Note 132 (revised December 1999), *Part. Accel.* **59**, pp. 93-106, (1998), <http://wwwslap.cern.ch/frs/report/lines97.ps.gz>.
- [15] M. Böge and F. Schmidt, "Tracking studies for the LHC optics version 4 at injection energy", LHC Project Report 103, presented in part at the Particle Accelerator Conference, Vancouver, May 1997.
- [16] É. Forest, "The DaLie code", 1986, unpublished.
- [17] F. Schmidt, F. Willeke and F. Zimmermann, "Comparison of methods to determine long-term stability in proton storage rings", *Part. Accel.* **35**, 1991, pp. 249-256.
- [18] G. Guignard, "A General Treatment of Resonance in accelerators", CERN 76-12, 1976.
- [19] R. Bartolini, L.H.A. Leunissen, Y. Papaphilippou, F. Schmidt, A. Verdier, "Measurement of Resonance Driving Terms from Turn-by-Turn Data", 1999 Particle Accelerator Conference - PAC '99 New York City, NY, USA, CERN-SL-99-032 AP, <http://wwwslap.cern.ch/frs/report/TUP36.ps.gz>.
- [20] W. Fischer et al., *Phys. Rev. E* Vol. **55**, no. 3, 3507 (1995).
- [21] F. Schmidt, CERN SL 94-56 (AP).
- [22] A.-S. Müller, 7<sup>th</sup> LEP Perf. Workshop, CERN SL 97-06 (DI).
- [23] H. Grote and C.H. Iselin, CERN SL 90-13 (AP).

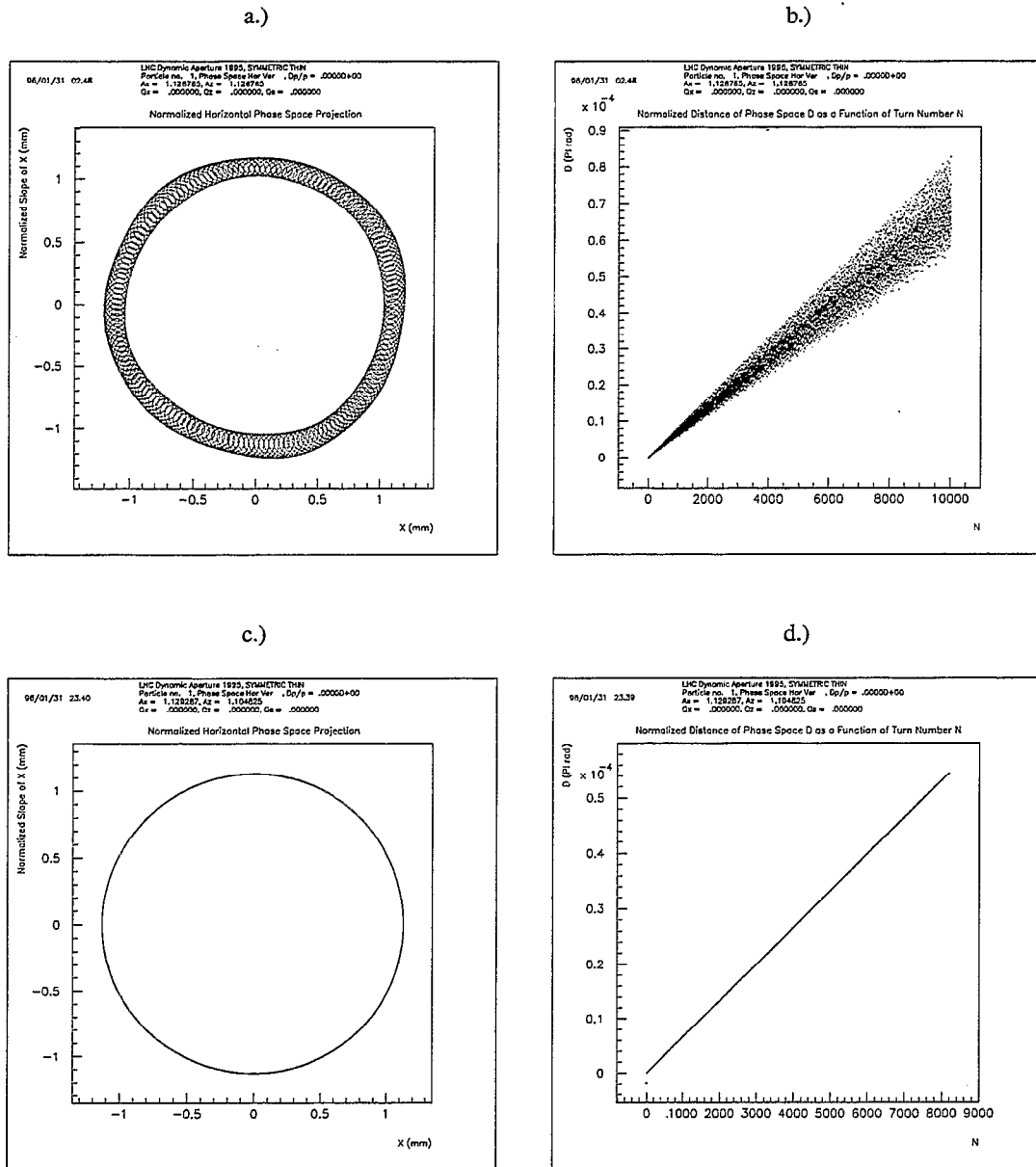


**Figure 2: Reducing Phase Space Distortions by Subtraction of dominant Lines**

Part a.) shows a typical horizontal phase space plot of nonlinear particle motion in a LHC structure. The linear increase of the distance of two initially close-by particles indicates that the motion is regular, that is to say stable forever. Taking out the most dominant lines (with the exception of the tune line) reduces the phase space to a near perfect circle part c.). Moreover the increase of the distance in phase space, the distance in phase space, which is shaped like a wedge as seen in part b.), reduces to a thin line after the subtraction part d.).

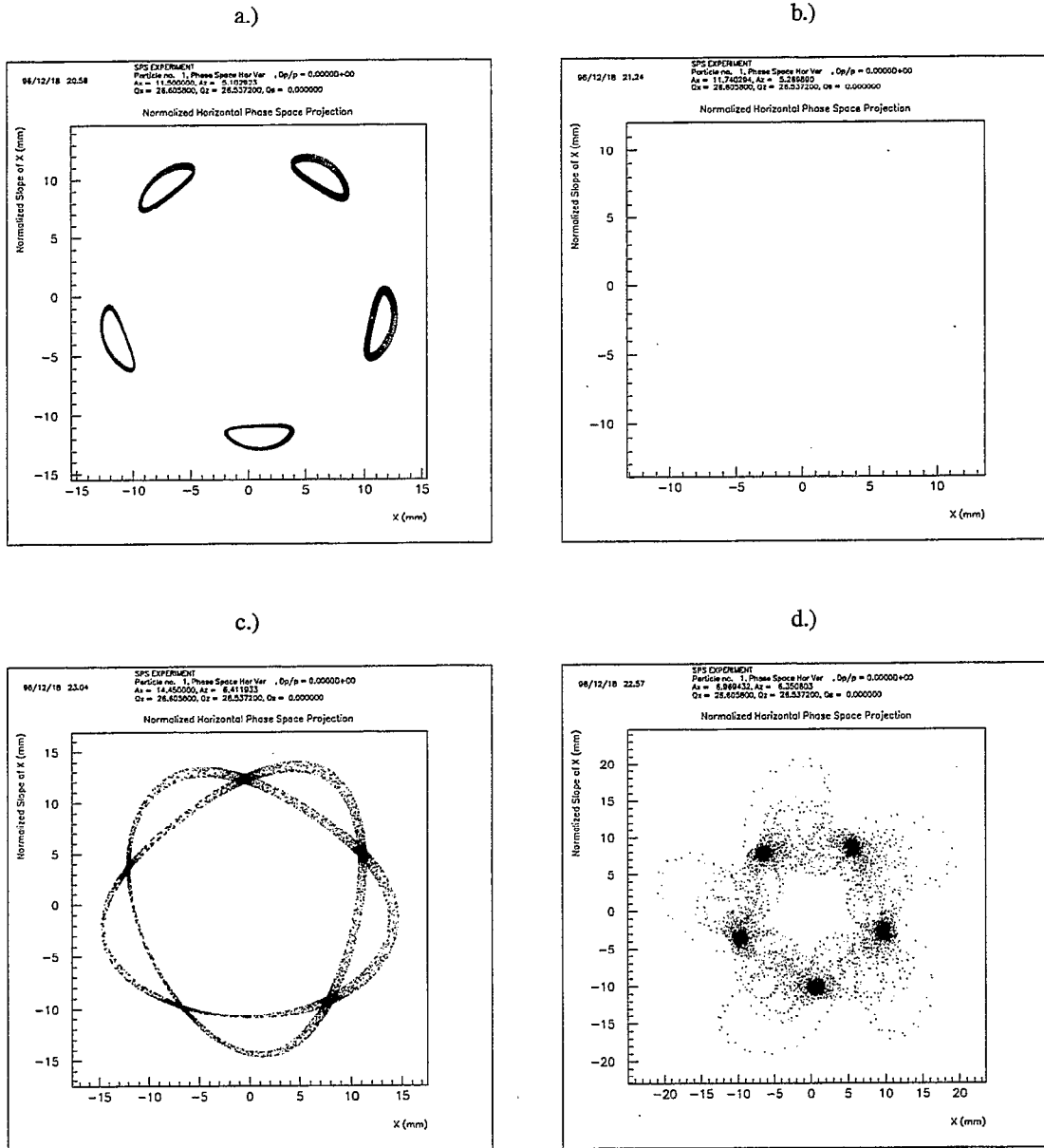


**Figure 3: Reducing Phase Space Distortions close to 5<sup>th</sup> Order Resonance**

The motion close to a 5<sup>th</sup> order resonance is shown in part a.). Taking out the 100 largest lines while keeping the tune line reduces the islands to points which are just visible in part b.). The method works of course only for regular motion. Once chaotic motion is considered, here by approaching the separatrix part c.), the subtraction of lines no longer leads to point-like objects part d.). On the contrary, one can argue that the phase space has become more distorted after this subtraction.

Position of Correctors for (3,0) Resonance.

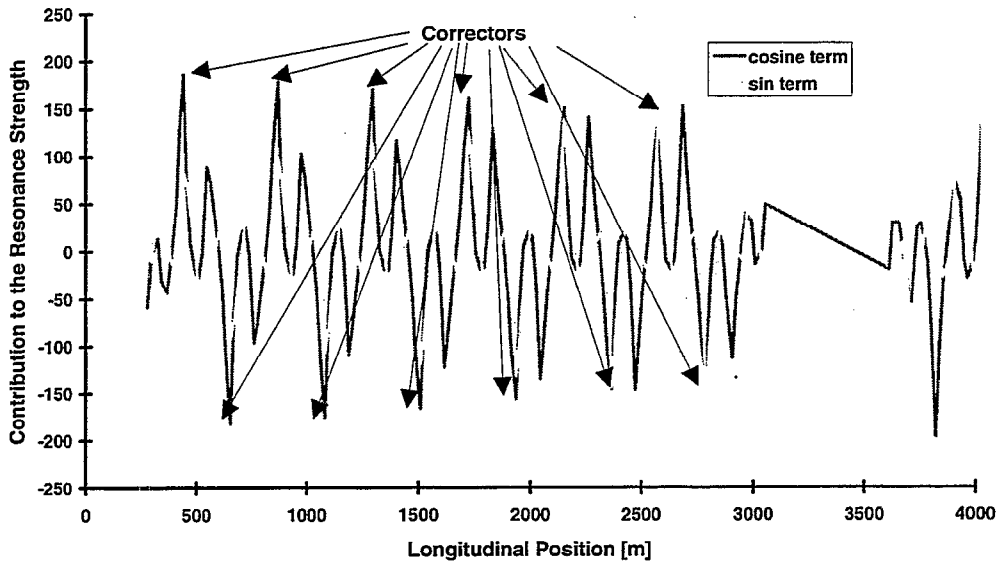
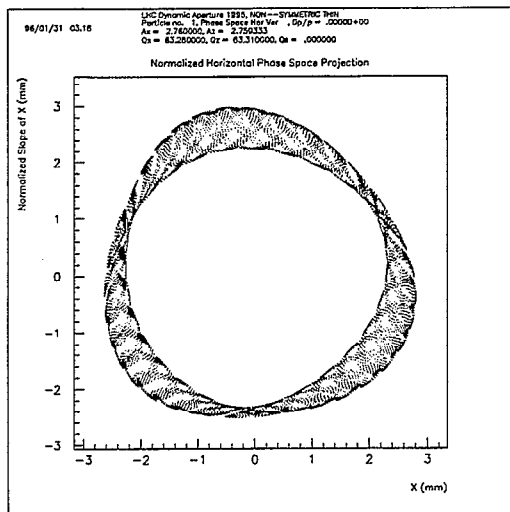


Figure 4: Choosing best places for correcting the (3,0) resonances with sextupoles

a.)



b.)

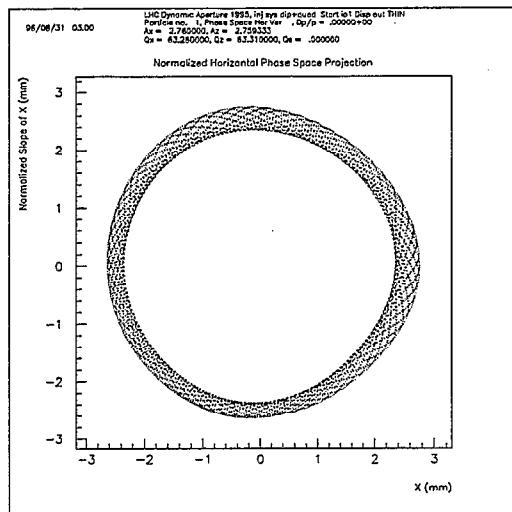
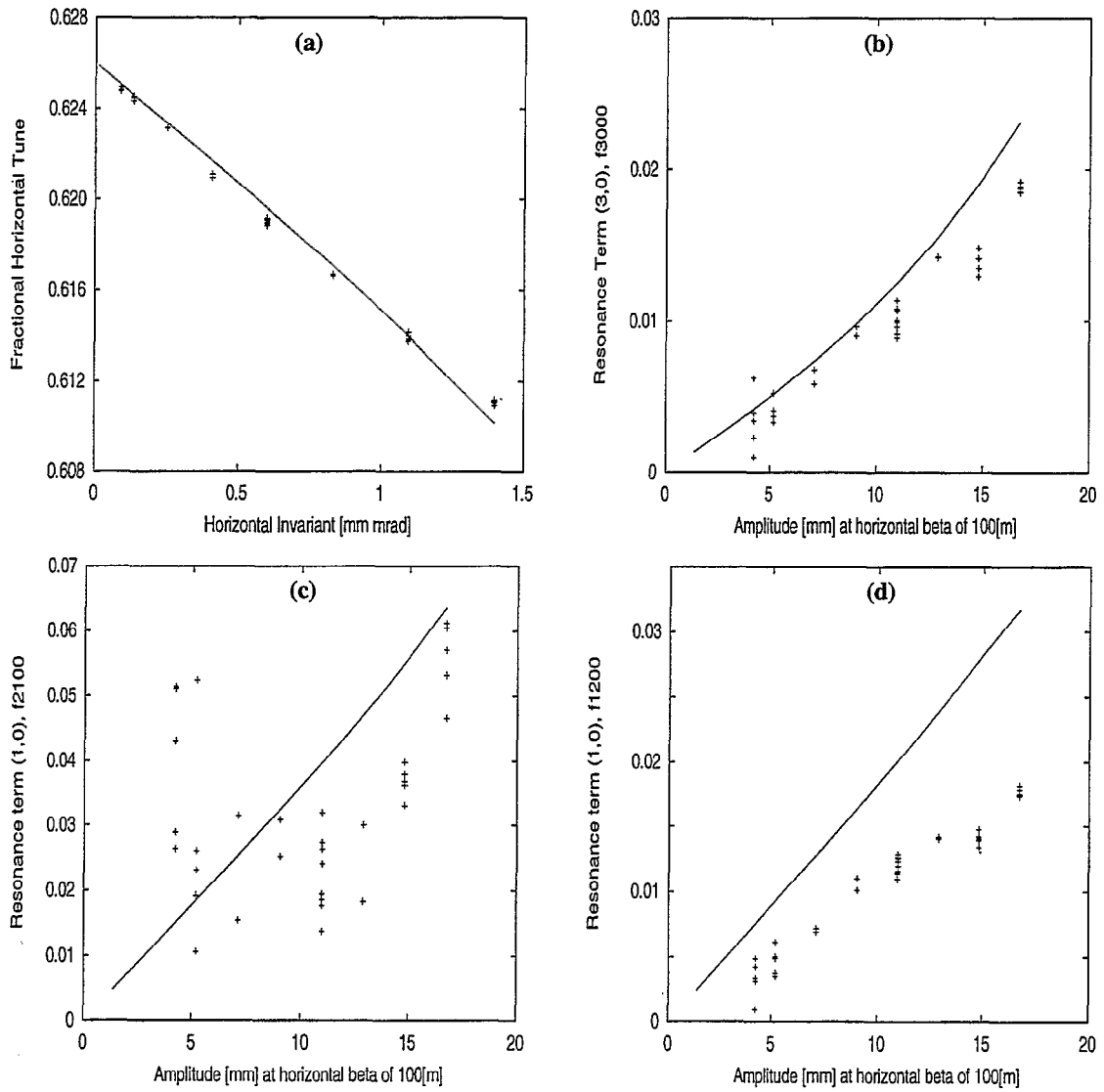


Figure 5: Reduction of Phase Space Distortion due to Correction of Resonances

In part a.) the horizontal phase space of particle motion is shown in a LHC lattice with the (3,0) and the (1,2) resonance strongly excited. These resonances have been corrected resulting in the corresponding phase space projection as depicted in part b.).



**Figure 6: Detuning and First Order Sextupole Driving Terms**

Part (a): Detuning versus linear Invariant  $I_x$ ; Part (b): (3, 0) Resonance versus Amplitude;

Part (c): (1, 0) Resonance ( $f_{2100}$ ) versus Amplitude; Part d.): (1, 0) Resonance ( $f_{1200}$ ) versus Amplitude;

–Lines are from tracking

–Symbols are experimental data

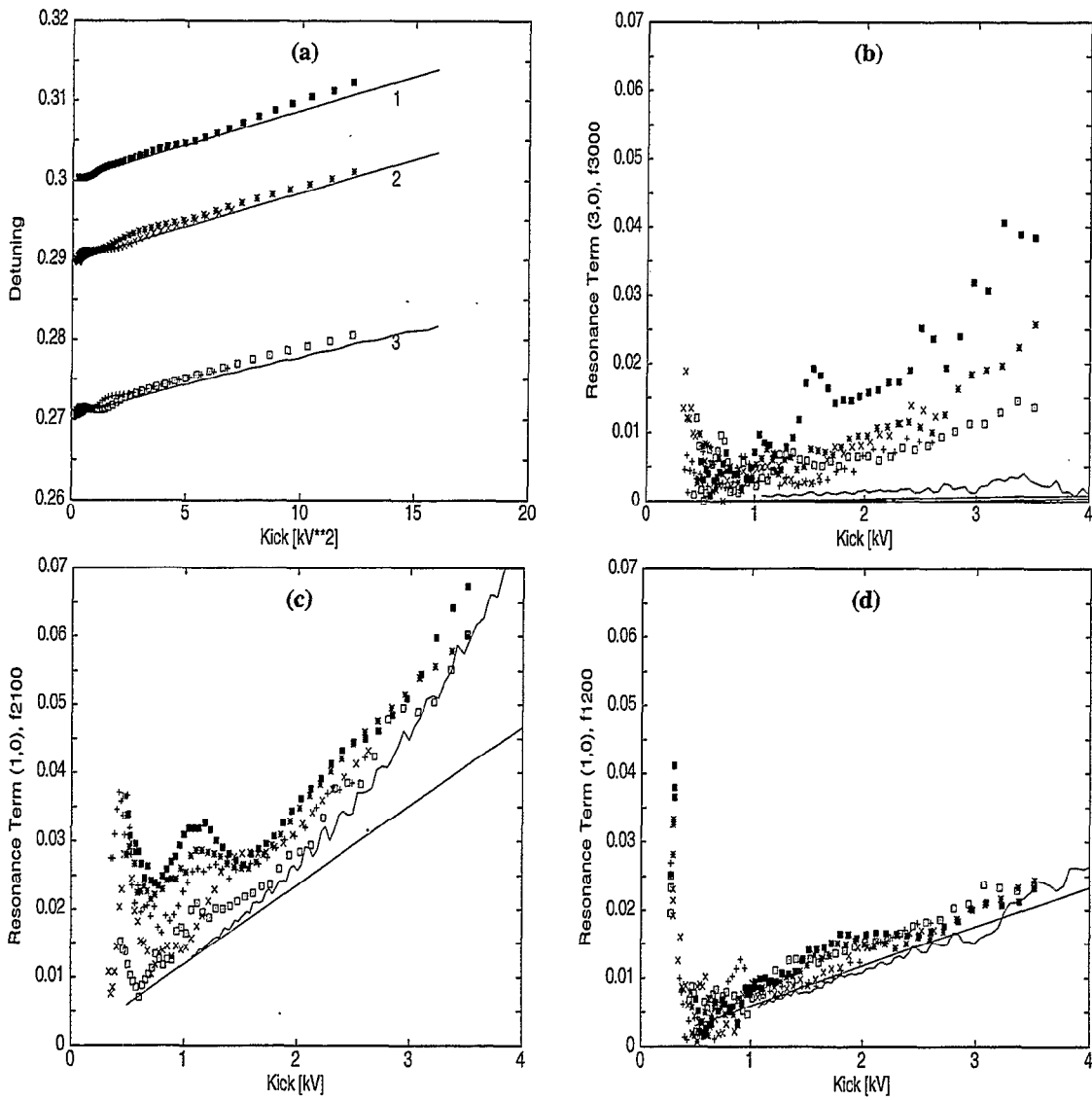


**Figure 7: Detuning and First Order Sextupole Driving Terms**

Part a.): Detuning versus kick amplitude [kV<sup>2</sup>]; Part b.): (3, 0) Resonance versus Amplitude;

Part c.): (1, 0) Resonance ( $f_{2100}$ ) versus Amplitude; Part d.): (1, 0) Resonance ( $f_{1200}$ ) versus Amplitude;

—Lines are from tracking

—Symbols are experimental data

# MEASUREMENTS OF COHERENT TUNE SHIFT AND HEAD-TAIL GROWTH RATES AT THE SPS

G. Arduini, H. Burkhardt, K. Cornelis, Y. Papaphilippou\*, F. Zimmermann, M.P. Zorzano, CERN, Geneva, Switzerland

## Abstract

A series of measurements of the coherent tune shifts with intensity and of head-tail growth rates have been performed with single proton bunches in the SPS, at 26 GeV. From these, the real and imaginary part of the transverse impedance can be estimated. This study, together with earlier and future measurements, will be used to experimentally document and follow up the effect of the impedance improvements on the SPS as injector to the LHC. A reproducibility at the 20% level was achieved for the value of the effective vertical impedance inferred from the coherent tune shift measurements.

## 1 INTRODUCTION

Several measurements, similar to those described in this article have been performed in the past, in the SPS. The main results are summarized in table 2. Most of these measurements, however, are quite old. Furthermore, they present a significant spread in the obtained vertical and horizontal broadband impedance parameters, covering about a factor of 3 from 12 to 48 M $\Omega$ /m in  $Z_v/Q$ .

In the present measurements, we aimed for an uncertainty below 20% in the impedance estimation. This would allow us to follow up and document experimentally the various steps of improvements planned to reduce the impedance of the SPS as injector into the LHC. As much as possible, we try to perform the measurements with the same bunch dimensions. This minimizes the model dependence and uncertainties due to variation in bunch parameters.

## 2 BEAM CONDITIONS

The measurements were all performed using single and relatively short bunches ( $\sigma_z \approx 16$  cm or 5.5 ns) injected at 26 GeV in the SPS machine development (MD) cycle. Single short bunches were chosen for simplicity and in order to have a significant effect. The fixed beam energy of 26 GeV was rather imposed by beam availability. It would be useful in the future to confirm these measurements at a higher energy, to exclude any bias from space-charge effects [1].

The measurements were performed close to "standard tunes" ( $Q_x = 26.62$ ,  $Q_y = 26.58$ ). Chromaticity was carefully measured and corrected in order to be slightly positive (this was achieved with settings of typically  $\xi_x = -0.16$ ,  $\xi_y = +0.26$ ). The octupole components in the machine were compensated using octupole settings of typi-

cally  $-0.70$  for the radial and  $-0.75$  for the horizontal component. The damper was switched off and the tune measurements were done using 1 mm (nominal) kicks. With these settings and for small intensities ( $\sim 10^{10}$  protons), one obtains rather clean sinusoidal oscillations with little damping, observable online over  $2^{12} = 4096$  turns using the SPS tune application.

The variation of proton intensity in the range of 1 to  $10 \cdot 10^{10}$  protons was performed in the PS. Ideally, the bunch dimensions and in particular the bunch length should not vary. The best compromise was achieved by adjusting the beam in the PS for the highest intensity first (close to  $10 \cdot 10^{10}$ ), and then reducing it by vertical scraping. In this way, the bunch length and horizontal beam size remained nearly constant.

Longitudinal bunch parameters were also recorded on the PS side for every step in intensity. Typical numbers were: longitudinal emittance  $\epsilon_z = 0.2$  eVs ( $2\sigma$ ), total ( $\sim \pm 2\sigma$ ) bunch length  $l = 4$  ns and  $\Delta p/p = 1.9 \cdot 10^{-3}$  ( $\pm 2\sigma$ ).

On the SPS side, the 200 MHz rf was adjusted to obtain good capture and matching. Depending on intensity, this was achieved with voltages in the range of 0.5 - 0.8 MV.

In order to be independent of injection optimization and to have shorter bunches with a larger effect on the coherent tune shift, the rf was ramped adiabatically to 3 MV nominal (corresponding to about 2.5 MV measured) just before the time of the measurements. Details are given in Table 1.

Table 1: MD-cycle timing and RF-voltage

event	$\Delta t$ start / $\Delta t$ inj. (ms)	turns	$V_{rf}$ (MV)
cycle start	0		0.5
injection	972 / 0	0	0.5
rf-ramp start	1000 / 28	1214	0.5
rf-ramp end	1080 / 108	4685	3
$Q_y$ meas. start	1080 / 108	4685	3
$Q_x$ meas. start	1110 / 138	5986	3
cycle end	1700 / 728	31578	3

## 3 BUNCH DIMENSION

The vertical and horizontal bunch dimensions were recorded as a function of the proton intensity using wire-scanners. The results are shown in Figures 1, 2 and 3. Note that typical horizontal emittances from PS on the experiment of the 17/9/1999 were 0.36, 0.46, 0.4, 0.38 [ $\mu$ m] at  $2\sigma$ . The horizontal measurements are scattered with max-

\* Present address: BNL, Upton, NY 11973, USA

Table 2: Broadband resonance parameters found in earlier transverse impedance measurements and calculations.

$Z/Q$ in $M\Omega/m$		year	studies performed
vertical	horizontal		
18		1980	head-tail growth rates (protons @ 270 GeV) [2]
47.7		1984	tune difference of high/low intensity bunches [3]
13 / 12.5	-8 / -5.2	1986	coherent tune shift (corrected for space-charge) / computed [4]
26.8	-16.88	1988	coherent tune shift @ 31.5 GeV [5]
$(23 \pm 2)$		1993	leptons, TMCI threshold [6]

imal variations of about 40%. As we mentioned previously, the PS beam was used at its maximum intensity and then it was scraped vertically to obtain the desired number of protons. This had an effect on the vertical dimension of the beam which was bigger at higher currents.

An approximately constant voltage of  $V_{rf} = 0.8$  MV was used on the first MD, on the 23/08/1999. A shorter and better controlled bunch length was obtained in the subsequent MD's using the voltage ramp described above. The bunch length was systematically recorded. The results at the time relevant for the tune measurements<sup>1</sup> are shown in Figure 4.

A good knowledge of the bunch length  $\sigma$  is needed to extract the parameters of the broad band impedance model. Since the bunch length is not constant we will use the average  $\langle\sigma\rangle$  of all individual length measurements in our calculations. The r.m.s. spread in the measured bunch length is used as the error in the determination of  $\sigma$  and will lead to an error in the impedance estimate. These values are summarized in Table 3.

#### 4 METHOD OF ANALYSIS OF TUNE AND GROWTH RATE MEASUREMENTS

The frequency analysis method is a refined Fourier analysis which can be applied on experimental or tracking data. More details about the mathematical details of the method can be found in papers of Laskar who introduced it in celestial mechanics [7] and accelerator dynamics [8].

The basic feature of the method is to produce a quasi-periodic approximation, truncated to order  $N$ ,

$$f'(t) = \sum_{k=1}^N a_k e^{i\omega_k t}, \quad (1)$$

with  $f'(t)$ ,  $a_k \in \mathbb{C}$ , of a numerical function  $f(t) = q(t) + ip(t)$ , usually representing in complex form the position and conjugate momenta associated with one of the degrees of freedom of a Hamiltonian dynamical system. This function can be either obtained by usual numerical integration or by real experimental data, recorded for a finite time span  $t = T$ . As we assume that the signal is quasi-periodic, the different frequencies of the series should be a linear combination of some base or fundamental frequencies  $\omega_k = k \cdot \omega$ .

<sup>1</sup>Closer to injection, for the capture voltage of  $V \approx 0.62$  MV and  $N_p = 2.5 \times 10^{10}$  we get  $\sigma = 0.7$  ns, which is consistent with the value of 0.7 ns for the longitudinal  $\sigma$  given by the PS at these intensities.

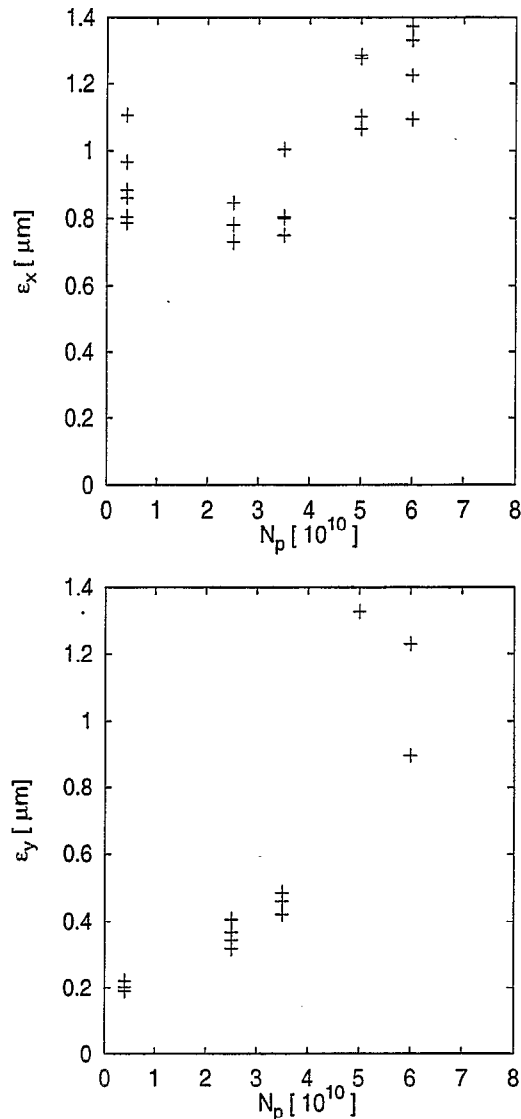


Figure 1: Proton horizontal emittance (top) and vertical emittance (bottom) as a function of bunch population, for an effective voltage  $V_{rf} \approx 2.5$  MV (measured on 23/08/1999).

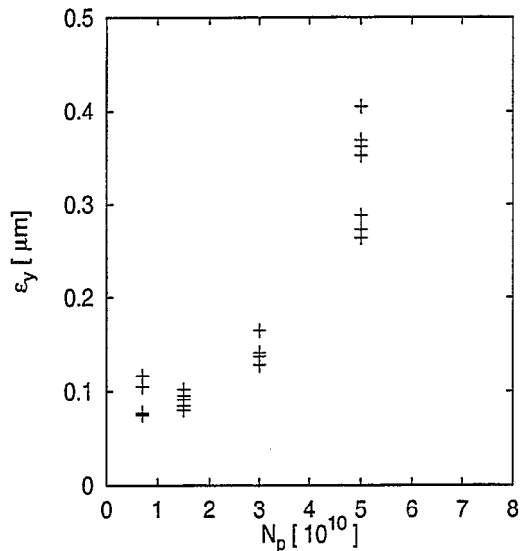


Figure 2: Vertical proton emittance ( $4\sigma_y^2/\beta_y$ ) as a function of bunch population. Measured with a wire-scanner at a location with  $\beta_y = 22$  m (measured on 17/9/1999).

Through an advanced filtering algorithm using the Hanning window, the method guaranties the asymptotic accuracy of the determination of the base tunes to be of the order of  $1/T^4$  [9] for quasi-periodic signals, compared to  $1/T$  of an FFT. Actually for the noisy signals associated with experimental data, we can expect an accuracy of the order of  $1/T^2$  [10]. In that way, the horizontal and vertical coherent tune shifts can be efficiently estimated by applying the method to the raw data representing the coherent bunch oscillations.

Another interesting application of the method is the determination of the damping or growth rates, associated to some kind of collective instability, in a real accelerator. In fact, we may consider that the amplitudes of the series, instead of being constant, depend exponentially on time  $a_k(t) = A_k e^{t/\tau}$ , with  $1/\tau$  denoting the growth or damping rate. A straightforward calculation of this rate can be achieved by estimating one of the amplitudes of the series (e.g. the one corresponding to the base frequency  $a_1(t)$ ), for successive time spans (e.g. every 100 turns) and then fit an exponential to represent the function  $a_1(t)$ .

As example, we present in Fig. 5 one of the measurements effectuated in the SPS while the vertical chromaticity was slightly negative, producing a growth from the head-tail instability in the vertical plane. In Fig. 5, the actual measurement from the SPS acquisition system and the exponential fit with the calculated growth rate are plotted. We may note the good accuracy with which the growth rate is obtained (the  $R^2$  of the fit is very close to 1).

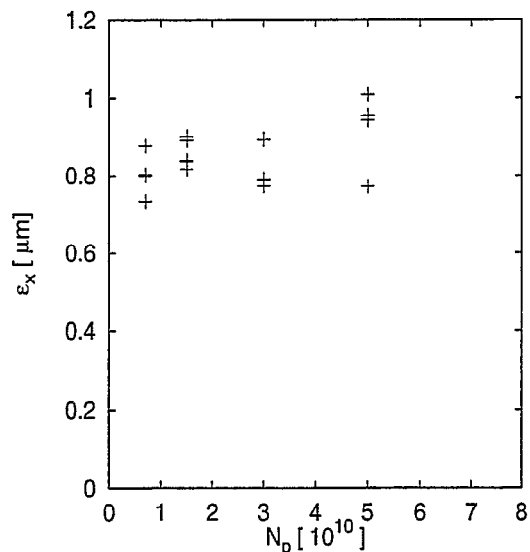
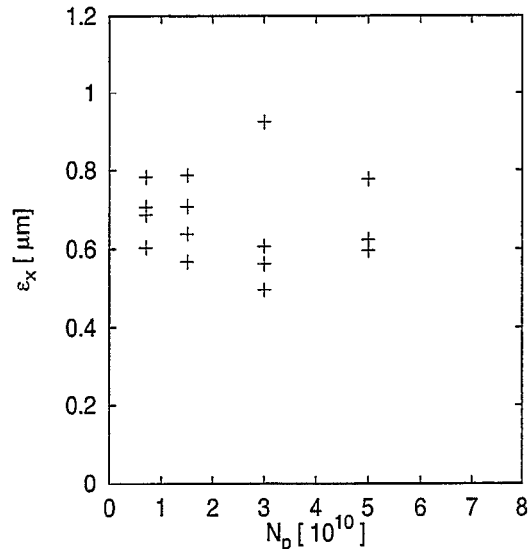


Figure 3: Horizontal proton emittance ( $4\sigma_x^2/\beta_x$ ) as a function of bunch population, for the capture voltage (top) and after the ramp at  $V_{rf} \approx 2.5$  MV (bottom). Measured with the wire-scanner on 17/9/1999 at a location with  $\beta_x = 97$  m and dispersion  $D = 2.9$  m. Typical  $\Delta p/p$  reported from PS:  $1.6 \times 10^{-3}$ ,  $2 \times 10^{-3}$ ,  $1.6 \times 10^{-3}$  and therefore  $(D\Delta p/p)^2/\beta_x \approx 0.35$  at injection.

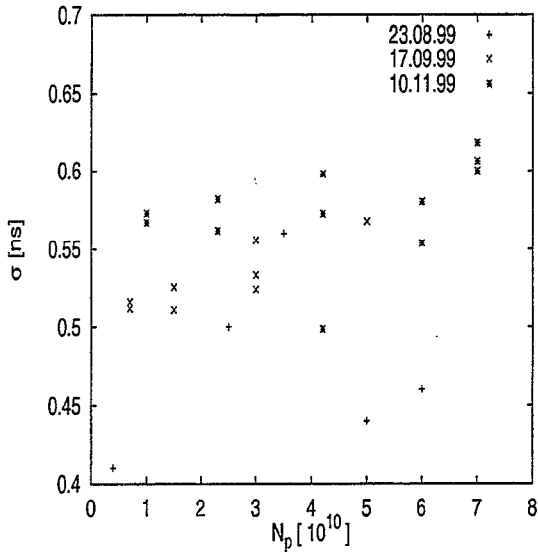


Figure 4: Longitudinal  $\sigma$  as a function of bunch population, as found by fitting the longitudinal profile with a Gaussian distribution. Measured when the actual voltage is  $V \approx 2.5$  MV (or 3 MV nominal voltage).

## 5 HORIZONTAL AND VERTICAL TUNE SHIFT AS A FUNCTION OF BUNCH POPULATION

The vertical and horizontal tunes were obtained by kicking the beam and post-processing the time sequence (1024 to 4096 turns) of the beam position. Using the frequency analysis technique, the precision of the measurement was increased. We have measured the tunes after the adiabatic ramp for bunch population between  $10^{10}$  and  $5 \times 10^{10}$ .

In Figures 6, 7, 8 and 9 we show the measured tune as a function of bunch population, for the horizontal and vertical plane. As expected from measurements performed in the past, with increasing current the vertical tune decreases and the horizontal tune increases. The slope of these plots is related to the imaginary part of the impedance. The difference in sign and magnitude between the two planes is due to the flat dimensions of the chamber: the horizontal mean radius is about 7 cm and the vertical mean radius of the SPS chamber is about 2.4 cm.

The data was fit to a straight line  $f(x) = a \cdot x + b$ . To obtain realistic errors for the slope, the uncertainties in each tune point were scaled to obtain  $\chi^2 = 1$  for the fit.

### 5.1 Summary Of Tune-shift Measurement

In Table 3 we summarize the slopes found and the errors, as well as the  $\sigma$  of the longitudinal distribution. Note that the measurement on the 13/08/1999 was done without ramp of the rf-voltage, *i.e.* with longer bunches.

The bunch mode spectrum for these  $\sigma$  extends up to  $f =$

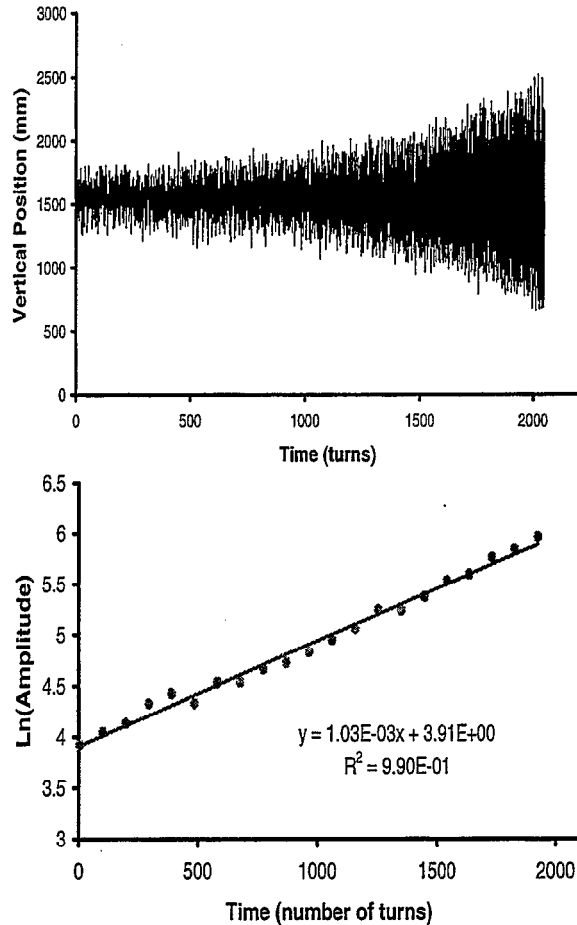


Figure 5: Vertical position of a bunch with slightly negative chromaticity, as measured by the SPS acquisition system (top) and growth rate obtained by fitting an exponential to the leading oscillating amplitude of the series issued by the frequency analysis method (bottom).

$$1/(2\pi \cdot \sigma) \approx 300 \text{ MHz.}$$

## 6 GROWTH RATE AS A FUNCTION OF CHROMATICITY

For negative chromaticity, and operating above transition, the head-tail mode ( $l = 0$ ) becomes unstable and drives the motion of the centroid of the beam. The amplitude of these oscillations increases exponentially in time. Analyzing this exponential growth, we get the growth rate  $1/\tau$  which increases with  $|\xi|$ . The slope of this plot is related to the real part of the impedance.

During our most recent experimental attempt on the 10/11/1999, we studied the head-tail mode for low currents ( $N_p = 1.6 \times 10^{10}$  protons per bunch). The chromaticity was reduced with respect to the previous settings by changing the strength of the sextupoles.

Table 3: Coherent tune shift measurements

date	$\Delta Q_x/\Delta N_p [10^{10}]$	$\Delta Q_y/\Delta N_p [10^{10}]$	$\sigma$ [ns]
13/08/1999	$+0.00024 \pm 2 \times 10^{-5}$	$-0.0018 \pm 2 \times 10^{-4}$	$0.77 \pm 0.14$
23/08/1999	$+0.00058 \pm 6 \times 10^{-5}$	$-0.0029 \pm 1 \times 10^{-4}$	$0.47 \pm 0.05$
17/09/1999	$+0.00021 \pm 4 \times 10^{-5}$	$-0.0036 \pm 2 \times 10^{-4}$	$0.53 \pm 0.02$
10/11/1999	$+0.00023 \pm 2 \times 10^{-5}$	$-0.0029 \pm 1 \times 10^{-4}$	$0.58 \pm 0.03$

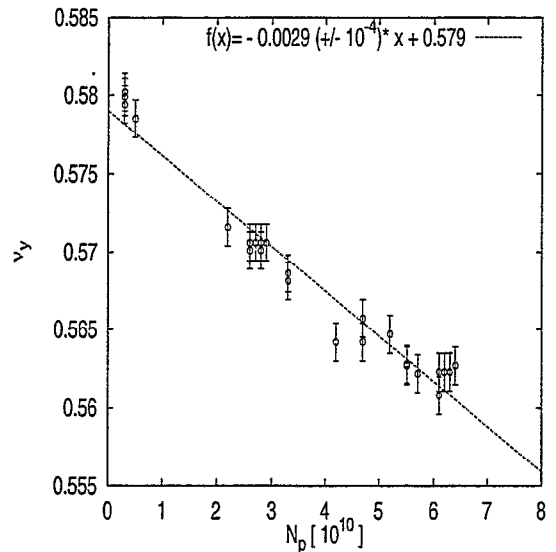
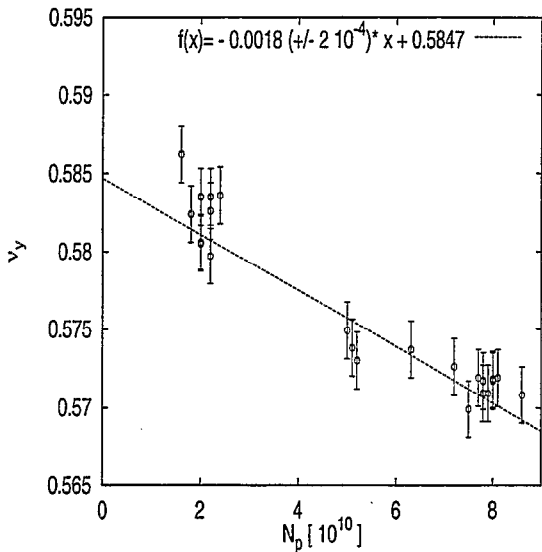
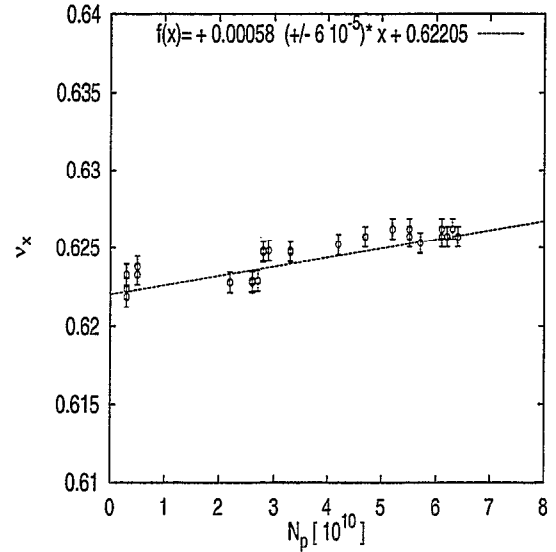
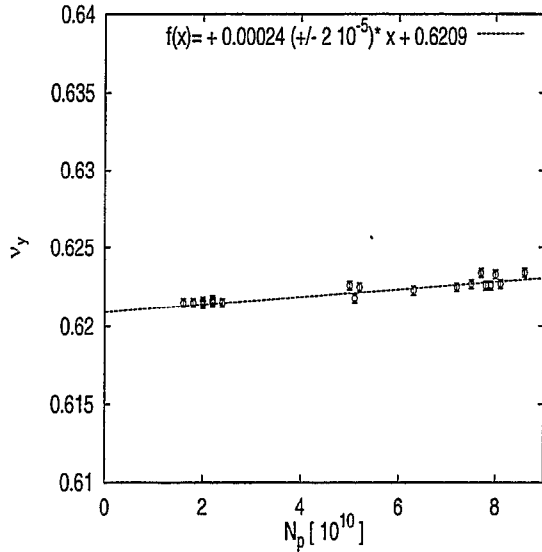


Figure 6: Horizontal (top) and vertical (bottom) tune as a function of the bunch population and fit with errors (measured on 13/08/1999 with RF voltage  $V_{rf}=0.8$  MV). Tune error bars are  $e_y = 1.8 \times 10^{-3}$  and  $e_x = 3 \times 10^{-4}$ .

Figure 7: Horizontal (top) and vertical (bottom) tune as a function of the bunch population and fit with errors (measured on 23/08/1999 with RF voltage  $V_{rf}=2.5$  MV). Tune error bars  $e_y = 1.2 \times 10^{-3}$  and  $e_x = 6.5 \times 10^{-4}$ .

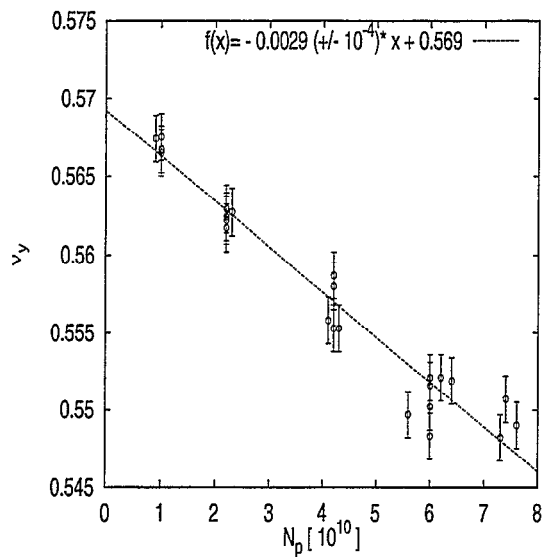
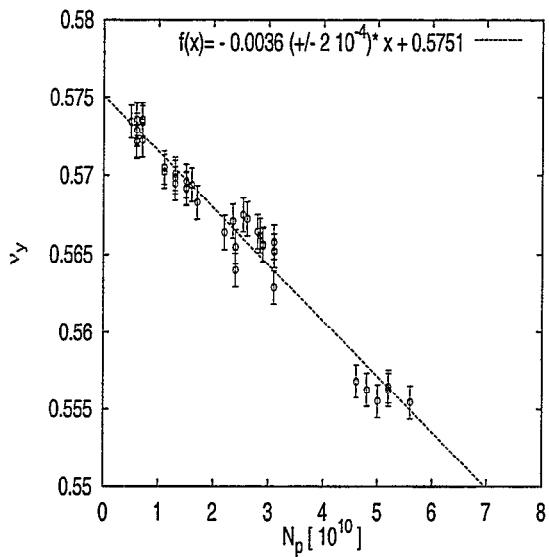
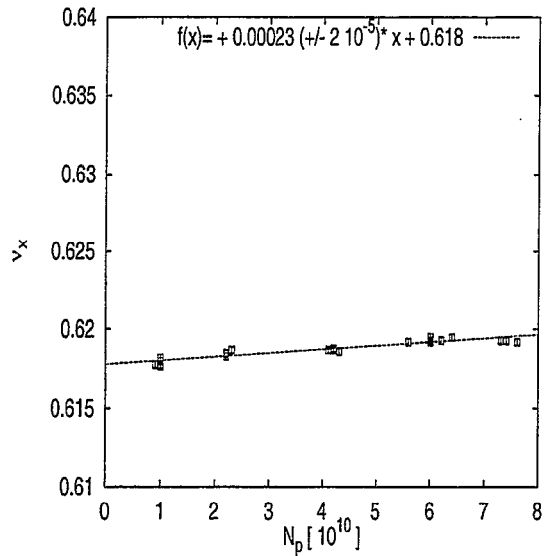
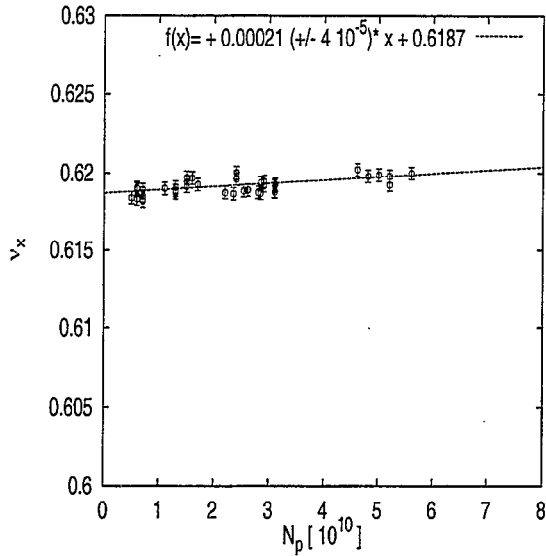


Figure 8: Horizontal (top) and vertical (bottom) tune as a function of the bunch population (measured on 17/09/1999 with  $V_{rf}=2.5$  MV). Tune error bars  $e_y = 1 \times 10^{-3}$  and  $e_x = 4 \times 10^{-4}$ .

Figure 9: Horizontal (top) and vertical (bottom) tune as a function of the bunch population and fit with errors (measured on 10/11/1999 with  $V_{rf}=2.5$  MV). Tune error bars  $e_y = 1.5 \times 10^{-3}$  and  $e_x = 2 \times 10^{-4}$ .

In Figure 10 we show the vertical growth rate as a function of the variation in the setting of the vertical chromaticity  $\Delta\xi_v$ , with respect to our setting used for the tune shift measurements. For negative chromaticity the bunch population was constant and equal to  $1.6 \times 10^{10}$ . The values at  $\Delta\xi_v = 0$  were taken from the tune shift measurements which were performed with slightly positive chromaticity that lead to damping of the centroid motion. These points were measured with a bunch population of  $N_p = 10^{10}$  and  $N_p = 2.2 \times 10^{10}$  and their values were rescaled by the intensity ratio to compare with the measurements at

$N_p = 1.6 \times 10^{10}$ .

The zero crossing of the linear fit suggests that our standard setting  $\Delta\xi_v = 0$  corresponds to a slightly positive chromaticity of  $\xi = 0.011$ .

A first attempt to measure growth rates was already undertaken earlier, on the 17/9/1999, with  $N_p$  between  $3.5 \times 10^{10}$  and  $5 \times 10^{10}$  and  $\sigma = 0.53$  ns. The results are more scattered but are still shown for completeness in Figure 10 (bottom). The y-axis is scaled to the bunch population of  $1.6 \times 10^{10}$  and  $\sigma = 0.58$  ns to be directly comparable to the linear fit of the measurements of the 10/11/1999.

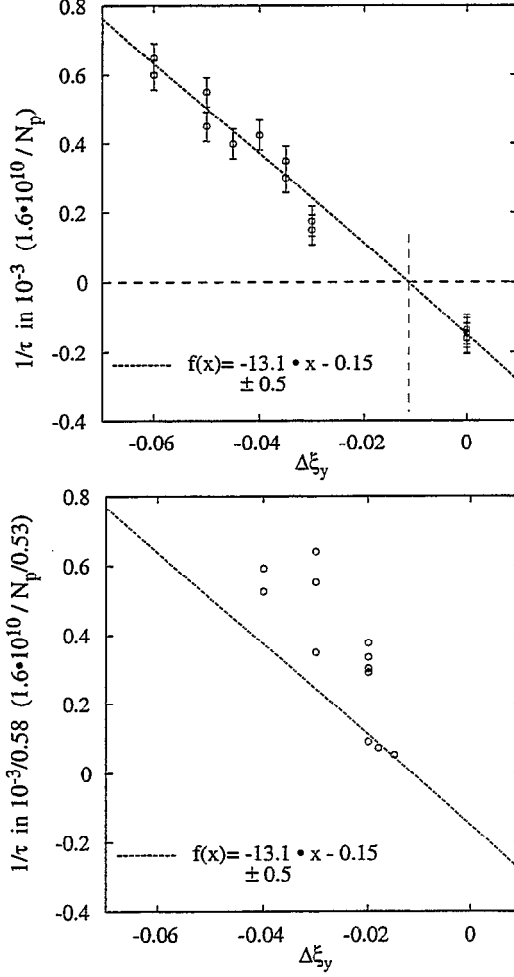


Figure 10: Growth rate of the head-tail mode instability (in units of  $10^{-3}$  turns), as a function of the decrement of chromaticity. Top: measurement on the 10/11/1999. Error bars are  $e = 0.043$  (in units of  $10^{-3}$ ). Bottom: Data of a first attempt on the 17/09/1999 and the straight line as obtained on the 10/11/1999.

## 7 FITTING THE RESULTS WITH A BROAD-BAND IMPEDENCE MODEL

For a single bunch, the longitudinal impedance has been modelled by an equivalent parallel LRC resonator circuit with resonance frequency  $w_R = 1/\sqrt{CL}$ , resistance  $R_s$  and quality factor  $Q = R_s\sqrt{C/L}$ . The Panofsky-Wenzel theorem requires that the same resonator gives a transverse impedance

$$Z_1^\perp = \frac{w_R}{w} \frac{Z_t}{1 + iQ \left( \frac{w_R}{w} - \frac{w}{w_R} \right)} \quad (2)$$

where  $Z_t = c/w_R R_s$ . For  $w \rightarrow w_R$  the impedance is purely resistive with  $\Re(Z_1^\perp) = Z_t = c/w_R R_s$  and  $\Im(Z_1^\perp) = 0$ .

Let  $\xi$  be the chromaticity,  $\eta$  the slip factor,  $w_0$  the revolution frequency,  $w_\beta = Q_\beta w_0$  the betatron frequency and  $Q_\beta$  the betatron tune (including the integer part). Defining  $w_\xi = \frac{\xi w_\beta}{\eta}$  and  $w_p = p w_0 + w_\beta$  with  $p$  an integer number we can evaluate the effective transverse impedance [11]

$$(Z_1^\perp)_{eff} = \frac{\sum_{p=-\infty}^{\infty} Z_1^\perp(w_p) h_l(w_p - w_\xi)}{\sum_{p=-\infty}^{\infty} h_l(w_p - w_\xi)} \quad (3)$$

where we take  $h_l$  as defined for a Gaussian beam model

$$h(w_p) = e^{-w_p^2 \sigma_z^2 / c^2} \quad (4)$$

with  $\sigma_z = c\sigma$  the bunch length,  $c$  the speed of light and  $\sigma$  the r.m.s of the Gaussian distribution in units of time.

Then the tune shift is given by

$$\Delta Q = \frac{\Omega - w_\beta}{w_0} \approx \frac{1}{w_0} \frac{N_p e c^2}{2E/eT_0 w_\beta 2\sqrt{\pi}\sigma_z} \Im(Z_1^\perp)_{eff} \quad (5)$$

with  $N_p$  the number of particles per bunch,  $e$  charge of the particle,  $E$  the particle energy, and  $T_0 = 2\pi/w_0$  the revolution period. Similarly the growth rate (in turns $^{-1}$ ) is given by

$$\frac{1}{\tau} \approx -T_0 \frac{N_p e c^2}{2E/eT_0 w_\beta 2\sqrt{\pi}\sigma_z} \Re(Z_1^\perp)_{eff} \quad (6)$$

The real part of the effective impedance is different from zero if the chromaticity is not zero. Above transition, this leads to a negative growth rate (damping) for positive chromaticity, and to a positive growth rate otherwise.

In Table 4 we summarize parameters, relevant to our experiment.

Table 4: Parameters and their values

$E$	26.017 GeV	beam energy
$T_0$	23.05 $\mu$ s	time for one revolution
$Q_\beta$	26.6	betatron tune
$\eta$	$5.55 \times 10^{-4}$	phase slip factor
$N_p$	$1 - 8 \times 10^{10}$	number of protons in the bunch

### 7.1 Tune Shift

We fit the broad band resonator with a quality factor  $Q = 1$  and a resonance frequency  $w_R = 2\pi \times 1.3$  GHz.

The ratio  $\Delta Q/\Delta N_p [10^{10}]$  is directly proportional to the impedance  $Z_1^\perp$ . For each plane we determine the impedance such that  $\Delta Q/\Delta N_p [10^{10}]$  equals the slope found in our measurements. In Table 5 we summarize the impedances inferred from the tune shifts. The uncertainty reflects both the error of the fitted slope and the spread in the measured bunch length  $\sigma$ .

The averages and uncertainties from combining the four measurements are also given. The four numbers of  $Z_v$  are

Table 5: Impedance results obtained by fitting coherent tune shifts with a broad-band model.

date	$Z_v$ in $M\Omega/m$	$Z_h$ in $M\Omega/m$
13/08/1999	$25 \pm 6$	$-3.3 \pm 0.7$
23/08/1999	$24 \pm 2$	$-4.8 \pm 0.7$
17/09/1999	$33 \pm 3$	$-2.0 \pm 0.4$
10/11/1999	$30 \pm 2$	$-2.4 \pm 0.3$
average	$28 \pm 2$	$-2.6 \pm 0.2$

all compatible with the mean within 20%. This makes us confident that the measurements presented here are in fact relevant to document and follow the improvements of the SPS as LHC injector. The effect in the horizontal plane is much smaller, and has clearly the opposite sign.

The uncertainties given above are effectively only from the scatter in the data, as relevant for a comparison of data taken under similar conditions. The model dependence should be considered in addition when this is compared to results obtained with different methods or under different conditions.

## 7.2 Growth Rate

On the experiment of the 10/11/1999 (see Figure 10), we found that the growth rate increases linearly with the decrement of chromaticity. This can be understood as follows. If the bunch is longer than the range of the wake field ( $\sigma c > c/w_R = 3.6$  cm for  $w_R = 2\pi \times 1.3$  GHz) then  $(Z_1^\perp)_{eff} \approx Z_1^\perp(w_\xi)$ . The growth rate  $1/\tau$  which is proportional to  $\Re(Z_1^\perp)_{eff}$  is then

$$\begin{aligned} \frac{1}{\tau} &\approx -T_0 \frac{N_p e c^2}{2E/eT_0 w_\beta 2\sqrt{\pi}\sigma_z} \frac{Z_1 w_\xi}{w_R} \\ &= -T_0 \frac{N_p e c^2 Z_1}{2E/eT_0 w_\beta 2\sqrt{\pi}\sigma_z w_R} \frac{\xi w_\beta}{\eta} \end{aligned} \quad (7)$$

which increases linearly with  $-\xi$ .

Using the complete formula (Eq. 3) and assuming  $Q = 1$ , the impedance that fits the measured dependence on the chromaticity is  $Z_t = 8.3 \pm 0.6$   $M\Omega/m$ . This impedance is 3.7 times smaller than the impedance found by fitting the coherent tune shift.

We can fit both measurements simultaneously with  $Z_t = 108$   $M\Omega/m$  by changing the quality factor to  $Q = 3.6$ . In this broad band model  $Z_t/Q = 30$   $M\Omega/m$ .

## 8 ACKNOWLEDGMENTS

We would like to thank the SPS shift leaders for their support, D. Manglunki for providing high-quality beams from the PS, P. Baudrenghien for the setup of the SPS-RF and L. Jensen, A. Mostacci, J. Klem and H. Tsutsui for their participation in some of these MD's and H. Tsutsui once more for help in the data analysis

## 9 REFERENCES

- [1] L. Vos, "Decoherence from space-charge to the SPS", CERN SL/98-056, 1998.
- [2] D. Boussard, J. Gareyte, "Measurements of the SPS coupling impedance", CERN Improvement report No. 181, 1980.
- [3] T. Linnecar, W. Scandale, "Measurement of the coupling impedance of the SPS", CERN SPS/DI MST/ME 84-12, 1984.
- [4] L. Vos, "Computer calculation of the longitudinal impedance of cylindrical symmetric structures and its application to the SPS", CERN SPS/86-21 MS, 1986.
- [5] D. Brandt, J. Gareyte, C. Niquille, F. Schmidt, "Tune shift measurements in the SPS", CERN SPS/AMS/Note/88-14, 1988.
- [6] T. Linnecar, E. Chapirochnikova, "Analysis of the transverse mode coupling instability of the leptons in the SPS", CERN SL/Note 93-00 (RFS), 1993.
- [7] J. Laskar, "Secular evolution of the solar system over 10 million years", *Astronomy and Astrophysics* 198, 341, 1988; J. Laskar, "The chaotic behavior of the solar system: A numerical estimate of the size of the chaotic zones", *Icarus* 88, 266, 1990.
- [8] J. Laskar, "Frequency analysis for multi-dimensional systems. Global dynamics and diffusion", *Physica D* 67, 257 1993; J. Laskar and D. Robin, "Application of Frequency Map Analysis to the ALS", Part. Acc. 54, 183, 1996.
- [9] J. Laskar, "Introduction to Frequency Map Analysis", in Proc. of the NATO Advanced Series Institute, on Hamiltonian Systems with 3 or more Degrees of Freedom, S'Agaró, Spain, 1995, ed. C. Simó 1999.
- [10] F. Harris, "On the use of windows for the harmonic analysis with the discrete Fourier transform", *Proc. of the IEEE* 60, 51, 1978.
- [11] A. Chao, "Physics of collective instabilities in high energy accelerators", Wiley, 1993.

## Measurements With AC Dipoles\*

M. Bai, M. Meth, B. Parker, S. Peggs, T. Roser, D. Trbojevic  
 Brookhaven National Laboratory, Upton, NY 11973, USA

### Abstract

Two AC dipoles with horizontal and vertical oscillating magnetic fields will be installed in RHIC. Both of the magnets are expected to be able to induce maximum  $5\sigma$  coherent oscillations in the two transverse planes. This is desired for measuring betatron functions and phase advances in the machine as well as for nonlinear beam dynamic studies. The AC dipole with horizontal magnetic field will also be used as a spin flipper for RHIC polarized proton experiments. This paper discusses the possible measurements with the AC dipoles in RHIC.

### 1 INTRODUCTION

In accelerators, coherent oscillation can be excited by an AC dipole oscillating magnetic field  $\Delta B$  where

$$\Delta B = \Delta B_m \cos \nu_m \phi(s). \quad (1)$$

Here,  $\Delta B_m$  is the magnetic field oscillating amplitude,  $\nu_m = \frac{f_m}{f_{rev}}$  is the modulation tune where  $f_m$  is the AC dipole oscillating frequency and  $f_{rev}$  is the beam revolution frequency, and  $\phi(s)$  is azimuthal angle along the accelerator. The amplitude of the coherent oscillation is determined by the AC dipole field strength and frequency. In an accelerator without any nonlinear components, the coherent oscillation amplitude is given by Eq.(2).

$$Z_{coh} = \sqrt{2\beta_z J} = \frac{\Delta B_m \ell}{4\pi(B\rho)|\nu_m - \nu_z|} \beta_z. \quad (2)$$

With a fixed magnetic field amplitude, the closer the AC dipole frequency is to the intrinsic beam betatron oscillation  $\nu_z$ , the stronger the coherent oscillation is. When the AC dipole is right at resonance, the beam then becomes unstable. Here, we use  $z$  to stand for either horizontal coordinate or vertical coordinate.  $\beta_z$  is the betatron functions where the dipole is located and  $B\rho$  is the magnetic rigidity.

The advantage of using an AC dipole to induce a coherent oscillation is that it can be done in an adiabatic fashion as we have already demonstrated in the Brookhaven AGS[1, 2]. Fig. 1 is experimental data taken during the AGS AC dipole experiment with gold beam. The measured transverse beam size before the AC dipole was turned on and after it was turned off shows that by slowly turning the magnet on and off, the beam emittance remained unperturbed during the whole process. In this way, the length of this sustained coherent excitation is also controllable. This non-destructive manipulation of the beam then allows

one to perform beam studies or diagnostics without continuously reinjecting beam and interrupting the normal machine operation.

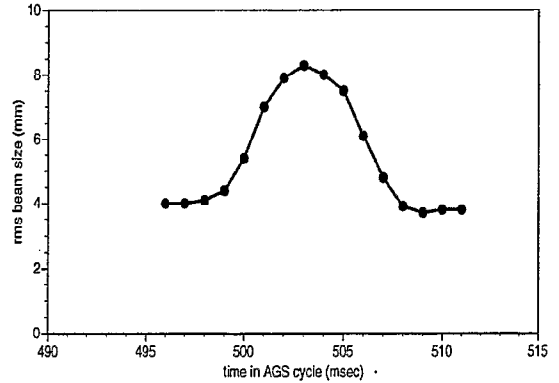


Figure 1: Measured vertical rms beam size as a function of time during the AGS AC dipole experiment with gold beam. The time span covers the whole AC dipole operation process.

### 2 AC DIPOLE APPLICATIONS

#### 2.1 Measure betatron function and phase advance

The betatron functions and phase advances are measured by analyzing turn by turn beam position data from two beam position monitors (BPMs). The transfer matrix between the two BPMs with the AC dipole excluded in between is given by

$$\begin{pmatrix} x_2 \\ x_2' \end{pmatrix} = \begin{pmatrix} \sqrt{\frac{\beta_2}{\beta_1}}(c + \alpha_1 s) & \sqrt{\beta_1 \beta_2} s \\ -\frac{1 + \alpha_1 \alpha_2}{\sqrt{\beta_1 \beta_2}} s + \frac{\alpha_1 - \alpha_2}{\sqrt{\beta_1 \beta_2}} c & \sqrt{\frac{\beta_1}{\beta_2}}(c - \alpha_2 s) \end{pmatrix} \begin{pmatrix} x_1 \\ x_1' \end{pmatrix} \quad (3)$$

where  $c = \cos\phi_{21}$ ,  $s = \sin\phi_{21}$  and the AC dipole is not in between. Therefore,  $x_1'$  can then be expressed by the positions at the two BPMs, i.e.

$$x_1' = \frac{x_2}{\sqrt{\beta_1 \beta_2} \sin \phi_{21}} - \frac{\cot \phi_{21} + \alpha_1}{\beta_1} x_1. \quad (4)$$

where  $\beta_i$  and  $\alpha_i$ ,  $i=1,2$ , are the Twiss parameters at BPM1 and BPM2, respectively,  $\phi_{21}$  is the phase advance between the two BPMs. Since

$$x_1^2 + (\beta_1 x_1' + \alpha_1 x_1)^2 = 2\beta_1 J, \quad (5)$$

\* Work supported by US Department of Energy

$x_1$  and  $x_2$  satisfy the elliptical equation

$$x_1^2 + \left( \sqrt{\frac{\beta_1}{\beta_2}} \frac{x_2}{\sin \phi_{21}} - \cot \phi_{21} x_1 \right)^2 = 2\beta_1 J. \quad (6)$$

where  $J$  is the action. Hence, the ratio of the betatron functions  $\sqrt{\frac{\beta_1}{\beta_2}}$ , the phase advance between the two BPMs  $\phi_{21}$  and  $\beta_1 J$  can be obtained by fitting the turn-by-turn data of the two BPMs [3, 4, 5]. In accelerators with many BPMs distributed around the ring, turn by turn beam position data at all the BPMs can be measured simultaneously which then allows one to derive betatron functions around the ring.

## 2.2 Measure the detuning effect

The octupole and sextupole's field generate detuning effect, in which different particles with different betatron oscillation amplitude have different tunes

$$\nu_z = \nu_{z0} + \frac{1}{2} \alpha a^2, \quad (7)$$

where  $\nu_{z0}$  is the betatron tune of the center particle and  $a$  is the betatron oscillation amplitude. In the presence of detuning, the simple linear relation of Eq.(2) no longer holds. The top part of Fig. 2 shows the fixed points as a function of the proximity parameter  $\delta = \nu_m - \nu_z$  [6]. Two islands are developed after the bifurcation point as shown in the bottom figure. The detuning coefficient  $\alpha$  can be measured by ramping the AC dipole frequency through the resonance and measuring the amplitude of the excited oscillation as a function of the modulation.

## 2.3 Other applications

- Measure the nonlinear harmonics of the one turn Hamiltonian.

In high energy colliders like RHIC and LHC, IR correction is one of the important issues to improve the luminosity. In order to meet this requirement, reliable measurements of the non-linear components in the accelerator is necessary. To achieve this, turn by turn BPM data of a sustained large amplitude coherent oscillation are desired. Unlike the linear case, the phase space is distorted due to the non-linearities in the machine. By analyzing the spectrum of the turn by turn beam position data, one can then extract the information of the non-linear components [7, 8, 9].

- Spin flipper.

Beside the gold operation, another important project in RHIC is the polarized proton physics which often prefers to have collisions with different spin patterns to cancel systematic experimental errors. This requires one to reverse the polarization of the beam. In RHIC, polarized protons are acceleration with two snakes to eliminate all the first order spin resonances. So, in the presence of two snakes, spin flipping can be

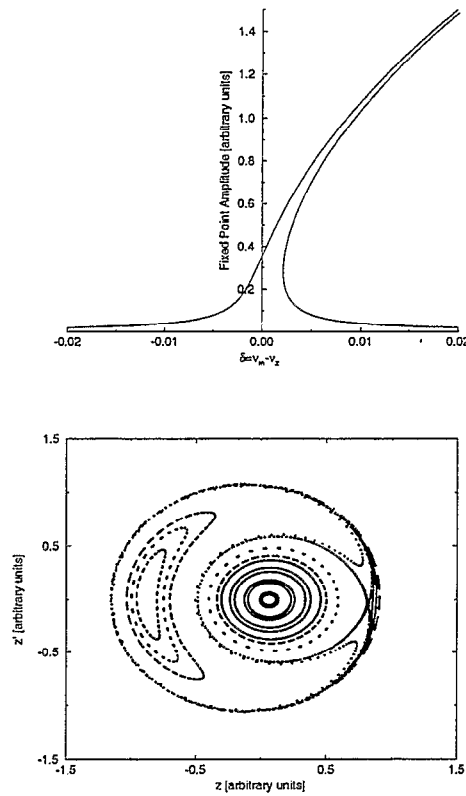


Figure 2: The top plot is the calculated fixed points as a function of the proximity parameter  $\delta$ . The bottom plot shows the phase plot in the rotating frame, namely the frame which rotates along with the modulation frequency.

achieved by introducing a oscillating magnetic field to excite an artificial spin resonance. By slowly ramping its frequency through the spin precession frequency, a full spin flip can be obtained [10]. Fig. 3 is the tracking result of a single particle.

In RHIC, two AC dipoles will be installed in sector 3 between the D0 magnet and the interaction point. The betatron functions at the AC dipole location are about 11 m. Both magnets are about 1 m long. Table 1 lists their design parameters.

In order to minimize power losses, the AC dipole is designed as an air-core magnet using Litz wire. Unlike regular conductor, Litz wire consists of thousands of fine strands. Its AC resistance is greatly reduced

## 3 CONCLUSION

A sustained coherent oscillation with large amplitude can be adiabatically excited by an AC dipole preserving the emittance. This method has been successfully applied in the AGS polarized proton acceleration to overcome

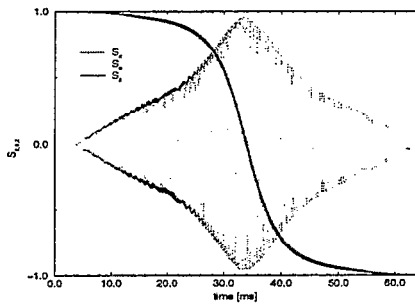


Figure 3: Spin tracking of 1000 particles using an AC dipole to induce a spin flip. The nominal spin tune in RHIC is  $\frac{1}{2}$ . In this particular case, we moved the spin tune slightly away from its nominal value by tuning the two snakes' axis. The AC dipole strength is 500G-m and its modulation tune was swept from 0.443 to 0.457 in 2700 turns.

[7] S. Peggs, and C. Tang, RHIC AP Tech. Notes: RHIC/AP/159, October 1998.  
 [8] S. Peggs, *Handbook of Accelerator Physics and Engineering*, P. 93, edited by A. Chao and M. Tigner.  
 [9] S. Peggs, Proc. 2nd ICFA workshop, CERN 88-04, and SSC-175 (1988).  
 [10] T. Roser, *Handbook of Accelerator Physics and Engineering*, P. 150, edited by A. Chao and M. Tigner.

Table 1: Margin specifications

field	application	desired B [G-m]	resonant frequency	maximum coherence
Hori.	nonlinear beam dynamic studies	380	63.95 kHz	$5\sigma$
	betatron function measurement	78		$1\sigma$
	spin flipper	100	37.5 kHz	-
vert.	beam studies	380	63.73 kHz	$5\sigma$
	betatron function measurement	78		$1\sigma$

strong intrinsic spin depolarizing resonances. As a non-destructive method, several other other applications in beam diagnostics and dynamics studies, spin manipulations have been proposed.

#### 4 ACKNOWLEDGEMENT

The authors would like to thank M. Brenann, H. Harn, D. Lehn, C. Pai, T. Russo, R. Spitz, J. Tuozzolo, C. Trabocchi and A. Zaltsman for the fruitful discussions and support.

#### 5 REFERENCES

[1] M. Bai *et al.*, Phys. Rev. E56, 5 (1997).  
 [2] M. Bai *et al.*, Phys. Rev. Lett. 80 (1998).  
 [3] S. Y. Lee, *Accelerator Physics*, P. 97, World Scientific.  
 [4] /rap/lattice.tools/bin/SUN/tevex  
 [5] N. Merminga, *A Study of Nonlinear Dynamics in the Fermi-Lab TEVATRON*, Ph. D thesis  
 [6] M. Bai, S. Y. Lee, H. Huang, T. Roser and M. Syphers, AGS/RHIC/SN No. 055.

## TRANSVERSE ECHOS IN RHIC\*

W. Fischer and B. Parker, BNL, USA  
O. Brüning, CERN, Switzerland

### Abstract

Echo phenomena are well known in plasma physics and have been observed in accelerators in the longitudinal plane. Echo measurements are appealing since they allow the determination of small diffusion coefficients in a relatively short time. In this paper we explore the possibility of observing transverse echos in RHIC, created by a dipole kick followed by a quadrupole kick. We describe a technical solution for a pulsed quadrupole, present analytical estimates and show simulations of echo signals.

### 1 INTRODUCTION

Well known in plasma physics, echo phenomena have only been recently introduced to accelerator physics. First measurements of longitudinal echo signals have been reported [1–8].

In the simplest case, a transverse echo is generated by a dipole kick followed by a quadrupole kick. The echo signal appears as a dipole moment long after the initial dipole oscillations have disappeared. We consider only this case. Fig. 1–2 illustrate the creation of such an echo signal in normalized phase space. A particle distribution is displaced by several  $\sigma$  of the transverse beam distribution through a dipole kick. If the particle tune is amplitude dependent the distribution filaments but information on the phase relations between the particles is still retained if the filamentation time is not too long. A quadrupole kick after time  $\tau$  changes the distribution although it does not affect the dipole moment. After a time  $\tau_{echo} = 2\tau$  a transient dipole moment appears, the echo signal. The left hand side of Fig. 3 shows the dipole moment of the same distribution with a dipole kick only and the right hand side of Fig. 3 shows the dipole moment with an additional quadrupole kick, thus creating an echo signal. Such a signal can be observed with beam position monitors.

A particularly interesting aspect of echo measurements is the possibility of diffusion coefficient measurements in short time intervals since any form of diffusion reduces the echo signal.

One reason for the lack of transverse echo measurements is the difficulty of applying a short quadrupole kick to the beam. In the following section we will review the technical options of applying one-turn dipole and one-turn quadrupole kicks in RHIC. The next sections determine the

expected maximum echo signal from theoretical computations and simulations. We consider the case of RHIC in proton operation at injection. In proton operation intra-beam scattering is less destructive to echo signals than in gold operation. At injection energy the quadrupole kick is most effective.

### 2 RHIC INSTRUMENTATION FOR TRANSVERSE ECHOS

This section describes the possibilities of applying dipole and quadrupole kicks in RHIC as well as the detectors that can record an echo signal. While dipole kickers and detectors are installed and available the quadrupole kicker is still under construction.

#### 2.1 Dipole Kickers

In RHIC there are three types of dipole kickers available: the injection kickers [9, 10], the tune kickers [11] and the abort kickers [12]. Their properties are summarized in Tab. 1. Only the injection kickers can provide a one-turn kick of several  $\sigma$  and restricts our investigations to the vertical plane. However, a dipole kick can also be achieved, by injecting the beam under an angle.

Table 1: RHIC dipole kickers at injection energy.

Kicker	Strength range		Kick length
	$[\mu\text{rad}]$	$\sigma$	
Injection (ver)	300–1500	4.7–23.5	60 ns
Tune (hor)	0–11	0–0.2	90 ns
Tune (ver)	0–11	0–0.1	90 ns
Abort (hor)	250–2500	4.2–390	> 12 $\mu\text{s}$

#### 2.2 Quadrupole Kicker

The quadrupole kicker is the real challenge in producing transverse echos. We have available a special air core quadrupole magnet [13] that can be used for a quadrupole kicker. This magnet had been installed at the IP4 interaction region and is common to both rings.

The magnet is designed for a maximum current of 50 A which corresponds to a focal length of 500 m at injection energy. However, in pulsed operation the current could be raised above the 50 A design value.

\* Work performed under the auspices of the US Department of Energy.

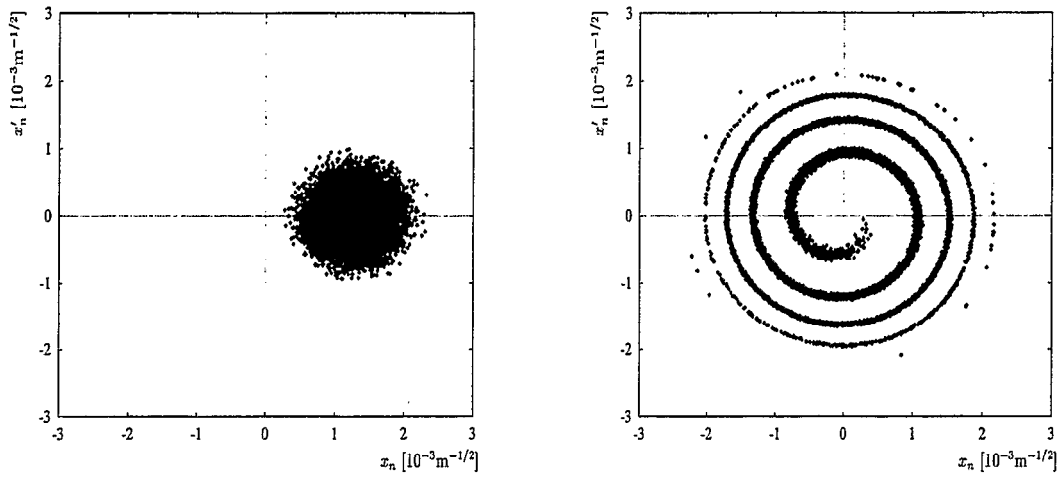


Figure 1: Left: Horizontal particle distribution in normalized phase space after the initial dipole offset. Right: The same distribution 500 turns later.

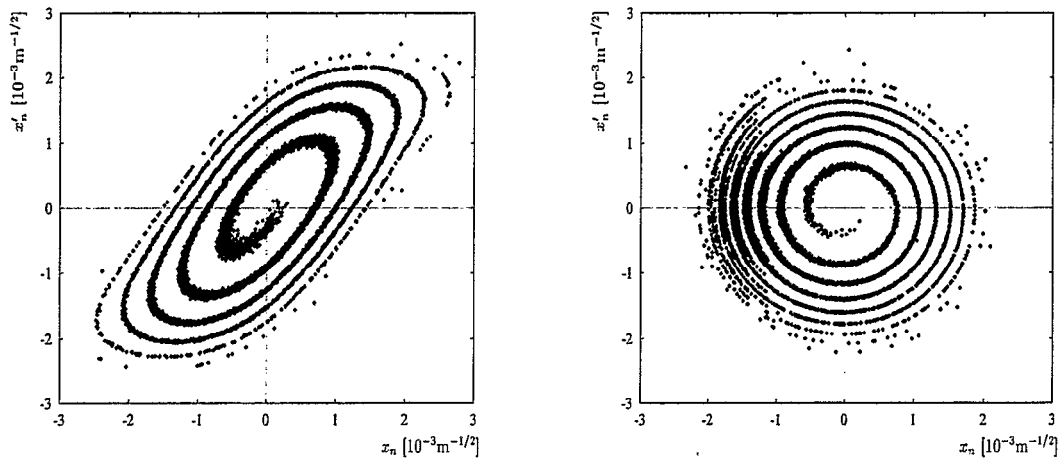


Figure 2: Left: Horizontal particle distribution in normalized phase space right after a 1 turn long quadrupole kick placed 500 turns after the dipole kick. Right: The same distribution 500 turns after the quadrupole kick.

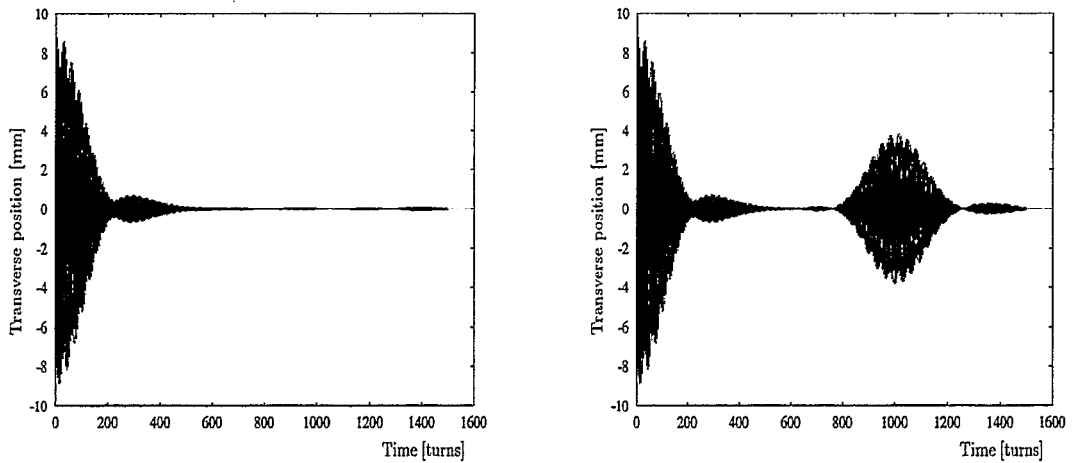


Figure 3: Left: The dipole moment of the distribution versus time after a dipole kick. Right: The same signal with an additional quadrupole kick at 500 turns after the dipole kick.

Fig. 4 shows resistance and Fig. 5 the inductance measurements for the quadrupole as a function of frequency. In one case it is assumed that resistance and inductance are in series while in the other case it is assumed that they are in parallel. In the parallel case the inductance is relatively constant at  $125 \mu\text{H}$  up to a frequency of 1 kHz and drops to about  $105 \mu\text{H}$  at a frequencies beyond 1 kHz. A one-turn pulse would correspond to a frequency of 20kHz.

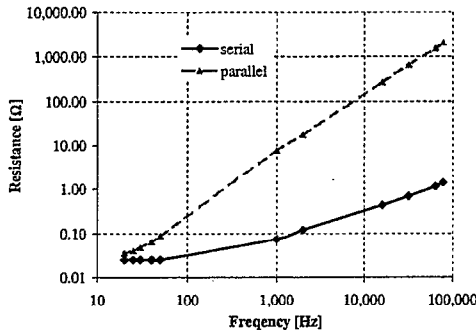


Figure 4: Resistance measurements of the quadrupole. Results labeled “serial” assume that resistance and inductance are in series, results labeled “parallel” assume that resistance and inductance are in parallel.

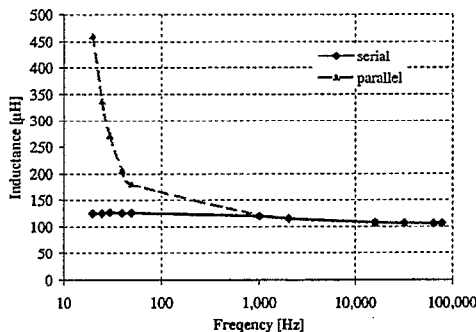


Figure 5: Inductance measurement of the quadrupole. Results labeled “serial” assume that resistance and inductance are in series, results labeled “parallel” assume that resistance and inductance are in parallel.

A relatively simple design for the pulsed operation of the quadrupole is the one shown in Fig. 6. By closing the switch  $S1$  a power supply charges the capacitor  $C$ . When charged the switch  $S1$  opens again. By closing the switch  $S2$  at the time  $t_0$  the capacitor  $C$  will start to discharge over the quadrupole with the inductance  $L = 105 \mu\text{H}$ . We neglect for the moment magnet and cable resistance as well as switching time.

The current in the coil  $L$  reaches a maximum after the time  $t_1$  when the switch  $S2$  can be opened again. The energy stored in the coil is then discharged in the resistor  $R$ . By choosing  $R$  appropriately the current in the coil can be zero after the time  $t_2$  with little further oscillation. During the time  $t_2 - t_0$  there is a field in the quadrupole that would create a quadrupole kick. The time  $t_2 - t_0$  can therefore be

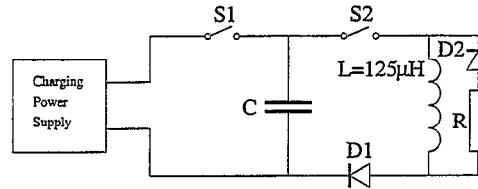


Figure 6: Electric circuit for a pulsed quadrupole.

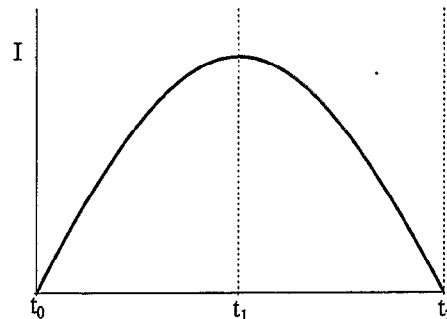


Figure 7: Current in the coil  $L$  after the switch  $S2$  is closed.

2 turns long, one turn to raise the current and one turn to bring it to zero again.

For the angular frequency  $\omega_0$  of the electric circuit, the capacitance  $C$  and the voltage  $V$  over the coil  $L$  the relations

$$\omega_0 = \frac{2\pi}{2(t_2 - t_0)}, \quad C = \frac{1}{\omega_0^2 L} \quad \text{and} \quad V = \omega_0 L I. \quad (1)$$

hold. Fig. 8 shows the capacitance  $C$  and the voltage  $V$  as a function of the quadrupole kick length assuming that the peak current  $I_{max}$  in the coil is 50 A. According to Eq. (1) the voltage over the quadrupole will increase proportionally with the current, which in turn is proportional to the quadrupole kick strength.

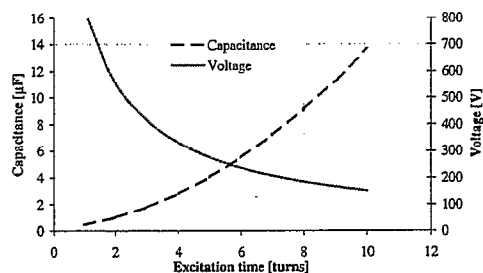


Figure 8: Capacitance and voltage as a function of the quadrupole excitation time for a peak current of 50 A in the quadrupole.

### 2.3 Detectors

For the observation of transverse echos only beam position monitors (BPMs) are needed. The RHIC arc BPMs are located at positions where the  $\beta$ -function reaches a local maximum of 48m. The arc BPMs have a resolution of at least 0.1 mm if there are no less than  $10^9$  charges per bunch [14]. For protons this is about 1% of the design intensity [15]. The detection of echo signals of several millimeters should therefore pose no problem.

During the RHIC commissioning a turn-by-turn ionization profile monitor (IPM) has been tested successfully [16]. While the BPMs can only detect the center of charge, the IPM would give the projection of the phase space distribution onto the x- or y-axis.

## 3 ANALYTICAL ESTIMATES OF ECHO SIGNALS

In this section we follow closely Ref. [17]. We use normalized phase space coordinates  $(x_N, x'_N)$  according to

$$x_N = \frac{1}{\sqrt{\beta}} x \quad \text{and} \quad x'_N = \frac{1}{\sqrt{\beta}} (\alpha x + \beta x') \quad (2)$$

where  $(x, x')$  are the unnormalized transverse phase space coordinates and  $\alpha$  and  $\beta$  are the lattice functions. The initial particle distribution is assumed to be Gaussian with an rms emittance  $\epsilon$ :

$$\psi(x_N, x'_N) = \frac{1}{2\pi\epsilon} \exp\left\{-\frac{x_N^2 + x'^2_N}{2\epsilon}\right\} \quad (3)$$

We furthermore define  $Q$  as the ratio of the  $\beta$ -function at the quadrupole location to the focal length of the quadrupole,  $a$  the dipole kick strength in normalized coordinates and  $\tau$  the time between dipole and quadrupole kick.  $\mu$  gives the amplitude dependent tune shift at one  $\sigma$  of the unkickd particle distribution,

$$\nu = \nu_0 - \mu \frac{x_N^2 + x'^2_N}{\epsilon} \quad (4)$$

Second order perturbation theory gives for the echo amplitude  $\eta = \sqrt{x_N^2 + x'^2_N}$  after a one-turn dipole and a one-turn quadrupole kick

$$\eta = aF\left(\frac{\tau}{\tau_0} \frac{t - \tau}{\tau_d}\right) \quad (5)$$

where  $\tau_0 = Q\tau$ ,  $\tau_d = T_0/4\pi\mu$  and the function  $F$

$$F(x, y) = \frac{x}{[(1 + x^2 - y^2)^2 + 4y^2]^{2/3}} \quad (6)$$

The effect of diffusion on the echo amplitude can be computed for the case when the time  $\tau$  is small compared to the decoherence time  $\tau_d$  and the parameter  $Q$  is small [18]. In this case one has

$$\eta^{max} = \frac{aQ}{\tau_d} \frac{\tau}{1 + 8D_0\mu^2\omega_0^2\tau^3/3\epsilon} \quad (7)$$

where  $\omega_0 = 2\pi/T_0$  is the angular revolution frequency and  $D_0$  the diffusion coefficient. For the parameters in Tab. 2 Eq. (7) gives a maximum echo amplitude of 0.44 of the dipole kick and 5000 turns between the dipole and the quadrupole kick. Such an echo amplitude would be observable.

## 4 SIMULATIONS

In the simulations we assume that the quadrupole kick can be extended over a few turns. This mode of operation is not covered in Sec. 3. The simulations are used to determine the maximum acceptable kick length of a pulsed quadrupole kick, the optimum time  $\tau$  between dipole and quadrupole kick and the minimum required kick amplitude. In all cases we assume that the quadrupole signal increases over half the kick length (ramp-up) reaches its maximum signal at half the kick length and decreases again during the second half of the kick length (ramp-down).

The left hand side of Fig. 9 shows such an excitation versus time. The right hand side of Fig. 9 shows the maximum echo response (dipole signal) versus the excitation time  $\Delta T$  for a quadrupole kick 5,000 turns after the dipole offset with an quadrupole kick amplitude corresponding to 25A. The signal decreases rapidly for a pulsed excitation which is longer than 10 turns. Note that dipole kick was 9 mm and the computed echo amplitude for one turn from Eq. (7) is 2 mm in agreement with the simulation.

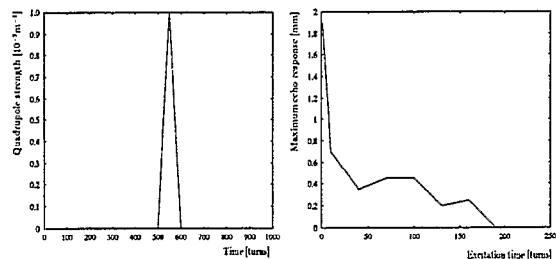


Figure 9: Left: The quadrupole excitation versus time for an amplitude of  $k = 1.0 \cdot 10^{-3} \text{m}^{-1}$  and an excitation time of 100 turns. Right: The maximum echo response versus the excitation time  $\Delta T$ .

Because the particle distribution rotates in the transverse phase space with the betatron frequency a long quadrupole excitation does not lead to a simple elongation and tilt of the phase space distribution but rather to a perturbation which looks approximately uniform over the azimuthal angle of the transverse phase space. Since the echo signal relies on local density deformation along the azimuthal angle of the transverse phase space this uniformity of the distribution reduces the final echo amplitude. For a perfectly uniform azimuthal perturbation of the transverse distribution the echo signal vanishes entirely.

The left hand side of Fig. 10 shows the maximum echo response versus the time separation between the initial dipole offset and a 10 turn long quadrupole kick. The echo

Table 2: RHIC machine parameters, proton beam at injection.

Parameter	Symbol	Unit	Value
Revolution frequency	$f_{rev}$	kHz	78.196
Particle momentum	$p$	GeV/c	25
Maximum transverse rms beam size	$\sigma_{x,y}$	mm	2.42
Maximum transverse $\beta$ -function in arcs	$\beta_{x,y}$	m	48.6
Transverse tune	$\nu_{x,y}$	1	28.19/29.18
Detuning	$\mu$	1	0.0035
Quadrupole kick strength (at 50A current)	$Q$	1	0.02

signal has a maximum amplitude for a time separation of 60,000 turns between the dipole kick and the quadrupole kick. Assuming that the maximum echo response varies linearly with the quadrupole excitation amplitude and requiring a maximum echo response of at least 1/10 of the initial 9 mm dipole signal one needs a quadrupole kick of

$$k \geq 1.8 \cdot 10^{-4} \text{m}^{-1} \text{ and } \Delta T \leq 10 \text{ turns.} \quad (8)$$

The right hand side of Fig. 10 shows the dipole signal of the distribution versus the number of turns for a 10 turn long quadrupole kick with  $k = 1.0 \cdot 10^{-3} \text{m}^{-1}$  at turn 50,000 after the initial dipole offset.

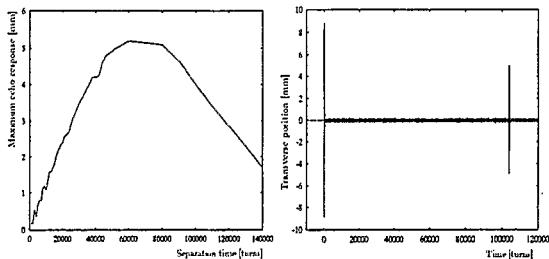


Figure 10: Left: The maximum echo response versus the separation time  $T$  between the initial dipole kick and a 10 turn long quadrupole kick with  $k = 1.0 \cdot 10^{-3} \text{m}^{-1}$ . Right: The dipole signal of the distribution versus time for a 10 turn long pulsed quadrupole kick with  $k = 1.0 \cdot 10^{-3} \text{m}^{-1}$  at turn 50,000 after the initial dipole offset.

## 5 SUMMARY

It should be possible to build a quadrupole kicker for RHIC that gives a one-turn normalized quadrupole kick of  $Q = 0.02$ . Analytical estimates and simulations predict that with such a quadrupole kick a transverse echo should be overvailable in at injection. Transverse echo measurement may allow the fast determination of diffusion coefficients.

## 6 REFERENCES

[1] T.M. O'Neil and R.W. Gould, Phys. Fluids **11**, 1 (1968).  
 [2] G. Stupakov, "Echo effect in hadron colliders", SSCL-579 (1992).  
 [3] G. Stupakov and S. Kauffmann, "Echo effect in accelerators", SSCL-587 (1992).

[4] N. Mahale et al., "Displaced bunch synchrotron oscillation echoes in accelerators", SSCL-N-817 (1993).  
 [5] L.K. Spentzouris, J.-F. Ostiguy and P.L. Colestock, "Direct measurement of diffusion rates in high energy synchrotrons using longitudinal beam echoes", PRL Vol. 76, No 4, pp. 620 (1996).  
 [6] O. Brüning, "On the possibility of measuring longitudinal echos in the SPS", CERN SL/95-83 (AP) (1995).  
 [7] O. Brüning et al., "Beam echos in the CERN SPS", proceedings of the 1997 Particle Accelerator Conference, Vancouver, (1997).  
 [8] J. Kewisch and M. Brennan, "Bunched beam echos in the AGS", proceedings of the 1998 European Particle Accelerator Conference, Stockholm (1998).  
 [9] W. Fischer et al., "Beam Injection into RHIC", proceedings of the 1997 Particle Accelerator Conference, Vancouver (1997).  
 [10] H. Hahn, J.E. Tuozzolo, "The RHIC injection kicker", proceedings of the 1997 Particle Accelerator Conference, Vancouver (1997).  
 [11] P. Cameron et al., "ARTUS: A Rhic TUne monitor System", BNL RHIC/AP/156 (1998).  
 [12] H. Hahn et al., "The RHIC Beam Abort Kicker System", proceedings of the 1999 Particle Accelerator Conference, New York, (1999).  
 [13] W. Fischer, A. Jain and D. Trbojevic, "The AC quadrupole in RHIC", RHIC/AP/164 (1999).  
 [14] P. Cameron and T. Shea, private communication (1999).  
 [15] "RHIC Design Manual", revision of April 1998.  
 [16] P. Cameron et al., "The RHIC Ionization Beam Profile Monitor", proceedings of the 1999 Particle Accelerator Conference, New York, (1999).  
 [17] G.V. Stupakov, "Echo", in A.W. Chao and M. Tigner (editors), "Handbook of Accelerator Physics and Engineering", World Scientific (1999).  
 [18] G.V. Stupakov and A.W. Chao, "Effect of Diffusion on Bunched Beam Echo", proceedings of the 1997 Particle Accelerator Conference, Vancouver, (1997).

## LIST OF PARTICIPANTS

Mai Bai  
BNL, Upton, NY 11973-5000, USA  
mbai@bnl.gov

Peter Bagley  
FNAL, Batavia, IL 60510-0500, USA  
ppb@fnal.gov

Oliver Brüning  
CERN, 1211 Geneva 23, Switzerland  
Oliver.Bruning@cern.ch

Nuria Catalan-Lasheras  
BNL, Upton, NY 11973-5000, USA  
catalan@bnl.gov

Angelika Drees  
BNL, Upton, NY 11973-5000, USA  
drees@bnl.gov

Andreas Lehrach  
BNL, Upton, NY 11973-5000, USA  
lehrach@bnl.gov

Wolfram Fischer  
BNL, Upton, NY 11973-5000, USA  
Wolfram.Fischer@bnl.gov

Miguel Furman  
LBNL, Berkeley, CA 94720, USA  
MAFurman@lbl.gov

William MacKay  
BNL, Upton, NY 11973-5000, USA  
mackay@bnl.gov

Ernest Malamud  
FNAL, Batavia, IL 60510-0500, USA  
malamud@fnal.gov

Christoph Montag  
DESY, Hamburg, 22603, Germany  
montag@mail.desy.de

Yannis Papaphilippou  
BNL, Upton, NY 11973-5000, USA  
papap@bnl.gov

Fulvia Pilat  
BNL, Upton, NY 11973-5000, USA  
pilat@bnl.gov

Vadim Ptitsyn  
BNL, Upton, NY 11973-5000, USA  
vadimp@bnl.gov

Thomas Roser  
BNL, Upton, NY 11973-5000, USA  
roser@bnl.gov

Todd Satogata  
BNL, Upton, NY 11973-5000, USA  
satogata@bnl.gov

Frank Schmidt  
CERN, 1211 Geneva 23, Switzerland  
Frank.Schmidt@cern.ch

Tanaji Sen  
FNAL, Batavia, IL 60510-0500, USA  
sen@fnal.gov

Vladimir Shiltsev  
FNAL, Batavia, IL 60510-0500, USA  
shiltsev@fnal.gov

Mike Syphers  
FNAL, Batavia, IL 60510-0500, USA  
syphers@fnal.gov

Steve Tepikian  
BNL, Upton, NY 11973-5000, USA  
tepikian@bnl.gov

Dejan Trbojevic  
BNL, Upton, NY 11973-5000, USA  
dejan@bnl.gov

Richard Talman  
Cornell, Ithaca, NY 14853-2801, USA  
talman@lns61.tn.cornell.edu

William Turner  
LBNL, Berkeley, CA 94720, USA  
WCTurner@lbl.gov